Quasi-Static Fluid-Structure Interactions Based on a Geometric Description of Fluids

Zur Erlangung des akademischen Grades eines

DOKTOR-INGENIEURS

von der Fakultät für

Bauingenieur-, Geo- und Umweltwissenschaften
der Universität Fridericiana zu Karlsruhe (TH)

genehmigte

DISSERTATION

von

Dipl.-Ing. Marc Haßler
aus Wedern

Tag der mündlichen Prüfung	:	22. Juli 2009
Hauptreferent	:	Prof. Dr.-Ing. K. Schweizerhof
Korreferent	:	Prof. J. Bonet

Karlsruhe 2009

Abstract

This thesis deals with the description of quasi-static fluid-structure interactions. Regarding an efficient computation of such kind of problems all relevant properties of the fluid, such as density, pressure or fluid level, will be captured using only the geometry of the surrounding wetted structure. This allows an analytical description of the fluid, with its strain energy implemented in a volume-dependent energetic equivalent loading acting on the structure. Thus, for the description of the interaction of the structure and the fluid only the structural geometry is necessary.

Apart from providing the thermodynamical fundamentals a special focus of this work is on the geometrical capturing of all energetic terms (including the height of the fluid level and a possible overpressure) describing the state of equilibrium only in terms of the surrounding wetted structure. After a consistent linearization of the equations and their discretization with finite element mapping functions, several solution schemes for this kind of equations will be discussed. Further, the influence of such volume-dependent pressure loadings on the structural stability is investigated.

Some practical examples covering the fields of hydraulic engineering, metal sheet forming and ship building complete this work.

Although a reduction of the fluid – where the inner state variables are generally field quantities – to a single phase system with position-invariant state variables restricts the consideration to quasi-static applications, however, in the last numerical example the transition to acoustics is presented, in order to expand the applicability of the algorithms derived in this work.

Kurzfassung

Diese Arbeit beschäftigt sich mit der Beschreibung quasistatischer Fluid-Struktur-Interaktionen. Im Hinblick auf eine effiziente Berechnung derartiger Problemstellungen werden alle relevanten Eigenschaften, wie Dichte, Druck oder Fluidspiegellage, des mit der Struktur in Kontakt stehenden Fluids über eine rein geometrische Darstellung erfasst. Dies ermöglicht somit eine analytische Fluidbeschreibung, deren Formänderungsenergie Eingang in eine energetisch äquivalente, auf die Strukturoberfläche wirkende Ersatzlast findet. Zur Beschreibung der Wirkung des Fluids auf die Struktur dient damit also lediglich die strukturelle Oberfläche.

Neben der Bereitstellung der notwendigen thermodynamischen Werkzeuge liegt ein erster Schwerpunkt in der geometrischen Erfassung aller energetischen Anteile, um den Gleichgewichtszustand in Abhängigkeit der das Fluid berandenden Strukturoberfläche darstellen zu können. Nach konsistenter Linearisierung der Gleichgewichtsbedingungen und deren Einbettung in die Methode der Finiten Elemente werden verschiedene Methoden zur effizienten Lösung des so erhaltenen Gleichungssystems behandelt. Des Weiteren wird der Einfluss einer derartigen volumenabhängigen Druckbelastung auf die strukturelle Stabilität diskutiert. Mehrere praxisnahe Beispiele aus den Bereichen Wasserbau, Metallumformung und Schiffbau bilden den Abschluss dieser Arbeit.

Die Reduktion eines Fluids, dessen Zustandsvariablen im Allgemeinen Feldgrößen sind, auf eine einfache Phase mit ortsunabhängigen Zustandsvariablen bewirkt zunächst, dass die Anwendbarkeit dieser Betrachtung auf quasistatische Prozesse beschränkt werden muss; in einem letzten numerischen Beispiel erfolgt jedoch auch der Übergang zur Akustik, um die Anwendbarkeit der hier behandelten Algorithmen in einem weiteren Kontext aufzuzeigen.

Acknowledgments

The present work was accomplished during my employment at the Institut für Mechanik, Universität Karlsruhe (TH), Germany.

Special thanks is addressed to my supervisor Prof. Dr.-Ing. K. Schweizerhof for his enduring support, valuable guidance and the inspiration for the development of this work.

I express my gratitude also to my external supervisor Prof. J. Bonet, Swansea University, Wales, for his many advice and the efficient proofreading of this work.

For their feedback and their expert talks I would like to thank Prof. Dr.-Ing. habil. P. Vielsack, Prof. Dr.-Ing. habil. Th. Seelig and especially Dr. rer. nat. J. Lenz, who first and foremost encouraged me to join the institute as a PhD student.

I would also like to thank all my colleagues at the Institut für Mechanik for the passionate discussions, the extraordinarily good collaboration and the creation of a very amicable atmosphere.

As this thesis would not have been possible without the excellent preliminary work of Dr.-Ing. Thorsten Rumpel, I would like to address my thanks also to him.

For his support in the field of hydraulic engineering I would like to thank Dr.-Ing. Michael Gebhardt.

Finally, I would like to acknowledge the support by my parents and my brother Jörg. Their moral assistance and advice in all other views engaged me to successfully finish this work.

Munich, August 14, 2009 M. Haßler

Contents

Notations **VI**

Introduction **1**

1 Continuum mechanics **6**

1.1 Kinematics 6

1.1.1 Configuration 6

1.1.2 Deformation gradient and strains 7

1.2 Stresses 10

1.3 Velocity and time derivatives 11

1.3.1 Objective derivation of a tensor field 11

1.4 Mechanical balance laws 12

1.4.1 Balance of mass 12

1.4.2 Balance of linear momentum 13

1.4.3 Balance of rotational momentum 14

2 Thermodynamics **15**

2.1 First law of thermodynamics 15

2.1.1 Kinetic energy 15

2.1.2 Specific internal energy 16

2.1.3 Power of the external forces 16

2.1.4 Heat flow and heat production 17

2.1.5 Strong form of the first law of thermodynamics 17

2.2 The second law of thermodynamics 18

2.3 Fundamental equations for solids and fluids 19

2.3.1 Constitutive laws for hyperelastic materials 20
St. Venant-Kirchhoff material 20
Neo-Hooke material 22
2.3.2 State equations of fluid phases 24
State equations for ideal gases 25
State equation of an incompressible fluid 30
State equation of a compressible fluid 30

3 Weak form of equilibrium 32
3.1 Variation of the potential energies 32
3.1.1 Variation of the elastic potential energy 33
Variation of the strains 34
3.1.2 Variation of the potential energy of the gas 34
3.1.3 Variation of the potential energy of a heavy fluid 35
3.1.4 Geometric dependencies 36
3.1.5 Boundary integral representation of the geometry 38
Variation of the geometry 40
Only gas filling 42
Complete fluid filling 42
3.1.6 Virtual work of the absolute fluid and gas pressures 43
3.1.7 Derivation of specific load cases 44
Gas filled control volume 44
Incompressible fluid with free fluid surface 45
Incompressible fluid with free fluid surface and additional gas loading 46
Compressible fluid with free fluid surface 47
Control volume completely filled with a compressible fluid . . . 47
Control volume containing compressible fluid and gas 48
3.1.8 Weak form of equilibrium 50
3.2 Linearization of the weak form 50
3.2.1 Linearization of the elastic part 51
Material tangent 51

Geometric part 51
3.2.2 Linearization of the fluid and gas parts 52
Incremental pressure changes 52
Incremental changes of the geometric quantities 52
Incremental change of the fluid level 54
Pressure changes due to volume compression 54
Incremental pressure change in the center of gravity 55
Incremental pressure change at the phase intersection 56
Incremental pressure change at a wetted structural surface point 57
3.2.3 Terms including the change of normals 57
3.2.4 Proof of conservativeness 58

4 The finite element method 63
4.1 Basics 63
4.2 Discretization 64
4.2.1 Discretization of the geometry 64
4.2.2 Discretization of the kinematics 65
4.2.3 Discretization of the fluid and gas parts 67
4.2.4 Hybrid approach 69
4.2.5 Derivation of special load cases 70
Incompressible heavy fluid with free fluid surface and additional gas loading 70
Compressible heavy fluid with free fluid surface and additional gas loading 72
4.2.6 Interaction of multiple control volumes 73

5 Discussion of deformation dependent loadings 75
5.1 Loadings with deformation dependent directions 75
5.2 Gas filled control volume 78
5.3 Control volume filled with incompressible heavy fluid 80
5.3.1 Discussion of stability 83

6 Numerical solution schemes 87

6.1 Direct solution scheme 87
6.1.1 Solution procedure for a rank-3-update of $\underline{K}$ 88
Starting point: recursive step $i = 0$ 88
Recursive step $i = 1$ 89
Recursive step $i = 2$ 90
Recursive step $i = 3$ 91
General solution scheme 91
Memory requirements 91
6.2 Iterative solution of the hybrid equation system 92
6.2.1 Benchmark: Gas filled multi-chamber system 94
6.3 Eigenvalue analysis 97
6.3.1 Computation of shifted eigenvalues 97
Case 1: All coordinates unequal zero $(\bar{a}_j \neq 0)$ 99
Case 2: Coordinate $\bar{a}_j = 0$ 101
6.3.2 Computation of eigenvectors 101
6.3.3 Efficiency considerations: How many eigenpairs needed? 102
6.3.4 Multiple rank-updates 104

7 Numerical examples **107**
7.1 Rubber dam 107
7.1.1 2D model of the rubber dam 109
Air inflated rubber dam subjected to hydrostatic loading 109
Water filled rubber dam subjected to hydrostatic loading . . . 110
7.1.2 3D model of the rubber dam 112
Air inflated rubber dam subjected to hydrostatic loading 113
Water filled dam subjected to hydrostatic loading 114
7.2 High-pressure tube hydroforming 116
7.3 Stability 120
7.3.1 Buckling analysis of fluid/gas filled cylinders 120
Empty cylinder 121
Gas filled cylinder 122
Partially fluid filled cylinder 123

Partially gas and fluid filled cylinder . . . 123
Completely fluid filled cylinder . . . 124
Discussion . . . 124
7.3.2 Buckling analysis of an inflatable beam . . . 126
Mechanics of an inflatable beam . . . 126
Buckling analysis of an inflatable beam using a membrane formulation . . . 128
7.4 Buoyancy simulation . . . 133
7.5 Acoustical simulation . . . 136

Conclusions/Outlook **142**

Bibliography **144**

A Mathematical basics **153**
A.1 Linearizations . . . 153
A.2 Some fundamentals of variational calculus . . . 154
A.2.1 Eulerian equation of the variational problem . . . 156
A.3 Legendre transformation . . . 156
A.4 Some fundamentals of tensor calculus . . . 157
A.4.1 Triple product . . . 157
A.4.2 Product of two tensors . . . 158
A.4.3 Expanding double cross products . . . 158
A.4.4 Separation of a matrix . . . 158
A.4.5 Trace of a tensor . . . 158
A.4.6 Convective coordinates on a surface . . . 158
A.4.7 Gauß' theorem . . . 158
A.5 Computation of the volume . . . 159
A.5.1 Variation of the volume . . . 159
A.6 First order volume moment . . . 161
A.6.1 Variation of the first order volume moment . . . 163
A.7 Derivatives of the invariants in direction of the strains . . . 165

Notations

Tensors

$\boldsymbol{X}$	position vector to initial configuration
$\boldsymbol{x}$	position vector to current configuration
$\boldsymbol{u}$	displacement vector
$\boldsymbol{v}$	velocity vector
$\boldsymbol{l}$	velocity gradient
$\boldsymbol{d}$	rate of deformation
$\boldsymbol{\omega}$	spin tensor
$\boldsymbol{F}$	deformation gradient
$\boldsymbol{R}$	rotation tensor
$\boldsymbol{U}$	right stretch tensor
$\boldsymbol{V}$	left stretch tensor
$\boldsymbol{C}$	right Cauchy-Green strain tensor
$\boldsymbol{b}$	left Cauchy-Green strain tensor
$\boldsymbol{G}$	metric tensor of the initial configuration
$\boldsymbol{g}$	metric tensor of the current configuration
$\boldsymbol{G}_\alpha$, $\boldsymbol{G}^\alpha$	co- and contravariant base vectors in the initial configuration
$\boldsymbol{g}_\alpha$, $\boldsymbol{g}^\alpha$	co- and contravariant base vectors in the current configuration
$\boldsymbol{E}$	Green-Lagrange strain tensor
$\boldsymbol{e}$	Almansi strain tensor
$\boldsymbol{t}$	stress vector
$\boldsymbol{N}$	normal vector in the initial configuration
$\boldsymbol{n}$	normal vector in the current configuration
$\boldsymbol{F}_S$	cutting force vector in the initial configuration
$\boldsymbol{f}_S$	cutting force vector in the current configuration
$\boldsymbol{\sigma}$	Cauchy stress tensor
$\boldsymbol{P}$	first Piola-Kirchhoff stress tensor
$\boldsymbol{S}$	second Piola-Kirchhoff stress tensor
$\boldsymbol{\tau}$	Kirchhoff stress tensor
$\boldsymbol{N}^\alpha$	principal directions in the initial configuration
$\boldsymbol{n}^\alpha$	principal directions in the current configuration
$\bar{\boldsymbol{t}}$	surface loads
$\bar{\boldsymbol{b}}$	volume loads
$\boldsymbol{p}$	impulse
$\boldsymbol{q}$	heat flow density
$\boldsymbol{s}$	first order volume moment
$\boldsymbol{c}$	position vector to the center of gravity of the fluid
$\boldsymbol{I}$	identity tensor

$\widehat{\boldsymbol{W}}$	skew symmetric tensor
$\mathbb{C}$	fourth order material tensor
$\mathbb{I}$	symmetric fourth order metric tensor
$\mathbb{J}$, $\mathbb{T}$	symmetric fourth order tensors

Exceptions in chapters 3, A.5 and A.6

$\boldsymbol{g}$	gravitation

Scalars

J	determinant of the deformation gradient
ξ_α, ξ^α	co- and contravariant coordinates
λ_α	eigenvalues of the deformation gradient
m	mass
t	time
V	initial volume
v	current volume
ρ	density
$\mathcal{B}$	material solid body
$\partial\mathcal{B}$	surface of the material solid body
$\mathcal{E}$	total energy of the system
$\mathcal{K}$	kinetic energy of the system
$\mathcal{A}$	work done by the external forces
$\mathcal{Q}$	heat stored in the system
$\mathcal{V}$	potential energy of system
r	heat rate density produced in the system
s	specific entropy
T	thermodynamical temperature
f	Helmholtz function
g	Gibbs function
h	specific enthalpy
W_S	strain energy density
$I_{\boldsymbol{T}}$, $II_{\boldsymbol{T}}$, $III_{\boldsymbol{T}}$	invariants of a tensor $\boldsymbol{T}$
Λ, μ	Lamé constants
ν	specific volume
p	pressure
c_p	isobaric heat capacity
c_ν	isochoric heat capacity

R	specific gas constant
R_m	universal gas constant
M	molar mass
n	amount of substance
κ	adiabatic exponent
K_0	bulk modulus
κ_0	isothermal coefficient of the compressibility
β_0	coefficient of volumetric expansion
α, β, γ	pressure volume gradients
$\bar{\alpha}$, $\bar{\beta}$	dimensionless pressure volume gradients
Ω	domain of a finite element
δ	operator of variation
Δ	operator of linearization
C_i	constants

Exceptions in chapter 2.3.1

ν	Poisson ratio
κ	shear correction factor

Matrices

$\underline{X}$	position vector to initial configuration
$\underline{x}$	position vector to current configuration
$\underline{u}$	displacement vector
$\underline{\hat{X}}$	vector of the discrete nodal coordinates
$\underline{d}$	vector of the discrete nodal displacements
$\underline{N}$	interpolation matrix
$\underline{J}$	Jacobian matrix
$\underline{\xi}$	convective coordinates
$\underline{G}_\alpha$, $\underline{G}^\alpha$	co- and contravariant base vectors in the initial configuration
$\underline{g}_\alpha$, $\underline{g}^\alpha$	co- and contravariant base vectors in the current configuration
$\underline{E}$	Green-Lagrange strains
$\underline{S}$	second Piola-Kirchhoff stresses
$\underline{B}$	geometrically linear part of strains
$\underline{H}$	geometrically nonlinear part of strains
$\underline{K}$	stiffness matrix
$\underline{f}$	load vector
$\underline{a}$, $\underline{b}$, $\underline{c}$	coupling vectors

$\underline{\hat{a}}$, $\underline{\hat{b}}$, $\underline{\hat{c}}$	modified coupling vectors
$\underline{\underline{\mathbb{C}}}$	fourth order material matrix
$\underline{\underline{D}}$	simplified second order material matrix

Superscripts

o	concerning the fluid level
$*$	non-conservative
f	concerning the part of the structural surface wetted by fluid
g	concerning the part of the structural surface wetted by gas
ext	concerning external loadings
k	resulting from gas or fluid compressibility
x	concerning an arbitrary structural surface point
c	concerning the center of gravity of the fluid
Δn	resulting from the linearization of the normal vector
Δp	resulting from the linearization of the pressure
Cpl	volume coupling term
h	spatially discrete quantity
α	curvilinear coordinate index $\alpha = 1, 2$
$,\alpha$	partial derivative to the covariant coordinate ξ_α

Subscripts

f	concerning the part of the structural surface wetted by fluid
g	concerning the part of the structural surface wetted by gas
ext	concerning external loadings
el	concerning the elastic strains of a solid body
t	computed at time t
0	computed in the initial configuration
$\square$	computed in the reference configuration
e	denoting size on element level
α	curvilinear coordinate index $\alpha = 1, 2$
$,\alpha$	partial derivative to the contravariant coordinate ξ^α

Introduction

The expression fluid-structure interaction covers a wide variety of physical problems, which are of interest mainly in the field of engineering and nowadays also in medicine. The applications range from the computations of pneumatic structures as e.g. airbags or pontoon bridges to the simulation of fluid flow inside blood vessels. Since this vast diversification led to different computation methods only appropriate for a specific class of problems, for a better classification of this work these types of problems shall be briefly mentioned here. In general it has to be distinguished between quasi-static fluid-structure interaction problems, where dynamical effects can be neglected and dynamical fluid-structure interaction problems, which again can be subdivided into acoustic type problems and problems involving fluid flow.

Classification

Highly dynamical fluid-structure interactions

In case of highly dynamical fluid-structure interactions, such as aerodynamical flow problems or underwater explosions in the vicinity of elastic solid bodies, very high fluid velocities arise interacting with the elastic solid body. A major difficulty for the numerical description of these kinds of problems is, that on one hand an Eulerian description of the fluid with its high velocities and possible turbulences is necessary with a fixed spatial mesh. On the other hand large deformations in solid bodies can be described best using a Lagrangian formulation, because here the development of the material properties of a material point and the capturing of boundary conditions are directly given. This fundamental problem can be overcome by the ALE-method managing the coupling of the Navier-Stokes equations of the fluid, given in an Eulerian formulation and the Lagrangian formulation of the solid body. In the vicinity of the deformable structure, where the fluid mesh undergoes heavy distortions, the ALE algorithms guarantee a permanent mesh adaptation, see also Hughes et al.[43], Wall[108]. The disadvantages of this method are mainly the high numerical effort necessary for the mesh adaptation and the fact that those algorithms are not robust enough for the computation of more complex three-dimensional structures, see e.g. Souli et al.[97].

An alternative way for the numerical simulation of complex flow problems can be found e.g. in the smooth particle hydrodynamics (SPH), a so-called meshless

method, where the continuum is represented by a set of points or particles. This method was initially developed for the simulation of astrophysical problems, see GINGOLD&MONAGHAN[34],[35]. In SPH a given function, e.g. the fluid density, is approximated in terms of values of the function at a number of neighbouring particles and a kernel function featuring a specific smoothing length, which determines the support of the kernel. Thus e.g. the fluid density at an arbitrary point can then be interpreted as the the smoothing of the discrete masses of particles over a finite region of space. This procedure offers the opportunity to describe both the fluid and the solid domain in Lagrangian coordinates and allows to simulate large deformation problems, as e.g. arising in metal forming, see BONET ET AL.[12], or even free surface flows, see BONET ET AL.[13].

Acoustic fluid-structure interaction

The simulation of acoustic fluid-structure interaction problems is e.g. of interest in the field of civil engineering, motivated by earthquake damages of fluid filled tanks. But also in aeronautics and astronautics the vibration behaviour of e.g. liquid-fuel tanks is of interest. Premise for such kind of investigations are small deflections, allowing a linear composition of the response of the system by different eigenmodes. Further the velocities of the fluid have to be small enough to neglect viscous and convective effects in the fluid, see ZIENKIEWICZ&TAYLOR[115]. A general overview of acoustic fluid-structure interaction can be found in MORAND&OHAYON[61]. A relatively simple method for a vibration analysis of fluid filled systems is the added mass concept, which merely adds a certain amount of mass to the elastic structure to consider the inertia of the fluid, see e.g. VIRELLA ET AL.[105] and KIANOUSH[46]. The development of fluid elements for the investigation of vibrations of compressible and incompressible fluids including also free fluid surface effects is described in ANDRIANARISON&OHAYON[1] and SCHOTTÉ&OHAYON[83],[84]. Besides elements based on a velocity potential, as in KOCK&OLSON[49] and EVERSTINE[26], purely displacement based elements exist as well, see BELYTSCHKO&KENNEDY[8], OLSON&BATHE[65] or BERMÚDEZ ET AL.[9]. However, the latter elements suffer from spurious rotation eigenmodes. To overcome this effect, it is referred to the works of HAMDI ET AL.[38] and WANG&BATHE[109]. In order to reduce the number of degrees of freedom and thus reduce the computation time for time integration purposes the system response can be also composed by a reduced modal basis, see OHAYON[64] and ANDRIANARISON&OHAYON[2].

Analytical description of fluids

All previously discussed methods (except for the added-mass concept) have in common that the fluid has to be discretized, leading to a remarkable increase of computation time. Therefore achievements were made to model the fluid as a homogeneous phase with a minimum number of unknowns, e.g. the density or the pressure, in order to save computation time. Early works on fluid filled membrane structures, considering the coupling of the fluid level with the structural displacements, were presented in

SCHNEIDER[82] or KATSIKADELIS&NERANTZAKI[45]. However, they are restricted to two-dimensional or simple three-dimensional geometries. The exact capturing of a gas volume using the geometry of its boundary as well as proposing a consistent linearization of all terms with respect to the solution can be found in BERRY&YANG[10], although also only for the 2D case. Identical formulations for gas filled systems, but meanwhile extended to the general 3D case, are given in BONET ET AL.[15] and RUMPEL&SCHWEIZERHOF[79], where a major focus of the last work was also on the investigation of the stability of gas filled structures. Also in commercial state-of-the-art codes surface integral descriptions of volume dependent gas loadings can be found already. For example in the airbag model in LS-Dyna, where the inflation process is controlled by a mass flow of gas, see HALLQUIST[37]. Based on the work of BERRY&YANG[10] VAN DIJK ET AL.[24] developed the equations for simulations of structures filled with gas and an incompressible fluid. To avoid difficulties during the iteration process the incompressibility of the fluid was included using a penalty formulation. Since no gravitational effects of the fluid and no coupling of the fluid level with the structural deformations were considered, the applicability of these routines is restricted to relatively small structures, such as deformable, water filled PET-bottles. A derivation of the state of equilibrium of thin-walled structures, either filled with an incompressible or a compressible heavy fluid was given in RUMPEL&SCHWEIZERHOF[80]. Starting from the variation of the potential energy of the fluid a consistent linearization and application of physically correct boundary conditions leads to a symmetric stiffness matrix. Further, in the literature other derivations can be found for the analytical description of specific gas filled continua, such as cylindrical gas supported beams. Their basic assumption is that both the cross-section and the internal gas pressure remain constant throughout the deformation, see FICHTER[28]. However, a disadvantage is the introduction of an effective beam length and of an effective radius for the compensation of initial deformations during the inflation process. More detailed information is given in WIELGOSZ ET AL.[16],[23],[52],[53],[101],[111]; although the real coupling influence of the fluid and the structural deformation is missing.

Since the literature mentioned in this section is mostly concerned with quasi-static computations of gas and fluid filled structures, the relevance of such kind of problems in the engineering sector will now be briefly discussed. In the field of hydraulic engineering air or water filled rubber dams are a relatively new class of structures, with only a few decades of experience and thus still a lot of questions have to be answered. The algorithms derived later in this thesis can be of particular interest for these kinds of problems, because an analytical description of the fluid offers a very efficient method to simulate problems as the final geometry of the dam and wrinkling at the cheeks of a dam. An early work on this topic can be found in ANWAR[3], which is restricted to a two-dimensional analysis. Further investigations on the bearing behaviour of gas filled membranes, e.g. applied to airhouses, were made by WAGNER&RAIBLE[107]. But also in the field of aeronautics and astronautics inflatable and deployable structures are of particular interest. For example in the works of FREELAND ET AL.[29], PALISOC ET AL.[69], TAN&BAIER[100] and TUAN[104] the quasi-static deployments of solar sails, telescopes, reflectors and shields are simulated. The computation of the

stability properties of atmospheric balloons, subjected to different temperatures and thus different gas pressures concerning the day time and altitude, is also a field of applications for quasi-static fluid-structure interactions, see PELLEGRINO ET AL.[67],[66]. Further, the high-pressure tube hydroforming sector, using instead of deep drawing tools fluid pressure to form a metal sheet, is in need of appropriate fluid-structure interaction algorithms, especially in the automotive industry, because the manufacturing tolerances are shrinking and due to the high pressures in these processes it can be important to consider also the deformation of the fluid. More detailed information about hydroforming can be found in VOLLERTSEN ET AL.[106], SIEGERT[93], NAKAGAWA[62], KLEINER[47]. A concept restricted rather to architectural applications than real civil engineering applications is the so-called Tensairity concept, see LUCHSINGER ET AL.[55],[73], where the load bearing behaviour of a beam is directed to a separate compression chord and a tension chord. The maintenance of the moment arm is guaranteed by a gas filled membrane, also having the effect of stabilizing the compression chord to a certain degree. Hence, in contrast to conventional materials with equal strength very light structures can be obtained.

Outline

In chapter 1 the basic equations of nonlinear continuum mechanics are provided. Besides the kinematical behaviour of elastic structures, the stresses as the representative quantities in the mechanical balance laws are discussed. With respect to a consistent linearization of the balance laws an additional focus is also on the incremental changes of stresses and strains in time.

Chapter 2 provides the connection between the stresses and strains, both for material solid bodies and fluids, using two fundamental laws of thermodynamics. As this thesis is primarily concentrated on capturing the physical behaviour of fluids and gases by their geometry, the final formulation of these constitutive laws consequently has to be given also only in terms of the fluid and gas geometry.

Chapter 3 deals with the derivation of the equilibrium equations of fluid and/or gas filled elastic structures using the variational principle, as a state of equilibrium is characterized by a stationary value of its total potential energy. A further focus is on the transformation of all relevant quantities concerning the fluid or gas into a boundary integral formulation, as the fluid and gas is to be represented by its surface only.

Chapter 4 presents with the finite element method a common tool for the numerical computation of (initial) boundary value problems. Both the global displacement field as the unknown target function and the geometry are discretized using isoparametric mapping functions. Finally, all element matrices, necessary for a finite element implementation of the discussed fluid-structure interaction algorithms, are given.

As the derived equations and matrices are considerably large and therefore lack of physical clearness, chapter 5 provides with several simple one-degree of freedom systems a more transparent insight into deformation dependent loadings, also with respect to

their stabilizing influence on the structure.

The fact that the considered fluid loading is deformation dependent results in matrices with a considerably large bandwidth. Therefore in chapter 6 two schemes are presented, which allow both an efficient solution of the equilibrium equations and the extraction of the eigenvalues and eigenmodes of the global stiffness matrix.

Chapter 7 demonstrates both the performance and the restrictions of the derived finite element formulation for the computation of quasi-static fluid-structure interaction problems by means of several practically relevant numerical examples, as e.g. the inflation and hydrostatic loading of a rubber dam, the high-pressure tube hydroforming of a thin metal tube or stability investigations of axially loaded fluid filled cylinders.

The last chapter finally concludes this thesis with a summary and a discussion of the presented algorithms regarding their applicability and their performance and provides an outlook to open future work in the field of fluid-structure interaction.

Chapter 1

Continuum mechanics

In this chapter the basic equations of continuum mechanics, necessary for the finite element formulation, will be provided. First, the kinematics of an elastic body, describing the geometric behaviour of its deformation and thus allowing the introduction of strain quantities, will be discussed. Afterwards the stresses are covered, because they have to satisfy the balance equations for a state of equilibrium. To embed the final algorithm in a Newton-type solution scheme a consistent linearization is necessary, therefore an additional focus will be on the incremental changes of stresses and strains in time. As this chapter only briefly summarizes the well-known basics of continuum mechanics for notational purposes, for more detailed information about these topics it is referred to the standard literature, such as Bonet[14], Crisfield[21], Parisch[70], Malvern[56] *or* Marsden&Hughes[57]. *The connection of stresses and strains using constitutive material laws will be part of chapter 2.*

1.1 Kinematics

An arbitrary deformation of a body can be separated into a rigid body motion and a change of shape. The change of the shape of the body leads to strains and thus to stresses. The fact that for the description of physical problems balance laws are needed implies a strict decomposition of the deformation, which is guaranteed by the introduction of objective state variables. These are unaffected by rigid body motions and therefore adequate for the description of the physical balance laws.

1.1.1 Configuration

In continuum mechanics a material body $\mathcal{B}$ is a contiguous set of material points. To capture the properties of the body at a time t the material points are mapped in the Euclidean vector space $\mathcal{E}^3$ with the bijective rule $\boldsymbol{\Phi} : \mathcal{B} \Rightarrow \mathcal{E}^3$. The configuration at time $t_0 = 0$, described by the material or Lagrangian coordinates $\boldsymbol{X}$, is called initial configuration $\mathcal{C}_0$, the configuration at any other time $t_i > 0$, described by the spatial

or Eulerian coordinates $\boldsymbol{x}$, is called current configuration c_i. Subsequently only fixed Cartesian coordinate systems with a common origin are used for the description of the initial and actual configurations. Their metric tensors are given by $\boldsymbol{I}$.

1.1.2 Deformation gradient and strains

The motion of the body can be described by the unique nonlinear mapping

$$\boldsymbol{x} = \boldsymbol{x}(\boldsymbol{X}, t) \ , \tag{1.1}$$

also called material or Lagrangian description of motion, because here the material coordinates are the independent variables. The inverse mapping

$$\boldsymbol{X} = \boldsymbol{X}(\boldsymbol{x}, t) \tag{1.2}$$

uses Eulerian coordinates and thus is called Eulerian description of motion. To allow for the requested unique reversibility of the mapping at any time t, as a sufficient condition the determinant of the deformation gradient $\boldsymbol{F}$ has to be positive for all t.

$$\det\left(\frac{\partial \boldsymbol{x}}{\partial \boldsymbol{X}}\right) = \det\left(\boldsymbol{F}\right) = J > 0 \tag{1.3}$$

Thus the deformation gradient maps the material tangent vector $d\boldsymbol{X}$ in the spatial tangent vector $d\boldsymbol{x}$ respectively in the current configuration.

$$d\boldsymbol{x} = \boldsymbol{F} d\boldsymbol{X} = \boldsymbol{\Phi}_* \left(d\boldsymbol{X}\right) \tag{1.4}$$

This transformation from the initial to the current configuration is also called push forward $\boldsymbol{\Phi}_*$. A reverse mapping from the current to the initial configuration is called a pull back operation $\boldsymbol{\Phi}^* = \boldsymbol{\Phi}_*^{-1}$.

$$d\boldsymbol{X} = \boldsymbol{F}^{-1} d\boldsymbol{x} = \boldsymbol{\Phi}^* \left(d\boldsymbol{x}\right) \tag{1.5}$$

See also figure 1.1. To obtain the objective state variables mentioned above, which are free of rigid body motions, a temporary configuration $\tilde{c}$ is used to achieve a polar decomposition of the deformation gradient. This yields the proper orthogonal rotation tensor

$$\boldsymbol{R} = \frac{\partial \boldsymbol{x}}{\partial \tilde{\boldsymbol{X}}} \ , \quad \text{with} \quad \boldsymbol{R}\boldsymbol{R}^T = \boldsymbol{I} \tag{1.6}$$

and the right stretch tensor

$$\boldsymbol{U} = \frac{\partial \tilde{\boldsymbol{X}}}{\partial \boldsymbol{X}} \ , \quad \text{with} \quad d\boldsymbol{x} = \boldsymbol{R}\boldsymbol{U} d\boldsymbol{X} \ . \tag{1.7}$$

Hence, the tangent vector $d\boldsymbol{x}$ is then given by a stretch of $d\boldsymbol{X}$ with $\boldsymbol{U}$ and a subsequent rotation with $\boldsymbol{R}$. In analogy the left stretch tensor can be introduced by

$$\boldsymbol{V} = \frac{\partial \boldsymbol{x}}{\partial \tilde{\boldsymbol{X}}} \ , \quad \text{with} \quad d\boldsymbol{x} = \boldsymbol{V}\boldsymbol{R} d\boldsymbol{X} \ . \tag{1.8}$$

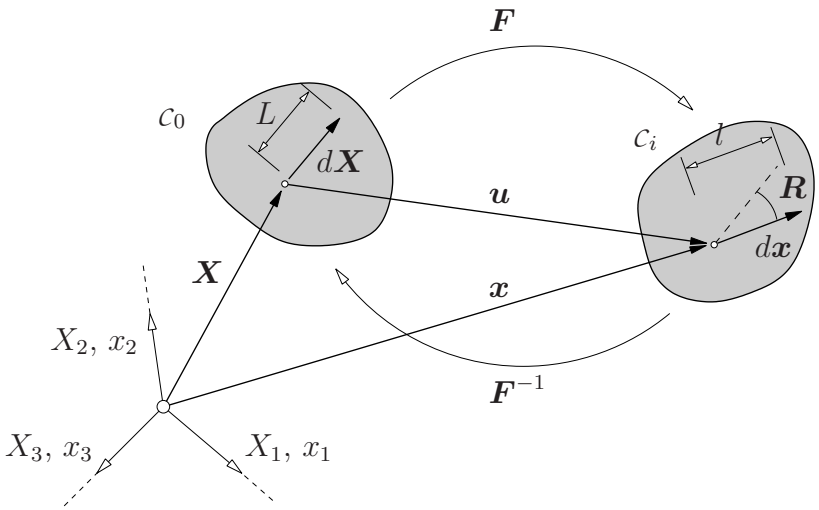

Figure 1.1: Mapping of the material tangent vector $d\boldsymbol{X}$ into the spatial tangent vector $d\boldsymbol{x}$

Thus the deformation gradient follows as

$$\boldsymbol{F} = \boldsymbol{R}\boldsymbol{U} \quad \text{and} \quad \boldsymbol{F} = \boldsymbol{V}\boldsymbol{R} \,. \tag{1.9}$$

Exploiting the orthonormality of the rotation tensor $\boldsymbol{R}$ the rotational parts in (1.9), representing the rigid body motions, can be eliminated. This yields the right Cauchy-Green tensor

$$\boldsymbol{C} = \boldsymbol{F}^T\boldsymbol{F} \,, \tag{1.10}$$

given in the initial configuration and the left Cauchy-Green tensor

$$\boldsymbol{b} = \boldsymbol{F}\boldsymbol{F}^T \,, \tag{1.11}$$

given in the current configuration. Although in both tensors the rotational parts are now eliminated, they are still not adequate as proper strain measures, because in case of a pure rigid body motion they become the identity tensor instead of a zero tensor. Therefore the Green-Lagrangian strain tensor defines the strain as the average difference between the current metric $\boldsymbol{C}$ and the undeformed metric $\boldsymbol{I}$.

$$\boldsymbol{E} = \frac{1}{2}\left(\boldsymbol{C} - \boldsymbol{I}\right) \tag{1.12}$$

From equation (1.12) the relations

$$\frac{\partial \boldsymbol{E}}{\partial \boldsymbol{C}} = \frac{1}{2} \,, \quad \text{resp.} \quad \frac{\partial}{\partial \boldsymbol{E}} = 2\frac{\partial}{\partial \boldsymbol{C}} \tag{1.13}$$

between both strain tensors can be given, which will be used later on. In the same manner the Almansi strain tensor defines the strains as the average difference of the metric $\boldsymbol{I}$ and the undeformed metric $\boldsymbol{b}^{-1}$.

$$\boldsymbol{e} = \frac{1}{2}\left(\boldsymbol{I} - \boldsymbol{b}^{-1}\right) \tag{1.14}$$

In a finite element formulation a parameterization of the geometry $\boldsymbol{X} = \boldsymbol{X}(\xi^\alpha)$, $\boldsymbol{x} = \boldsymbol{x}(\xi^\alpha)$ and the displacements $\boldsymbol{u} = \boldsymbol{u}(\xi^\alpha)$ is often advantageous. Using the covariant tangent vectors

$$\boldsymbol{G}_\alpha = \frac{\partial \boldsymbol{X}}{\partial \xi^\alpha} \,, \qquad \boldsymbol{g}_\alpha = \frac{\partial \boldsymbol{x}}{\partial \xi^\alpha} \tag{1.15}$$

along with an application of the chain rule as well as condition $\boldsymbol{G}^\gamma \cdot \boldsymbol{G}_\alpha = \delta^\gamma{}_\alpha$ yields the relation

$$\boldsymbol{g}_\alpha = \frac{\partial \boldsymbol{x}}{\partial \boldsymbol{X}} \frac{\partial \boldsymbol{X}}{\partial \xi^\alpha} = \boldsymbol{F}\boldsymbol{G}_\alpha = \left(F^\beta{}_\gamma \boldsymbol{g}_\beta \otimes \boldsymbol{G}^\gamma\right) \boldsymbol{G}_\alpha = F^\beta{}_\alpha \boldsymbol{g}_\beta \,. \tag{1.16}$$

The deformation gradient in a convective basis then follows by a subsequent right-hand multiplication with $\boldsymbol{G}^\alpha$.

$$\boldsymbol{F} = \boldsymbol{g}_\alpha \otimes \boldsymbol{G}^\alpha \tag{1.17}$$

Using (1.17) in (1.10) resp. in (1.11) yields with equations (1.12) resp. (1.14) both strain tensors in a convective coordinate system (see also figure 1.2).

$$\boldsymbol{E} = \frac{1}{2} \left(g_{\alpha\beta} - G_{\alpha\beta}\right) \boldsymbol{G}^\alpha \otimes \boldsymbol{G}^\beta \tag{1.18}$$

$$\boldsymbol{e} = \frac{1}{2} \left(g_{\alpha\beta} - G_{\alpha\beta}\right) \boldsymbol{g}^\alpha \otimes \boldsymbol{g}^\beta \tag{1.19}$$

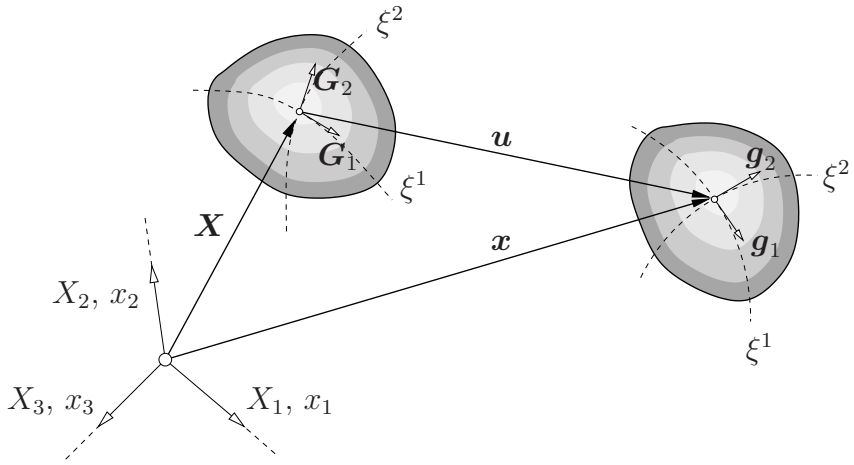

Figure 1.2: Spanning the tangent plane at a curvilinear surface

1.2 Stresses

The external loads are conducted to the bearings in forms of stresses inside the continuum. These stresses can be dissected by an imaginary cut free of the system. According to Cauchy the stress vector $\boldsymbol{t}$ is defined as the relation of the cutting force $d\boldsymbol{f}_S$ and the cutting area da.

$$\boldsymbol{t} = \lim_{\Delta a \to 0} \frac{\Delta \boldsymbol{f}_S}{\Delta a} = \frac{d\boldsymbol{f}_S}{da} \tag{1.20}$$

For the description of the internal stress state 3 orthogonal sectionings are sufficient. The 9 coordinates of all 3 dissected stress vectors add up to form the symmetric Cauchy stress tensor $\boldsymbol{\sigma}$. The Cauchy stress tensor specifies the true stresses, because it measures the stresses acting on the deformed volume element with the deformed area element. With a transformation of the normal vector $\boldsymbol{n}$ on the cutting area, besides the Cauchy stress tensor, other stress tensors can be obtained. Using the stress vector

$$\boldsymbol{t} = \boldsymbol{\sigma}\boldsymbol{n} \ , \tag{1.21}$$

equation (1.20) and the resulting cutting force vector

$$d\boldsymbol{f}_S = \boldsymbol{t}da = \boldsymbol{\sigma}\boldsymbol{n}\ da \tag{1.22}$$

a transformation of the normal vector $\boldsymbol{n}da$ to the initial configuration $\mathcal{C}_0$ yields the first Piola-Kirchhoff stress tensor $\boldsymbol{P}$:

$$d\boldsymbol{f}_S = \boldsymbol{\sigma}\boldsymbol{n}\ da = J\boldsymbol{\sigma}\boldsymbol{F}^{-T}\boldsymbol{N}dA = \boldsymbol{P}\boldsymbol{N}dA \ , \tag{1.23}$$

with

$$\boldsymbol{P} = J\boldsymbol{\sigma}\boldsymbol{F}^{-T} \ . \tag{1.24}$$

Due to the pull back operation of the normal $\boldsymbol{n}da$ the first Piola-Kirchhoff stress tensor measures the stresses at the deformed volume element with the undeformed area element dA. Thus a 2-point tensor with an unsymmetric coordinate matrix was generated. An additional pull back of the cutting force vector $d\boldsymbol{f}_S$ to the initial configuration $\mathcal{C}_0$ results in the second Piola-Kirchhoff stress tensor $\boldsymbol{S}$, holding for

$$d\boldsymbol{F}_S = \boldsymbol{F}^{-1}d\boldsymbol{f}_S = J\boldsymbol{F}^{-1}\boldsymbol{\sigma}\boldsymbol{F}^{-T}\boldsymbol{N}dA \ , \tag{1.25}$$

with

$$\boldsymbol{S} = J\boldsymbol{F}^{-1}\boldsymbol{\sigma}\boldsymbol{F}^{-T} \ . \tag{1.26}$$

The second Piola-Kirchhoff stress tensor is a symmetric tensor and completely related to the material configuration, although it has no physical significance any more. Besides the Cauchy stress tensor and the Piola-Kirchhoff stress tensors, introducing the Kirchhoff stress tensor

$$\boldsymbol{\tau} = J\boldsymbol{\sigma} \tag{1.27}$$

has the advantage, that in a pull back operation of $\boldsymbol{\tau}$ or a push forward operation of $\boldsymbol{S}$ the metric does not need to be scaled with J.

$$\boldsymbol{S} = \boldsymbol{\Phi}^*(\boldsymbol{\tau}) \quad \text{resp.} \quad \boldsymbol{\tau} = \boldsymbol{\Phi}_*(\boldsymbol{S}) \tag{1.28}$$

1.3 Velocity and time derivatives

For the embedding of all derived quantities in a numerical solution procedure, such as the Newton algorithm, a consistent linearization of stresses and strains is required. Therefore this section considers the time derivatives of several tensor fields. In case of a Lagrangian tensor field $\boldsymbol{T}(\boldsymbol{X}, t)$ the material coordinates $\boldsymbol{X}$ are independent of time, thus its time derivative yields

$$\frac{d}{dt}\boldsymbol{T}(\boldsymbol{X}, t) = \frac{\partial \boldsymbol{T}}{\partial t} = \dot{\boldsymbol{T}} \ , \tag{1.29}$$

whereas the time dependency of the spatial coordinates $\boldsymbol{x}(t)$ in an Eulerian tensor field $\boldsymbol{t}(\boldsymbol{x}, t)$ has to be considered in its derivation:

$$\frac{d}{dt}\boldsymbol{t}(\boldsymbol{x}, t) = \frac{\partial \boldsymbol{t}}{\partial t} + \frac{\partial \boldsymbol{t}}{\partial \boldsymbol{x}}\frac{\partial \boldsymbol{x}}{\partial t} = \dot{\boldsymbol{t}} + (\text{grad } \boldsymbol{t})\dot{\boldsymbol{x}} \tag{1.30}$$

Introducing the velocity $\dot{\boldsymbol{x}} = \boldsymbol{v}$ and using equation (1.29), the time derivative of the deformation gradient can be given as

$$\frac{d}{dt}\boldsymbol{F} = \dot{\boldsymbol{F}} = \frac{\partial}{\partial t}\frac{\partial \boldsymbol{x}}{\partial \boldsymbol{X}} = \frac{\partial}{\partial \boldsymbol{X}}\dot{\boldsymbol{x}} = \text{Grad } \boldsymbol{v} \ . \tag{1.31}$$

By applying the chain rule it can be mapped to the current configuration.

$$\dot{\boldsymbol{F}} = \frac{\partial \boldsymbol{v}}{\partial \boldsymbol{X}} = \frac{\partial \boldsymbol{v}}{\partial \boldsymbol{x}}\frac{\partial \boldsymbol{x}}{\partial \boldsymbol{X}} = (\text{grad } \boldsymbol{v})\boldsymbol{F} = \boldsymbol{l}\boldsymbol{F} \tag{1.32}$$

The resulting 2-point tensor

$$\boldsymbol{l} = \text{grad } \boldsymbol{v} = \dot{\boldsymbol{F}}\boldsymbol{F}^{-1} \tag{1.33}$$

is called spatial velocity gradient. For a future application in thermodynamical balance laws the spatial velocity gradient $\boldsymbol{l}$ is split into a symmetric part $\boldsymbol{d}$, called rate of deformation and into an antisymmetric part $\boldsymbol{\omega}$, called spin tensor.

$$\boldsymbol{l} = \frac{1}{2}\left(\boldsymbol{l} + \boldsymbol{l}^T\right) + \frac{1}{2}\left(\boldsymbol{l} - \boldsymbol{l}^T\right) = \boldsymbol{d} + \boldsymbol{\omega} \tag{1.34}$$

Containing the time variance of the tangent vector $d\boldsymbol{x}$, the velocity gradient $\boldsymbol{l}$ maps $d\boldsymbol{x}$ in the velocity tangent vector $d\dot{\boldsymbol{x}}$.

$$d\dot{\boldsymbol{x}} = \boldsymbol{l}d\boldsymbol{x} \tag{1.35}$$

1.3.1 Objective derivation of a tensor field

Both quantities describing the physical state of a continuum and their derivatives must be independent of the current coordinate system. A Lagrangian tensor field as well as its derivative is time-independent and thus objective. According to equation (1.32)

with the rate of the deformation tensor $\dot{\boldsymbol{F}} = \boldsymbol{l}\boldsymbol{F}$ the time derivative of the Green strain tensor follows as:

$$\dot{\boldsymbol{E}} = \frac{1}{2}\left(\dot{\boldsymbol{F}}^T\boldsymbol{F} + \boldsymbol{F}^T\dot{\boldsymbol{F}}\right) = \boldsymbol{F}^T\frac{1}{2}\left(\boldsymbol{l}^T + \boldsymbol{l}\right)\boldsymbol{F} \tag{1.36}$$

Comparing this result with equation (1.34) shows, that the rate of the Green strain tensor matches a pull back operation of the rate of deformation $\boldsymbol{d}$.

$$\dot{\boldsymbol{E}} = \boldsymbol{F}^T\boldsymbol{d}\boldsymbol{F} = \boldsymbol{\Phi}^*(\boldsymbol{d}) \tag{1.37}$$

Further, an additional push forward of $\dot{\boldsymbol{E}}$ leads to the rate of deformation $\boldsymbol{d}$.

$$\boldsymbol{\Phi}_*(\dot{\boldsymbol{E}}) = \boldsymbol{d} \tag{1.38}$$

Generally it can be posted that an Eulerian tensor field in a first step has to be pulled back to the initial configuration, where the derivation D can be accomplished. Afterwards it can be pushed forward again to the current configuration. These steps can be combined in the operator

$$\pounds_\Phi(\cdot) = \boldsymbol{\Phi}_*\left[D\boldsymbol{\Phi}^*(\cdot)\right] \ , \tag{1.39}$$

also known as Lie-derivative. Thus follows for the strain rate tensor $\boldsymbol{d}$:

$$\boldsymbol{d} = \pounds_\Phi(\boldsymbol{e}) \tag{1.40}$$

Although in chapters 3.1 and 3.2 the derivations are not carried out in direction of time but in direction of the virtual and incremental displacements, it can be shown that the operator D can be replaced by both the total differential and the variational δ.

1.4 Mechanical balance laws

The specification of a state of equilibrium, in local form at a differential volume element or in an integral form at the continuum, is performed using balance laws. In contrast to the linear theory, where balance laws are established at the undeformed element, these balance laws have to be established in the current configuration at the deformed element, if finite deformations are to be considered.

1.4.1 Balance of mass

The balance of mass postulates that the mass m of the body $\mathcal{B}$ remains constant in any coordinate system.

$$\frac{dm}{dt} = \frac{d}{dt}\int\limits_{\mathcal{B}} \rho(\boldsymbol{x},t)dv = \frac{d}{dt}\int\limits_{\mathcal{B}_0} \rho(\boldsymbol{x},t)JdV = 0 \tag{1.41}$$

Since the balance of mass has to be valid for any initial volume the transition to a local form can be performed. Using this relation along with the change of volume $J = dv/dV$ a connection between the density ρ_0 in the initial configuration and the density ρ in the current configuration can be given.

$$dm = \rho_0 dV = \rho J dV \quad \Leftrightarrow \quad \rho = \frac{1}{J}\rho_0 \tag{1.42}$$

1.4.2 Balance of linear momentum

According to Newton the sum of all external forces a body is subjected to equal the rate of its linear momentum. Considering area loads $\bar{\boldsymbol{t}}(\boldsymbol{x}, t)$ and volume loads $\rho\bar{\boldsymbol{b}}(\boldsymbol{x}, t)$, after integrating over the appropriate domain the balance of linear momentum in the current configuration follows as

$$\int_{\partial\mathcal{B}} \bar{\boldsymbol{t}} da + \int_{\mathcal{B}} \rho\bar{\boldsymbol{b}} dv = \frac{d}{dt}\int_{\mathcal{B}} \rho\boldsymbol{v}\ dv\ . \tag{1.43}$$

In order to express the balance of linear momentum in its strong form the Gauß theorem (A.31) and the stress boundary condition

$$\boldsymbol{t} = \boldsymbol{\sigma}\boldsymbol{n} = \bar{\boldsymbol{t}}\ : \quad \text{on} \quad \partial\mathcal{B}_\sigma \tag{1.44}$$

can be used to transform the area integral into a volume integral.

$$\int_{\partial\mathcal{B}} \bar{\boldsymbol{t}}\ da = \int_{\partial\mathcal{B}} \boldsymbol{\sigma}\boldsymbol{n}\ da = \int_{\mathcal{B}} \mathrm{div}\boldsymbol{\sigma}\ dv \tag{1.45}$$

To accomplish the time derivative on the right-hand side of equation (1.43) it is necessary to switch to the initial configuration using (1.42), because ρ is a time-variant field. Afterwards the rate of the momentum can be pushed forward again to the current configuration.

$$\frac{d}{dt}\int_{\mathcal{B}} \rho\boldsymbol{v}\ dv = \frac{d}{dt}\int_{\mathcal{B}_0} \rho_0\boldsymbol{v}\ dV = \int_{\mathcal{B}_0} \rho_0\dot{\boldsymbol{v}}\ dV = \int_{\mathcal{B}} \rho\dot{\boldsymbol{v}}\ dv \tag{1.46}$$

Inserting equations (1.45) and (1.46) in (1.43) enables a combination of all terms under a volume integral.

$$\int_{\mathcal{B}} \left(\mathrm{div}\boldsymbol{\sigma} + \rho\bar{\boldsymbol{b}} - \rho\dot{\boldsymbol{v}}\right) dv = 0 \tag{1.47}$$

This relation has to be valid for an arbitrary body $\mathcal{B}$, thus the integrand has to vanish, which yields the balance of linear momentum in its local form, also known as Cauchy's first law of motion.

$$\mathrm{div}\boldsymbol{\sigma} + \rho\bar{\boldsymbol{b}} = \rho\dot{\boldsymbol{v}} \tag{1.48}$$

1.4.3 Balance of rotational momentum

Cauchy's second law of motion demands the balance of rotational momentum at a volume element. With the origin of the coordinate system as the reference point and along with the velocity vector $\boldsymbol{v}$ and the location vector $\boldsymbol{x}$ the rotational momentum $d\boldsymbol{p}$ of a mass element $dm = \rho dv$ can be given as

$$d\boldsymbol{p} = (\boldsymbol{x} \times \boldsymbol{v})\, \rho dv \ . \tag{1.49}$$

Its time derivative follows with $\dot{\boldsymbol{x}} = \boldsymbol{v}$ as

$$d\dot{\boldsymbol{p}} = (\dot{\boldsymbol{x}} \times \boldsymbol{v} + \boldsymbol{x} \times \dot{\boldsymbol{v}})\, \rho dv = (\boldsymbol{x} \times \dot{\boldsymbol{v}})\, \rho dv \ . \tag{1.50}$$

The balance of rotational momentum postulates the equality of the rate of the rotational momentum and the resulting moment of all external forces.

$$\int_{\partial\mathcal{B}} (\boldsymbol{x} \times \bar{\boldsymbol{t}})\ da + \int_{\mathcal{B}} \left(\boldsymbol{x} \times \bar{\boldsymbol{b}}\right)\ \rho dv = \int_{\mathcal{B}} (\boldsymbol{x} \times \dot{\boldsymbol{v}})\, \rho dv \tag{1.51}$$

It can be shown that the balance of rotational momentum does not provide any additional equations for the solution of the boundary value problem. In its strong form it merely demands the symmetry of the Cauchy stress tensor.

Chapter 2

Thermodynamics

The basic quantities of stresses and strains are introduced in chapter 1; in thermodynamics i.a. two fundamental laws are postulated. The first is describing the state of equilibrium via a balance of energy rates and the second is defining a physically reasonable direction of a process. This enables the connection of the initially independent stresses and strains with appropriate constitutive laws. Thus, several new state variables, such as the thermodynamical temperature and the entropy, have to be introduced. Finally the aim of this chapter is the derivation of the state variables of a fluid and its expression in terms of geometry. For more detailed information about thermodynamics it is referred to the standard literature, e.g. Baehr[4], Hutter[44], Truesdell&Noll[103], Truesdell[102] *and* Ziegler[113].

2.1 First law of thermodynamics

Each system features an extensive state variable called energy $\mathfrak{E}$, which is proportional to the mass of the system and which can only change with an energy transport in terms of heat or work over the boundary of the system. The first law of thermodynamics postulates the energetic equilibrium considering the kinetic energy $\mathfrak{K}$, the internal energy $\mathfrak{U}$ as well as the work $\mathfrak{A}$ done to the system and other fed or conducted energy terms $\mathfrak{Q}$. In a state of equilibrium $\boldsymbol{x}$ for the rate $\dot{\mathfrak{E}}$ of the total energy yields

$$\dot{\mathfrak{E}}\,dt = D\mathfrak{E}(\boldsymbol{x})[t] = \left(\dot{\mathfrak{K}} + \dot{\mathfrak{U}}\right) dt = \left(\dot{\mathfrak{A}} + \dot{\mathfrak{Q}}\right) dt \ . \tag{2.1}$$

In order to compare two time adjacent states of energy it is assembled as a balance of powers.

2.1.1 Kinetic energy

The time derivation of the kinetic energy has to be carried out in the initial configuration, because the velocity $\boldsymbol{v}$, the density ρ and the volume differential dv are

time-variant. Thereafter the rate of the kinetic energy can be pushed forward again to the current configuration.

$$\dot{\mathcal{K}} = \frac{d\mathcal{K}}{dt} = \frac{d}{dt}\int\limits_{\mathcal{B}} \frac{1}{2}\boldsymbol{v}^2 \rho dv = \int\limits_{\mathcal{B}_0} \frac{1}{2}\frac{d\boldsymbol{v}^2}{dt}\rho_0 dV = \int\limits_{\mathcal{B}_0} \dot{\boldsymbol{v}} \cdot \boldsymbol{v}\rho_0 dV = \int\limits_{\mathcal{B}} \dot{\boldsymbol{v}} \cdot \boldsymbol{v}\rho dv \tag{2.2}$$

2.1.2 Specific internal energy

However, the kinetic energy is just a part of the total energy. A system at rest can also store energy. This energy is called internal energy $\mathcal{U}$, with

$$\mathcal{U} = \mathcal{E} - \mathcal{K} \ . \tag{2.3}$$

It can be interpreted as the kinetic energy of the molecular components of the system. The specific internal energy u can be obtained by a division of $\mathcal{U}$ by the mass m of the system.

$$u = \mathcal{U}/m \tag{2.4}$$

Thus the rate of internal energy $\mathcal{U}$ can be given in terms of the rate of the specific internal energy $\dot{u}$.

$$\dot{\mathcal{U}} = \frac{d\mathcal{U}}{dt} = \int\limits_{\mathcal{B}} \dot{u}\rho \ dv \tag{2.5}$$

I.a. this allows both a local formulation of the balance of energy at the volume element dv and the derivation of constitutive material laws connecting stresses and strains. Chapter 2.3.2 gives a more detailed insight into the specific internal energy.

2.1.3 Power of the external forces

In order to combine both the power of the area loads $\bar{\boldsymbol{t}}(\boldsymbol{x}, t)$ and the power of the volume loads $\bar{\boldsymbol{b}}(\boldsymbol{x}, t)$ in a common volume integral, the first term on the right hand side of equation (2.1) has to be transformed with the Gauß theorem (A.31) including the condition

$$\bar{\boldsymbol{t}}(\boldsymbol{x}, t) = \boldsymbol{\sigma}\boldsymbol{n} \ . \tag{2.6}$$

Thus follows

$$\begin{aligned} \dot{\mathcal{A}} = \frac{d\mathcal{A}}{dt} &= \int\limits_{\partial\mathcal{B}} \boldsymbol{v} \cdot \bar{\boldsymbol{t}} da + \int\limits_{\mathcal{B}} \boldsymbol{v} \cdot \bar{\boldsymbol{b}}\rho \ dv \\ &= \int\limits_{\mathcal{B}} \operatorname{div}(\boldsymbol{\sigma}\boldsymbol{v}) \, dv + \int\limits_{\mathcal{B}} \boldsymbol{v} \cdot \bar{\boldsymbol{b}}\rho \ dv \ . \end{aligned} \tag{2.7}$$

Subsequent application of the chain rule to the first term gives the power of the external forces as

$$\dot{\mathcal{A}} = \int_{\mathcal{B}} \boldsymbol{v} \cdot \left(\mathrm{div}\boldsymbol{\sigma} + \rho\bar{\boldsymbol{b}}\right) dv + \int_{\mathcal{B}} \boldsymbol{\sigma} : \mathrm{grad}\boldsymbol{v}\ dv\ . \tag{2.8}$$

Using the local balance of linear momentum (1.48)

$$\mathrm{div}\boldsymbol{\sigma} + \rho\bar{\boldsymbol{b}} = \dot{\boldsymbol{v}}\rho \tag{2.9}$$

along with the fact, that the spatial velocity gradient $\boldsymbol{l} = \boldsymbol{d} + \boldsymbol{\omega}$ from equation (1.33), due to the skew symmetry of the spin tensor $\boldsymbol{\omega}$, features

$$\boldsymbol{\sigma} : \boldsymbol{l} = \boldsymbol{\sigma} : \boldsymbol{d}\ , \tag{2.10}$$

leads to the following form for the power of the external forces:

$$\dot{\mathcal{A}} = \int_{\mathcal{B}} \rho\boldsymbol{v} \cdot \dot{\boldsymbol{v}}\ dv + \int_{\mathcal{B}} \boldsymbol{\sigma} : \boldsymbol{d}\ dv \tag{2.11}$$

2.1.4 Heat flow and heat production

The change of heat in the system results from the rate of the internal heat production r and the heat flow $\boldsymbol{q}$, emitted from the boundary of the system.

$$\dot{\mathcal{Q}} = \frac{d\mathcal{Q}}{dt} = -\int_{\partial\mathcal{B}} \boldsymbol{q} \cdot \boldsymbol{n}\ da + \int_{\mathcal{B}} r\rho\ dv = -\int_{\mathcal{B}} \mathrm{div}\boldsymbol{q}\ dv + \int_{\mathcal{B}} r\rho\ dv \tag{2.12}$$

2.1.5 Strong form of the first law of thermodynamics

Using the terms (2.2), (2.5), (2.11) and (2.12) in the balance of energy (2.1) yields the the first law of thermodynamics in its global form:

$$\int_{\mathcal{B}} \dot{u}\rho\ dv = \int_{\mathcal{B}} \boldsymbol{\sigma} : \boldsymbol{d}\ dv - \int_{\mathcal{B}} \mathrm{div}\boldsymbol{q}\ dv + \int_{\mathcal{B}} r\rho\ dv \tag{2.13}$$

Since the first law must be valid for an arbitrary volume, it can be expressed by its strong form, describing the balance of energy at a differential element.

$$\dot{u}\rho = \boldsymbol{\sigma} : \boldsymbol{d} - \mathrm{div}\boldsymbol{q} + r\rho \tag{2.14}$$

Within this work especially purely adiabatic processes without any heat production are of interest, thus $\boldsymbol{q} = \boldsymbol{0}$ and $r = 0$. Hence the specific rate of the internal energy

equals the power of the stresses and strain rates, which complies with the rate of the strain energy density.

$$\dot{u}\rho = \boldsymbol{\sigma} : \boldsymbol{d} \tag{2.15}$$

Thus the internal energy as an invariant of the system can be expressed alternatively in terms of several energetically conjugated field sizes.

$$\dot{u} = \frac{1}{\rho}\boldsymbol{\sigma} : \boldsymbol{d} = \frac{1}{\rho_0}\boldsymbol{\tau} : \boldsymbol{d} = \frac{1}{\rho_0}\boldsymbol{P} : \dot{\boldsymbol{F}} = \frac{1}{\rho_0}\boldsymbol{S} : \dot{\boldsymbol{E}} \tag{2.16}$$

By reasons of convenience the internal energy rate $\dot{u}$ is usually expressed using the stresses $\boldsymbol{S}$ and strain rates $\dot{\boldsymbol{E}}$ related to the initial configuration.

2.2 The second law of thermodynamics

Since all natural processes are irreversible ones, a further restriction is necessary, postulating that heat does only flow from a warm body to a cold one. Because of the equality sign, the first law of thermodynamics (2.14) omits this restriction concerning the direction of a process. However, the second law of thermodynamics postulates this unsymmetry in the direction of energy transformations and thus enables the derivation of physically meaningful constitutive material laws. Two basic energetically conjugated variables of the second law of thermodynamics are the specific entropy s as an extensive state variable and the thermodynamical temperature T as an intensive state variable. Their derivation was at first mathematically driven: Starting from equation (2.16) in a simple adiabatic system for a reversible process the differential

$$df = 1 \cdot du - \frac{1}{\rho_0}\boldsymbol{S} : d\boldsymbol{E} \tag{2.17}$$

is not a complete one, because it does not satisfy the Maxwell relation

$$\frac{\partial}{\partial \boldsymbol{E}}\left(\frac{\partial f}{\partial u}\right) = \frac{\partial}{\partial u}\left(\frac{\partial f}{\partial \boldsymbol{E}}\right) \ . \tag{2.18}$$

This means, that the integral $\int_1^2 df$ from $(u_1, \boldsymbol{E}_1)$ to $(u_2, \boldsymbol{E}_2)$ is not path independent, which is in conflict with the reversible process conduction. A division of (2.17) by an integrating denominator $T = T(u, \boldsymbol{E})$, which always exists for this kind of equations (see e.g. COLLATZ[20]) allows to fulfill the Maxwell relation (2.18). Thus the generated differential

$$ds = \frac{df}{T(u, \boldsymbol{E})} = \frac{1}{T}du - \frac{1}{\rho_0 T}\boldsymbol{S} : d\boldsymbol{E} \tag{2.19}$$

is a complete one and is called Gibbs' fundamental equation if recast in the following form:

$$du = Tds + \frac{1}{\rho_0}\boldsymbol{S} : d\boldsymbol{E} \tag{2.20}$$

Here T denotes the thermodynamical temperature and s the specific entropy immanent to the system. Besides, the entropy of a system can be increased also by an external heat transfer (2.12). The second law of thermodynamics postulates that the internal production of entropy is never less than the entropy provided by external sources. In case of reversible processes internal and external entropy production are equal, whereas in case of irreversible processes the production of internal entropy is always larger than the entropy conducted from outside. This postulate finds its mathematical expression in the Clausius-Duhem inequality:

$$\int_{\mathcal{B}} \dot{s}\rho \; dv \geq \int_{\mathcal{B}} \frac{r}{T}\rho \; dv - \int_{\partial\mathcal{B}} \frac{1}{T}\boldsymbol{q}\cdot\boldsymbol{n} \; da \tag{2.21}$$

For the derivation of constitutive material laws the specific entropy is not appropriate, because this quantity is hard to measure. Referring to Gibbs' equation (2.20), which defines the differential of the internal energy $u = u(s, \boldsymbol{E})$, it is possible to eliminate the specific entropy. A Legendre transformation, see also appendix A.3, achieves a change of the independent variables and thus the equivalent form $f = f(\boldsymbol{E}, T)$, known as Helmholtz function or free internal energy.

$$f = f(\boldsymbol{E}, T) = u - Ts \tag{2.22}$$

The subtraction of the entropy term Ts from u only leaves the part of the internal energy provided for reversible resp. elastic deformations. Using (2.20) the complete differential can be given as

$$df = du - sdT - Tds = -sdT + \frac{1}{\rho_0}\boldsymbol{S} : d\boldsymbol{E} \; . \tag{2.23}$$

From equation (2.23) it is evident, that in case of isothermal processes, with $dT = 0$, the Helmholtz function f represents a potential for the stresses. Hence, introducing a strain energy function $W_{0S} = \rho_0 f$ defined in the current configuration yields along with equation (1.13)

$$\left.\frac{\partial W_{0S}}{\partial \boldsymbol{E}}\right|_{T=const} = 2\left.\frac{\partial W_{0S}}{\partial \boldsymbol{C}}\right|_{T=const} = \boldsymbol{S} \; . \tag{2.24}$$

Thus the second law of thermodynamics restricts the constitutive material laws in such a way, that the entire solutions of the field equations obtained with these material laws only cover the physically possible solutions. The next section is devoted to the derivation of these constitutive material laws both for hyperelastic solid bodies and fluid phases, using the previously given variables.

2.3 Fundamental equations for solids and fluids

The amount of balance laws provided so far and describing the thermodynamical equilibrium is still not sufficient to eliminate all the unknowns they contain. Therefore the surplus unknowns have to be connected by constitutive material laws, which in general are to be identified experimentally.

2.3.1 Constitutive laws for hyperelastic materials

Almost all materials used in this work can be described with hyperelastic material laws. Thermal effects are not considered in this work, because the Helmholtz function f, as a basis for the derivation of all subsequent material laws, only provides a potential for the stresses in case of isothermal processes. The following publications provide more detailed information on hyperelastic and plastic material laws: OGDEN[63], WRIGGERS[112], REESE[76], BARTHOLD[5] and DOLL[25]. Further, we restrict us on isotropic materials requiring the constitutive laws to be invariant in terms of the directions. This restricts the relation between the strain energy function W_{0S} and the strains to be a function only dependent on the invariants of the strain tensor. The invariants of e.g. the Green-Lagrangian strains $\boldsymbol{E}$ are defined as:

$$I_{\boldsymbol{E}} = \boldsymbol{E} : \boldsymbol{G} = E_{ij} G^{ij} \tag{2.25}$$

$$II_{\boldsymbol{E}} = (\boldsymbol{E}\boldsymbol{E}) : \boldsymbol{G} = E_{ij} G^{jk} E_{kl} G^{il} \tag{2.26}$$

$$III_{\boldsymbol{E}} = \det \boldsymbol{E} \tag{2.27}$$

The invariants of the Cauchy-Green strain tensor follow analogously.

St. Venant-Kirchhoff material

The most simple hyperelastic material model is the St. Venant-Kirchhoff constitutive law, which is obtained by transferring Hooke's law for small deformations to the nonlinear Green-Lagrangian strains. It is defined by the following strain energy function:

$$W_{0S}(\boldsymbol{E}) = \frac{1}{2} \Lambda I_{\boldsymbol{E}}^2 + \mu II_{\boldsymbol{E}} \tag{2.28}$$

However, this strain energy function does not satisfy specific requirements, as e.g. in case of a complete compression an unrealistic stress state $\boldsymbol{S} = \boldsymbol{0}$ exists. Therefore it can only be used for problems with small strains. The constants Λ and μ are the Lamé constants. A derivation in the direction of $\boldsymbol{E}$ gives according to equation (2.24) the stresses

$$\boldsymbol{S} = \frac{\partial W_{0S}}{\partial \boldsymbol{E}} = \Lambda I_{\boldsymbol{E}} \boldsymbol{G} + 2\mu \boldsymbol{E} \ . \tag{2.29}$$

The second order metric tensor $\boldsymbol{G}$ in a covariant basis can be given as

$$\boldsymbol{G} = G^{ij} \boldsymbol{G}_i \otimes \boldsymbol{G}_j \ . \tag{2.30}$$

The fourth order material tensor $\mathbb{C}$ as the tangent of the stress-strain relation (2.29) follows as

$$\mathbb{C} = \frac{\partial \boldsymbol{S}}{\partial \boldsymbol{E}} = \Lambda \boldsymbol{G} \otimes \boldsymbol{G} + 2\mu \mathbb{I} \ , \tag{2.31}$$

where $\mathbb{I}$ denotes the covariant symmetric fourth order tensor

$$\mathbb{I} = \frac{1}{2}\left(G^{ik}G^{jl} + G^{jk}G^{il}\right)\boldsymbol{G}_i \otimes \boldsymbol{G}_j \otimes \boldsymbol{G}_k \otimes \boldsymbol{G}_l \ . \tag{2.32}$$

For reasons of a more convenient programming the symmetry

$$\mathbb{C}^{ijkl} = \mathbb{C}^{jikl} = \mathbb{C}^{ijlk} \tag{2.33}$$

of the material tensor can be exploited assembling its coordinates in a matrix.

$$\underline{D} = \begin{pmatrix} \mathbb{C}^{1111} & \mathbb{C}^{1122} & \mathbb{C}^{1133} & \mathbb{C}^{1112} & \mathbb{C}^{1123} & \mathbb{C}^{1113} \\ \mathbb{C}^{2211} & \mathbb{C}^{2222} & \mathbb{C}^{2233} & \mathbb{C}^{2212} & \mathbb{C}^{2223} & \mathbb{C}^{2213} \\ \mathbb{C}^{3311} & \mathbb{C}^{3322} & \mathbb{C}^{3333} & \mathbb{C}^{3312} & \mathbb{C}^{3323} & \mathbb{C}^{3313} \\ \mathbb{C}^{1211} & \mathbb{C}^{1222} & \mathbb{C}^{1233} & \mathbb{C}^{1212} & \mathbb{C}^{1223} & \mathbb{C}^{1213} \\ \mathbb{C}^{2311} & \mathbb{C}^{2322} & \mathbb{C}^{2333} & \mathbb{C}^{2312} & \mathbb{C}^{2323} & \mathbb{C}^{2313} \\ \mathbb{C}^{1311} & \mathbb{C}^{1322} & \mathbb{C}^{1333} & \mathbb{C}^{1312} & \mathbb{C}^{1323} & \mathbb{C}^{1313} \end{pmatrix} \tag{2.34}$$

The fact, that the material tangent was derived from a potential leads with $\mathbb{C}_{ijkl} = \mathbb{C}_{klij}$ to a symmetric material matrix.

Particular case: material law for solid shells

For the solid shell elements (see also HAUPTMANN&SCHWEIZERHOF[41]) it is assumed that the shell director is always perpendicular to the shell surface. This means that all metric coefficients $\boldsymbol{G}^{\alpha 3}$ and $\boldsymbol{G}^{3\alpha}$ $(\alpha = 1, 2)$ vanish. Thus the St. Venant-Kirchhoff material in a covariant basis can be reduced to

$$\begin{aligned} \underline{D} \ = \ & \Lambda \begin{pmatrix} G^{11}G^{11} & G^{11}G^{22} & G^{11}G^{33} & G^{11}G^{12} & 0 & 0 \\ G^{22}G^{11} & G^{22}G^{22} & G^{22}G^{33} & G^{22}G^{12} & 0 & 0 \\ G^{33}G^{11} & G^{33}G^{22} & G^{33}G^{33} & G^{33}G^{12} & 0 & 0 \\ G^{12}G^{11} & G^{12}G^{22} & G^{12}G^{33} & G^{12}G^{12} & 0 & 0 \\ 0 & 0 & 0 & 0 & 0 & 0 \\ 0 & 0 & 0 & 0 & 0 & 0 \end{pmatrix} \\ + \ & \mu \begin{pmatrix} 2G^{11}G^{11} & 2G^{12}G^{12} & 0 & 2G^{11}G^{12} & 0 & 0 \\ 2G^{12}G^{12} & 2G^{22}G^{22} & 0 & 2G^{12}G^{22} & 0 & 0 \\ 0 & 0 & 2G^{33}G^{33} & 0 & 0 & 0 \\ 2G^{11}G^{12} & 2G^{12}G^{22} & 0 & G^{11}G^{22} + G^{12}G^{12} & 0 & 0 \\ 0 & 0 & 0 & 0 & \kappa G^{22}G^{33} & \kappa G^{12}G^{33} \\ 0 & 0 & 0 & 0 & \kappa G^{12}G^{33} & \kappa G^{11}G^{33} \end{pmatrix} \end{aligned} \tag{2.35}$$

The parameter κ denotes the shear correction factor. Although such an element is called solid shell element it is still a conventional volume element with all characteristic locking effects, e.g. in case of bending. For the improvement of the behaviour of the element several proposals have been made, mostly based on a mixed formulation: The EAS concept for linear elements by SIMO&RIFAI[96] enriches the kinematics by an additional strain field and has been afterwards extended to geometric nonlinear kinematics by SIMO ET AL.[94], [95]. The ANS concept by BATHE&DVORKIN[6], used in

the MITC elements to overcome the transversal shear locking and the membrane locking, assumes a strain field, which is reduced of spurious strains. BISCHOFF&RAMM[11] extended this formulation also for the normal strains in thickness direction.

Particular case: Plain stress state

In the particular case of a plain stress state with

$$S_{33} = 0 \tag{2.36}$$

a constraint equation for the normal strain in thickness direction can be given. Using the relation

$$\lambda = \frac{2\Lambda\mu}{\Lambda + 2\mu} \tag{2.37}$$

the St. Venant-Kirchhoff material can be further simplified:

$$\begin{aligned} \underline{D} &= \lambda \begin{pmatrix} G^{11}G^{11} & G^{11}G^{22} & G^{11}G^{12} \\ G^{22}G^{11} & G^{22}G^{22} & G^{22}G^{12} \\ G^{12}G^{11} & G^{12}G^{22} & G^{12}G^{12} \end{pmatrix} \\ &+ \mu \begin{pmatrix} 2G^{11}G^{11} & 2G^{12}G^{12} & 2G^{11}G^{12} \\ 2G^{12}G^{12} & 2G^{22}G^{22} & 2G^{22}G^{12} \\ 2G^{12}G^{11} & 2G^{12}G^{22} & G^{11}G^{22} + G^{12}G^{12} \end{pmatrix} . \end{aligned} \tag{2.38}$$

This material law in a covariant basis is appropriate especially for a small strain membrane element. In this case using an incompressible material is possible, because the volume conservation can be guaranteed by the contraction of the membrane in thickness direction.

Neo-Hooke material

If shell problems with locally large bending strains are to be solved a different constitutive model should be used. To correct the defects of the St. Venant-Kirchhoff materials the strain energy function is enriched by a logarithmic term, leading to a function dependent on the right Cauchy-Green tensor.

$$W_{0S}(\boldsymbol{C}) = \frac{\mu}{2}(I_C - 3) - \mu \ln J + \frac{\Lambda}{2} \ln^2 J \tag{2.39}$$

Using the derivation rule (see appendix A.7)

$$\frac{\partial \ln J}{\partial \boldsymbol{C}} = \frac{1}{2}\boldsymbol{C}^{-1} \tag{2.40}$$

yields the second Piola-Kirchhoff stress tensor.

$$\boldsymbol{S} = 2\frac{\partial W_{0S}}{\partial \boldsymbol{C}} = \mu\left(\boldsymbol{G} - \boldsymbol{C}^{-1}\right) + \Lambda \ln J \boldsymbol{C}^{-1} \tag{2.41}$$

A further derivation in the direction of the strains gives the fourth order material tensor

$$\mathbb{C} = 2\frac{\partial \boldsymbol{S}}{\partial \boldsymbol{C}} = 4\frac{\partial^2 W_{0S}}{\partial \boldsymbol{C}^2} = \Lambda \boldsymbol{C}^{-1} \otimes \boldsymbol{C}^{-1} + 2\left(\mu - \Lambda \ln J\right) \mathbb{J}^{sym} \ . \tag{2.42}$$

As in engineering the shear deformation $\gamma_{12} = 2E_{12}$ is used rather than the strains E_{12} and E_{21}, the symmetric part $\mathbb{J}^{sym}$ of the derivation of the inverse Cauchy-Green tensor in direction of $\boldsymbol{C}$ has to be used for the connection of $\boldsymbol{S}$ and $\boldsymbol{E}$.

$$\mathbb{J}^{sym} = \frac{1}{2}\left(\left(\boldsymbol{C}^{-1}\right)^{ik}\left(\boldsymbol{C}^{-1}\right)^{jl} + \left(\boldsymbol{C}^{-1}\right)^{il}\left(\boldsymbol{C}^{-1}\right)^{jk}\right) \boldsymbol{G}_i \otimes \boldsymbol{G}_j \otimes \boldsymbol{G}_k \otimes \boldsymbol{G}_l \tag{2.43}$$

Particular case: incompressible Neo-Hooke material

Neo-Hooke materials, capturing an incompressible material behaviour, can be achieved by e.g. penalty methods, with $J \approx 0$. However, if the dimension in thickness direction is much smaller than the other directions and by restricting to a plain stress state, the volume conservation can be ensured again by the contraction in thickness direction. With the constraint $J = 1$ the strain energy function (2.39) reduces to:

$$W_{0S}(\boldsymbol{C}) = \frac{\mu}{2}(I_C - 3) \tag{2.44}$$

Using the two Jacobian matrices

$$\boldsymbol{J} = \frac{\partial \boldsymbol{X}}{\partial \boldsymbol{\xi}} \quad \text{and} \quad \boldsymbol{j} = \frac{\partial \boldsymbol{x}}{\partial \boldsymbol{\xi}} \tag{2.45}$$

for setting up the two Cauchy-Green strain tensors in convective coordinates[1]

$$\boldsymbol{C}_0 = \boldsymbol{J}^T\boldsymbol{J} \quad \text{and} \quad \boldsymbol{C}_n = \boldsymbol{j}^T\boldsymbol{j} \tag{2.46}$$

the material tangent, see also BONET ET AL.[15], can be given as:

$$\mathbb{C} = 2\mu\frac{\det \boldsymbol{C}_0}{\det \boldsymbol{C}_n}\left(\mathbb{T}^{sym} + \boldsymbol{C}_n^{-1} \otimes \boldsymbol{C}_n^{-1}\right) \tag{2.47}$$

The symmetric part $\mathbb{T}^{sym}$ follows as:

$$\mathbb{T}^{sym} = \frac{1}{2}\left(\left(\boldsymbol{C}_n^{-1}\right)^{ik}\left(\boldsymbol{C}_n^{-1}\right)^{jl} + \left(\boldsymbol{C}_n^{-1}\right)^{il}\left(\boldsymbol{C}_n^{-1}\right)^{jk}\right) \boldsymbol{G}_i \otimes \boldsymbol{G}_j \otimes \boldsymbol{G}_k \otimes \boldsymbol{G}_l \tag{2.48}$$

Assembling all coordinates of the fourth order tensor in a symmetric matrix $\underline{D}$, only 6 of 81 coordinates of $\mathbb{C}$ have to be computed.

$$\underline{D} \ = \ \begin{pmatrix} \mathbb{C}^{1111} & \mathbb{C}^{1122} & \mathbb{C}^{1133} \\ \mathbb{C}^{2211} & \mathbb{C}^{2222} & \mathbb{C}^{2233} \\ \mathbb{C}^{3311} & \mathbb{C}^{3322} & \mathbb{C}^{3333} \end{pmatrix} \tag{2.49}$$

A comprehensive discussion on hyperelastic anisotropic constitutive laws for small and finite deformations basing on structural tensors can be found in SPENCER&RIVLIN[98] and SCHRÖDER[85]. For the specifics of capturing the material behaviour of fibre tissues it is referred to RAIBLE[75].

[1] $\boldsymbol{C}_0$ measures the strains between an element in a fictive reference configuration and the initial configuration, whereas $\boldsymbol{C}_n$ measures the strains between the reference configuration and the current configuration.

2.3.2 State equations of fluid phases

Besides the constitutive laws provided so far for hyperelastic solid bodies, the focus in this work is mainly on the description of fluids. For reasons of simplicity their electrical, magnetic and chemical properties shall be neglected, thus a so-called simple system is obtained. The consideration of the gravitational properties of the fluid is part of chapter 3.1.3 and is not considered here. Further, the complicated description of state variables as field sizes changing with their position is simplified by regarding the fluid as a phase, where the intensive state variables are independent of the position. Therefore in proceeding in this chapter the formulation for the state variables will change from a tensor formulation to a scalar formulation. Following the notation in the standard literature, e.g. HUTTER[44], the stress tensor $\boldsymbol{S}$ can then be represented by the hydrostatic pressure p and the strains $\boldsymbol{E}$ of the fluid are replaced by the change of its specific volume ν. An empirical law of thermodynamics (see also HUTTER[44]) postulates, that in case of a simple phase two independent intensive state variables (e.g. the specific volume ν and the thermodynamical temperature T) are sufficient for the characterization of the actual state of a fluid phase. As an example the caloric state equation

$$u = u(\nu, T) \tag{2.50}$$

provides a connection between the internal energy u and the independent intensive state variables ν and T. For the derivation of such state equations for ideal gases or (in)compressible fluids the variables introduced so far, namely the specific entropy s, the specific internal energy u and the specific free energy f, can be used. Since it is the goal to describe the fluid behaviour as efficient as possible, the subsequent achievements aim on the elimination of most of the state variables and on a final constitutive law $p = p(\nu)$. As the gravitational properties of the fluid will be derived later on, its stress state is characterized at first only by the compression of its specific volume ν. In order to achieve this kind of material law, as the last two state variables the specific enthalpy h and the specific free enthalpy g are introduced.

Specific enthalpy

Analogously to the caloric state equation (2.50), featuring the temperature and the specific volume as independent state variables, the specific enthalpy

$$h = u + p\nu \tag{2.51}$$

provides a further caloric state equation. Building the complete differential

$$dh = du + pd\nu + \nu dp \tag{2.52}$$

along with Gibbs' equation (2.20)[2] yields the differential

$$dh = Tds + \nu dp \ . \tag{2.53}$$

[2]It shall be briefly mentioned here, that the tensor formulation of the energy differential $\frac{1}{\rho_0}\boldsymbol{S} : d\boldsymbol{E}$ from equation (2.20) in case of simple phases complies with the scalar formulation $-pd\nu$. Thus follows: $\frac{1}{\rho_0}\boldsymbol{S} : d\boldsymbol{E} = \nu_0 \boldsymbol{S} : d\boldsymbol{E} = -p\nu_0 \boldsymbol{G} : d\boldsymbol{E} = -p\nu_0 \ \mathrm{Tr}(\boldsymbol{E}) = -pd\nu$

Hence, besides $u = u(s, \nu)$ as the inverse function of equation (2.20), the important connection $h = h(s, p)$ was generated. As syntheses of the caloric state equation $u = u(T, \nu)$, the thermal state equation $p = p(T, \nu)$ and the entropy state equation $s = s(T, \nu)$ each of these so-called fundamental equations $h = h(s, p)$ and $u = u(s, \nu)$ contain the whole information of all relevant thermodynamical properties of the phase. However, it is more convenient to work with fundamental equations featuring the state sizes T, p or T, ν as independent variables, as they are easier to measure. Equations of this kind can be easily extracted from the two fundamental equations $s = s(u, \nu)$ and $h = h(s, \nu)$ by a Legendre transformation.

Specific free enthalpy

Switching from $h = h(s, p)$ to $g = g(T, p)$ leads with the Legendre transformation (A.21) to the specific free enthalpy or Gibbs' function

$$g = h - Ts = g(T, p) \ . \tag{2.54}$$

Using dh from equation (2.53) its differential can be given as

$$dg = dh - sdT - Tds = -sdT + \nu dp \ . \tag{2.55}$$

As already mentioned, the fundamental equations (2.20), (2.51), (2.54) and (2.22) contain all relevant thermodynamical information of a phase. Therfore all concerning characteristics can be derived using these equations. Table 2.1 provides an overview of all connections resulting from the derivations of f and g in direction of the independent variables. These connections serve as the basis for the derivation of all necessary constitutive laws of fluids or gases, which are to be implemented in the finite element formulation.

State equations for ideal gases

The thermal state equation

With decreasing pressure p all real gases show an identical behaviour, which, in the limit case of an evanescent pressure, is expressed by the ideal gas law

$$\lim_{p \to 0}(pV_m)\Big|_{T=const} = R_m T \ , \tag{2.56}$$

valid for all types of gases. Thus, the product of the gas pressure p and the molar volume

$$V_m = V/n \tag{2.57}$$

of the gas, given as volume V per amount of substance n, in the limit case $p \to 0$ is proportional to the temperature T of the gas. The universal gas constant R_m can be

	Helmholtz function	**Gibbs' function**
definition	$f = f(T,\nu) := u - Ts$	$g = g(T,p) := h - Ts$
differential	$df = -s\ dT - p\ d\nu$	$dg = -s\ dT + \nu\ dp$
state equations	$s(T,\nu) = -\left.\frac{\partial f}{\partial T}\right\|_\nu$	$s(T,p) = -\left.\frac{\partial g}{\partial T}\right\|_p$
	$p(T,\nu) = -\left.\frac{\partial f}{\partial \nu}\right\|_T$	$\nu(T,p) = \left.\frac{\partial g}{\partial p}\right\|_T$
	$u(T,\nu) = f - T\left.\frac{\partial f}{\partial T}\right\|_\nu$	$h(T,p) = g - T\left.\frac{\partial g}{\partial T}\right\|_p$
derivations of the caloric state equation	$\left.\frac{\partial u}{\partial T}\right\|_\nu = -T\left.\frac{\partial^2 f}{\partial T^2}\right\|_\nu =: c_\nu(T,\nu)$	$\left.\frac{\partial h}{\partial T}\right\|_p = -T\left.\frac{\partial^2 g}{\partial T^2}\right\|_p =: c_p(T,p)$
	$\left.\frac{\partial u}{\partial \nu}\right\|_T = -p + T\left.\frac{\partial p}{\partial T}\right\|_\nu$	$\left.\frac{\partial h}{\partial p}\right\|_T = \nu - T\left.\frac{\partial \nu}{\partial T}\right\|_p$
derivations of the entropy	$\left.\frac{\partial s}{\partial T}\right\|_\nu = \frac{1}{T}c_\nu(T,\nu)$	$\left.\frac{\partial s}{\partial T}\right\|_p = \frac{1}{T}c_p(T,p)$
	$\left.\frac{\partial s}{\partial \nu}\right\|_T = \left.\frac{\partial p}{\partial T}\right\|_\nu$	$\left.\frac{\partial s}{\partial p}\right\|_T = -\left.\frac{\partial \nu}{\partial T}\right\|_p$

Table 2.1: Helmholtz function $f = f(T,\nu)$, Gibbs' function $g = g(T,p)$ and their derivatives for the description of the fluid phases

approximated by $R_m \approx 8.314\,\mathrm{J/molK}$. This idealized gas model, characterized by the thermal state equation (2.56)

$$pV_m = R_m T\ , \tag{2.58}$$

is called ideal gas. Assuming a pressure $p < 0.5\,\mathrm{MPa}$, see also BAEHR[4], the variations arising from the approximation of real gases by the thermal state equation (2.58) of an ideal gas are negligible in most of the technical applications. Usually, besides (2.58), a different form of the thermal state equation of ideal gases is used. Along with the amount of substance n, the mass m and the molar mass

$$M = m/n \tag{2.59}$$

of the ideal gas, introducing the special gas constant

$$R = R_m/M \tag{2.60}$$

and using equation (2.57), the thermal state equation yields

$$npV_m = pV = nR_mT = m\frac{R_m}{M}T = mRT \ . \tag{2.61}$$

A further division by the mass m leads with the specific volume

$$\nu = \frac{V}{m} = \frac{1}{\rho} \ , \tag{2.62}$$

which can be also seen as the reciprocal of the density ρ, to a simplified thermal state equation:

$$p(\nu, T) = R\frac{T}{\nu} \tag{2.63}$$

Specific heat capacities of ideal gases

Employing the derivations of the free energy functions g and h given in table 2.1, in the particular case of an ideal gas a state equation for the specific entropy s can be found, which is advantageous for the derivation of two different constitutive laws describing short-time compressions and quasi-static compressions. The basis for this derivation is the internal energy u, featuring the complete differential

$$du = \left.\frac{\partial u}{\partial T}\right|_{\nu} dT + \left.\frac{\partial u}{\partial \nu}\right|_{T} d\nu \tag{2.64}$$

as it is a state equation. Its partial derivative in direction of the temperature T

$$c_\nu(T, \nu) = \left.\frac{\partial u}{\partial T}\right|_{\nu} dT \tag{2.65}$$

is called specific isochoric heat capacity. Using the thermal state equation (2.63) and table 2.1, it can be demonstrated that for ideal gases the specific internal energy is only a function of the temperature, which means

$$\left.\frac{\partial u}{\partial \nu}\right|_{T} d\nu \equiv 0 \ . \tag{2.66}$$

Thus follows

$$u = u(T) \ . \tag{2.67}$$

Hence, the isochoric heat capacity is in case of an ideal gas the complete differential of the internal energy.

$$c_\nu^0(T) = \frac{du}{dT} \tag{2.68}$$

The index 0 denotes the material parameter of an ideal gas. Analogously to (2.64) the specific enthalpy h features a complete differential as well:

$$dh = \left.\frac{\partial h}{\partial T}\right|_{p} dT + \left.\frac{\partial h}{\partial p}\right|_{T} dp \tag{2.69}$$

Its partial derivative in direction of the temperature T

$$c_p(T,p) = \left.\frac{\partial h}{\partial T}\right|_p dT \tag{2.70}$$

is called specific isobaric heat capacity. Using equations (2.63) and (2.67) likewise exhibits, that for an ideal gas the specific enthalpy h is also only a function of the temperature T.

$$h = u + p\nu = u(T) + RT = h(T) \tag{2.71}$$

Similar to equation (2.68), in this case the isobaric heat capacity forms the complete differential of the specific enthalpy h.

$$c_p^0(T) = \frac{dh}{dT} \tag{2.72}$$

Inserting equation (2.71) in (2.72) leads to the relation

$$c_p^0(T) = \frac{du}{dT} + R = c_\nu^0 + R \ , \tag{2.73}$$

which shows, that the difference of the specific isobaric heat capacity c_p^0 and the specific isochoric heat capacity c_ν^0 for any ideal gas is independent of the temperature T and is always constant ($= R$). By sorting the conditional equation (2.53) of the specific enthalpy h by the differential ds of the specific entropy and inserting the isobaric heat capacity (2.72), the thermal state equation (2.63) as well as equation (2.73), the change of the entropy ds^0 of an ideal gas in terms of the easily measurable quantities T and p is obtained.

$$ds^0(T,p) = \frac{1}{T}\left(dh - \nu dp\right) = c_p^0\frac{dT}{T} - R\frac{dp}{p} = c_p^0\frac{dT}{T} - (c_p^0 - c_\nu^0)\frac{dp}{p} \tag{2.74}$$

In a similar fashion the differential of the specific entropy ds^0 of an ideal gas can be developed by recasting the caloric state equation (2.20)[3]. Using the isochoric heat capacity (2.68) along with the thermal state equation (2.63) and equation (2.73) yields then the differential of the entropy as a function of T and ν.

$$ds^0(T,\nu) = c_\nu^0\frac{dT}{T} + R\frac{d\nu}{\nu} = c_\nu^0\frac{dT}{T} + (c_p^0 - c_\nu^0)\frac{d\nu}{\nu} \tag{2.75}$$

Finally, with (2.74) and (2.75) two equations have been provided enabling the elimination of the temperature as an independent variable and thus keep, as initially required, the pressure p and the geometric variable ν as the only remaining variables describing the state of the ideal gas.

[3]Again it is essential: $du = Tds + \frac{1}{\rho_0}\boldsymbol{S} : d\boldsymbol{E} = Tds - pd\nu$.

The isentropic state equation

In case of an isentropic change of state the differential of the entropy has to vanish in both cases. Introducing the adiabatic exponent

$$\kappa = \frac{c_p^0}{c_\nu^0} \tag{2.76}$$

and using $ds^0 = 0$ according to equation (2.74) yields the relation

$$\frac{dT}{T} = \frac{(c_p^0 - c_\nu^0)}{c_p^0}\frac{dp}{p} = \frac{\kappa - 1}{\kappa}\frac{dp}{p} \ . \tag{2.77}$$

Integration gives

$$\frac{T}{T_0} = \left(\frac{p}{p_0}\right)^{\frac{\kappa-1}{\kappa}} \ . \tag{2.78}$$

The integration can be accomplished without any difficulties, because in the particular case of an ideal gas the specific heat capacities c_p^0 and c_ν^0 are constants. Analogously for the isentropic change of state of an ideal gas using $ds^0 = 0$ according to equation (2.75) yields the relation

$$\frac{dT}{T} = -\frac{(c_p^0 - c_\nu^0)}{c_\nu^0}\frac{d\nu}{\nu} = -(\kappa - 1)\frac{d\nu}{\nu} \ . \tag{2.79}$$

Integration gives

$$\frac{T}{T_0} = \left(\frac{\nu}{\nu_0}\right)^{-(\kappa-1)} \ . \tag{2.80}$$

Equalizing equations (2.78) and (2.80) finally leads to an equation describing the isentropic change of state of an ideal gas only in terms of the two intensive state variables p and ν.

$$\frac{p}{p_0} = \left(\frac{\nu_0}{\nu}\right)^{\kappa} \tag{2.81}$$

Isothermal state equation

Besides the isentropic change of state of an ideal gas, involving a rise of temperature of the adiabatic system, the isothermal compression of an ideal gas is to be discussed as well. Imagine a closed, gas filled system embedded in a very large adiabatic system keeping the gas system at a constant temperature. Due to the isothermal behaviour the reversible compression of the gas filled system does not lead to a change of the internal energy $u = u(T)$, however, the compression yields a change of the entropy conducted to the surrounding system as a heat flow. Thus the compression of an ideal gas always involves a rise of its temperature. Hence an almost isothermal process conduction is possible only if the compression is performed very slowly. In this case the entropy of

the system is conserved as well. Considering both an isentropic change of state and the constraint $T = T_0$ for isothermal processes in equation (2.80) yields an adiabatic exponent $\kappa = 1$, turning equation (2.81) into Boyle's law

$$\frac{p}{p_0} = \frac{\nu_0}{\nu} \ , \tag{2.82}$$

which is appropriate for quasi-static processes. On the other hand, the isentropic state equation (2.81) is valid for an adiabatic gas filled system, which is hard to realize due to imperfect isolation. Therefore this constitutive law is appropriate only for short-time compressions (e.g. assumed in automotive applications in the design of air springs, see also BERRY&YANG[10]).

State equation of an incompressible fluid

As apparent from the universal thermal state equation $\nu = \nu(T, p)$, the thermal state equation of an incompressible fluid, given by

$$\nu = \nu_0 = const \ , \tag{2.83}$$

can be used as a constitutive law only under the premise of an isothermal process conduction.

State equation of a compressible fluid

Besides the state equations discussed so far, state equations for compressible fluids have also been developed. However, within the limits of low pressures and a relatively small temperature interval the model of an incompressible fluid can be seen as an adequate approximation of reality. For the description of an elastic system completely filled with fluid considering the compressibility of the fluid is advantageous, if the complicated assembling of constraint equations for the elastic domain is to be bypassed. Usually, for the thermal state equation $\nu(T, p)$ an approach linear in T and p (see also BAEHR[4]) is chosen.

$$\nu(T, p) = \nu_0 \left[1 + \beta_0 (T - T_0) - \kappa_0 (p - p_0)\right] \tag{2.84}$$

In a reference state marked with 0 the constant β_0 denotes the coefficient of the volume expansion

$$\beta_0 := \frac{1}{\nu_0} \left(\frac{\partial \nu}{\partial T} \right) \Bigg|_p \tag{2.85}$$

and κ_0 denotes the isothermal coefficient of the compressibility

$$\kappa_0 := -\frac{1}{\nu_0} \left(\frac{\partial \nu}{\partial p} \right) \Bigg|_T \ . \tag{2.86}$$

Specific values for β_0 and κ_0 can be found e.g. in Landolt[51]. Generally, the bulk modulus

$$K_0 = -\nu_0 \left(\frac{\partial p}{\partial \nu} \right) \Bigg|_T = \frac{1}{\kappa_0} \, , \tag{2.87}$$

is used rather than κ_0. Inserting K_0 in equation (2.84) gives a connection of the isothermal volume dilatation and the pressure change:

$$p = p(\nu) = p_0 - K_0 \frac{\nu - \nu_0}{\nu_0} \tag{2.88}$$

With the equations (2.29) and (2.41) for hyperelastic solid bodies and the equations (2.81), (2.82), (2.83) and (2.88) for simple fluid phases all necessary constitutive laws connecting the stresses and strains have been provided by the second law of thermodynamics. In the subsequent achievements these constitutive laws find their application in the first law of thermodynamics, which is the basis for the numerical computation of a state of equilibrium, using the finite element method.

Chapter 3

Weak form of equilibrium

This chapter deals with the derivation of the state of equilibrium of an arbitrarily deformable structure – for simplicity consisting of elastic material – filled with gas and fluid. With the principle of virtual work, focusing on a variation of the total potential energy caused by a virtual displacement field applied to the system, this goal is achieved. Thus a variation of the strain energy functions for hyperelastic solid bodies and – in particular – fluid phases is needed. In addition, a special focus is on the variation of the gravitational potential of a fluid phase. An important observation is that the derived variations of all energy terms for the fluid can be transformed from a formulation over the fluid volume to a boundary integral formulation and thus can be expressed completely in geometrical terms of the structural surface surrounding the fluid. In a further step, each – in general nonlinear – energy term is subjected to a consistent linearization, enabling the application of standard solution schemes. Although this thesis is based on Bonet et al.[15] *and* Rumpel[78]*, where the specific cases of pure gas loadings and pure fluid loadings have been derived separately, the current formulation considers the most general load case of an elastic structure enclosing a compressible heavy fluid with a free fluid surface and an additional gas volume. By introducing two dimensionless parameters the transition between all possible load cases, including those in* Bonet et al.[15] *and* Rumpel[78]*, is performed.*

3.1 Variation of the potential energies

One possibility for the determination of the state of equilibrium of an arbitrary structure, as depicted in figure 3.1, is the principle of virtual work. It states that for a real system (with current total potential energy level $\mathcal{E}$) in a state of equilibrium the virtual energy change $\delta\mathcal{E}$, caused by a virtual displacement field $\delta\boldsymbol{u}$, equals the virtual work $\delta\mathcal{A}^*_{ext}$ of the external non-conservative forces. As the only constraint the arbitrary virtual displacement field has to satisfy the kinematical boundary conditions. In its basic form the principle of virtual work complies with the first law of thermodynamics, which also demands a stationary value for the total potential energy. In contrast to

the first law of thermodynamics the change of energy is not derived in direction of the time t but in direction of the virtual displacements $\delta\boldsymbol{u}$, which are orthogonal to the time axis. Nevertheless, the derivations of the virtual energy can be obtained from the derivations of the energy rates given in chapter 2 by merely changing the differential operator. For the virtual change in direction of $\delta\boldsymbol{u}$ thus follows:

$$\delta\mathcal{E} = D\mathcal{E}(\boldsymbol{x})[\delta\boldsymbol{u}] \tag{3.1}$$

Here a total Lagrangian formulation is taken as a basis, mapping the initial configuration to the current configuration according to

$$\boldsymbol{x} = \boldsymbol{x}(\boldsymbol{X}, t) \ . \tag{3.2}$$

As shown in equation (2.3), the total potential energy stored in the system can be split in the internal energy part $\mathcal{E}_{el}$ of the elastic solid structure, in the internal energy parts $\mathcal{E}_f$ and $\mathcal{E}_g$ stored in the fluid and gas as well as in the kinetic energy $\mathcal{K}$. Hence, for the real state of equilibrium $\boldsymbol{x}$ the principle of virtual work yields the following conditional equation:

$$\delta\mathcal{K}(\boldsymbol{x}) + \delta\mathcal{E}_{el}(\boldsymbol{x}) + \delta\mathcal{E}_f(\boldsymbol{x}) + \delta\mathcal{E}_g(\boldsymbol{x}) - \delta\mathcal{A}^*_{ext} = 0 \tag{3.3}$$

As a start only quasi-static processes are investigated, thus the variation of the kinetic energy can be neglected.

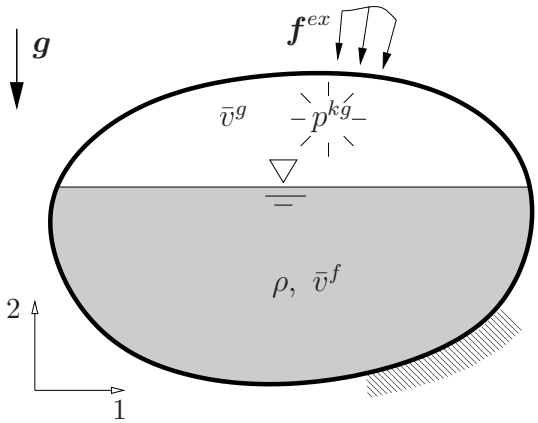

Figure 3.1: Elastic, thin-walled structure, filled with gas and compressible heavy fluid.

3.1.1 Variation of the elastic potential energy

The strain energy functions (2.28), (2.39) or (2.44), derived in chapter 2.3.1, are taken as a basis for the variation of the elastic potential energy, because in the case of an isothermal process conduction they constitute a potential for the stresses. If the system

is additionally subjected to conservative volume loads $\boldsymbol{f}_0$ (as e.g. the dead load) or surface loads $\boldsymbol{t}_0$, deriving from a potential

$$\mathcal{E}_{ext}(\boldsymbol{x}) = -\int_{\mathcal{B}_0} \boldsymbol{f}_0 \cdot \boldsymbol{x}\; dV - \int_{\partial\mathcal{B}_0} \boldsymbol{t}_0 \cdot \boldsymbol{x}\; dA\;, \tag{3.4}$$

using the second Piola-Kirchhoff stress tensor as given in (2.24) yields

$$\begin{aligned}
\delta\mathcal{E}_{el} &= D\mathcal{E}_{el}(\boldsymbol{x})[\delta\boldsymbol{u}] \\
&= \int_{\mathcal{B}_0} \frac{\partial W_{0S}}{\partial \boldsymbol{E}} : D\boldsymbol{E}(\boldsymbol{x})[\delta\boldsymbol{u}]\; dV - \int_{\mathcal{B}_0} \boldsymbol{f}_0 \cdot \delta\boldsymbol{u}\; dV - \int_{\partial\mathcal{B}_0} \boldsymbol{t}_0 \cdot \delta\boldsymbol{u}\; dA \\
&= \int_{\mathcal{B}_0} \boldsymbol{S} : D\boldsymbol{E}(\boldsymbol{x})[\delta\boldsymbol{u}]\; dV - \int_{\mathcal{B}_0} \boldsymbol{f}_0 \cdot \delta\boldsymbol{u}\; dV - \int_{\partial\mathcal{B}_0} \boldsymbol{t}_0 \cdot \delta\boldsymbol{u}\; dA\;.
\end{aligned} \tag{3.5}$$

Variation of the strains

Since in this work only membrane and solid shell elements are employed, which are described by curvilinear coordinates ξ^α (with $\alpha = 1, 2$ and assuming $\xi^3 \perp \xi^\alpha$), for the variation of the strains the Green strain tensor (1.18) in a contravariant basis is taken. By means of the variation

$$D\boldsymbol{g}_\alpha(\boldsymbol{x})[\delta\boldsymbol{u}] = \frac{\partial \delta\boldsymbol{u}}{\partial \xi^\alpha} = \delta\boldsymbol{u}_{,\alpha} \tag{3.6}$$

of the current base vector

$$\boldsymbol{g}_\alpha = \boldsymbol{G}_\alpha + \frac{\partial \boldsymbol{u}}{\partial \xi^\alpha} \tag{3.7}$$

and an application of the chain rule to the covariant metric tensor $g_{\alpha\beta} = \boldsymbol{g}_\alpha \cdot \boldsymbol{g}_\beta$ the variation of the Green strain tensor (1.18) can be given as follows:

$$D\boldsymbol{E}(\boldsymbol{x})[\delta\boldsymbol{u}] = \frac{1}{2}\left(\delta\boldsymbol{u}_{,\alpha} \cdot \boldsymbol{g}_\beta + \boldsymbol{g}_\alpha \cdot \delta\boldsymbol{u}_{,\beta}\right) \boldsymbol{G}^\alpha \otimes \boldsymbol{G}^\beta \tag{3.8}$$

3.1.2 Variation of the potential energy of the gas

A variation of the internal energy $\mathcal{U}$ stored in the gas yields

$$\delta\mathcal{E}_g = D\mathcal{E}_g(\boldsymbol{x})[\delta\boldsymbol{u}] = D\mathcal{U}(\boldsymbol{x})[\delta\boldsymbol{u}]\;. \tag{3.9}$$

As the variations of the energy terms can be obtained by merely exchanging the differential operator D in the rates of the energies given in (2.15), using equation (2.16) leads to the variation of the internal energy of an ideal gas.

$$D\mathcal{U}(\boldsymbol{x})[\delta\boldsymbol{u}] = mDu(\boldsymbol{x})[\delta\boldsymbol{u}] = \bar{v}_0^g \boldsymbol{S} : D\boldsymbol{E}(\boldsymbol{x})[\delta\boldsymbol{u}] \tag{3.10}$$

As the stress tensor $\boldsymbol{S}$ can be completely replaced by an expression containing the hydrostatic pressure p, the variation of the internal energy can be given in terms of the conjugated quantities[1] p^{kg} and $\delta\bar{v}^g(\boldsymbol{x})$.

$$D\mathcal{U}(\boldsymbol{x})[\delta\boldsymbol{u}] = -p^{kg}\bar{v}_0^g\boldsymbol{G} : D\boldsymbol{E}(\boldsymbol{x})[\delta\boldsymbol{u}] = -p^{kg}\bar{v}_0^g\mathrm{Tr}(\delta\boldsymbol{E}) = -p^{kg}\delta\bar{v}^g \ . \tag{3.11}$$

Thus follows

$$\delta\mathcal{E}_g = -p^{kg}\delta\bar{v}^g \tag{3.12}$$

for the variation of the internal energy stored in a gas volume $\bar{v}^g$ featuring a gas pressure p^{kg}.

3.1.3 Variation of the potential energy of a heavy fluid

Assuming a compressible fluid $\mathcal{B}_f$ subjected to a gravity field, the variation of the stored energy results from the variation of the internal energy $\mathcal{U}$

$$D\mathcal{U}(\boldsymbol{x})[\delta\boldsymbol{u}] = -p^f D\bar{v}^f(\boldsymbol{x})[\delta\boldsymbol{u}] \tag{3.13}$$

and from the variation of its gravitational potential $D\mathcal{V}(\boldsymbol{x})[\delta\boldsymbol{u}]$. Introducing the static moment

$$\bar{\boldsymbol{s}}^f = \int\limits_{\mathcal{B}_f} \boldsymbol{x}\ dv \tag{3.14}$$

the gravitational potential can be expressed by

$$\mathcal{V}(\boldsymbol{x}) = -\int\limits_{\mathcal{B}_f} \rho\boldsymbol{g}\cdot\boldsymbol{x}\ dv = -\rho\boldsymbol{g}\cdot\bar{\boldsymbol{s}}^f \ . \tag{3.15}$$

In this equation extracting the density from the integral is only valid under the assumption that the fluid can be considered as a phase, where the density is not a field term but only a variable varying with time. Often in presence of a gravity field an exponential approximation for the increase of the density $\Delta\rho$ with increasing fluid depth h is chosen (see also RUMPEL[78])

$$\frac{\Delta\rho}{\rho_0} = \exp\left(\frac{|\boldsymbol{g}|\rho_0}{K_0}h\right) - 1 \ , \tag{3.16}$$

with K_0 denoting the initial bulk modulus of the fluid. However, this is a very small number, thus for most technically relevant applications the description of the fluid

[1] The superscript k denotes the origin of the specific pressure term: it is caused by a volume compression. Other superscripts arising in the further developments may be c for a pressure in the center of gravity, or x for a pressure at an arbitrary structural point. The second superscript g denotes that this pressure term is associated to the gas volume.

as a phase, where ρ is not position dependent, is appropriate. The variation of the gravitational potential follows then as:

$$D\mathcal{V}(\boldsymbol{x})[\delta\boldsymbol{u}] = -D\rho(\boldsymbol{x})[\delta\boldsymbol{u}]\boldsymbol{g}\cdot\bar{\boldsymbol{s}}^f - \rho\boldsymbol{g}\cdot\bar{\boldsymbol{s}}^f(\boldsymbol{x})[\delta\boldsymbol{u}] \tag{3.17}$$

Hence, the entire variation of the potential energy of a fluid can be given as:

$$\delta\mathcal{E}_f = D\mathcal{E}_f(\boldsymbol{x})[\delta\boldsymbol{u}] = -p^f\delta\bar{v}^f - \delta\rho\boldsymbol{g}\cdot\bar{\boldsymbol{s}}^f - \rho\boldsymbol{g}\cdot\delta\bar{\boldsymbol{s}}^f \tag{3.18}$$

3.1.4 Geometric dependencies

One of the major goals of this work is the capturing of the potentials $\mathcal{E}_f$ and $\mathcal{E}_g$ of fluid and gas in terms of the geometry of the structural surface surrounding the fluid and gas. This interaction between fluid, gas and the – here – elastic structure can be regarded as an energetically equivalent surface loading acting on the structure, however, considering also the change of the internal state variables due to structural deformations. Though, this implies that all energy terms arising in the variational formulations (3.12) and (3.18) are given in terms only of the geometry surrounding the fluid and gas. For the local fluid volume change

$$J = \frac{d\bar{v}^f}{d\bar{v}_0^f} \tag{3.19}$$

from equation (A.24), we can assume that the fluid can be considered as a simple phase, where the state variables, such as the density, are not position-dependent. Thus J can be given also as the mean strain value $\bar{v}^f/\bar{v}_0^f$ of the entire volume and for its variation then yields

$$\delta J = \frac{\delta\bar{v}^f}{\bar{v}_0^f}\ . \tag{3.20}$$

The conservation of mass (1.42) leads for the variation of the volume differential to

$$\delta J = -\frac{1}{\rho_0}\delta\rho\ . \tag{3.21}$$

Equalizing (3.20) and (3.21) results in the variation of the fluid density in the following form:

$$\delta\rho = -\frac{\rho_0}{\bar{v}_0^f}\delta\bar{v}^f \tag{3.22}$$

Since local deformations of the differential fluid or gas volume, as e.g. occurring in case of a wave propagation, are not covered by the intended surface integral representation of the fluid or gas, all further developments are restricted to quasi-static processes. In order to connect the fluid pressures with the geometry, the constitutive laws (2.81), (2.82) and (2.88) provided in section 2.3.2 can be used. Hence, the isentropic state

equation (2.81) gives the pressure of an ideal gas enclosed in an adiabatic control volume in terms of the volume change[2].

$$\frac{p^{kg}}{p_0^{kg}} = \left(\frac{\bar{v}_0^g}{\bar{v}^g}\right)^{\kappa} \tag{3.23}$$

p_0^{kg} and $\bar{v}_0^g$ denote the pressure and the volume of the gas in the initial configuration and p^{kg} and $\bar{v}^g$ denote the pressure and the volume of the gas in the current configuration. For a two-atomic gas (e.g. nitrogen N_2 as the major part of air) we can set the adiabatic exponent to $\kappa = 1.4$, see also BAEHR[4]. As already mentioned, this state equation is appropriate rather for short-time compressions than for quasi-static ones. For quasi-static processes conducted in non-adiabatic control volumes[3] the particular case of an isothermal compression with $\kappa = 1.0$ is the more appropriate model. Hooke's law (2.88) provides the constitutive law for the current pressure p^{kf} of a fluid due to a volume compression.

$$p^{kf} = p_0^{kf} - K_0 \frac{\bar{v}^f - \bar{v}_0^f}{\bar{v}_0^f} \tag{3.24}$$

Here $\bar{v}_0^f$ and p_0^{kf} represent the initial fluid volume and the initial fluid pressure, $\bar{v}^f$ and p^{kf} represent the respective state variables in the current configuration. According to equation (2.87), K_0 denotes the bulk modulus of a fluid. The further developments aim at a general description of an elastic structure filled with fluid and gas, which can be used to derive all relevant particular cases. Therefore a relation between (3.23) and (3.24) is needed. A closer look at figure 3.1 reveals that both pressures must be identical at the phase intersection, because gravitational effects are acting only below the intersection. Since the pressures due to volume compression are assumed to be constant, inside of each phase the equivalence

$$p^{kg} = p^{kf} = p^k \tag{3.25}$$

must hold generally. At this point it shall be mentioned, that a possible separation of a control volume, as depicted in figure 3.2b), during the deformation process is not included in this work, although such configurations can be in general investigated. All control volumes are given a definite pressure. The number of control volumes has to be specified at the beginning of a computation and remains fixed throughout the computation. Although equation (3.25) implies the assumption[4] $p^{kg} = p^{kf} = p^k$, to avoid misunderstandings concerning the origin of the volume compression terms, despite their identity the different notations p^{kg} and p^{kf} will be used further on.

[2]Although in equation (2.81) the specific volume $\nu = \bar{v}^g/m$ is used, description (3.23) is equivalent, because the mass of the system is conserved throughout the process conduction and thus it can be eliminated leaving the ratio of the volumes.

[3]It shall be remarked that this insufficiently isolated control volume is nevertheless embedded in an overall adiabatic system.

[4]This assumption will be proven later on.

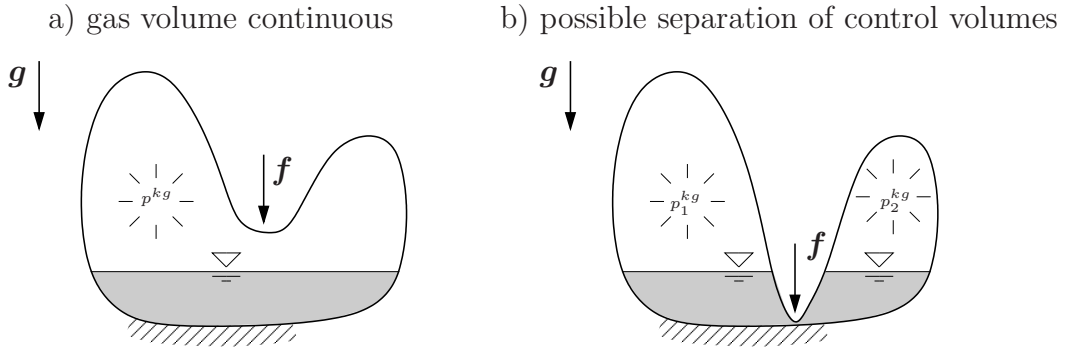

Figure 3.2: a) Considered configurations and b) not treated configurations of gas and fluid filled structures

3.1.5 Boundary integral representation of the geometry

In the previous section all relevant terms, contained in the variations of the potential energies of the fluid and gas, have been connected with the current geometry (e.g. $\bar{v}^g$, $\bar{v}^f$ and $\bar{\boldsymbol{s}}^f$) or its variation, thus providing the basis for an energetically equivalent surface loading. Consequently, the next step in the analytical formulation of this substitute loading will be the representation of these geometric quantities by the surfaces surrounding the gas and the fluid. Hence, the geometry of the surrounding structure, which will be approximated by finite elements in the further developments, contains the complete information of the thermodynamical state of the enclosed fluid and gas making a discretization of the fluid and gas domains redundant. In order to achieve this consistent boundary integral representation of the geometry, both control volumes $\bar{v}^g$ and $\bar{v}^f$[5] have to be cut free, see also figure 3.3.

The appropriate quantities for the geometry can be given using the average of the projections in all three directions x_1, x_2, x_3 (see also figure 3.4) of their particular boundaries ($\partial\mathcal{B}^g$, $\partial\mathcal{B}^g$ and $\partial\mathcal{B}^o$) along with the unit normal vectors $\bar{\boldsymbol{n}}^g$, $\bar{\boldsymbol{n}}^f$ and $\bar{\boldsymbol{n}}^o$.

$$\bar{v}^g = v^g - v^o = \frac{1}{3}\int\limits_{\partial\mathcal{B}^g} \bar{\boldsymbol{n}}^g \cdot \boldsymbol{x}^g \; da - \frac{1}{3}\int\limits_{\partial\mathcal{B}^o} \bar{\boldsymbol{n}}^o \cdot \boldsymbol{x}^o \; da \tag{3.26}$$

$$\bar{v}^f = v^f + v^o = \frac{1}{3}\int\limits_{\partial\mathcal{B}^f} \bar{\boldsymbol{n}}^f \cdot \boldsymbol{x}^f \; da + \frac{1}{3}\int\limits_{\partial\mathcal{B}^o} \bar{\boldsymbol{n}}^o \cdot \boldsymbol{x}^o \; da \tag{3.27}$$

$$\bar{\boldsymbol{s}}^f = \boldsymbol{s}^f + \boldsymbol{s}^o = \frac{1}{4}\int\limits_{\partial\mathcal{B}^f} \left(\bar{\boldsymbol{n}}^f \cdot \boldsymbol{x}^f\right)\boldsymbol{x}^f \; da + \frac{1}{4}\int\limits_{\partial\mathcal{B}^o} \left(\bar{\boldsymbol{n}}^o \cdot \boldsymbol{x}^o\right)\boldsymbol{x}^o \; da \tag{3.28}$$

The fact, that the normal on the negative cutting area, as a boundary of the gas domain, points in the opposite direction of $\boldsymbol{n}^o$ was considered in equation (3.26) with a negative

[5]To avoid misunderstanding concerning the geometry, in the further text a bar is denoting the geometrical quantities describing the fluid or gas domain, whereas the geometrical quantities arising from the structural surface surrounding the fluid or gas are used without a bar.

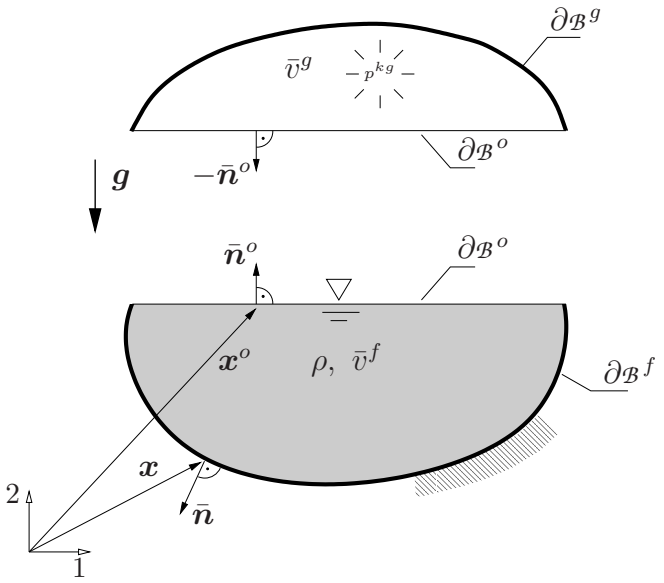

Figure 3.3: Sectioning of control volumes $\bar{v}^g$ and $\bar{v}^f$

sign for the part of v^o. If the gravitation $\boldsymbol{g}$ and a global base vector $\boldsymbol{e}_i$ are colinear, no

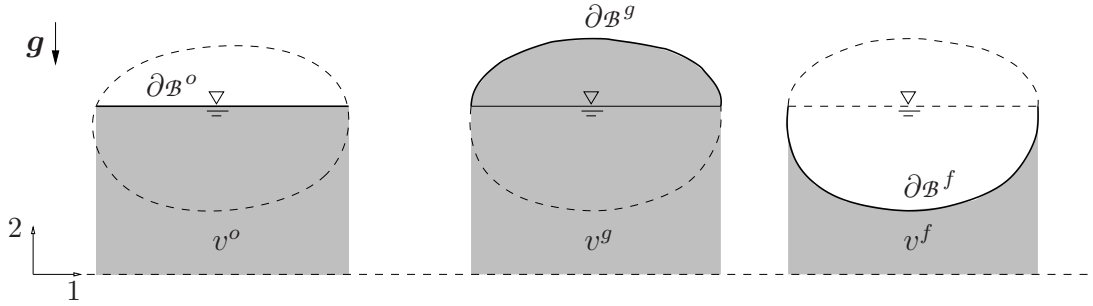

Figure 3.4: Volumes v^o, v^g and v^f generated by a projection of the surfaces $\partial\mathcal{B}^o$, $\partial\mathcal{B}^g$ and $\partial\mathcal{B}^f$ in 2-direction

averaging of v^o must be carried out as the projections of v^o in direction of the other two base vectors $\boldsymbol{e}_j$ (with $j \neq i$) are zero in this case. The volume is computed merely by the projection in direction of $\boldsymbol{e}_i$. Hence, the coefficient for the static moment must be set to 1/2. Analogously in case of a reduction to a two-dimensional or a one-dimensional projection of the geometry $\partial\mathcal{B}^g$ or $\partial\mathcal{B}^f$, the denominators of the averaging coefficients have to be diminished by 1 respectively by 2. The derivations of the boundary integral formulation of a volume or the static moment can be found in the appendices A.5 and A.6 or to some extend in de Boer[22].

Variation of the geometry

The equations for the computation of all geometric quantities presented above can be varied by application of the chain rule. A subsequent partial integration leads to a split of these terms in a domain part and a boundary part (see also BONET ET AL.[15], RUMPEL[78] or appendices A.5 and A.6).

It can be shown that the boundary terms, arising from the partial integration, either vanish, because a control volume completely surrounded by the structural surface does not feature a boundary, or they eliminate each other, because in case of multiple fluid layers the boundary terms eliminate each other, because of the different signs of their tangent vectors on the boundary. For the variation of the geometric terms thus follows:

$$\delta\bar{v}^g = \delta v^g - \delta v^o = \int\limits_{\partial\mathcal{B}^g} \bar{\boldsymbol{n}}^g \cdot \delta\boldsymbol{u}^g \; da - \int\limits_{\partial\mathcal{B}^o} \bar{\boldsymbol{n}}^o \cdot \delta\boldsymbol{u}^o \; da \; , \tag{3.29}$$

$$\delta\bar{v}^f = \delta v^f + \delta v^o = \int\limits_{\partial\mathcal{B}^f} \bar{\boldsymbol{n}}^f \cdot \delta\boldsymbol{u}^f \; da + \int\limits_{\partial\mathcal{B}^o} \bar{\boldsymbol{n}}^o \cdot \delta\boldsymbol{u}^o \; da \; , \tag{3.30}$$

$$\delta\bar{\boldsymbol{s}}^f = \delta\boldsymbol{s}^f + \delta\boldsymbol{s}^o \; = \int\limits_{\partial\mathcal{B}^f} \left(\bar{\boldsymbol{n}}^f \cdot \delta\boldsymbol{u}^f\right) \boldsymbol{x}^f \; da + \int\limits_{\partial\mathcal{B}^o} \left(\bar{\boldsymbol{n}}^o \cdot \delta\boldsymbol{u}^o\right) \boldsymbol{x}^o \; da \; . \tag{3.31}$$

An important simplification can be given for the variation of the static moment $\delta\boldsymbol{s}^o$ of the volume v^o, obtained by a projection of the fluid level. As in equation (3.18) the projection of the static moment is crucial only in direction of the gravity

$$\boldsymbol{g} \cdot \delta\boldsymbol{s}^o = \int\limits_{\partial\mathcal{B}^o} (\boldsymbol{n}^o \cdot \delta\boldsymbol{u}^o)(\boldsymbol{g} \cdot \boldsymbol{x}^o) \; da \; , \tag{3.32}$$

but the projection of the position vector to the phase intersection $\boldsymbol{g} \cdot \boldsymbol{x}^o$ is constant in the entire domain $\partial\mathcal{B}^o$, it can be shifted out of the integral. Using the virtual volume change (A.44) yields

$$\boldsymbol{g} \cdot \delta\boldsymbol{s}^o = (\boldsymbol{g} \cdot \boldsymbol{x}^o) \int\limits_{\partial\mathcal{B}^o} \boldsymbol{n}^o \cdot \delta\boldsymbol{u}^o \; da = (\boldsymbol{g} \cdot \boldsymbol{x}^o)\delta v^o \; . \tag{3.33}$$

For the application of the previously derived equations in a computation of the geometry it has to be considered that they are formulated in Eulerian coordinates. $\boldsymbol{x}$ denotes the current position vector to an arbitrary point on the structural surface surrounding the fluid or gas, $\boldsymbol{x}^o$ denotes current position vector of the phase intersection, and $\bar{\boldsymbol{n}}$ represents the normalized normal vector[6] of the differential area element

$$da = |\boldsymbol{x}_{,1} \times \boldsymbol{x}_{,2}| \; d\xi^1 d\xi^2 = |\boldsymbol{n}| \; d\xi^1 d\xi^2 \tag{3.34}$$

[6]For the purpose of a unified notation for the convective base vectors the identifiers $\boldsymbol{g}_\alpha = \boldsymbol{x}_{,\alpha}$ resp. $\boldsymbol{g}^\alpha = \boldsymbol{x}^{,\alpha}$ introduced in chapter 1 should be maintained. However, in order to avoid confusions concerning the acceleration of gravity $\boldsymbol{g}$ the notations $\boldsymbol{x}_{,\alpha}$ and $\boldsymbol{x}^{,\alpha}$ are used for the convective base vectors.

in the current configuration. It can be obtained from the vector cross product of the covariant base vectors.

$$\bar{\boldsymbol{n}} = \frac{\boldsymbol{x}_{,1} \times \boldsymbol{x}_{,2}}{|\boldsymbol{x}_{,1} \times \boldsymbol{x}_{,2}|} = \frac{\boldsymbol{n}}{|\boldsymbol{n}|} \tag{3.35}$$

By performing the integration over da in equations (3.29)-(3.31) the lengths of the normal vectors are cancelled. Thus in the further formulations only the non-normalized normal vector $\boldsymbol{n}$ is needed and the area differential da is replaced by the product of the line differentials $d\xi^1 d\xi^2$. Then equations (3.29)-(3.31) can be rewritten as

$$\delta\bar{v}^g = \int\limits_{\partial\mathcal{B}^g} \boldsymbol{n}^g \cdot \delta\boldsymbol{u}^g \; d\xi^1 d\xi^2 - \int\limits_{\partial\mathcal{B}^o} \boldsymbol{n}^o \cdot \delta\boldsymbol{u}^o \; d\xi^1 d\xi^2 \; , \tag{3.36}$$

$$\delta\bar{v}^f = \int\limits_{\partial\mathcal{B}^f} \boldsymbol{n}^f \cdot \delta\boldsymbol{u}^f \; d\xi^1 d\xi^2 + \int\limits_{\partial\mathcal{B}^o} \boldsymbol{n}^o \cdot \delta\boldsymbol{u}^o \; d\xi^1 d\xi^2 \; , \tag{3.37}$$

$$\boldsymbol{g} \cdot \delta\bar{\boldsymbol{s}}^f = \int\limits_{\partial\mathcal{B}^f} \left(\boldsymbol{n}^f \cdot \delta\boldsymbol{u}^f\right) \left(\boldsymbol{g} \cdot \boldsymbol{x}^f\right) \; d\xi^1 d\xi^2 + (\boldsymbol{g} \cdot \boldsymbol{x}^o)\delta v^o \; . \tag{3.38}$$

We have to note further that the fluid and gas control volumes are not only defined by the structural surface (leading to the projections δv^g, δv^f and $\delta\boldsymbol{s}^f$), but also by the phase intersection $\partial\mathcal{B}^o$. For this reason the terms $\delta\bar{v}^g$, $\delta\bar{v}^f$ and $\delta\bar{\boldsymbol{s}}$ in equations (3.36) to (3.38) have to include the domain $\partial\mathcal{B}^o$ in the projection as well. This results in the terms δv^o and $\delta\boldsymbol{s}^o$. For the description of the volume change δv^o due to a virtual displacement of the phase intersection equation (3.25), describing the equivalence of the pressures p^{kg} and p^{kf}, can be used. This implies that their variations

$$\delta p^{kg} = -\kappa \frac{p^{kg}}{\bar{v}^g} \delta\bar{v}^g = -\alpha\delta\bar{v}^g \; , \quad \text{with} \quad \alpha = \kappa\frac{p^{kg}}{\bar{v}^g} \tag{3.39}$$

and

$$\delta p^{kf} = -\frac{K_0}{\bar{v}_0^f} \delta\bar{v}^f = -\beta\delta\bar{v}^f \; , \quad \text{with} \quad \beta = \frac{K_0}{\bar{v}_0^f} \tag{3.40}$$

are equivalent as well. For reasons of simplicity the pressure volume gradients α and β, describing the stiffness of the gas and the fluid, have been introduced. Equalizing both pressure variations (3.39) and (3.40) and using the projections of the geometry (3.29) and (3.30) of the elastic structure gives finally a relation for the virtual volume change δv^o.

$$\begin{aligned} -\alpha\left(\delta v^g - \delta v^o\right) &= -\beta\left(\delta v^f + \delta v^o\right) \\ \delta v^o(\alpha+\beta) &= \alpha\delta v^g - \beta\delta v^f \\ \delta v^o &= \frac{\alpha}{\alpha+\beta}\delta v^g - \frac{\beta}{\alpha+\beta}\delta v^f \end{aligned} \tag{3.41}$$

For reasons of convenience the dimensionless stiffness parameters

$$\bar{\alpha} = \frac{\alpha}{\alpha + \beta} \quad \text{and} \quad \bar{\beta} = \frac{\beta}{\alpha + \beta} \tag{3.42}$$

are introduced, enabling a description of the unknown volume variation δv^o only in terms of the surrounding structural surface $\partial \mathcal{B}^g \cup \partial \mathcal{B}^f$ (see also figure 3.5).

$$\delta v^o \;=\; \bar{\alpha}\delta v^g - \bar{\beta}\delta v^f \tag{3.43}$$

For the derivations following later the features of the stiffness parameters $\bar{\alpha}$ and $\bar{\beta}$ shall be briefly outlined here.

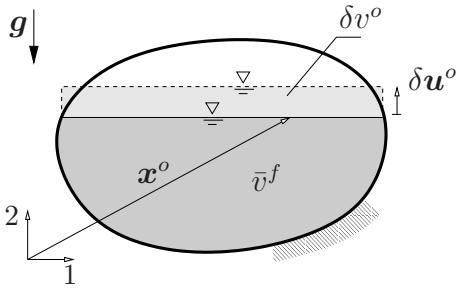

Figure 3.5: Virtual volume change δv^o under the fluid level $\partial \mathcal{B}^o$ caused by a virtual displacement $\delta \boldsymbol{u}^o$

Only gas filling

In case of a control volume as depicted in figure 3.1, but containing only a negligible fluid volume $\bar{v}_0^f \to 0$, the pressure volume gradient β from equation (3.40) tends to infinity.

$$\lim_{\bar{v}_0^f \to 0} \beta = \lim_{\bar{v}_0^f \to 0} \frac{K_0}{\bar{v}_0^f} = \infty \tag{3.44}$$

Thus for a system only filled with an ideal gas both dimensionless pressure volume gradients from (3.42) – the stiffness parameters – yield

$$\bar{\alpha} = 0 \quad \text{and} \quad \bar{\beta} = 1 \; . \tag{3.45}$$

Complete fluid filling

Considering a control volume containing only a negligible gas volume $\bar{v}^g \to 0$, but still with a finite gas pressure p^{kg}, the pressure volume gradient α tends to infinity.

$$\lim_{\bar{v}^g \to 0} \alpha = \lim_{\bar{v}^g \to 0} \kappa \frac{p^{kg}}{\bar{v}^g} = \infty \; . \tag{3.46}$$

Hence for a completely fluid filled system the stiffness parameters follow as:

$$\bar{\alpha} = 1 \quad \text{and} \quad \bar{\beta} = 0 \tag{3.47}$$

As shown, the parameters $\bar{\alpha}$ and $\bar{\beta}$ allow a universal description of all physically possible combinations of fluid and gas fillings in a closed volume.

3.1.6 Virtual work of the absolute fluid and gas pressures

After all geometric and constitutive equations have been set up, the variations of the potentials (3.12) and (3.18) can be given as follows:

$$\delta \mathcal{E}_{f \cup g} = -\delta\rho \boldsymbol{g} \cdot \bar{\boldsymbol{s}}^f - \rho \boldsymbol{g} \cdot \delta \bar{\boldsymbol{s}}^f - p^{kf} \delta \bar{v}^f - p^{kg} \delta \bar{v}^g \tag{3.48}$$

Inserting (3.22), (3.26)-(3.31) and (3.33) leads to

$$\begin{aligned} \delta \mathcal{E}_{f \cup g} = & \frac{\rho}{\bar{v}^f} \boldsymbol{g} \cdot \bar{\boldsymbol{s}}^f \left(\delta v^f + \delta v^o \right) - \rho \boldsymbol{g} \cdot \left(\delta \boldsymbol{s}^f + \boldsymbol{x}^o \delta v^o \right) \\ & - p^{kf} \left(\delta v^f + \delta v^o \right) - p^{kg} \left(\delta v^g - \delta v^o \right) \ . \end{aligned} \tag{3.49}$$

A subsequent elimination of the volume change δv^o using equation (3.43) finally yields

$$\begin{aligned} \delta \mathcal{E}_{f \cup g} = & \frac{\rho}{\bar{v}^f} \boldsymbol{g} \cdot \bar{\boldsymbol{s}}^f \left(\delta v^f + \bar{\alpha} \delta v^g - \bar{\beta} \delta v^f \right) - \rho \boldsymbol{g} \cdot \left(\delta \boldsymbol{s}^f + \boldsymbol{x}^o \left[\bar{\alpha} \delta v^g - \bar{\beta} \delta v^f \right] \right) \\ & - p^{kf} \left(\delta v^f + \bar{\alpha} \delta v^g - \bar{\beta} \delta v^f \right) - p^{kg} \left(\delta v^g - \bar{\alpha} \delta v^g + \bar{\beta} \delta v^f \right) \ . \end{aligned} \tag{3.50}$$

For a clearer expression, containing only the virtual works of volume changes caused by different pressures, in addition to the pressures p^{kg} and p^{kf} two other pressure quantities derived by a potential[7] are introduced. Dividing the first order moment $\bar{\boldsymbol{s}}^f$ by the fluid volume $\bar{v}^f$ yields the center of gravity of the fluid.

$$\boldsymbol{c}^f = \frac{\bar{\boldsymbol{s}}^f}{\bar{v}^f} \tag{3.51}$$

Introducing the pressure in the center of gravity of the fluid

$$p^c = \rho \boldsymbol{g} \cdot \boldsymbol{c}^f \tag{3.52}$$

and the pressure at the fluid level

$$p^o = \rho \boldsymbol{g} \cdot \boldsymbol{x}^o \tag{3.53}$$

and inserting both equations (3.52) and (3.53) in (3.50) leads after some reordering to a general form of the variation of the fluid and gas potentials. Their physical meaning

[7] To avoid misunderstanding concerning the following figures, conventional pressures as p^{kg} (having a positive sign) and pressures arising from a potential, as p^c and thus having a negative sign, have to be distinguished. Compare also equation (3.4).

can now be directly interpreted as the virtual work of different pressure terms acting on the volume changes δv^g and δv^f resulting from the projections of $\partial \mathcal{B}^g$ and $\partial \mathcal{B}^f$.

$$\begin{aligned} \delta \mathcal{E}_{f \cup g} &= \left[\left(1-\bar{\beta}\right) p^c - \left(1-\bar{\beta}\right) p^{kf} - \bar{\beta} p^{kg} + \bar{\beta} p^o \right] \delta v^f \\ &\quad + \left[\bar{\alpha} \left(p^c - p^o\right) - \left(1-\bar{\alpha}\right) p^{kg} - \bar{\alpha} p^{kf} \right] \delta v^g - \rho \boldsymbol{g} \cdot \delta \boldsymbol{s}^f \end{aligned} \tag{3.54}$$

The physical meaning of the projection of the static moment in gravity direction will be discussed later on. Although equation (3.54) contains the identical pressures p^{kf} and p^{kg}, which cancel each other in

$$\bar{\beta} p^{kf} - \bar{\beta} p^{kg} = 0 \qquad \text{and} \qquad \bar{\alpha} p^{kg} - \bar{\alpha} p^{kf} = 0 \ , \tag{3.55}$$

they are kept in the formulation to allow the derivation of several particular cases, which have already been discussed in BONET ET AL.[15] and RUMPEL&SCHWEIZERHOF [78], [79], [80] and [81]. However, in these publications only some of the load cases were derived separately and were not part of an overall formulation, which allows combining them arbitrarily. Therefore in the following developments all possible load cases are briefly discussed.

3.1.7 Derivation of specific load cases

Due to the fact that the pressures p^o, p^x and p^c were derived from a potential, they have to be multiplied by -1 to obtain the physically acting pressure comparable to the pressures defined before. For a better understanding of the following figures, which will focus on specific load cases, these physical pressure terms are used.

Gas filled control volume

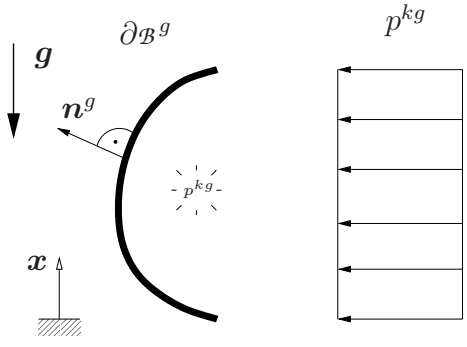

Figure 3.6: Hydrostatic pressure distribution in a gas filled control volume

In this case no fluid boundary $\partial \mathcal{B}^f$ and no fluid volume $\bar{v}^f$ exists, therefore all terms defined by the fluid surface integrals and fluid volume vanish. Further, no fluid level

$\partial\mathcal{B}^o$ exists, which means no projected volume v^o respectively no volume change δv^o. Using $\delta v^f = 0$ and $\delta v^o = 0$ in equation (3.43) yields

$$\bar{\alpha}\delta v^g = 0 \ . \tag{3.56}$$

This condition can only be satisfied if $\bar{\alpha} = 0$, because for an existing finite gas volume a change $\delta v^g \neq 0$ exists as well. The constraint equation $\bar{\alpha} = 0$ also follows directly from equation (3.45). For the variation $\delta\mathcal{E}_{f\cup g}$ in equation (3.54) only the virtual work of the gas compression remains (see also figure 3.6):

$$\delta\mathcal{E}_g = -p^{kg}\delta v^g = -p^{kg}\int\limits_{\partial\mathcal{B}^g} \boldsymbol{n}^g \cdot \delta\boldsymbol{u}^g \ d\xi^1 d\xi^2 \tag{3.57}$$

Incompressible fluid with free fluid surface

In this case we consider containments with partial fluid filling, where e.g. a vent hole is existing in the non-wetted region ensuring that no overpressure can arise in the interior. Thus all gas pressure terms can be neglected. In the case of an incompressible fluid, which means $K_0 \to \infty$, the limit for the pressure volume gradient β becomes:

$$\lim_{K_0\to\infty} \beta = \lim_{K_0\to\infty} \frac{K_0}{\bar{v}^f} = \infty \tag{3.58}$$

Thus for the dimensionless parameters $\bar{\alpha}$ and $\bar{\beta}$ the limits for $\beta \to \infty$ are

$$\lim_{\beta\to\infty} \bar{\alpha} = \lim_{\beta\to\infty} \frac{\alpha}{\alpha+\beta} = 0 \tag{3.59}$$

and

$$\lim_{\beta\to\infty} \bar{\beta} = \lim_{\beta\to\infty} \frac{\beta}{\alpha+\beta} = \lim_{\beta\to\infty} \frac{1}{\frac{\alpha}{\beta}+1} = 1 \ . \tag{3.60}$$

Hence, for an incompressible fluid with a free fluid surface we obtain

$$\bar{\alpha} = 0 \qquad \text{and} \qquad \bar{\beta} = 1 \ . \tag{3.61}$$

Thus with (3.61) and $p^{kg} = 0$ all gas terms are cancelled in equation (3.54) and the variation of the potential becomes

$$\delta\mathcal{E}_f \ = \ p^o\delta v^f - \rho\boldsymbol{g}\cdot\delta\boldsymbol{s}^f \ . \tag{3.62}$$

Using the static moment $\delta\boldsymbol{s}^f$ given in terms of surface integrals as in equation (3.38) and introducing the gravitational pressure term

$$p^x = \rho\boldsymbol{g}\cdot\boldsymbol{x} \ , \tag{3.63}$$

denoting the pressure at a structural surface point on $\partial\mathcal{B}^f$, $\delta\boldsymbol{s}^f$ now reveals its physical meaning.

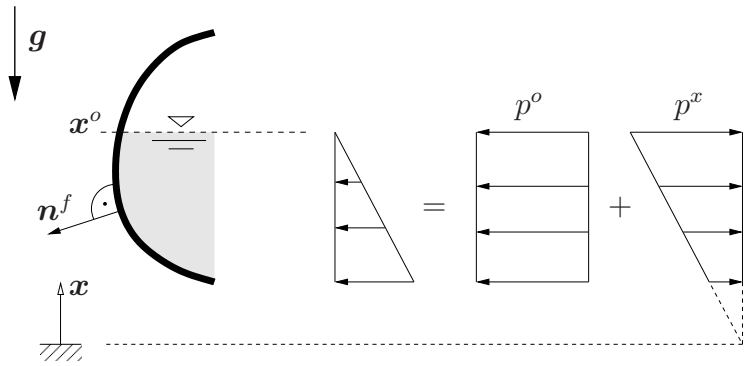

Figure 3.7: Hydrostatic pressure distribution in a single chamber partially filled with an incompressible heavy fluid

The virtual works of p^x and p^o can be given as:

$$\begin{aligned} \delta\mathcal{E}_f &= \int_{\partial\mathcal{B}^f} (p^o - \rho\boldsymbol{g}\cdot\boldsymbol{x})\,\boldsymbol{n}^f\cdot\delta\boldsymbol{u}^f\; d\xi^1 d\xi^2 \\ &= \int_{\partial\mathcal{B}^f} (p^o - p^x)\,\boldsymbol{n}^f\cdot\delta\boldsymbol{u}^f\; d\xi^1 d\xi^2 \end{aligned} \tag{3.64}$$

As depicted in figure 3.7 they arise from from the overall virtual work done by the difference of the pressures p^o and p^x acting on a structural surface point.

Incompressible fluid with free fluid surface and additional gas loading

As already mentioned, in contrast to former developments, the current formulation also enables the combination of fluid and gas loadings. For completely closed control

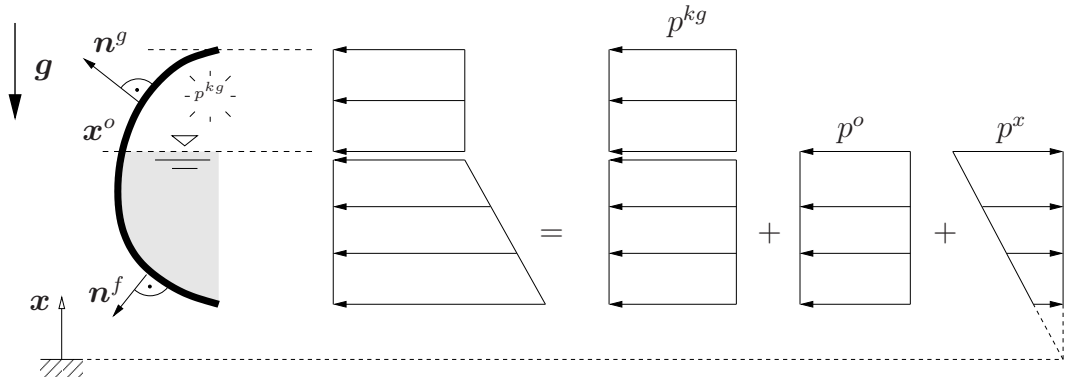

Figure 3.8: Hydrostatic pressure distribution in a chamber filled with gas and an incompressible heavy fluid

volumes, containing both a fluid filling and a gas filling with pressure $p^{kg} \neq 0$, an

additional gas boundary $\partial\mathcal{B}^g$ appears. Therefore in contrast to equation (3.64) two gas terms remain in equation (3.54) resulting in the variation of the gas and the fluid potential.

$$\begin{aligned}\delta\mathcal{E}_{f\cup g} &= \left(-p^{kg}+p^o\right)\delta v^f - \rho\boldsymbol{g}\cdot\delta\boldsymbol{s}^f - p^{kg}\;\delta v^g \\ &= \int\limits_{\partial\mathcal{B}^f}\left(p^o-p^x-p^{kg}\right)\boldsymbol{n}^f\cdot\delta\boldsymbol{u}^f\;d\xi^1d\xi^2 - \int\limits_{\partial\mathcal{B}^g} p^{kg}\boldsymbol{n}^g\cdot\delta\boldsymbol{u}^g\;d\xi^1d\xi^2\end{aligned} \tag{3.65}$$

The gas and fluid pressure distributions are depicted in figure 3.8.

Compressible fluid with free fluid surface

As for the case of an incompressible fluid with free fluid surface, all surface integrals over the gas domain can be removed, as no gas boundary $\partial\mathcal{B}^g$ exists. Therefore the gas pressure p^{kg} is zero, which means $\alpha(p^{kg})=0$. For the stiffness parameters $\bar{\alpha}$ and $\bar{\beta}$ then follows

$$\bar{\alpha}=0 \quad\text{and}\quad \bar{\beta}=1\;. \tag{3.66}$$

The fact that with $\bar{\beta}=1$ the term p^{kf} in equation (3.54) is canceled implies, that for a heavy fluid subjected to a gravity field, no volume compression needs to be considered[8]. Thus a compressible heavy fluid in absence of an exterior pressure is treated like an incompressible heavy fluid.

$$\delta\mathcal{E}_f = \int\limits_{\partial\mathcal{B}^f}\left(p^o-p^x\right)\boldsymbol{n}^f\cdot\delta\boldsymbol{u}^f\;d\xi^1d\xi^2 \tag{3.67}$$

Control volume completely filled with a compressible fluid

For chambers completely filled with fluid the deformation of the surrounding structure in general goes along with both a volumetric and a deviatoric deformation. Therefore the compressibility of the fluid must be considered, because otherwise complicated constraint equations have to be set up in order to couple the degrees of freedom. This is comparable to a contact formulation with a penalty parameter. Again no gas parts appear in the formulation for the variation of the potential and also no free fluid surface parts ($\partial\mathcal{B}^o=0$), which is reflected in the stiffness parameters

$$\bar{\alpha}=1 \quad\text{and}\quad \bar{\beta}=0\;, \tag{3.68}$$

[8]This complies with the calculation of cutting forces in case of statically determined systems, which can be performed without considering the deformation of the systems.

see also equation (3.47). Thus only the fluid potential terms remain with equation (3.54):

$$\begin{aligned} \delta\mathcal{E}_f &= \left(p^c - p^{kf}\right)\delta v^f - \rho\boldsymbol{g}\cdot\delta\boldsymbol{s}^f \\ &= \int\limits_{\partial\mathcal{B}^f} \left(p^c - p^{kf} - p^x\right)\boldsymbol{n}^f\cdot\delta\boldsymbol{u}^f \; d\xi^1 d\xi^2 \end{aligned} \tag{3.69}$$

Figure 3.9 illustrates the pressure distribution.

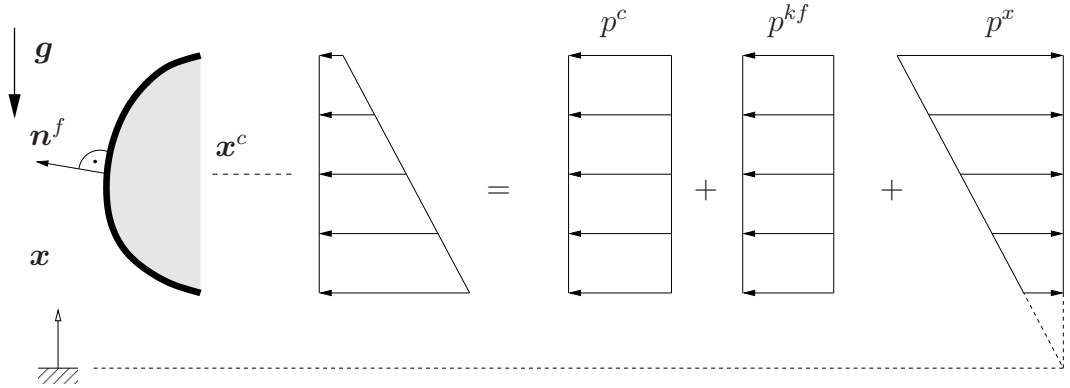

Figure 3.9: Hydrostatic pressure distribution in a chamber completely filled with a compressible heavy fluid

Control volume containing compressible fluid and gas

In the most general case all terms remain in the variational formulation (3.54). However, this case is more an academical one, as in general the virtual work, done for the compression of the fluid, is negligible compared to the virtual work done for the compression of a gas volume[9]. Thus for stiffness parameters $\bar{\alpha} \ll \bar{\beta}$, with $\bar{\alpha}, \bar{\beta} \in [0, 1]$, this case converges to a volume containing an incompressible fluid and gas. Since from this most general case all other cases discussed so far can be derived by a simple adjustment of the stiffness parameters it will be included here. Finally, the assumption (3.25), concerning the identity of the pressures due to volume compression, shall be verified. Combining the pressure terms in equation (3.54) acting in the fluid with

$$p^f = \left(1-\bar{\beta}\right)p^c - \left(1-\bar{\beta}\right)p^{kf} - \bar{\beta}p^{kg} + \bar{\beta}p^o - p^x \tag{3.70}$$

and the ones acting in the gas with

$$p^g = \bar{\alpha}\left(p^c - p^o\right) - \left(1-\bar{\alpha}\right)p^{kg} - \bar{\alpha}p^{kf} \;, \tag{3.71}$$

[9]This can be illustrated by a serial connection of two springs featuring highly different stiffnesses. Although in both springs the same force is acting their displacements and thus the stored energies are of different sizes. The major part of the external work is stored in the more flexible spring.

for reasons of equilibrium both pressures have to be identical at the phase intersection $\boldsymbol{x} = \boldsymbol{x}^o$. The gas pressure in equation (3.71) is constant and thus maintains its value at the phase intersection. According to equation (3.70) at the position $\boldsymbol{x} = \boldsymbol{x}^o$ the fluid pressure can be given as

$$\begin{aligned} p^f(\boldsymbol{x}^o) &= \left(1-\bar{\beta}\right) p^c - \left(1-\bar{\beta}\right) p^{kf} - \bar{\beta} p^{kg} + \bar{\beta} p^o - p^o \\ &= \left(1-\bar{\beta}\right) p^c - \left(1-\bar{\beta}\right) p^{kf} - \bar{\beta} p^{kg} - (1-\bar{\beta}) p^o \ . \end{aligned} \tag{3.72}$$

As gas and fluid share a common control volume $\bar{v} = \bar{v}^f + \bar{v}^g$ the conditional equation (3.42) yields the following relation between both parameters:

$$\bar{\alpha} = \frac{\alpha}{\alpha+\beta} = \frac{\alpha+\beta}{\alpha+\beta} - \frac{\beta}{\alpha+\beta} = 1 - \bar{\beta} \tag{3.73}$$

This relation was set up assuming (3.25), therefore a substitution of $\bar{\beta}$ by $1-\bar{\alpha}$ in equation (3.72) must lead to the gas pressure (3.71) again.

$$p^f(\boldsymbol{x}^o) = \bar{\alpha}(p^c - p^o) - \bar{\alpha} p^{kf} - (1-\bar{\alpha}) p^{kg} = p^g \tag{3.74}$$

As the assumption of identical pressures of volume compression finally leads to the necessary equilibrium of the pressures at the phase intersection, the identical pressures in equations (3.70) and (3.71) can be cancelled[10]. Thus the total fluid and gas pressures can be given as

$$\hat{p}^g = \bar{\alpha}\left(p^c - p^o\right) - p^{kg} \ , \tag{3.75}$$

$$\hat{p}^f = \bar{\alpha} p^c + \bar{\beta} p^o - p^{kg} - p^x \ . \tag{3.76}$$

Canceling the identical pressure terms in equation (3.54) and using (3.73), (3.75) and (3.76) yields the variational formulation of the fluid and gas potentials in case of a control volume filled with a compressible heavy fluid and gas.

$$\begin{aligned} \delta \mathcal{E}_{f \cup g} &= \left[\bar{\alpha} p^c + \bar{\beta} p^o - p^{kg}\right] \delta v^f - \rho \boldsymbol{g} \cdot \delta \boldsymbol{s}^f + \left[\bar{\alpha}\left(p^c - p^o\right) - p^{kg}\right] \delta v^g \\ &= \int\limits_{\partial \mathcal{B}^f} \hat{p}^f \boldsymbol{n}^f \cdot \delta \boldsymbol{u}^f \ d\xi^1 d\xi^2 + \int\limits_{\partial \mathcal{B}^g} \hat{p}^g \boldsymbol{n}^g \cdot \delta \boldsymbol{u}^g \ d\xi^1 d\xi^2 \ . \end{aligned} \tag{3.77}$$

The general pressure distribution and its separation into specific terms are depicted in figure 3.10. The term $\bar{\alpha} p^c - p^x$ represents the gravitational pressure distribution in the fluid, which is superimposed by the constant gas pressure p^{kg}. p^c has its origin in the variation of the fluid density, see the first term in equation (3.48). However, the computation of the variation of the density $\delta\rho = \delta\rho(\delta\bar{v}^f)$ implies with $\delta\bar{v}^f = \delta\bar{v}^f(\delta v^f, \delta v^o)$ and $\delta v^o = \delta v^o(\delta v^f, \delta v^g)$ according to equation (3.43) also the variation δv^g. Thus the term $\bar{\alpha} p^c$ has also an effect on the structural surface enclosing the gas.

[10] Due to the fact that the information concerning the origin of the pressure is lost in this case, they are exceptionally denoted by the pointer $\hat{}$. However, in the further developments of this thesis the general pressures (3.70) and (3.71) are used.

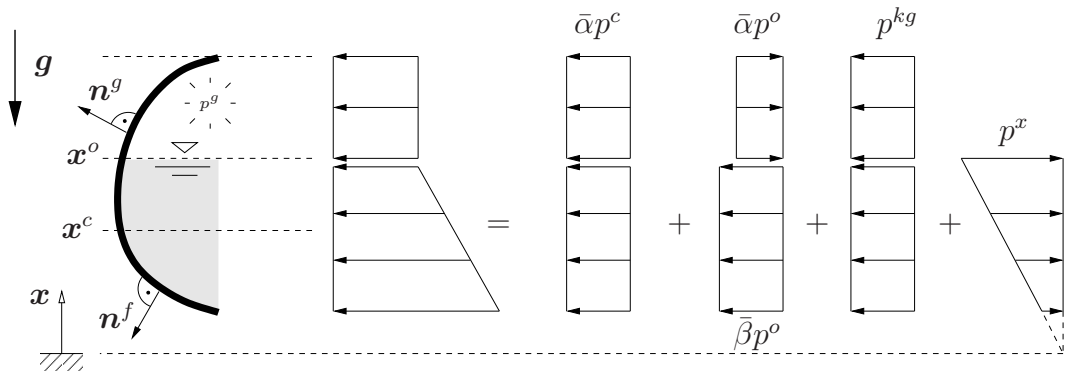

Figure 3.10: Hydrostatic pressure distribution in a control volume filled with gas and a compressible heavy fluid

3.1.8 Weak form of equilibrium

Summarizing the previous results the weak form of equilibrium (presuming isothermal conditions) of an elastic structure filled with an arbitrary combination of gas and (in)compressible fluid can be given as:

$$\begin{aligned}
\delta\mathcal{E} &= D\mathcal{E}_{el}(\boldsymbol{x})[\delta\boldsymbol{u}] + D\mathcal{E}_f(\boldsymbol{x})[\delta\boldsymbol{u}] + D\mathcal{E}_g(\boldsymbol{x})[\delta\boldsymbol{u}] - \delta\mathcal{A}^*_{ext} = 0 \\
&= \int_{\mathcal{B}_0} \boldsymbol{S} : D\boldsymbol{E}[\delta\boldsymbol{u}]\; dV - \int_{\mathcal{B}_0} \boldsymbol{f}_0 \cdot \delta\boldsymbol{u}\; dV - \int_{\partial\mathcal{B}_0} \boldsymbol{t}_0 \cdot \delta\boldsymbol{u}\; dA \\
&\quad + \int_{\partial\mathcal{B}^f} p^f \boldsymbol{n}^f \cdot \delta\boldsymbol{u}^f\; d\xi^1 d\xi^2 + \int_{\partial\mathcal{B}^g} p^g \boldsymbol{n}^g \cdot \delta\boldsymbol{u}^g\; d\xi^1 d\xi^2 = 0
\end{aligned} \tag{3.78}$$

To embed this nonlinear formulation of equilibrium in a numerical solution scheme, as e.g. the Newton-Raphson algorithm, all terms in (3.78) have to be linearized consistently, which will be part of the following section.

3.2 Linearization of the weak form

The previously derived weak form of equilibrium (3.78) is nonlinear in its motion $\boldsymbol{x} = \boldsymbol{x}(\boldsymbol{X}, t)$ and therefore has to be linearized in order to use numerical methods for its solution. Developing the weak form into a Taylor series about $\epsilon = 0$ (see also appendix A.1), corresponding to $\boldsymbol{x} = \boldsymbol{x}_t$, and neglecting higher order terms $R(\boldsymbol{u})$ yields a piecewise linear system of equations

$$\delta\mathcal{E}(\boldsymbol{x}_t + \Delta\boldsymbol{u}) = \delta\mathcal{E}(\boldsymbol{x}_t) + D\delta\mathcal{E}(\boldsymbol{x}_t)[\boldsymbol{u}] + R(\boldsymbol{u}) = 0\ . \tag{3.79}$$

The incremental change $D\delta\mathcal{E}(\boldsymbol{x}_t)[\boldsymbol{u}]$ of the weak form at the current position $\boldsymbol{x}_t$ in direction of the displacements $\boldsymbol{u}$ can be obtained by the directional derivative.

$$D\delta\mathcal{E}(\boldsymbol{x}_t)[\boldsymbol{u}] = \frac{\partial \delta\mathcal{E}(\boldsymbol{x}_t)}{\partial \boldsymbol{u}} \cdot \Delta\boldsymbol{u} \tag{3.80}$$

Hence, in this section the focus is on the determination of the directional derivatives of the elastic part $\delta\mathcal{E}_{el}(\boldsymbol{x}_t)$ and of the fluid and gas parts $\delta\mathcal{E}_{f\cup g}(\boldsymbol{x}_t)$ contained in the weak form. For reasons of simplicity all forces, which do not originate from the fluid or gas, are assumed to be deformation invariant and thus can be excluded from the linearization process.

3.2.1 Linearization of the elastic part

$$\delta\mathcal{E}_{el}(\boldsymbol{x}_t + \Delta\boldsymbol{u}) = \delta\mathcal{E}_{el}(\boldsymbol{x}_t) + D\delta\mathcal{E}_{el}(\boldsymbol{x}_t)[\boldsymbol{u}] \tag{3.81}$$

The incremental change of the potential in direction of $\boldsymbol{u}$ can be divided in the standard nonlinear material tangent and a nonlinear geometric part.

$$D\delta\mathcal{E}_{el}(\boldsymbol{x}_t)[\boldsymbol{u}] = \int_{\mathcal{B}_0} \left(D\boldsymbol{S}(\boldsymbol{x}_t)[\boldsymbol{u}] : \delta\boldsymbol{E}(\boldsymbol{x}_t) + \boldsymbol{S}(\boldsymbol{x}_t) : D\delta\boldsymbol{E}(\boldsymbol{x}_t)[\boldsymbol{u}]\right) dV \tag{3.82}$$

Material tangent

By applying the chain rule the derivation of the stresses $\boldsymbol{S}$ in direction of the displacements $\boldsymbol{u}$ yields

$$D\boldsymbol{S}(\boldsymbol{x}_t)[\boldsymbol{u}] = \frac{\partial \boldsymbol{S}}{\partial \boldsymbol{E}} : \frac{\partial \boldsymbol{E}}{\partial \boldsymbol{u}}\Delta\boldsymbol{u} \ . \tag{3.83}$$

For hyperelastic solid bodies – the model used in this thesis – the change of the stresses in direction of the strains was given as the symmetric fourth order tensor $\mathbb{C}$ in equations (2.31), (2.42) and (2.47). Thus follows:

$$D\boldsymbol{S}(\boldsymbol{x}_t)[\boldsymbol{u}] = \mathbb{C} : \frac{\partial \boldsymbol{E}}{\partial \boldsymbol{u}}\Delta\boldsymbol{u} \tag{3.84}$$

Geometric part

The linearization of the geometric part is performed analogously to the variation (3.8) of the strain tensor $\boldsymbol{E}$. Using the incremental change

$$D\boldsymbol{g}_\alpha(\boldsymbol{x}_t)[\boldsymbol{u}] = \frac{\partial \Delta\boldsymbol{u}}{\partial \xi^\alpha} = \Delta\boldsymbol{u}_{,\alpha} \tag{3.85}$$

of the current base vector $\boldsymbol{g}_\alpha$ yields

$$D\delta\boldsymbol{E}(\boldsymbol{x}_t)[\boldsymbol{u}] = \frac{1}{2}\left(\delta\boldsymbol{u}_{,\alpha} \cdot \Delta\boldsymbol{u}_{,\beta} + \Delta\boldsymbol{u}_{,\alpha} \cdot \delta\boldsymbol{u}_{,\beta}\right)\boldsymbol{G}^\alpha \otimes \boldsymbol{G}^\beta \ . \tag{3.86}$$

3.2.2 Linearization of the fluid and gas parts

After an application of the chain rule the linearization of the fluid and gas parts in equation (3.78) for the domain $\partial\mathcal{B}^g \cup \partial\mathcal{B}^f$ leads to a pressure change part $D\delta\mathcal{E}_{f\cup g}^{\Delta p}(\boldsymbol{x}_t)[\boldsymbol{u}]$ and a normal change part $D\delta\mathcal{E}_{f\cup g}^{\Delta n}(\boldsymbol{x}_t)[\boldsymbol{u}]$.

$$\begin{aligned} D\delta\mathcal{E}_{f\cup g}(\boldsymbol{x}_t)[\boldsymbol{u}] &= D\delta\mathcal{E}_{f\cup g}^{\Delta p}(\boldsymbol{x}_t)[\boldsymbol{u}] + D\delta\mathcal{E}_{f\cup g}^{\Delta n}(\boldsymbol{x}_t)[\boldsymbol{u}] \\ &= \int\limits_{\partial\mathcal{B}^f} \Delta p^f \boldsymbol{n}_t^f \cdot \delta\boldsymbol{u}^f \; d\xi^1 d\xi^2 + \int\limits_{\partial\mathcal{B}^g} \Delta p^g \boldsymbol{n}_t^g \cdot \delta\boldsymbol{u}^g \; d\xi^1 d\xi^2 \\ &\quad + \int\limits_{\partial\mathcal{B}^f} p_t^f \Delta\boldsymbol{n}^f \cdot \delta\boldsymbol{u}^f \; d\xi^1 d\xi^2 + \int\limits_{\partial\mathcal{B}^g} p_t^g \Delta\boldsymbol{n}^g \cdot \delta\boldsymbol{u}^g \; d\xi^1 d\xi^2 \end{aligned} \tag{3.87}$$

The linearization of each of these parts will be the aim of the following sections.

Incremental pressure changes

As it is obvious in equations (3.70) and (3.71), in the general case the fluid and gas pressures are assembled by the different parts Δp^c, Δp^o, Δp^{kg}, Δp^{kf} and Δp^x, which have to be considered using the directional derivative[11]. For the incremental change of the fluid pressure follows

$$\Delta p^f = \left(1-\bar{\beta}\right)\Delta p^c - \left(1-\bar{\beta}\right)\Delta p^{kf} - \bar{\beta}\Delta p^{kg} + \bar{\beta}\Delta p^o - \Delta p^x \tag{3.88}$$

and for the incremental change of the gas pressure

$$\Delta p^g = \bar{\alpha}\left(\Delta p^c - \Delta p^o\right) - \left(1-\bar{\alpha}\right)\Delta p^{kg} - \bar{\alpha}\Delta p^{kf} \; . \tag{3.89}$$

Within the linearization process of the state equations for the acting pressures (3.23) and (3.24) respectively for the pressures (3.52), (3.53) and (3.63), deducted from a potential, the implied incremental geometric terms have to be captured.

Incremental changes of the geometric quantities

In analogy to equation (3.43) the identity of the pressures due to volume compression (3.25) allows the computation of the volume change Δv^o caused by an incremental displacement $\Delta\boldsymbol{u}^o$ of the fluid level.

$$\Delta v^o = \bar{\alpha}\Delta v^g - \bar{\beta}\Delta v^f \tag{3.90}$$

[11] In a strict sense the dimensionless parameters $\bar{\alpha}$ and $\bar{\beta}$ have to be linearized as well. However, even in the general case of a compressible fluid and an additional gas loading (assuming a physically realistic fluid compressibility, which is much smaller than the compressibility of the gas) for the parameters follows $\bar{\alpha} \approx 0$ and $\bar{\beta} \approx 1$. Thus the changes of $\bar{\alpha}$ and $\bar{\beta}$ will be sufficiently small enough to neglect them in the linearization process for the sake of efficiency.

In a similar fashion changing the operator in equations (3.29) and (3.30) using equation (3.90) leads to the fluid volume change

$$\begin{aligned}\Delta\bar{v}^f &= \Delta\left(v^f + v^o\right)\\ &= \Delta v^f + \Delta v^o\\ &= \Delta v^f + \bar{\alpha}\Delta v^g - \bar{\beta}\Delta v^f\\ &= \left(1-\bar{\beta}\right)\Delta v^f + \bar{\alpha}\Delta v^g \end{aligned} \tag{3.91}$$

and the gas volume change

$$\begin{aligned}\Delta\bar{v}^g &= \Delta\left(v^g - v^o\right)\\ &= \Delta v^g - \Delta v^o\\ &= \Delta v^g - \left(\bar{\alpha}\Delta v^g - \bar{\beta}\Delta v^f\right)\\ &= \left(1-\bar{\alpha}\right)\Delta v^g + \bar{\beta}\Delta v^f\ . \end{aligned} \tag{3.92}$$

The linearization of the projection of the static moment $\Delta\bar{\boldsymbol{s}}^f$ in direction of gravity can be obtained by a change of the operator in (3.31) and (3.33) as well.

$$\begin{aligned}\boldsymbol{g}\cdot\Delta\bar{\boldsymbol{s}}^f &= \boldsymbol{g}\cdot\Delta\boldsymbol{s}^f + \Delta v^o\left(\boldsymbol{g}\cdot\boldsymbol{x}_t^o\right)\\ &= \boldsymbol{g}\cdot\Delta\boldsymbol{s}^f + \left(\bar{\alpha}\Delta v^g - \bar{\beta}\Delta v^f\right)\left(\boldsymbol{g}\cdot\boldsymbol{x}_t^o\right)\end{aligned} \tag{3.93}$$

The changes of the geometrical quantities derived so far are decomposed into the incremental volume changes

$$\Delta v^f = \int\limits_{\partial\mathcal{B}^f} \boldsymbol{n}_t^f\cdot\Delta\boldsymbol{u}^f\ d\xi^1 d\xi^2 \tag{3.94}$$

and

$$\Delta v^g = \int\limits_{\partial\mathcal{B}^g} \boldsymbol{n}_t^g\cdot\Delta\boldsymbol{u}^g\ d\xi^1 d\xi^2\ , \tag{3.95}$$

which can be obtained in analogy to (3.29) and (3.30) by a projection and subsequent integration of the structural displacements in direction of the normal. In a similar fashion, using equation (3.38) the part of the static moment can be derived by a projection of the wetted surface $\partial\mathcal{B}^f$.

$$\boldsymbol{g}\cdot\Delta\boldsymbol{s}^f = \int\limits_{\partial\mathcal{B}^f}\left(\boldsymbol{n}_t^f\cdot\Delta\boldsymbol{u}^f\right)\left(\boldsymbol{x}_t^f\cdot\boldsymbol{g}\right)d\xi^1 d\xi^2 \tag{3.96}$$

Incremental change of the fluid level

As the projected position of the fluid level $\boldsymbol{x}_t^o$ in direction of $\boldsymbol{g}$ remains constant at a state t in the whole area $\partial\mathcal{B}_t^o$, the volume change Δv^o of the fluid can also be seen as an incremental change $\Delta\boldsymbol{u}^o$ of the position of the fluid surface $\partial\mathcal{B}_t^o$.

$$\Delta v^o = \int_{\partial\mathcal{B}^o} \boldsymbol{n}_t^o \cdot \Delta\boldsymbol{u}^o \, d\xi^1 d\xi^2 = \int_{\partial\mathcal{B}^o} \underbrace{\boldsymbol{n}_t^o \cdot \frac{\boldsymbol{g}}{|\boldsymbol{g}|}}_{-n_t^o} \underbrace{\Delta\boldsymbol{u}^o \cdot \frac{\boldsymbol{g}}{|\boldsymbol{g}|}}_{-\Delta u^o} \, d\xi^1 d\xi^2 \tag{3.97}$$

Since the normal $\boldsymbol{n}_t^o$ and the displacement $\Delta\boldsymbol{u}^o$ are colinear to the gravity $\boldsymbol{g}$, but pointing in the opposite direction, the scalar product $\boldsymbol{n}_t^o \cdot \Delta\boldsymbol{u}^o$ in the equation above can be also expressed by the product of the two scalars n_t^o and Δu^o. As already mentioned $\boldsymbol{x}_t^o$ and thus $\Delta\boldsymbol{u}^o$ only change in a direction perpendicular to the fluid surface (which means in direction of its normal $\boldsymbol{n}_t^o$), the projection of $\Delta\boldsymbol{u}^o$ can be moved out of the fluid surface integral.

$$\Delta v^o = \Delta\boldsymbol{u}^o \cdot \frac{\boldsymbol{g}}{|\boldsymbol{g}|} \int_{\partial\mathcal{B}^o} \boldsymbol{n}_t^o \cdot \frac{\boldsymbol{g}}{|\boldsymbol{g}|} \, d\xi^1 d\xi^2 \tag{3.98}$$

The remaining integral can be evaluated directly and provides the total fluid surface[12] $\partial\mathcal{B}_t^o$ at a given state t.

$$\Delta v^o = \Delta\boldsymbol{u}^o \cdot \frac{\boldsymbol{g}}{|\boldsymbol{g}|}(-\partial\mathcal{B}_t^o) \tag{3.99}$$

As the linearized state of equilibrium shall be written only in terms of the surrounding structure $\boldsymbol{u}^f$ and $\boldsymbol{u}^g$, we insert (3.90) into (3.99), which yields the correlation of $\Delta\boldsymbol{u}^o$ and the volume changes due to the projected displacements of the structure.

$$\begin{aligned} \Delta v^o = \Delta\boldsymbol{u}^o \cdot \frac{\boldsymbol{g}}{|\boldsymbol{g}|}(-\partial\mathcal{B}_t^o) &= \bar{\alpha}\Delta v^g - \bar{\beta}\Delta v^f \\ \Delta\boldsymbol{u}^o \cdot \boldsymbol{g} &= -\frac{|\boldsymbol{g}|}{\partial\mathcal{B}_t^o}\left(\bar{\alpha}\Delta v^g - \bar{\beta}\Delta v^f\right) \end{aligned} \tag{3.100}$$

Pressure changes due to volume compression

As already mentioned, in case of a compressible fluid under gas pressure the pressure changes Δp^{kf} and Δp^{kg} are identical. But in order to keep a clear notation and a consequent derivation between all cases we continue using both pressure changes, which

[12] Since for the scalar product holds $\boldsymbol{n}_t^o \cdot \boldsymbol{g}/|\boldsymbol{g}| = -n_t^o$, evaluating the integral yields the negative free fluid surface.

follow (3.23), (3.24), (3.94) and (3.95). Hence we obtain the pressure change due to fluid compression

$$\begin{aligned}\Delta p^{kf} &= -\beta_t \Delta \bar{v}^f \\ &= -\beta_t \left[\left(1-\bar{\beta}\right) \Delta v^f + \bar{\alpha} \Delta v^g \right] \\ &= -\beta_t \left(1-\bar{\beta}\right) \int\limits_{\partial \mathcal{B}^f} \boldsymbol{n}_t^f \cdot \Delta \boldsymbol{u}^f d\xi^1 d\xi^2 - \beta_t \bar{\alpha} \int\limits_{\partial \mathcal{B}^g} \boldsymbol{n}_t^g \cdot \Delta \boldsymbol{u}^g d\xi^1 d\xi^2 \end{aligned} \tag{3.101}$$

and the pressure change due to gas compression

$$\begin{aligned}\Delta p^{kg} &= -\alpha_t \Delta \bar{v}^g \\ &= -\alpha_t \left[\left(1-\bar{\alpha}\right) \Delta v^g + \bar{\beta} \Delta v^f \right] \\ &= -\alpha_t \left(1-\bar{\alpha}\right) \int\limits_{\partial \mathcal{B}^g} \boldsymbol{n}_t^g \cdot \Delta \boldsymbol{u}^g d\xi^1 d\xi^2 - \alpha_t \bar{\beta} \int\limits_{\partial \mathcal{B}^f} \boldsymbol{n}_t^f \cdot \Delta \boldsymbol{u}^f d\xi^1 d\xi^2 \ . \end{aligned} \tag{3.102}$$

Incremental pressure change in the center of gravity

Linearization of equation (3.52) yields

$$\begin{aligned}\Delta p^c &= \Delta \left(\rho \boldsymbol{g} \cdot \frac{\bar{\boldsymbol{s}}}{\bar{v}^f} \right) \\ &= \Delta \rho \boldsymbol{g} \cdot \frac{\bar{\boldsymbol{s}}_t}{\bar{v}_t^f} + \rho_t \boldsymbol{g} \cdot \Delta \left(\frac{\bar{\boldsymbol{s}}}{\bar{v}^f} \right) \\ &= \Delta \rho \boldsymbol{g} \cdot \boldsymbol{c}_t^f + \rho_t \boldsymbol{g} \cdot \left(\frac{\Delta \bar{\boldsymbol{s}}}{\bar{v}_t^f} - \Delta \bar{v}^f \frac{\bar{\boldsymbol{s}}_t}{(\bar{v}_t^f)^2} \right) \ . \end{aligned} \tag{3.103}$$

Applying mass conservation condition (3.22) in equation (3.103) and using equations (3.51), (3.52) along with the equations for the fluid and gas volume changes (3.91) and (3.92), we obtain after some minor reordering:

$$\begin{aligned}\Delta p^c &= -\frac{\rho_t}{\bar{v}_t^f} \Delta \bar{v}^f \boldsymbol{g} \cdot \boldsymbol{c}_t + \rho_t \boldsymbol{g} \cdot \left(\frac{\Delta \bar{\boldsymbol{s}}}{\bar{v}_t^f} - \frac{\boldsymbol{c}_t^f}{\bar{v}_t^f} \Delta \bar{v}^f \right) \\ &= -2 \frac{p_t^c}{\bar{v}_t^f} \Delta \bar{v}^f + \frac{\rho_t}{\bar{v}_t^f} \boldsymbol{g} \cdot \Delta \bar{\boldsymbol{s}} \\ &= -2 \frac{p_t^c}{\bar{v}_t^f} \left[\left(1-\bar{\beta}\right) \Delta v^f + \bar{\alpha} \Delta v^g \right] + \frac{\rho_t}{\bar{v}_t^f} \boldsymbol{g} \cdot \left(\Delta \boldsymbol{s}^f + \bar{\alpha} \Delta v^g \boldsymbol{x}_t^o - \bar{\beta} \Delta v^f \boldsymbol{x}_t^o \right) \end{aligned} \tag{3.104}$$

Sorting equation (3.104) by integration domains $\partial \mathcal{B}^f$ and $\partial \mathcal{B}^g$ and using the pressure change (3.63) as well as the volume changes (3.94) and (3.95) leads to the incremental

pressure change Δp^c in the current center of gravity of the fluid $\boldsymbol{c}_t$ in terms of the incremental displacements $\Delta \boldsymbol{u}^g$ and $\Delta \boldsymbol{u}^f$.

$$\begin{aligned}
\Delta p^c &= \left[-2\frac{p_t^c}{\bar{v}_t^f}\left(1-\bar{\beta}\right) - \frac{p_t^o}{\bar{v}_t^f}\bar{\beta}\right]\Delta v^f + \left[\frac{p_t^o}{\bar{v}_t^f}\bar{\alpha} - 2\frac{p_t^c}{\bar{v}_t^f}\bar{\alpha}\right]\Delta v^g + \frac{\rho_t}{\bar{v}_t^f}\boldsymbol{g}\cdot\Delta\boldsymbol{s}^f \\
&= \frac{1}{\bar{v}_t^f}\int\limits_{\partial\mathcal{B}^f}\left[-2p_t^c\left(1-\bar{\beta}\right) - p_t^o\bar{\beta} + p_t^x\right]\boldsymbol{n}_t^f\cdot\Delta\boldsymbol{u}^f d\xi^1 d\xi^2 \\
&\quad + \frac{1}{\bar{v}_t^f}\int\limits_{\partial\mathcal{B}^g}\bar{\alpha}\left(p_t^o - 2p_t^c\right)\boldsymbol{n}_t^g\cdot\Delta\boldsymbol{u}^g d\xi^1 d\xi^2
\end{aligned} \tag{3.105}$$

Incremental pressure change at the phase intersection

In order to integrate a fluid with a free surface into an algorithm using the projection of the boundary for a description of the geometry, a consistent separation of the fluid boundary into a part $\partial\mathcal{B}^f$ (bounded by the structural surface) and a part $\partial\mathcal{B}^o$ (bounded by the fluid level) was necessary. From this separation the pressure p^o at the fluid level results, compare equation (3.53). With equations (3.22), (3.91) and (3.92) the pressure change becomes then

$$\begin{aligned}
\Delta p^o &= \Delta\left(\rho\boldsymbol{g}\cdot\boldsymbol{x}^o\right) \\
&= \Delta\rho\boldsymbol{g}\cdot\boldsymbol{x}_t^o + \rho_t\boldsymbol{g}\cdot\Delta\boldsymbol{u}^o \\
&= -\frac{\rho_t}{\bar{v}_t^f}\Delta\bar{v}^f\boldsymbol{g}\cdot\boldsymbol{x}_t^o + \rho_t\boldsymbol{g}\cdot\Delta\boldsymbol{u}^o \\
&= -\frac{\rho_t}{\bar{v}_t^f}\left[\left(1-\bar{\beta}\right)\Delta v^f + \bar{\alpha}\Delta v^g\right]\boldsymbol{g}\cdot\boldsymbol{x}_t^o + \rho_t\boldsymbol{g}\cdot\Delta\boldsymbol{u}^o\ .
\end{aligned} \tag{3.106}$$

Inserting the projection of the displacement increment $\boldsymbol{g}\cdot\Delta\boldsymbol{u}^o$ of the fluid level (3.100) yields

$$\Delta p^o = -\frac{\rho_t}{\bar{v}_t^f}\left[\left(1-\bar{\beta}\right)\Delta v^f + \bar{\alpha}\Delta v^g\right]\boldsymbol{g}\cdot\boldsymbol{x}_t^o - \frac{\rho_t|\boldsymbol{g}|}{\partial\mathcal{B}_t^o}\left(\bar{\alpha}\Delta v^g - \bar{\beta}\Delta v^f\right)\ . \tag{3.107}$$

Again the terms with the same integration domains can be collected and with the volume changes (3.94) and (3.95) and the pressure volume gradient

$$\gamma_t = \frac{\rho_t|\boldsymbol{g}|}{\partial\mathcal{B}_t^o} \tag{3.108}$$

the pressure change Δp^o at the fluid level position $\boldsymbol{x}^o$ becomes

$$\begin{aligned}
\Delta p^o &= \left[-\frac{p_t^o}{\bar{v}_t^f}\left(1-\bar{\beta}\right)+\frac{\rho_t|\boldsymbol{g}|}{\partial \mathcal{B}_t^o}\bar{\beta}\right]\Delta v^f-\bar{\alpha}\left(\frac{\rho_t|\boldsymbol{g}|}{\partial \mathcal{B}_t^o}+\frac{p_t^o}{\bar{v}_t^f}\right)\Delta v^g \\
&= \left[-\frac{p_t^o}{\bar{v}_t^f}\left(1-\bar{\beta}\right)+\gamma_t\bar{\beta}\right]\Delta v^f-\bar{\alpha}\left(\gamma_t+\frac{p_t^o}{\bar{v}_t^f}\right)\Delta v^g \\
&= \left[-\frac{p_t^o}{\bar{v}_t^f}\left(1-\bar{\beta}\right)+\gamma_t\bar{\beta}\right]\int\limits_{\partial\mathcal{B}^f}\boldsymbol{n}_t^f\cdot\Delta\boldsymbol{u}^f d\xi^1 d\xi^2 \\
&\quad -\bar{\alpha}\left(\gamma_t+\frac{p_t^o}{\bar{v}_t^f}\right)\int\limits_{\partial\mathcal{B}^g}\boldsymbol{n}_t^g\cdot\Delta\boldsymbol{u}^g d\xi^1 d\xi^2\ . \qquad (3.109)
\end{aligned}$$

Incremental pressure change at a wetted structural surface point

As for the determination of Δp^o in equation (3.109), we use mass conservation condition (3.22) and the volume changes (3.94) and (3.95) to derive the pressure change Δp^x at an arbitrary structural surface point $\boldsymbol{x}^f$ wetted by the fluid.

$$\begin{aligned}
\Delta p^x &= \Delta\left(\rho\boldsymbol{g}\cdot\boldsymbol{x}^f\right) \\
&= \Delta\rho\boldsymbol{g}\cdot\boldsymbol{x}_t^f+\rho_t\boldsymbol{g}\cdot\Delta\boldsymbol{u} \\
&= -\frac{\rho_t}{\bar{v}_t^f}\Delta\bar{v}^f\boldsymbol{g}\cdot\boldsymbol{x}_t^f+\rho_t\boldsymbol{g}\cdot\Delta\boldsymbol{u} \\
&= -\frac{p_t^x}{\bar{v}_t^f}\left[\left(1-\bar{\beta}\right)\Delta v^f+\bar{\alpha}\Delta v^g\right]+\rho_t\boldsymbol{g}\cdot\Delta\boldsymbol{u} \\
&= -\frac{p_t^x}{\bar{v}_t^f}\left(1-\bar{\beta}\right)\int\limits_{\partial\mathcal{B}^f}\boldsymbol{n}_t^f\cdot\Delta\boldsymbol{u}^f d\xi^1 d\xi^2 \\
&\quad -\frac{p_t^x}{\bar{v}_t^f}\bar{\alpha}\int\limits_{\partial\mathcal{B}^g}\boldsymbol{n}_t^g\cdot\Delta\boldsymbol{u}^g d\xi^1 d\xi^2+\rho_t\boldsymbol{g}\cdot\Delta\boldsymbol{u} \qquad (3.110)
\end{aligned}$$

3.2.3 Terms including the change of normals

Since a pressure loading is a deformation dependent loading as it is always acting normal to the surface (see also Schweizerhof[86] and Schweizerhof&Ramm[90]), the linearizations have to take into account the directional changes of the normal vectors on the surface as well. The terms describing the incremental changes of the normals can be adapted from Schweizerhof[86], Knebel[48] or Rumpel[79]. For the fluid domain the additional part due to the non-constant pressure distribution p^x in $\boldsymbol{x}$ must be considered. This part describes the pressure change in direction of the convective

coordinates ξ^α. By introducing the skew symmetric tensors

$$\widehat{\boldsymbol{W}}^{\xi_1} = \boldsymbol{n}_t \otimes \boldsymbol{x}^{,1} - \boldsymbol{x}^{,1} \otimes \boldsymbol{n}_t \tag{3.111}$$

$$\widehat{\boldsymbol{W}}^{\xi_2} = \boldsymbol{n}_t \otimes \boldsymbol{x}^{,2} - \boldsymbol{x}^{,2} \otimes \boldsymbol{n}_t \ , \tag{3.112}$$

defined in a contravariant basis $\boldsymbol{x}^{,1} \otimes \boldsymbol{x}^{,2}$, the normal change parts for the gas domain

$$\Delta\delta\mathcal{E}_g^{\Delta n} = \int\limits_{\partial\mathcal{B}^g} \frac{p_t^g}{2} \begin{pmatrix} \delta\boldsymbol{u}^g \\ \delta\boldsymbol{u}^g_{,1} \\ \delta\boldsymbol{u}^g_{,2} \end{pmatrix} \cdot \begin{pmatrix} \mathbf{0} & \widehat{\boldsymbol{W}}^{\xi_1} & \widehat{\boldsymbol{W}}^{\xi_2} \\ \widehat{\boldsymbol{W}}^{\xi_1 T} & \mathbf{0} & \mathbf{0} \\ \widehat{\boldsymbol{W}}^{\xi_2 T} & \mathbf{0} & \mathbf{0} \end{pmatrix} \begin{pmatrix} \Delta\boldsymbol{u}^g \\ \Delta\boldsymbol{u}^g_{,1} \\ \Delta\boldsymbol{u}^g_{,2} \end{pmatrix} d\xi^1 d\xi^2 \tag{3.113}$$

as well as the normal change parts for the fluid domain

$$\begin{aligned} \Delta\delta\mathcal{E}_f^{\Delta n} = & \int\limits_{\partial\mathcal{B}^f} \frac{p_t^f}{2} \begin{pmatrix} \delta\boldsymbol{u}^f \\ \delta\boldsymbol{u}^f_{,1} \\ \delta\boldsymbol{u}^f_{,2} \end{pmatrix} \cdot \begin{pmatrix} \mathbf{0} & \widehat{\boldsymbol{W}}^{\xi_1} & \widehat{\boldsymbol{W}}^{\xi_2} \\ \widehat{\boldsymbol{W}}^{\xi_1 T} & \mathbf{0} & \mathbf{0} \\ \widehat{\boldsymbol{W}}^{\xi_2 T} & \mathbf{0} & \mathbf{0} \end{pmatrix} \begin{pmatrix} \Delta\boldsymbol{u}^f \\ \Delta\boldsymbol{u}^f_{,1} \\ \Delta\boldsymbol{u}^f_{,2} \end{pmatrix} d\xi^1 d\xi^2 \\ & - \int\limits_{\partial\mathcal{B}^f} \left[p^f_{t,1}(\boldsymbol{x}_{,2} \times \delta\boldsymbol{u}^f_{,1}) - p^f_{t,2}(\boldsymbol{x}_{,1} \times \delta\boldsymbol{u}^f_{,2}) \right] \cdot \Delta\boldsymbol{u}^f \ d\xi^1 d\xi^2 \ . \end{aligned} \tag{3.114}$$

are obtained. The position dependent pressure inside the fluid at a state t can be computed with equation (3.70)

$$p_t^f = \left(1 - \bar{\beta}\right) p_t^c - \left(1 - \bar{\beta}\right) p_t^{kf} - \bar{\beta} p_t^{kg} + \bar{\beta} p_t^o - p_t^x \ . \tag{3.115}$$

The constant pressure inside the gas volume at a state t follows with equation (3.71).

$$p_t^g = \bar{\alpha}\,(p_t^c - p_t^o) - (1 - \bar{\alpha})\, p_t^{kg} - \bar{\alpha} p_t^{kf} \tag{3.116}$$

3.2.4 Proof of conservativeness

As it was shown in SCHWEIZERHOF[86] and KNEBEL[48] by product integration and subsequent application of the Gauß theorem, the formally unsymmetric part in equation (3.114) can be transformed into a skew symmetric field term and an unsymmetric boundary term. Assuming physically realistic boundary conditions makes this boundary term vanish. A complete symmetry of $\Delta\delta\mathcal{E}_{f\cup g}$ will finally be obtained without any further assumption, if the linearized pressure parts (3.101), (3.102), (3.105), (3.109) and (3.110) along with the normal change parts (3.113) and (3.114) are inserted into the initial equation (3.87). If now the last term $\rho_t \boldsymbol{g} \cdot \Delta\boldsymbol{u}$ in equation (3.110) is split up into a symmetric and a skew symmetric part, this skew symmetric part neutralizes with the remaining skew symmetric term in equation (3.114). Thus only the symmetric part from the position dependent pressure over the domain $\partial\mathcal{B}^f$ remains. The linearized

virtual potential $\delta\mathcal{E}_{f\cup g}(\boldsymbol{x}_t + \Delta\boldsymbol{u})$ finally consists of the following five parts including the residual terms:

Residual terms computed over $\partial\mathcal{B}^g$ and $\partial\mathcal{B}^f$

$$\begin{aligned}\delta\mathcal{E}_{f\cup g}(\boldsymbol{x}_t) \;=\; & \int_{\partial\mathcal{B}^f}\Big[\big(1-\bar\beta\big)\,p_t^c-(1-\bar\beta)p_t^{kf}-\bar\beta p^{kg}+\bar\beta p_t^o-p_t^x\Big]\,\boldsymbol{n}_t^f\cdot\delta\boldsymbol{u}^f\;d\xi^1d\xi^2\\ & +\int_{\partial\mathcal{B}^g}\Big[\bar\alpha\,(p_t^c-p_t^o)-(1-\bar\alpha)p_t^{kg}-\bar\alpha p^{kf}\Big]\,\boldsymbol{n}_t^g\cdot\delta\boldsymbol{u}^g\;d\xi^1d\xi^2 \qquad (3.117)\end{aligned}$$

Coupling part computed over $\partial\mathcal{B}^f$

$$D\delta\mathcal{E}_f^{\Delta p}(\boldsymbol{x}_t)[\boldsymbol{u}] \;=$$

- *gravitational part in the center of gravity of the fluid:* $\big(1-\bar\beta\big)\,\Delta p^c\delta v^f$

$$\begin{aligned}&\int_{\partial\mathcal{B}^f}\left[\frac{1-\bar\beta}{\bar v_t^f}\int_{\partial\mathcal{B}^f}\left[-2p_t^c\left(1-\bar\beta\right)-p_t^o\bar\beta+p_t^x\right]\boldsymbol{n}_t^f\cdot\Delta\boldsymbol{u}^f d\xi^1d\xi^2\right]\boldsymbol{n}_t^f\cdot\delta\boldsymbol{u}^f d\xi^1d\xi^2\\ &+\int_{\partial\mathcal{B}^f}\left[\frac{1-\bar\beta}{\bar v_t^f}\int_{\partial\mathcal{B}^g}\bar\alpha\,(p_t^o-2p_t^c)\,\boldsymbol{n}_t^g\cdot\Delta\boldsymbol{u}^g d\xi^1d\xi^2\right]\boldsymbol{n}_t^f\cdot\delta\boldsymbol{u}^f d\xi^1d\xi^2\end{aligned}$$

- *virtual work due to fluid volume compression:* $-(1-\bar\beta)\Delta p^{kf}\delta v^f$

$$\begin{aligned}&-\int_{\partial\mathcal{B}^f}\left(1-\bar\beta\right)\left[-\beta_t\left(1-\bar\beta\right)\int_{\partial\mathcal{B}^f}\boldsymbol{n}_t^f\cdot\Delta\boldsymbol{u}^f d\xi^1d\xi^2\right]\boldsymbol{n}_t^f\cdot\delta\boldsymbol{u}^f\;d\xi^1d\xi^2\\ &-\int_{\partial\mathcal{B}^f}\left(1-\bar\beta\right)\left[-\beta_t\bar\alpha\int_{\partial\mathcal{B}^g}\boldsymbol{n}_t^g\cdot\Delta\boldsymbol{u}^g d\xi^1d\xi^2\right]\boldsymbol{n}_t^f\cdot\delta\boldsymbol{u}^f\;d\xi^1d\xi^2\end{aligned}$$

- *virtual work due to gas volume compression:* $-\bar\beta\Delta p^{kg}\delta v^f$

$$\begin{aligned}&-\int_{\partial\mathcal{B}^f}\bar\beta\left[-\alpha_t\left(1-\bar\alpha\right)\int_{\partial\mathcal{B}^g}\boldsymbol{n}_t^g\cdot\Delta\boldsymbol{u}^g d\xi^1d\xi^2\right]\boldsymbol{n}_t^f\cdot\delta\boldsymbol{u}^f\;d\xi^1d\xi^2\\ &-\int_{\partial\mathcal{B}^f}\bar\beta\left[-\alpha_t\bar\beta\int_{\partial\mathcal{B}^f}\boldsymbol{n}_t^f\cdot\Delta\boldsymbol{u}^f d\xi^1d\xi^2\right]\boldsymbol{n}_t^f\cdot\delta\boldsymbol{u}^f\;d\xi^1d\xi^2\end{aligned}$$

• *gravitational part at the fluid level:* $\bar{\beta}\Delta p^o \delta v^f$

$$+\int_{\partial\mathcal{B}^f}\left[\bar{\beta}\left(-\frac{p_t^o}{\bar{v}_t^f}\left(1-\bar{\beta}\right)+\gamma_t\bar{\beta}\right)\int_{\partial\mathcal{B}^f}\boldsymbol{n}_t^f\cdot\Delta\boldsymbol{u}^f d\xi^1 d\xi^2\right]\boldsymbol{n}_t^f\cdot\delta\boldsymbol{u}^f\ d\xi^1 d\xi^2$$
$$-\int_{\partial\mathcal{B}^f}\left[\bar{\beta}\bar{\alpha}\left(\gamma_t+\frac{p_t^o}{\bar{v}_t^f}\right)\int_{\partial\mathcal{B}^g}\boldsymbol{n}_t^g\cdot\Delta\boldsymbol{u}^g d\xi^1 d\xi^2\right]\boldsymbol{n}_t^f\cdot\delta\boldsymbol{u}^f\ d\xi^1 d\xi^2$$

• *gravitational part:* $-\Delta\left(\rho\boldsymbol{g}\cdot\delta\boldsymbol{s}^f\right)$ *(without term* $\rho_t\boldsymbol{g}\cdot\Delta\boldsymbol{u}$*)*

$$-\int_{\partial\mathcal{B}^f}\left[-\frac{p_t^x}{\bar{v}_t^f}\left(1-\bar{\beta}\right)\int_{\partial\mathcal{B}^f}\boldsymbol{n}_t^f\cdot\Delta\boldsymbol{u}^f d\xi^1 d\xi^2\right]\boldsymbol{n}_t^f\cdot\delta\boldsymbol{u}^f\ d\xi^1 d\xi^2$$
$$-\int_{\partial\mathcal{B}^f}\left[-\frac{p_t^x}{\bar{v}_t^f}\bar{\alpha}\int_{\partial\mathcal{B}^g}\boldsymbol{n}_t^g\cdot\Delta\boldsymbol{u}^g d\xi^1 d\xi^2\right]\boldsymbol{n}_t^f\cdot\delta\boldsymbol{u}^f\ d\xi^1 d\xi^2 \tag{3.118}$$

Coupling part computed over $\partial\mathcal{B}^g$

$$D\delta\mathcal{L}_g^{\Delta p}(\boldsymbol{x}_t)[\boldsymbol{u}] \ =$$

• *gravitational part in the center of gravity of the fluid:* $\bar{\alpha}\Delta p^c \delta v^g$

$$\int_{\partial\mathcal{B}^g}\bar{\alpha}\left[\frac{1}{\bar{v}_t^f}\int_{\partial\mathcal{B}^f}\left[-2p_t^c\left(1-\bar{\beta}\right)-p_t^o\bar{\beta}+p_t^x\right]\boldsymbol{n}_t^f\cdot\Delta\boldsymbol{u}^f d\xi^1 d\xi^2\right]\boldsymbol{n}_t^g\cdot\delta\boldsymbol{u}^g\ d\xi^1 d\xi^2$$
$$+\int_{\partial\mathcal{B}^g}\bar{\alpha}\left[\frac{1}{\bar{v}_t^f}\int_{\partial\mathcal{B}^g}\bar{\alpha}\left(p_t^o-2p_t^c\right)\boldsymbol{n}_t^g\cdot\Delta\boldsymbol{u}^g d\xi^1 d\xi^2\right]\boldsymbol{n}_t^g\cdot\delta\boldsymbol{u}^g\ d\xi^1 d\xi^2$$

• *gravitational part:* $-\bar{\alpha}\Delta p^o \delta v^g$

$$-\int_{\partial\mathcal{B}^g}\bar{\alpha}\left[\left(-\frac{p_t^o}{\bar{v}_t^f}\left(1-\bar{\beta}\right)+\gamma_t\bar{\beta}\right)\int_{\partial\mathcal{B}^f}\boldsymbol{n}_t^f\cdot\Delta\boldsymbol{u}^f d\xi^1 d\xi^2\right]\boldsymbol{n}_t^g\cdot\delta\boldsymbol{u}^g\ d\xi^1 d\xi^2$$
$$\int_{\partial\mathcal{B}^g}\bar{\alpha}\left[\bar{\alpha}\left(\gamma_t+\frac{p_t^o}{\bar{v}_t^f}\right)\int_{\partial\mathcal{B}^g}\boldsymbol{n}_t^g\cdot\Delta\boldsymbol{u}^g d\xi^1 d\xi^2\right]\boldsymbol{n}_t^g\cdot\delta\boldsymbol{u}^g\ d\xi^1 d\xi^2$$

• *virtual work due to gas volume compression:* $-(1-\bar{\alpha})\Delta p^{kg}\delta v^g$

$$
\begin{aligned}
&-\int_{\partial\mathcal{B}^g}(1-\bar{\alpha})\left[-\alpha_t(1-\bar{\alpha})\int_{\partial\mathcal{B}^g}\boldsymbol{n}_t^g\cdot\Delta\boldsymbol{u}^g d\xi^1 d\xi^2\right]\boldsymbol{n}_t^g\cdot\delta\boldsymbol{u}^g\; d\xi^1 d\xi^2\\
&-\int_{\partial\mathcal{B}^g}(1-\bar{\alpha})\left[-\alpha_t\bar{\beta}\int_{\partial\mathcal{B}^f}\boldsymbol{n}_t^f\cdot\Delta\boldsymbol{u}^f d\xi^1 d\xi^2\right]\boldsymbol{n}_t^g\cdot\delta\boldsymbol{u}^g\; d\xi^1 d\xi^2
\end{aligned}
$$

• *virtual work due to fluid volume compression:* $-\bar{\alpha}\Delta p^{kf}\delta v^g$

$$
\begin{aligned}
&-\int_{\partial\mathcal{B}^g}\bar{\alpha}\left[-\beta_t\left(1-\bar{\beta}\right)\int_{\partial\mathcal{B}^f}\boldsymbol{n}_t^f\cdot\Delta\boldsymbol{u}^f d\xi^1 d\xi^2\right]\boldsymbol{n}_t^g\cdot\delta\boldsymbol{u}^g\; d\xi^1 d\xi^2\\
&-\int_{\partial\mathcal{B}^g}\bar{\alpha}\left[-\beta_t\bar{\alpha}\int_{\partial\mathcal{B}^g}\boldsymbol{n}_t^g\cdot\Delta\boldsymbol{u}^g d\xi^1 d\xi^2\right]\boldsymbol{n}_t^g\cdot\delta\boldsymbol{u}^g\; d\xi^1 d\xi^2
\end{aligned}
\tag{3.119}
$$

Normal change part computed over $\partial\mathcal{B}^g$

$$
\begin{aligned}
D\delta\mathcal{E}_g^{\Delta n}(\boldsymbol{x}_t)[\boldsymbol{u}] \;=\;& \\
&\frac{1}{2}\int_{\partial\mathcal{B}^g}p_t^g\begin{pmatrix}\delta\boldsymbol{u}^g\\ \delta\boldsymbol{u}^g_{,1}\\ \delta\boldsymbol{u}^g_{,2}\end{pmatrix}\cdot\begin{pmatrix}\mathbf{0} & \widehat{\boldsymbol{W}}^{\xi_1} & \widehat{\boldsymbol{W}}^{\xi_2}\\ \widehat{\boldsymbol{W}}^{\xi_1 T} & \mathbf{0} & \mathbf{0}\\ \widehat{\boldsymbol{W}}^{\xi_2 T} & \mathbf{0} & \mathbf{0}\end{pmatrix}\begin{pmatrix}\Delta\boldsymbol{u}^g\\ \Delta\boldsymbol{u}^g_{,1}\\ \Delta\boldsymbol{u}^g_{,2}\end{pmatrix}\; d\xi^1 d\xi^2
\end{aligned}
\tag{3.120}
$$

Normal change part computed over $\partial\mathcal{B}^f$

The virtual work of the incremental pressure change $\Delta p^x = \rho_t\boldsymbol{g}\cdot\Delta\boldsymbol{u}$, taken from the gravitational part $-\Delta\left(\rho\boldsymbol{g}\cdot\delta\boldsymbol{s}^f\right)$, is added here. This leads to an elimination of all skew symmetric parts and only a symmetric part remains as essentially demanded by the conservativeness of the problem.

$$
\begin{aligned}
D\delta\mathcal{E}_f^{\Delta n}(\boldsymbol{x}_t)[\boldsymbol{u}] \;=\;& \frac{1}{2}\int_{\partial\mathcal{B}^f}p_t^f\begin{pmatrix}\delta\boldsymbol{u}^f\\ \delta\boldsymbol{u}^f_{,1}\\ \delta\boldsymbol{u}^f_{,2}\end{pmatrix}\cdot\begin{pmatrix}\mathbf{0} & \widehat{\boldsymbol{W}}^{\xi_1} & \widehat{\boldsymbol{W}}^{\xi_2}\\ \widehat{\boldsymbol{W}}^{\xi_1 T} & \mathbf{0} & \mathbf{0}\\ \widehat{\boldsymbol{W}}^{\xi_2 T} & \mathbf{0} & \mathbf{0}\end{pmatrix}\begin{pmatrix}\Delta\boldsymbol{u}^f\\ \Delta\boldsymbol{u}^f_{,1}\\ \Delta\boldsymbol{u}^f_{,2}\end{pmatrix}\; d\xi^1 d\xi^2\\
&-\frac{\rho_t}{2}\int_{\partial\mathcal{B}^f}\delta\boldsymbol{u}^f\cdot\left(\boldsymbol{n}_t^f\otimes\boldsymbol{g}+\boldsymbol{g}\otimes\boldsymbol{n}_t^f\right)\Delta\boldsymbol{u}^f\; d\xi^1 d\xi^2
\end{aligned}
\tag{3.121}
$$

Thus for the linearization of the virtual fluid and gas potentials follows:

$$\begin{aligned}\delta\mathcal{E}(\boldsymbol{x}_t+\Delta\boldsymbol{u}) &= \int_{\mathcal{B}_0}\boldsymbol{S}(\boldsymbol{x}_t):\delta\boldsymbol{E}(\boldsymbol{x}_t)dV+\delta\mathcal{E}_{f\cup g}(\boldsymbol{x}_t)\\ &\quad+\int_{\mathcal{B}_0}\left(D\boldsymbol{E}(\boldsymbol{x}_t)[\boldsymbol{u}]:\mathbb{C}:\delta\boldsymbol{E}(\boldsymbol{x}_t)+\boldsymbol{S}(\boldsymbol{x}_t):D\delta\boldsymbol{E}(\boldsymbol{x}_t)[\boldsymbol{u}]\right)dV\\ &\quad+D\delta\mathcal{E}_f^{\Delta p}(\boldsymbol{x}_t)[\boldsymbol{u}]+D\delta\mathcal{E}_f^{\Delta n}(\boldsymbol{x}_t)[\boldsymbol{u}]\\ &\quad+D\delta\mathcal{E}_g^{\Delta p}(\boldsymbol{x}_t)[\boldsymbol{u}]+D\delta\mathcal{E}_g^{\Delta n}(\boldsymbol{x}_t)[\boldsymbol{u}]\ .\end{aligned}\tag{3.122}$$

The symmetry of this expression emerges even more clearly after a finite element discretization of the domains and a subsequent substitution of the integrals by coupling vectors, which i.a. will be part of the next section. The bilinear form (3.122) features the relation

$$\delta\mathcal{E}(\delta\boldsymbol{u},\Delta\boldsymbol{u})=\delta\mathcal{E}(\Delta\boldsymbol{u},\delta\boldsymbol{u})\tag{3.123}$$

and thus forms a selfadjoint problem. This shows, that a conservative problem is described, as already stated by SEWELL[91], PEARSON[71] and BUFLER[17],[18],[19]. SCHWEIZERHOF&RAMM[90] and also RUMPEL[78] showed that for deformation dependent loadings, which have been derived from a potential, the application of physically realistic boundary conditions is essential to achieve the selfadjoint bilinear form (3.123).

Chapter 4

The finite element method

The finite element method, as a numerical approach for the solution of most elliptic partial differential equations with boundary conditions both in the target function and in its derivatives, is nowadays a common tool. The unknown target function is assembled by a series of finite functions defined in disjoint regions. The solution space is limited in such a way, that by defining an approximation of the target function only an algebraic boundary value problem has to be solved instead of a continuous one. More detailed information about this topic can be found in the standard literature as e.g. Zienkiewicz&Taylor[114], Hughes[42] *or* Wriggers[112]. *The focus of this chapter is on the discretization of the equations derived so far for the entire domain, using an interpolation for the displacements and the geometry. Finally, all element matrices, necessary for a finite element implementation of the discussed fluid-structure interaction algorithms, are given, followed by a brief overview of the assembly of the system matrix in case of multiple interacting fluid or gas filled control volumes. A particular solution scheme for equations of this kind will be presented in chapter 6.*

4.1 Basics

In order to solve the previously derived continuous thermodynamical boundary value problem (3.122) numerically, in a first step the entire domain $\mathcal{B}$ with its boundaries $\partial\mathcal{B}_f$ and $\partial\mathcal{B}_g$ is covered with a discrete number of subdomains Ω_e, called finite elements (see also figure 4.1). According to the interpolation rule

$$\mathcal{B}_0 \approx \mathcal{B}_0^h = \bigcup_{e=1}^{nel} \Omega_e \ , \quad \text{with} \quad \Omega_i \cap \Omega_j = \emptyset \quad \forall \quad \Omega_i \neq \Omega_j \tag{4.1}$$

the initial configuration $\mathcal{B}_0$ is approximated by a domain $\mathcal{B}_0^h$. For a more efficient handling of the tensors (bold face), in this chapter the transition to matrices (underlined) is made. In the next step the solution space $\mathcal{S}$ containing the target function $\underline{u}$ is restricted to a subspace $\mathcal{S}^h \subset \mathcal{S}$ by specification of an interpolation rule $\underline{N}(\underline{\xi})$, which is

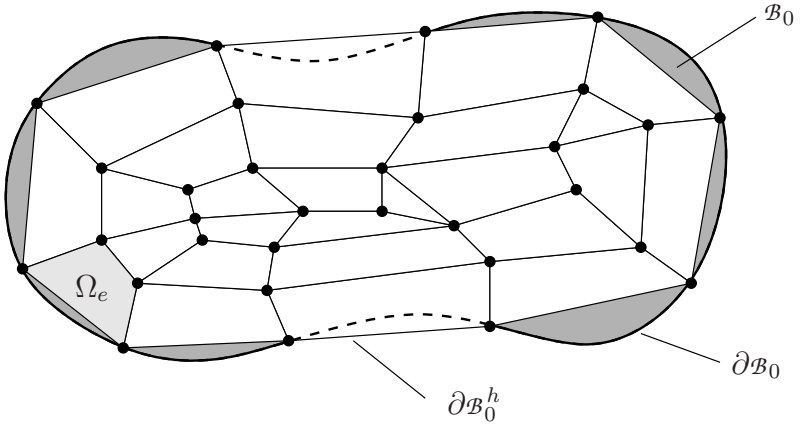

Figure 4.1: Discretization of the solid domain $\mathcal{B}$

defined element-wise and in the local coordinates $\underline{\xi}$ of a reference configuration $\Omega_\square$.

$$\underline{u}_e \approx \underline{u}_e^h(\underline{\xi}) = \underline{N}(\underline{\xi})\underline{d}_e \tag{4.2}$$

Analogously the incremental change $\Delta\underline{u}_e$ of the displacements can be approximated.

$$\Delta\underline{u}_e \approx \Delta\underline{u}_e^h(\underline{\xi}) = \underline{N}(\underline{\xi})\Delta\underline{d}_e \tag{4.3}$$

Although this procedure means a severe limitation of the solution space, instead of finding a continuous solution $\underline{u}$ only a discrete number of unknown nodal values $\underline{d}_e$, resp. $\Delta\underline{d}_e$ have to be found. Thus equation (3.122) has been transformed in an algebraic equation system, which can be solved numerically. Usually the weighting function $\delta\underline{u}$ is interpolated with (4.2) as well, leading to symmetric element matrices.

$$\delta\underline{u}_e \approx \delta\underline{u}_e^h(\underline{\xi}) = \underline{N}(\underline{\xi})\delta\underline{d}_e \tag{4.4}$$

It can be easily shown that the solution obtained by the Galerkin finite element method is the best solution contained in the solution space $\mathcal{S}^h$ and that the spatial discretization error $\underline{e}^h = \underline{u} - \underline{u}^h$ tends to zero for further mesh refinement, see e.g. HUGHES[42].

4.2 Discretization

4.2.1 Discretization of the geometry

For the approximation of the geometry mentioned in equation (4.1) the isoparametric concept, interpolating both the displacements and the geometry with the same functions, has been established within the finite element method. Using the nodal coordinates $\hat{\underline{X}}_e$, the position vector to an arbitrary point of the finite element Ω_e can be given (see also figure 4.2).

$$\underline{X}_e \approx \underline{X}_e^h(\underline{\xi}) = \underline{N}(\underline{\xi})\hat{\underline{X}}_e \tag{4.5}$$

In the same manner as the deformation gradient $\boldsymbol{F}$ maps the differential vector $d\boldsymbol{X}$ from the initial to the current configuration, the coordinate transformation from the reference configuration $\Omega_\square$ to the initial configuration Ω_e is performed using the Jacobian matrix $\underline{J}$.

$$d\underline{X}_e^h = \underline{J} d\underline{\xi} \ , \quad \text{with} \quad \underline{J} = \frac{\partial \underline{X}_e^h}{\partial \underline{\xi}} \tag{4.6}$$

$\underline{J}$ maps a vector $d\underline{\xi}$ of the reference configuration $\Omega_\square$ in the vector $d\underline{X}_e^h$ of the initial configuration. With the previous discretizations of geometry and displacements the finite element formulations of a geometric nonlinear membrane (see e.g. also GRUTTMANN[36] and BONET ET AL.[15]) and of a geometric nonlinear solid shell HAUPTMANN[41] will be discussed.

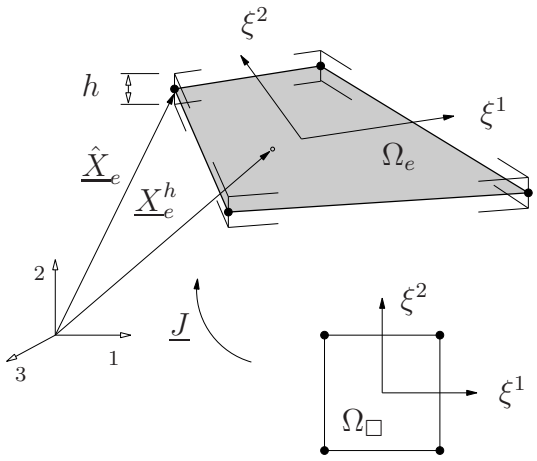

Figure 4.2: Reference configuration $\Omega_\square$ and initial configuration Ω_e of a bilinear membrane element

4.2.2 Discretization of the kinematics

First the discretizations of the covariant base vectors are given:

$$\underline{G}_\alpha \approx \frac{\partial \underline{X}_e^h}{\partial \xi^\alpha} = \underline{N}_{,\alpha} \hat{\underline{X}}_e \quad \text{and} \quad \underline{g}_\alpha \approx \frac{\partial (\underline{X}_e^h + \underline{u}_e^h)}{\partial \xi^\alpha} = \underline{G}_\alpha + \underline{N}_{,\alpha} \underline{d}_e \tag{4.7}$$

Inserting equations (4.4) and (4.7b) in equation (1.18) yields the discretized Green strain tensor $\boldsymbol{E}$, with its coordinates assembled in a matrix for reasons of more convenient programming[1].

$$E_{\alpha\beta} \approx \frac{1}{2} \left(\underline{G}_\alpha^T \underline{N}_{,\beta} + \underline{G}_\beta^T \underline{N}_{,\alpha} + \underline{d}_e^T \underline{N}_{,\alpha}^T \underline{N}_{,\beta} \right) \underline{d}_e \tag{4.8}$$

[1]From this point on it has to be kept in mind that the coordinates of $\boldsymbol{E}$ are given in a contravariant basis $\boldsymbol{G}^\alpha \otimes \boldsymbol{G}^\beta$, because assembling these coordinates in a matrix $\underline{E}$ implies the loss of the information about their basis.

In a similar fashion using equation (3.8) yields the discretized form of the first variation of the Green strain tensor

$$\delta E_{\alpha\beta} \approx \frac{1}{2}\left[\underline{G}_\beta^T \underline{N}_{,\alpha} + \underline{G}_\alpha^T \underline{N}_{,\beta} + \underline{d}_e^T \left(\underline{N}_{,\alpha}^T \underline{N}_{,\beta} + \underline{N}_{,\beta}^T \underline{N}_{,\alpha}\right)\right] \delta \underline{d}_e^T \ , \tag{4.9}$$

respectively the discretized form of its linearization.

$$\Delta E_{\alpha\beta} \approx \frac{1}{2}\left[\underline{G}_\beta^T \underline{N}_{,\alpha} + \underline{G}_\alpha^T \underline{N}_{,\beta} + \underline{d}_e^T \left(\underline{N}_{,\alpha}^T \underline{N}_{,\beta} + \underline{N}_{,\beta}^T \underline{N}_{,\alpha}\right)\right] \Delta \underline{d}_e^T \tag{4.10}$$

Equation (3.86) then leads to the discretized form of the linearized first variation of the Green strain tensor.

$$\Delta\delta E_{\alpha\beta} \approx \frac{1}{2} \delta \underline{d}_e^T \left(\underline{N}_{,\alpha}^T \underline{N}_{,\beta} + \underline{N}_{,\beta}^T \underline{N}_{,\alpha}\right) \Delta \underline{d}_e \tag{4.11}$$

Besides the strains, the contravariant coordinates $S^{\alpha\beta}$ of the second Piola-Kirchhoff stress tensor $\boldsymbol{S}$ are assembled in a matrix as well. This coordinate matrix $\underline{S}$ is obtained using the fourth order material matrix containing the coordinates of the material tensor $\mathbb{C}$ and the previously given matrix $\underline{E}$.

$$S^{\alpha\beta} \approx \mathbb{C}^{\alpha\beta\gamma\delta} E_{\gamma\delta} \tag{4.12}$$

For reasons of simplicity the matrices[2]

$$\underline{B}_{\alpha\beta} = \frac{1}{2}\left(\underline{G}_\beta^T \underline{N}_{,\alpha} + \underline{G}_\alpha^T \underline{N}_{,\beta}\right) \quad \text{and} \quad \underline{H}_{\alpha\beta} = \frac{1}{2} \underline{N}_{,\alpha}^T \underline{N}_{,\beta} \tag{4.13}$$

can be used to write the strains (4.8)-(4.11) and thus also the stresses (4.12) in a more compact form:

$$\underline{E} \approx \left(\underline{B} + \underline{d}_e^T \underline{H}\right) \underline{d}_e \ , \tag{4.14}$$

$$\underline{S} \approx \underline{\mathbb{C}} \left(\underline{B} + \underline{d}_e^T \underline{H}\right) \underline{d}_e \ , \tag{4.15}$$

$$\delta\underline{E} \approx \left(\underline{B} + \underline{d}_e^T (\underline{H} + \underline{H}^T)\right) \delta \underline{d}_e \ , \tag{4.16}$$

$$\Delta\underline{E} \approx \left(\underline{B} + \underline{d}_e^T (\underline{H} + \underline{H}^T)\right) \Delta \underline{d}_e \quad \text{and} \tag{4.17}$$

$$\Delta\delta E_{\alpha\beta} \approx \underline{d}_e^T (\underline{H} + \underline{H}^T) \Delta \underline{d}_e \ . \tag{4.18}$$

The tangent stiffness matrix $\underline{K}_e^{el}$, arising from the linearized first variation of the elastic potential

$$D\delta\mathfrak{E}_{el}(\underline{x}_t)[\underline{u}] \approx \delta \underline{d}_e^T \underline{K}_e^{el} \Delta \underline{d}_e \tag{4.19}$$

of a finite element Ω_e, thus yields

$$\underline{K}_e^{el} = \int_{\Omega_e} \left(\underline{B} + \underline{d}_e^T (\underline{H} + \underline{H}^T)\right)^T \underline{\mathbb{C}} \left(\underline{B} + \underline{d}_e^T (\underline{H} + \underline{H}^T)\right) + (\underline{H} + \underline{H}^T) \underline{S} \ d\Omega_e \ . \tag{4.20}$$

[2]Since the matrix $\underline{H}$ is obtained by derivation of the strains $\underline{E}$ in direction of the incremental displacements a fourth order matrix is produced.

Using equations (4.15) and (4.16) along with the vector

$$\underline{f}_e^{el} = \int_{\Omega_e} \underline{S}\left(\underline{B} + \underline{d}_e^T(\underline{H} + \underline{H}^T)\right)^T \underline{d}_e^T \, d\Omega_e \tag{4.21}$$

of the internal residual forces, the elastic residual energy $\delta\mathcal{E}_{el}(\underline{x}_t)$ can be given as

$$\delta\mathcal{E}_{el}(\underline{x}_t) \approx \delta\underline{d}_e^T \underline{f}_e^{el} \ . \tag{4.22}$$

The integration over the domain Ω_e is performed with a Gauß quadrature in the reference configuration $\Omega_\square$. The transformation of the differential $d\Omega_e$ to $d\square$ is achieved by scaling $d\square$ with the determinant of the Jacobian matrix $\det \underline{J}$.

$$d\Omega_e = \det \underline{J} \, d\square \tag{4.23}$$

4.2.3 Discretization of the fluid and gas parts

For the discretization of the pressure change terms $D\delta\mathcal{E}_{f\cup g}^{\Delta p}(\underline{x}_t)[\underline{u}]$ from equations (3.118) and (3.119), the following coupling vectors are introduced on element level.

$$\underline{a}_e = \int_{\square^g} \underline{N}^T \underline{n}_t^g \, d\square \qquad \text{(for element surfaces wetted with gas)} \tag{4.24}$$

$$\underline{b}_e = \int_{\square^f} \underline{N}^T \underline{n}_t^f \, d\square \qquad \text{(for element surfaces wetted with fluid)} \tag{4.25}$$

$$\underline{c}_e = \int_{\square^f} p_t^x \underline{N}^T \underline{n}_t^f \, d\square \qquad \text{(for element surfaces wetted with heavy fluid)} \tag{4.26}$$

Additionally the following pressure volume gradients are used:

$$\begin{aligned} C_1 &= \frac{1-\bar\beta}{\bar v_t^f}\left[-2p_t^c\left(1-\bar\beta\right) - p_t^o\bar\beta\right] + \beta_t\left(1-\bar\beta\right)^2 + \bar\beta^2\alpha_t \\ &\quad +\bar\beta\left(-\frac{p_t^o}{\bar v_t^f}\left(1-\bar\beta\right) + \gamma_t\bar\beta\right) \ , \end{aligned} \tag{4.27}$$

$$C_2 = \frac{1-\bar\beta}{\bar v_t^f} \ , \tag{4.28}$$

$$C_3 = \frac{\bar\alpha^2}{\bar v_t^f}\left(p_t^o - 2p_t^c\right) + \bar\alpha^2\left(\gamma_t + \frac{p_t^o}{\bar v_t^f}\right) + \alpha_t\left(1-\bar\alpha\right)^2 + \bar\alpha^2\beta_t \ , \tag{4.29}$$

$$C_4 = \frac{\bar\alpha}{\bar v_t^f} \quad \text{and} \tag{4.30}$$

$$C_5 = \frac{1-\bar\beta}{\bar v_t^f}\bar\alpha\left(p_t^o - 2p_t^c\right) + \left(1-\bar\beta\right)\beta_t\bar\alpha + \bar\beta\alpha_t\left(1-\bar\alpha\right) - \bar\beta\bar\alpha\left(\gamma_t + \frac{p_t^o}{\bar v_t^f}\right) \ . \tag{4.31}$$

Using the previous simplifications along with the usually fully occupied coupling matrix

$$\begin{aligned}\underline{K}_e^{Cpl} &= C_1\underline{b}_e\underline{b}_e^T + C_2\left(\underline{b}_e\underline{c}_e^T + \underline{c}_e\underline{b}_e^T\right) + C_3\underline{a}_e\underline{a}_e^T \\ &\quad + C_4\left(\underline{a}_e\underline{c}_e^T + \underline{c}_e\underline{a}_e^T\right) + C_5\left(\underline{b}_e\underline{a}_e^T + \underline{a}_e\underline{b}_e^T\right) \ , \end{aligned} \tag{4.32}$$

the discretization of the pressure change terms can be given.

$$D\delta\mathcal{E}_{f\cup g}^{\Delta p}(\underline{x}_t)[\underline{u}] \approx \delta\underline{d}_e^T\underline{K}_e^{Cpl}\Delta\underline{d}_e \tag{4.33}$$

With the discretization of the normal change parts from equations (3.120) and (3.121) the so-called load stiffness matrices are obtained

$$\underline{K}_e^g = \frac{1}{2}\int_{\square^g} p_t^g \begin{pmatrix} \underline{N} \\ \underline{N}_{,1} \\ \underline{N}_{,2} \end{pmatrix}^T \begin{pmatrix} \underline{0} & \underline{W}^{\xi_1} & \underline{W}^{\xi_2} \\ \underline{W}^{\xi_1 T} & \underline{0} & \underline{0} \\ \underline{W}^{\xi_2 T} & \underline{0} & \underline{0} \end{pmatrix} \begin{pmatrix} \underline{N} \\ \underline{N}_{,1} \\ \underline{N}_{,2} \end{pmatrix} d\square \quad \text{and} \tag{4.34}$$

$$\begin{aligned}\underline{K}_e^f &= \frac{1}{2}\int_{\square^f} p_t^f \begin{pmatrix} \underline{N} \\ \underline{N}_{,1} \\ \underline{N}_{,2} \end{pmatrix}^T \begin{pmatrix} \underline{0} & \underline{W}^{\xi_1} & \underline{W}^{\xi_2} \\ \underline{W}^{\xi_1 T} & \underline{0} & \underline{0} \\ \underline{W}^{\xi_2 T} & \underline{0} & \underline{0} \end{pmatrix} \begin{pmatrix} \underline{N} \\ \underline{N}_{,1} \\ \underline{N}_{,2} \end{pmatrix} d\square \\ &\quad -\frac{\rho_t}{2}\int_{\square^f} \underline{N}^T\left(\underline{n}_t^f \otimes \underline{g} + \underline{g} \otimes \underline{n}_t^f\right)\underline{N}\ d\square \ , \end{aligned} \tag{4.35}$$

and the linearized energy expression becomes:

$$D\delta\mathcal{E}_{f\cup g}^{\Delta n}(\underline{x}_t)[\underline{u}] \approx \delta\underline{d}_e^T\left(\underline{K}_e^g + \underline{K}_e^f\right)\Delta\underline{d}_e \ . \tag{4.36}$$

Using the load vectors

$$\underline{f}_e^g = \int_{\square^g}\left[\bar{\alpha}\left(p_t^c - p_t^o\right) - (1-\bar{\alpha})p_t^{kg} - \bar{\alpha}p_t^{kf}\right]\underline{N}^T\underline{n}_t^g\ d\square \quad \text{and} \tag{4.37}$$

$$\underline{f}_e^f = \int_{\square^f}\left[\left(1-\bar{\beta}\right)p_t^c - (1-\bar{\beta})p_t^{kf} - \bar{\beta}p_t^{kg} + \bar{\beta}p_t^o - p_t^x\right]\underline{N}^T\underline{n}_t^f\ d\square \tag{4.38}$$

finally gives the residual of the linearized first variation of the fluid and gas potential energy.

$$\delta\mathcal{E}_{f\cup g}(\underline{x}_t) \approx \delta\underline{d}_e^T\left(\underline{f}_e^g + \underline{f}_e^f\right) \tag{4.39}$$

Summarizing the previous derivations, the linearized state of equilibrium of a finite element becomes:

$$D\delta\mathcal{E}_{el}(\underline{x}_t)[\underline{u}] + D\delta\mathcal{E}_{f\cup g}^{\Delta p}(\underline{x}_t)[\underline{u}] + D\delta\mathcal{E}_{f\cup g}^{\Delta n}(\underline{x}_t)[\underline{u}] = \delta\mathcal{A}_{ext}^* - \delta\mathcal{E}_{f\cup g}(\underline{x}_t) - \delta\mathcal{E}_{el}(\underline{x}_t) \tag{4.40}$$

Inserting the element matrices from above results in:

$$\delta \underline{d}_e^T \left(\underline{K}_e^{el} + \underline{K}_e^g + \underline{K}_e^f + \underline{K}_e^{Cpl} \right) \Delta \underline{d}_e = \delta \underline{d}_e^T \left(\underline{f}_e^{ext} - \underline{f}_e^{el} - \underline{f}_e^g - \underline{f}_e^f \right) \ . \tag{4.41}$$

The global matrices and vectors are obtained by assembling all nel elements using e.g. the so-called direct stiffness method. Thus the global stiffness matrix follows as

$$\underline{K} = \bigcup_{e=1}^{nel} \left(\underline{K}_e^{el} + \underline{K}_e^g + \underline{K}_e^f + \underline{K}_e^{Cpl} \right) \tag{4.42}$$

and the global right-hand side vector as

$$\underline{f} = \bigcup_{e=1}^{nel} \left(\underline{f}_e^{ext} - \underline{f}_e^{el} - \underline{f}_e^g - \underline{f}_e^f \right) \ . \tag{4.43}$$

After implementing the Dirichlet boundary conditions and eliminating the virtual nodal displacements, for the determination of the incremental nodal displacements $\Delta \underline{d}$ the following linearized equation system has to be solved:

$$\underline{K} \Delta \underline{d} = \underline{f} \tag{4.44}$$

The matrices $\underline{K}_e^g$ and $\underline{K}_e^f$ simply led to extensions of the standard element matrices on the degrees of freedom associated to the surfaces wetted by gas or fluid. However, as already mentioned, the coupling of the pressure loading and the current geometry of the structure leads to an almost fully occupied global coupling matrix $\underline{K}^{Cpl}$ and thus to a considerable additional numerical effort, compared to a standard structure without gas or fluid filling. However, the special structure of $\underline{K}^{Cpl}$, a sum of rank-one-updates, can be exploited for establishing a more efficient solution scheme, which will be part of chapter 6.1.

4.2.4 Hybrid approach

It is not mandatory to derive a totally displacement dependent weak form as it was done in (3.122) respectively in (4.41). An alternative can be found in a hybrid approach, for which the increments Δp^{kg}, Δp^{kf}, Δp^c, Δp^o and Δp^x resp. $\Delta \rho$ in equation (3.88) and (3.89) can be taken as additional hybrid unknowns. Hence, with the coupling vectors (4.24), (4.25) and (4.26) the constraint equations (3.101), (3.102), (3.105), (3.109) and (3.110) for the hybrid unknowns can be rewritten:

$$-\frac{1}{\alpha_t} \Delta p^{kg} - \underline{\hat{a}} \cdot \Delta \underline{d} = 0 \ , \quad \text{with} \quad \underline{\hat{a}} = \left((1 - \bar{\alpha}) \, \underline{a} + \bar{\beta} \underline{b} \right) \ , \tag{4.45}$$

$$-\frac{1}{\beta_t} \Delta p^{kf} - \underline{\hat{b}} \cdot \Delta \underline{d} = 0 \ , \quad \text{with} \quad \underline{\hat{b}} = \left(\left(1 - \bar{\beta} \right) \underline{b} + \bar{\alpha} \underline{a} \right) \ , \tag{4.46}$$

$$-\frac{1}{\gamma_t} \Delta p^o + \frac{p_t^o}{\gamma_t} \frac{\Delta \rho}{\rho_t} - \left(\bar{\alpha} \underline{a} - \bar{\beta} \underline{b} \right) \cdot \Delta \underline{d} = 0 \quad \text{and} \tag{4.47}$$

$$\bar{v}_t^f \Delta p^c - 2p_t^c \bar{v}_t^f \frac{\Delta\rho}{\rho_t} - p_t^o \left(\bar{\alpha}\underline{a} - \bar{\beta}\underline{b}\right) \cdot \Delta\underline{d} - \underline{c} \cdot \Delta\underline{d} = 0 \ . \tag{4.48}$$

Substituting (4.47) in (4.48) leads to

$$\bar{v}_t^f \Delta p^c - \left(2p_t^c \bar{v}_t^f + \frac{p_t^{o2}}{\gamma_t}\right) \frac{\Delta\rho}{\rho_t} + \frac{p_t^o}{\gamma_t} \Delta p^o - \underline{c} \cdot \Delta\underline{d} = 0 \tag{4.49}$$

and

$$\Delta p^x = p_t^x \frac{\Delta\rho}{\rho_t} + \rho_t \underline{g} \cdot \underline{N} \Delta\underline{d} \ , \tag{4.50}$$

$$\frac{\Delta\rho}{\rho_t} = -\frac{1}{\bar{v}^f} \hat{\underline{b}} \cdot \Delta\underline{d} \ . \tag{4.51}$$

With the constraint equations (4.45)-(4.51) and the global arrays (4.42) and (4.43), the linearized state of equilibrium can be written in a hybrid formulation as:

$$\begin{bmatrix} \underline{K} & \hat{\underline{b}} & -\hat{\underline{b}} & -\hat{\underline{a}} & \bar{\beta}\underline{b} - \bar{\alpha}\underline{a} & -\underline{c} \\ \hat{\underline{b}}^T & 0 & 0 & 0 & 0 & \bar{v}_t^f \\ -\hat{\underline{b}}^T & 0 & -\frac{1}{\beta_t} & 0 & 0 & 0 \\ -\hat{\underline{a}}^T & 0 & 0 & -\frac{1}{\alpha_t} & 0 & 0 \\ \bar{\beta}\underline{b}^T - \bar{\alpha}\underline{a}^T & 0 & 0 & 0 & -\frac{1}{\gamma_t} & \frac{p_t^o}{\gamma_t} \\ -\underline{c}^T & \bar{v}_t^f & 0 & 0 & \frac{p_t^o}{\gamma_t} & -\left(2p_t^c \bar{v}_t^f + \frac{p_t^{o2}}{\gamma_t}\right) \end{bmatrix} \begin{bmatrix} \Delta\underline{d} \\ \Delta p^c \\ \Delta p^{kf} \\ \Delta p^{kg} \\ \Delta p^o \\ \frac{\Delta\rho}{\rho_t} \end{bmatrix} = \begin{bmatrix} \underline{f} \\ 0 \\ 0 \\ 0 \\ 0 \\ 0 \end{bmatrix} \tag{4.52}$$

This form gives a particular insight into the symmetric structure of the global matrix and allows also a direct development of a pure displacement form.

4.2.5 Derivation of special load cases

As some specific load cases, which are included in this overall description, have already been described in BONET ET AL.[15] and RUMPEL ET AL.[78], [79], [80] they are only briefly mentioned here in tabular form, see table 4.1 no. 1 to 3, whereas the finite element formulations for the load cases consisting of combinations of fluid and gas loadings are described in the following subsections.

Incompressible heavy fluid with free fluid surface and additional gas loading

To derive this particular load case the stiffness parameters in equation (4.33) have to be set to

$$\bar{\alpha} = 0 \quad \text{and} \quad \bar{\beta} = 1 \ . \tag{4.53}$$

#	load case	arrays/unknowns	stiffness param.
1	pure gas filling	$\underline{K}^f = \underline{0},\ \underline{b} = \underline{c} = \underline{f}^f = \underline{0}$ $\Rightarrow\ \underline{\hat{a}} = \underline{a},\ \underline{\hat{b}} = \underline{0},\ \Delta p^c = \Delta p^{kf} = \Delta p^o = \Delta\rho = 0$	$\bar{\alpha} = 0,\ \bar{\beta} = 1$
2	incompressible heavy fluid with free fluid surface	$\underline{K}^g = \underline{0},\ \underline{a} = \underline{c} = \underline{f}^g = \underline{0},$ $\Rightarrow\ \underline{\hat{a}} = \underline{b},\ \underline{\hat{b}} = \underline{0},\ \Delta p^c = \Delta p^{kf} = \Delta p^{kg} = \Delta\rho = 0$	$\bar{\alpha} = 0,\ \bar{\beta} = 1$
3	compressible heavy fluid without free fluid surface	$\underline{K}^g = \underline{0},\ \underline{a} = \underline{f}^g = \underline{0}$ $\Rightarrow\ \underline{\hat{a}} = \underline{0},\ \underline{\hat{b}} = \underline{b},$ $\Delta p^{kg} = \Delta p^o = 0$	$\bar{\alpha} = 1,\ \bar{\beta} = 0$
4	incompressible heavy fluid with free fluid surface and additional gas loading	$\underline{\hat{a}} = \underline{a} + \underline{b},\ \underline{\hat{b}} = \underline{b},\ \underline{c} = \underline{0},$ $\Delta p^c = \Delta\rho = 0$	$\bar{\alpha} = 0,\ \bar{\beta} = 1$
5	compressible heavy fluid with free fluid surface and additional gas loading	$\Delta p^{kg} = \Delta p^{kf}$	$0 \leq \bar{\alpha} < \bar{\beta} \leq 1$

Table 4.1: Derivation of specific cases with varying contents by adjustment of stiffness parameters $\bar{\alpha}$ and $\bar{\beta}$

The element coupling vectors then become

$$\underline{\hat{a}}_e = \underline{a}_e + \underline{b}_e \quad \text{and} \quad \underline{\hat{b}}_e = \underline{b}_e \tag{4.54}$$

In the case of an incompressible fluid, both the density change $\Delta\rho/\rho$ and the pressure increment Δp^{kf}, resulting from a volume compression, are zero. Therefore, the associated rows and columns 2, 3 and 6 in equation (4.52) can be canceled. Hence, the element coupling matrix consists only of a rank-two-update.

$$\underline{K}_e^{Cpl} = \alpha_t \left(\underline{a}_e + \underline{b}_e\right)\left(\underline{a}_e + \underline{b}_e\right)^T - \gamma_t \underline{b}_e \underline{b}_e^T \tag{4.55}$$

Along with the load vectors

$$\underline{f}_e^g = -\int_{\square^g} p_t^g \underline{N}^T \underline{n}_t^g \; d\square \tag{4.56}$$

and

$$\underline{f}_e^f = \int_{\square^f} \left(p_t^o - p_t^x - p_t^g\right) \underline{N}^T \underline{n}_t^f \; d\square \tag{4.57}$$

the linearized set of equations for an incompressible heavy fluid with a free fluid surface and additional gas loading can be written as:

$$\left(\underline{K}^{el} + \underline{K}^f + \underline{K}^g + \underline{K}^{Cpl}\right) \Delta\underline{d} = \underline{f}^{ext} - \underline{f}^{el} - \underline{f}^f - \underline{f}^g \ . \tag{4.58}$$

Alternatively equation (4.58) can be written in hybrid form:

$$\begin{bmatrix} \underline{K} & -(\underline{a}+\underline{b}) & \underline{b} \\ -(\underline{a}+\underline{b})^T & -\frac{1}{\alpha_t} & 0 \\ \underline{b}^T & 0 & -\frac{1}{\gamma_t} \end{bmatrix} \begin{bmatrix} \Delta\underline{d} \\ \Delta p^{kg} \\ \Delta p^o \end{bmatrix} = \begin{bmatrix} \underline{f} \\ 0 \\ 0 \end{bmatrix} , \tag{4.59}$$

with the complete stiffness matrix as

$$\underline{K} = \underline{K}^{el} + \underline{K}^{f} + \underline{K}^{g} + \underline{K}^{Cpl} \tag{4.60}$$

and the load vector for the structure

$$\underline{f} = \underline{f}^{ext} - \underline{f}^{el} - \underline{f}^{f} - \underline{f}^{g} \ . \tag{4.61}$$

Compressible heavy fluid with free fluid surface and additional gas loading

Although this specific load case is more of academical nature, because the virtual work due to a compression of the gas volume dominates in contrast to a compression of the fluid volume, for the sake of completeness this most general case shall be discussed at this point. Here all terms remain in equation (4.33). Because gas and fluid share a common volume the relation

$$\bar{\beta} = 1 - \bar{\alpha} \tag{4.62}$$

can be used to simplify the constants (4.27)-(4.31). In a next step from equations (4.33) the vectors with identical coefficients can be collected. Introducing the abbreviations

$$\bar{C}_1 = -\bar{\alpha}\alpha_t + \frac{1}{2}\bar{\alpha}^2\left(\alpha_t + \beta_t\right) + \bar{\alpha}^2\frac{p_t^o}{\bar{v}_t^f} + \frac{1}{2}\alpha_t + \frac{1}{2}\bar{\alpha}^2\gamma_t - \bar{\alpha}^2\frac{p_t^c}{\bar{v}_t^f} \ , \tag{4.63}$$

$$\bar{C}_2 = \frac{\bar{\alpha}}{\bar{v}_t^f} \ , \tag{4.64}$$

$$\bar{C}_3 = -\bar{\alpha}\frac{p_t^o}{\bar{v}_t^f} - \gamma_t\left(\bar{\alpha} - \frac{1}{2}\right) \quad \text{and} \tag{4.65}$$

$$\bar{C}_4 = -\bar{\alpha}\left(\gamma_t + \frac{p_t^o}{\bar{v}_t^f}\right) \tag{4.66}$$

we obtain for the volume coupling part

$$\begin{aligned} \underline{K}^{Cpl} \ &= \ 2\bar{C}_1\left(\underline{a}+\underline{b}\right)\left(\underline{a}+\underline{b}\right)^T + \bar{C}_2\left[\left(\underline{a}+\underline{b}\right)\underline{c}^T + \underline{c}\left(\underline{a}+\underline{b}\right)^T\right] \\ &\quad + 2\bar{C}_3\underline{b}\underline{b}^T + \bar{C}_4\left(\underline{a}\underline{b}^T + \underline{b}\underline{a}^T\right) \ . \end{aligned} \tag{4.67}$$

By using the modified coupling vectors

$$\hat{\underline{a}} = \bar{C}_4\underline{a} + \bar{C}_3\underline{b} \ , \quad \hat{\underline{b}} = \underline{a} + \underline{b} \quad \text{and} \quad \hat{\underline{c}} = \left[\bar{C}_1\left(\underline{a}+\underline{b}\right) + \bar{C}_2\underline{c}\right] \tag{4.68}$$

the coupling part $\underline{K}^{Cpl}$ can be further reduced to a rank-4-update.

$$\underline{K}^{Cpl} = \underline{\hat{a}}\underline{b}^T + \underline{b}\underline{\hat{a}}^T + \underline{\hat{c}}\underline{\hat{b}}^T + \underline{\hat{b}}\underline{\hat{c}}^T \tag{4.69}$$

These four rank updates reflect all possible degrees of freedom of the fluid-gas containment: the compression of the gas, the density change of the fluid, the gravitational pressure distribution inside the fluid and the displacement of the free fluid surface. Analogously to (4.41) the linearized set of equations for a compressible heavy fluid with a free fluid surface and additional gas loading can be written as:

$$\left(\underline{K}^{el} + \underline{K}^{f} + \underline{K}^{g} + \underline{K}^{Cpl}\right) \Delta\underline{d} = \underline{f}^{ext} - \underline{f}^{el} - \underline{f}^{f} - \underline{f}^{g} \ . \tag{4.70}$$

The load vectors $\underline{f}^g$ and $\underline{f}^f$ for the structure can be simplified by using $p^{kg} = p^{kf}$ and condition (4.62):

$$\underline{f}^{g} = \int\limits_{\square^g} \left(\bar{\alpha}\left(p_t^c - p_t^o\right) - p_t^{kg}\right) \underline{N}^T \underline{n}_t^g \ d\square \tag{4.71}$$

$$\underline{f}^{f} = \int\limits_{\square^f} \left(\bar{\alpha} p_t^c + \left(1-\bar{\alpha}\right) p_t^o - p_t^x - p_t^{kg}\right) \underline{N}^T \underline{n}_t^f \ d\square \tag{4.72}$$

The linearized set of equations can also be given in a hybrid form as:

$$\begin{bmatrix} \underline{K} & \bar{\alpha}\underline{\hat{a}} & (\bar{\alpha}-1)\underline{\hat{a}} & \underline{b} - \bar{\alpha}\underline{\hat{a}} & -\underline{c} \\ \bar{\alpha}\underline{\hat{a}}^T & 0 & 0 & 0 & \bar{v}_t^f \\ (\bar{\alpha}-1)\underline{\hat{a}}^T & 0 & -\frac{1}{\alpha_t} & 0 & 0 \\ \left(\underline{b} - \bar{\alpha}\underline{\hat{a}}\right)^T & 0 & 0 & -\frac{1}{\gamma_t} & \frac{p_t^o}{\gamma_t} \\ -\underline{c}^T & \bar{v}_t^f & 0 & \frac{p_t^o}{\gamma_t} & -\left(2p_t^c\bar{v}_t^f + \frac{p_t^{o2}}{\gamma_t}\right) \end{bmatrix} \begin{bmatrix} \Delta\underline{d} \\ \Delta p^c \\ \Delta p^{kg} \\ \Delta p^o \\ \frac{\Delta\rho}{\rho_t} \end{bmatrix} = \begin{bmatrix} \underline{f} \\ 0 \\ 0 \\ 0 \\ 0 \end{bmatrix} \tag{4.73}$$

4.2.6 Interaction of multiple control volumes

The derived procedure can directly be expanded to problems, where multiple fluid and/or gas filled chambers are connected to each other (see figure 4.3). For such systems the corresponding global arrays (load-stiffness matrices, coupling vectors and right-hand side vectors denoted by index i) have to be set up for each chamber i and must be summed up for all n chambers.

$$\left[\underline{K} + \sum_{i=1}^{n}\left(\underline{K}_i^g + \underline{K}_i^f + \underline{K}_i^{Cpl}\right)\right] \Delta\underline{d} = \underline{f}^{ext} - \underline{f}^{el} - \sum_{i=1}^{n}\left(\underline{f}_i^g + f_i^f\right) \tag{4.74}$$

In the hybrid approach the number of unknowns increases for each chamber by the number of internal state variables. In addition the load-stiffness matrices and the

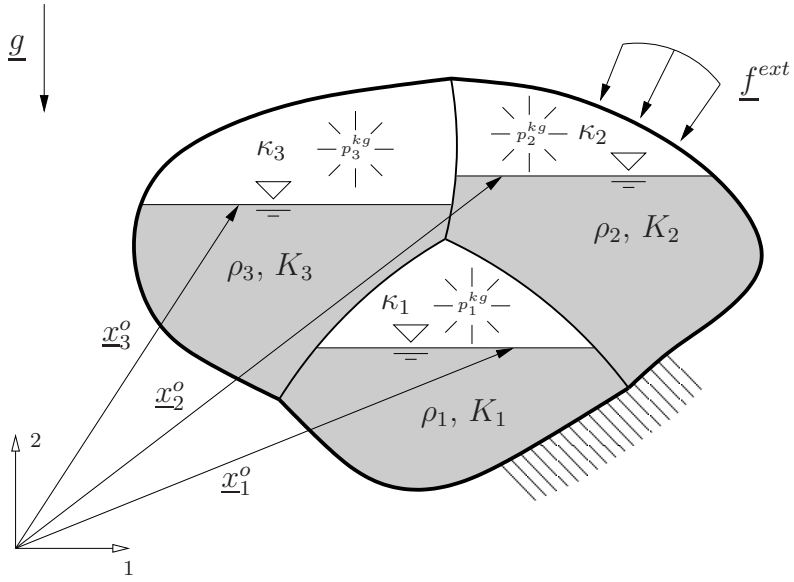

Figure 4.3: Multi chamber problem with 3 interacting fluid and gas filled control volumes

matrices due to the volume coupling have to be added to the system matrix. Further the right-hand side vector has to be modified by the appropriate pressure parts.

Chapter 5

Discussion of deformation dependent loadings

In the previous section all necessary finite element matrices for the quasi-static computation of structures subjected to an arbitrary combination of volume dependent fluid and gas loadings have been derived. For a better understanding of these matrices and coupling vectors, in this section, both a brief overview on deformation dependent loadings is given and several one-dimensional examples are presented, on which the basic features and restrictions of the general formulation can easily be discussed.

5.1 Loadings with deformation dependent directions

In order to understand the physical meaning of the load-stiffness matrices (4.34) and (4.35), several types of loadings, which are investigated in detail in SCHWEIZERHOF[86], are discussed first. As shown in table 5.1, loadings can be classified in two main groups: Loadings with constant global directions $\boldsymbol{n}_0$ and loadings maintaining their local direction relative to the structure, as e.g. pressure loadings, which are always perpendicular to the structural surface. Hence, for such kind of loadings in each state t the current load direction $\boldsymbol{n}_t$ has to be computed. Each group can be further splitted into the two subgroups of spatially fixed loadings, where the amplitude $f_t(\boldsymbol{x})$ of the loading is a function of the spatial position $\boldsymbol{x}$, and body-fixed loadings, where the load amplitude f_0 remains constant. For a proportional load application the load amplitudes can be additionally multiplied by a scaling factor λ_t.

In this work, mainly the type of loadings with displacement dependent directions $\boldsymbol{n}_t$ and spatially fixed load amplitude fields $f_t(\boldsymbol{x})$ is of interest, as it is e.g. the case for hydrostatic fluid loadings. In order to keep the following examples as simple as possible, each example is concerned with only one feature. The first one is shown in figure 5.1 and deals with the effect of a displacement dependent direction. For this purpose the resultant force $f_0\boldsymbol{n}$ of a constant gas pressure loading is applied on a rigid beam,

	loading with constant direction		loading changing its direction	
	spatially fixed	body-fixed (e.g. dead load)	spatially fixed (e.g. fluid load)	body-fixed
loading	$\boldsymbol{p} = \lambda_t f_t \boldsymbol{n}_0$	$\boldsymbol{p} = \lambda_t f_0 \boldsymbol{n}_0$	$\boldsymbol{p} = \lambda_t f_t \boldsymbol{n}_t$	$\boldsymbol{p} = \lambda_t f_0 \boldsymbol{n}_t$
definition of loading in state t	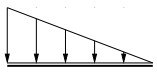	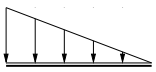	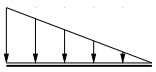	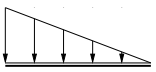
current configuration in state t	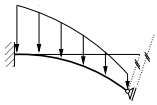	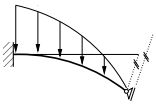	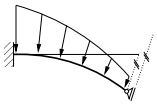	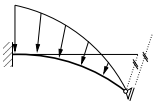

Table 5.1: Definition of different loadings according to SCHWEIZERHOF[86]

with its elasticity concentrated in the leg spring with stiffness k^{el}. The only degree of freedom is the rotation φ.

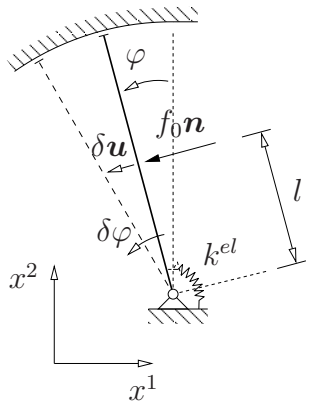

Figure 5.1: Elastic structure subjected to a loading with constant amplitude f_0 and deformation dependent direction $\boldsymbol{n}$.

Assuming a quasi-static process conduction the principle of virtual work leads to the following equilibrium condition in an arbitrary state t.

$$\delta\mathcal{L} = \delta\mathcal{U}^{\mathcal{B}} - \delta\mathcal{A}_{ext} = \delta\varphi k^{el}\varphi - f_0\boldsymbol{n}\cdot\delta\boldsymbol{u} \tag{5.1}$$

The virtual displacement of the force application point can be obtained by:

$$\boldsymbol{x} = \begin{pmatrix} -\sin\varphi \\ \cos\varphi \end{pmatrix} l \quad \Rightarrow \quad \delta\boldsymbol{u} = -\begin{pmatrix} \cos\varphi \\ \sin\varphi \end{pmatrix} l\delta\varphi \tag{5.2}$$

The direction of the force, as it is always perpendicular to the beam, is given by the normal.

$$\boldsymbol{n} = -\begin{pmatrix} \cos\varphi \\ \sin\varphi \end{pmatrix} \tag{5.3}$$

Thus a linearization of the equilibrium condition (5.1) at a current angle φ_t yields

$$\delta\mathcal{E}_{lin} = \delta\varphi\left(k^{el}\varphi_t - f_0 l\right) + \delta\varphi k^{el}\Delta\varphi - f_0\Delta\boldsymbol{n}\cdot\delta\boldsymbol{u} = 0 \tag{5.4}$$

Using the incremental change of the normal direction

$$\Delta\boldsymbol{n} = \begin{pmatrix} \sin\varphi_t \\ -\cos\varphi_t \end{pmatrix}\Delta\varphi \tag{5.5}$$

resulting from an incremental change of the rotation angle φ leads to the incremental energy contribution

$$\Delta\delta\mathcal{A}_{ext} = f_0\Delta\boldsymbol{n}\cdot\delta\boldsymbol{u} = -2l\sin\varphi_t\cos\varphi_t\Delta\varphi\delta\varphi = -l\sin(2\varphi_t)\Delta\varphi\delta\varphi \tag{5.6}$$

due a loading with a displacement dependent direction. With the right-hand side residual moment

$$m = -k^{el}\varphi_t + f_0 l \tag{5.7}$$

the conditional equation for the unknown rotation increment φ yields

$$\left(k^{el} + f_0 l\sin(2\varphi_t)\right)\Delta\varphi = m\ . \tag{5.8}$$

Since the volume coupling of the gas pressure loading will be part of the following section, its influence in the n-dimensional equation (4.41), reflecting in the coupling matrix $\underline{K}^{Cpl} = \alpha_t\underline{a}\underline{a}^T$ (for its setup see equation (4.32) and table 4.1), is here eliminated by setting the pressure-volume gradient $\alpha_t = 0$. For an arbitrary gas filled structure, this leaves the following terms, similar to equation (5.8):

$$\left(\underline{K}^{el} + \underline{K}^{g}\right)\Delta\underline{d} = \underline{f} \tag{5.9}$$

Although on the first sight a possible stiffness update of the structure is evident both in the one-dimensional and the n-dimensional equation, the one-dimensional example makes clear, that the additional stiffness term $f_0 l\sin(2\varphi_t)$ in the linearized equilibrium equation (5.8) not necessarily leads to a stabilization of the structure, because in an exact solution the virtual work $\delta\mathcal{A}_{ext}$ of the external force $f_0\boldsymbol{n}_t$ acting along $\delta\boldsymbol{u}$ always yields the constant value $f_0\boldsymbol{n}_t\cdot\delta\boldsymbol{u} = f_0 l\delta\varphi$ and thus no further stiffening term due to an incremental change $\Delta\delta\mathcal{A}_{ext}$ can appear. Hence, at least in this one-dimensional example the additional term is merely an artefact of the consistent linearization process, which approximates the exact motion of the structure by its tangent at state t. It leads to a certain gain of stiffness for $0 \le \varphi_t \le \pi/2$ and to a loss of stiffness for $\pi/2 \le \varphi_t \le \pi$. However, in order to find the equilibrium position of arbitrary structures subjected to displacement dependent loadings, a necessary precondition of embedding the nonlinear equilibrium equations in a numerical solution procedure is a consistent linearization of all terms and thus ensuring a quadratic convergence. Neglecting this load-stiffness matrix $\underline{K}^{g}$ would therefore result in a higher number of equilibrium iterations.

5.2 Gas filled control volume

After discussing the direction dependence of the loading and the associated load-stiffness matrices, the focus is now both on the volume dependence of the loading and its geometric description using the projections of the surfaces in contact with the fluid or gas. The one-degree of freedom model depicted in figure 5.2 will serve as an example for the derivation of the linearized equilibrium equation of a gas filled system. The elastic solid body domain is represented by a spring with stiffness k^{el} and the gas domain is characterized by its volume $\bar{v}$ and pressure p. The system is subjected to an external loading f^{ext}. Assuming a system at rest the energy conservation in equation

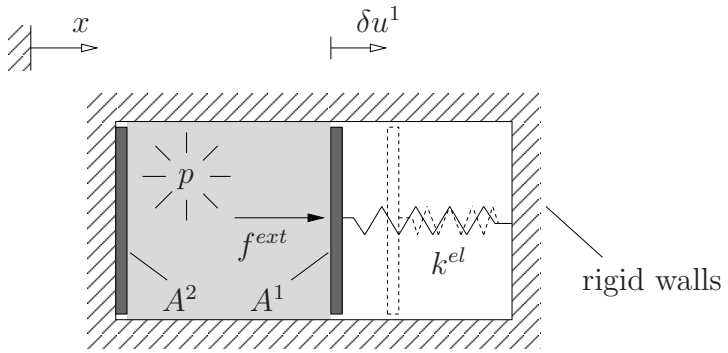

Figure 5.2: Virtual displacement δu acting on an equilibrated pneumatic one-degree of freedom system

(3.3) only contains the variation $\delta \mathcal{U}^{\mathcal{B}\cup\mathcal{F}}$ of the the internal energy, as well as the virtual work $\delta \mathcal{A}^{*}_{ext}$ of the external forces.

$$\delta \mathcal{E} = \delta \mathcal{U}^{\mathcal{B}\cup\mathcal{F}} - \delta \mathcal{A}^{*}_{ext} = 0 \tag{5.10}$$

The variation of the internal energy of the fluid and the elastic solid body is given by

$$\delta \mathcal{U}^{\mathcal{B}\cup\mathcal{F}} = -p\delta\bar{v} \tag{5.11}$$

In a state of equilibrium using equation (5.10) along with (5.11) leads to

$$\delta \mathcal{E} = k^{el}u^1\delta u^1 - p\delta\bar{v} - f^{ext}\delta u^1 = 0 \ . \tag{5.12}$$

As depicted in figure 5.3 the virtual volume change $\delta\bar{v}$ can be given in terms of the virtual displacement δu^i of the associated area A^i. With the fixed displacement $u^2 = 0$ and thus $\delta u^2 = 0$ only the contribution of A^1 remains.

$$\bar{v} = \sum_{i=1}^{2} A^i x^i \quad \Rightarrow \quad \delta\bar{v} = \sum_{i=1}^{2} A^i \delta u^i = A^1 \delta u^1 \tag{5.13}$$

A linearization of the equilibrium condition (5.12) at the current position u_t yields

$$\delta \mathcal{E}_{lin} = \left(k^{el}u^1_t - p_t A^1 - f^{ext}\right)\delta u^1 + k^{el}\Delta u^1 \delta u^1 + \Delta p A^1 \delta u^1 = 0 \ . \tag{5.14}$$

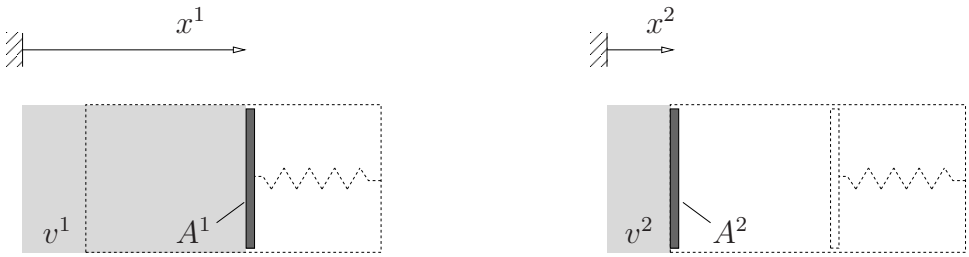

Figure 5.3: Volumes v^1 and v^2 obtained by projection of corresponding surfaces A^1 and A^2.

As a constitutive law for the gas the isentropic state equation (2.81) is used. Thus in analogy to equation (3.39), the incremental pressure change Δp, necessary in equation (5.14), can be given as

$$\Delta p = -\kappa \frac{p_t}{\bar{v}_t} \Delta \bar{v} = -\kappa \frac{p_t}{\bar{v}_t} A^1 \Delta u^1 \ . \tag{5.15}$$

Inserting equation (5.15) in equation (5.14) then yields a totally displacement based formulation of the linearized state of equilibrium t, with $u_{t+1} = u_t + \Delta u$.

$$\delta \mathcal{E}_{lin} = (k^{el} u_t^1 - p_t A^1 - f^{ext}) \delta u^1 + k^{el} \Delta u^1 \delta u^1 + \kappa \frac{p_t}{\bar{v}_t} A^1 A^1 \Delta u^1 \delta u^1 = 0 \tag{5.16}$$

Elimination of the virtual displacement δu^1 and introducing the vector

$$f = f^{ext} - k^{el} u_t^1 + p_t A^1 \ , \tag{5.17}$$

containing the internal and external forces, yields the conditional equation for the unknown displacement increment Δu.

$$\left(k^{el} + \alpha_t A^1 A^1\right) \Delta u^1 = f \ , \quad \text{with} \quad \alpha_t = \kappa \frac{p_t}{\bar{v}_t} \tag{5.18}$$

Apart from the missing normal change part $\underline{K}^g$, which has already been discussed in the previous section, this one-dimensional equation is identical to the n-dimensional equation (4.41) of an arbitrary gas filled structure, given in chapter 4.2.3. According to table 4.1 for the load case of a pure gas loading the following terms remain:

$$\left(\underline{K}^{el} + \underline{K}^g + \alpha_t \underline{a} \underline{a}^T\right) \Delta \underline{u} = \underline{f} \ , \quad \text{with} \quad \alpha_t = \kappa \frac{p_t}{\bar{v}_t} \tag{5.19}$$

A comparison of (5.18) with (5.19) shows, that the coupling vector $\underline{a}$ represents the surface of the finite elements surrounding the gas. The influence of the gas support on the structural stiffness k^{el} is predominantly defined by the factor $\alpha_t = \kappa p_t / \bar{v}_t$. For a large enclosed gas volume $\bar{v}_t \to \infty$ the effect of the volume coupling can be neglected, as $\alpha_t \to 0$. On the other hand for a relatively small enclosed gas volume $\bar{v}_t \to 0$ the pressure-volume gradient tends to infinity: $\alpha_t \to \infty$ and thus making the gas support the dominating part of the stiffness matrix of soft structures, see also section 5.3.1.

5.3 Control volume filled with incompressible heavy fluid

For a control volume at rest filled with an incompressible heavy fluid, as depicted in figure 5.4, the total potential energy $\mathcal{E}$ consists of the elastic energy of the solid domain, which is represented again by a spring with stiffness k^{el} and the gravitational potential energy $\mathcal{V}$ of the enclosed heavy fluid.

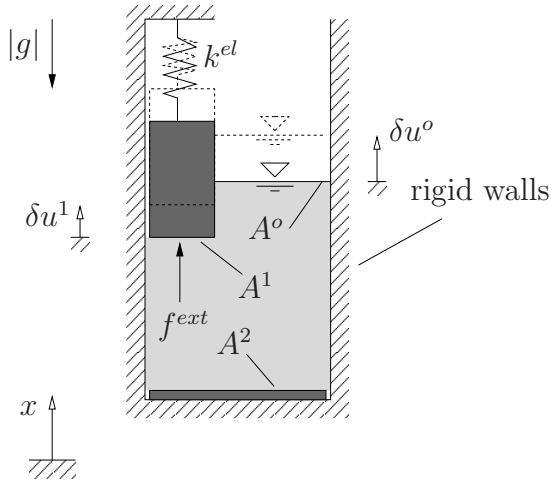

Figure 5.4: Virtual displacement δu acting on an equilibrated fluid-filled one-degree of freedom system

As the fluid is assumed to be incompressible, the internal energy $\mathcal{U}$ remains constant and thus its energy change vanishes. In a state of equilibrium the variation of the total potential energy has to fulfill:

$$\delta\mathcal{E} = \delta\mathcal{E}^{el} + \delta\mathcal{V} - \delta\mathcal{A}^*_{ext} = 0 \ , \tag{5.20}$$

with $\mathcal{A}^*_{ext}$ denoting the virtual work of the external loading f^{ext}. The gravitational potential $\mathcal{V}$ can be given in terms of the first order volume moment[1].

$$\mathcal{V} = -\rho g \int_{\mathcal{B}_f} x \ dv = -\rho g \bar{s} \tag{5.21}$$

The first order volume moment $\bar{s}$ can be given in terms of the volumes v^i times their distances to the center of gravity c^i, see also figure 5.5.

$$\bar{s} = \sum_{i=0}^{2} c_i v_i \tag{5.22}$$

[1]As g is negative $\mathcal{V}$ is given the minus sign.

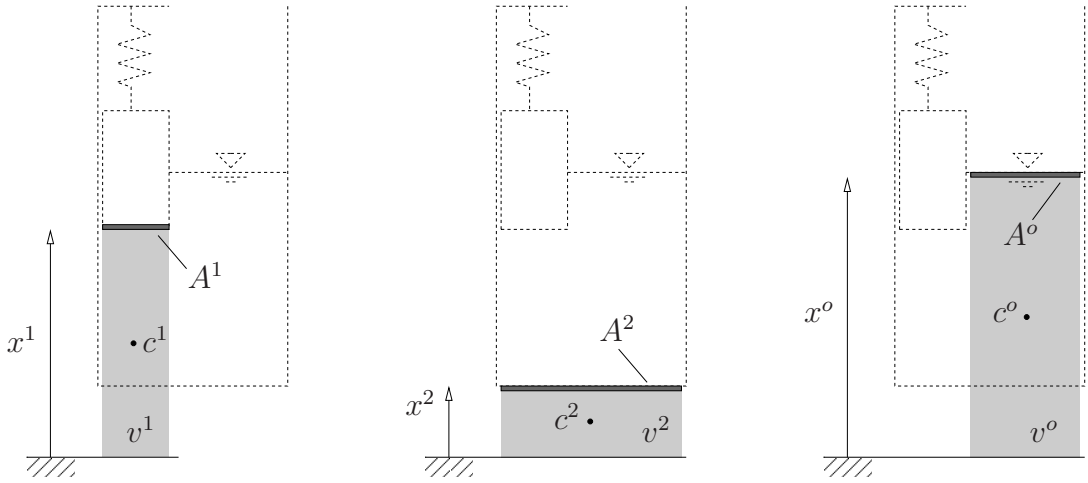

Figure 5.5: Volumes v^1, v^2 and v^o below the surfaces A^1, A^2 and A^o and their corresponding centers of gravity c^1, c^2 and c^o.

In a formulation using only the projections of the surrounding surfaces for the computation of the energy changes of the fluid the centers of gravity c^i can be substituted by the coordinates of the areas A^i

$$c^1 = \frac{1}{2}x^1 \ , \quad c^2 = \frac{1}{2}x^2 \quad \text{and} \quad c^o = \frac{1}{2}x^o \tag{5.23}$$

and the volumes v^i can be computed by

$$v^1 = A^1 x^1 \ , \quad v^2 = -A^2 x^2 \quad \text{and} \quad v^o = A^o x^o \ . \tag{5.24}$$

Thus the first order volume moment $\bar{s}$ can be given only in terms of the surrounding surfaces.

$$\bar{s} = \sum_{i=0}^{2} c^i v^i = \frac{1}{2}A^1 x^1 x^1 - \frac{1}{2}A^2 x^2 x^2 + \frac{1}{2}A^o x^o x^o \tag{5.25}$$

As in this case area A^2 is fixed, its corresponding virtual displacement yields $\delta u^2 = 0$ and thus the variation of the first order volume moment can be written as:

$$\delta\bar{s} = A^1 x^1 \delta u^1 + A^o x^o \delta u^o \ . \tag{5.26}$$

The incompressibility constraint $\delta\bar{v} = 0$ provides a connection between the virtual displacement δu^o of the free fluid surface and the structural displacement δu^1.

$$\delta\bar{v} = \sum_{i=0}^{2} \delta v^i = A^1 \delta u^1 + A^o \delta u^o \stackrel{!}{=} 0 \quad \Rightarrow \quad \delta u^o = -\frac{A^1}{A^o}\delta u^1 \tag{5.27}$$

With the gravitational pressures

$$p^o = \rho g x^o \quad \text{and} \quad p^x = \rho g x^1 \tag{5.28}$$

at the free fluid surface A^o and at area A^1 the variation of the gravitational potential yields

$$\delta\mathcal{V} = (p^o - p^x)\, A^1 \delta u^1 \ . \tag{5.29}$$

A linearization of the equilibrium equation (5.20) at a current position u_t^1 gives:

$$\delta\mathcal{E}_{lin} = \delta\mathcal{E}_t + k^{el}\Delta u^1 \delta u^1 + (\Delta p^o - \Delta p^x)\, A^1 \delta u^1 \ . \tag{5.30}$$

The incremental pressure changes

$$\Delta p^o = \rho g \Delta u^o \quad \text{and} \quad \Delta p^x = \rho g \Delta u^1 \tag{5.31}$$

can be obtained in analogy to (5.27) using the constitutive equation of an incompressible fluid, which provides the connection between the incremental displacements Δu^o and Δu^1.

$$\Delta u^o = -\frac{A^1}{A^o}\Delta u^1 \tag{5.32}$$

The resulting force of the internal and external forces is given by

$$f = -k^{el} u_t^1 - (p_t^o - p_t^x) A^1 + f^{ext} \ . \tag{5.33}$$

Since the acceleration of gravity g points in negative x-direction, its minus sign can be canceled with the minus sign in (5.32), if in the further development the absolute value $|g|$ is used.

$$\left(k^{el} - \rho g A^1 + \gamma_t A^1 A^1\right) \Delta u^1 = f \ , \quad \text{with} \quad \gamma_t = \frac{\rho|g|}{A^o} \tag{5.34}$$

Apart from the missing normal change part $\underline{K}^f$ this one-dimensional equation is identical to the n-dimensional equation (4.41) of an arbitrary structure filled with an incompressible heavy fluid, given in chapter 4.2.3. According to table 4.1 for the load case of an incompressible fluid with a free fluid surface the following terms remain:

$$\left(\underline{K}^{el} + \underline{K}^f + \gamma_t \underline{b}\underline{b}^T\right) \Delta\underline{d} = \underline{f} \ , \quad \text{with} \quad \gamma_t = \frac{\rho|\underline{g}|}{\partial\mathcal{B}_t^o} \tag{5.35}$$

In the one-dimensional formulation (5.34) the term $-\rho g A^1$ corresponds to the additional term

$$-\frac{\rho_t}{2}\int_{\square^f} \underline{N}^T \left(\underline{n}_t^f \otimes \underline{g} + \underline{g} \otimes \underline{n}_t^f\right) \underline{N}\ d\square$$

in the load-stiffness matrix $\underline{K}^f$ in (4.35) to account for a non-constant pressure distribution. A closer look at the stiffness term

$$k = k^{el} \underbrace{-\rho g A^1}_{k_f^x = \Delta p^x_{,u}} \underbrace{+\frac{\rho|g|}{A^o} A^1 A^1}_{k_f^o = \Delta p^o_{,u}} \tag{5.36}$$

of the one-dimensional problem shows, that in the limit case of $A^o \to 0$ the stiffening term k^f due to volume coupling becomes infinity.

$$\lim_{A^o \to 0} k_f^o = \infty \tag{5.37}$$

In this case a kind of volumetric locking is at hand, as for the incompressible fluid an infinite fluid level displacement would be necessary to conserve its volume. On the other hand, if the fluid surface is much larger than the structural surface $A^o \gg A^1$, the stiffening effect due to an infinitesimal change of the fluid surface can be neglected.

$$\lim_{A^o \to \infty} k_f^o = 0 \tag{5.38}$$

Nevertheless, the structure is still supported by the change of the fluid pressure $k_f^x = \Delta p_{,u}^x = \rho|g|A^1$ with increasing depth. From the numerical point of view this has the advantage, that although no Dirichlet boundary conditions in the vertical direction are present, no regularization with a mass matrix and thus no transient analysis is necessary, as the stiffness matrix does not feature zero eigenvalues. However, this one-dimensional example still suffers from the assumption, that the stiffening buoyance force continuously increases with increasing depth, which is only valid if the solid body is not completely submerged. Otherwise the buoyance force remains constant, because the changes $\Delta p_{,u_1}^x = \rho|g|A^1$ on the upper and lower side of the solid body cancel each other due to their opposite orientation. Hence, a completely submerged solid body is kinematic and therefore needs a mass matrix for computing the equilibrium.

5.3.1 Discussion of stability

In order to emphasize again the effect of a volume dependent fluid loading on structural stability, which will be described in particular in chapter 6.3, the three hinged arch, depicted in figure 5.6, will serve as an example: It is subjected to an external loading F and supported by an internal gas pressure. This example aims on presenting the differences between a computation using a constant gas pressure $p = p_0 = const.$ and a computation using a gas pressure $p = p(v)$, which is dependent on the enclosed volume v, resp. the displacements u of the surrounding structure.

The state of equilibrium is formulated using the principle of virtual work. Along with the normal strain ε of the trusses and its variation $\delta\varepsilon$

$$\varepsilon = \frac{\sqrt{L^2 - 2hu + u^2} - L}{L} \quad \text{and} \quad \delta\varepsilon = -\frac{h-u}{L\sqrt{L^2 - 2hu + u^2}}\delta u \tag{5.39}$$

the virtual work of the inner forces inside the elastic trusses yields (see e.g. also Pflüger[74]):

$$\delta\mathcal{E} = 2\int_L EA\varepsilon\delta\varepsilon dL = -2\frac{EA}{L}\left(1 - \frac{L}{\sqrt{L^2 - 2hu + u^2}}\right)(h-u)\delta u \ . \tag{5.40}$$

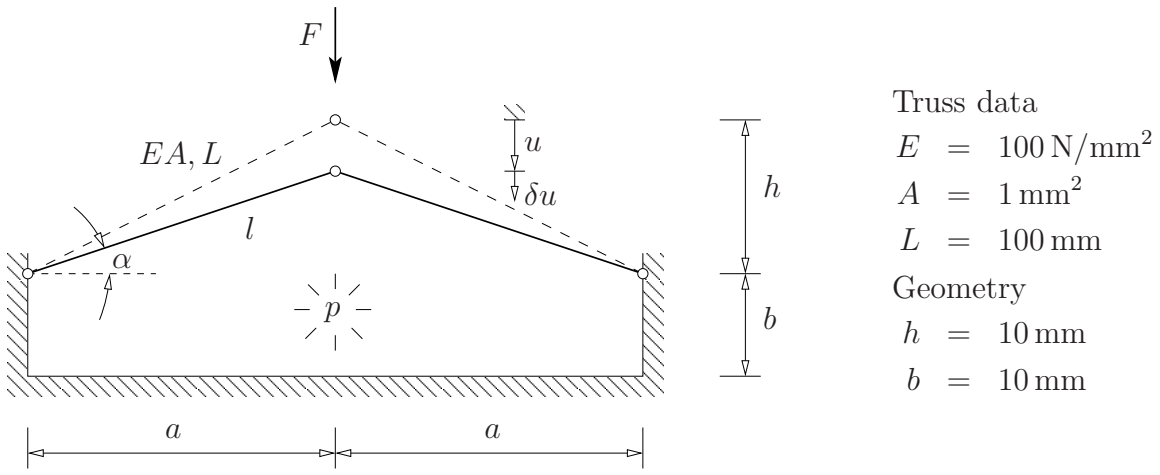

Figure 5.6: Snap-through problem of three hinged arch with gas support

Using the current gas volume

$$v(u) = \sqrt{L^2 - h^2}(b + h - u) \tag{5.41}$$

and its variation

$$\delta v = -\sqrt{L^2 - h^2}\delta u \tag{5.42}$$

the virtual work $\delta\mathcal{A}$ done by the gas pressure p and by the external loading can be given as

$$\delta\mathcal{A} = p\delta v + F\delta u = -p\sqrt{L^2 - h^2}\delta u + F\delta u \ . \tag{5.43}$$

Rewriting the equilibrium condition

$$\delta\mathcal{E} - \delta\mathcal{A} = 0 \tag{5.44}$$

by collecting the external force F and eliminating the virtual displacement δu leads to a set of curves $F(u)$ describing the load deflection behaviour for both a) the case of a constant gas pressure $p = p_0 = const$

$$F_a(u) = -2\frac{EA}{L}\left(1 - \frac{L}{\sqrt{L^2 - 2hu + u^2}}\right)(h - u) + p_0\sqrt{L^2 - h^2} \tag{5.45}$$

and b) the case of a volume dependent gas pressure $p = p(v)$, e.g. using the constitutive equation (2.82).

$$F_b(u) = -2\frac{EA}{L}\left(1 - \frac{L}{\sqrt{L^2 - 2hu + u^2}}\right)(h - u) + \frac{p_0 v_0}{v(u)}\sqrt{L^2 - h^2} \tag{5.46}$$

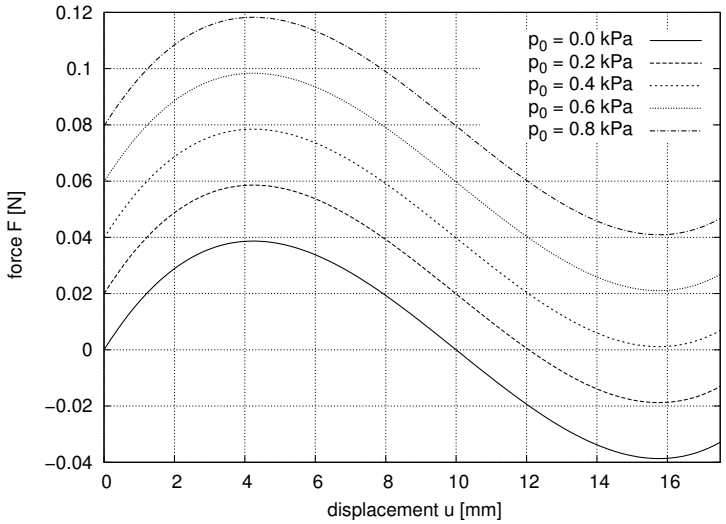

Figure 5.7: Load deflection curves of the snap-through problem with a constant gas support $p = p_0 = const$, plotted for different initial pressures p_0.

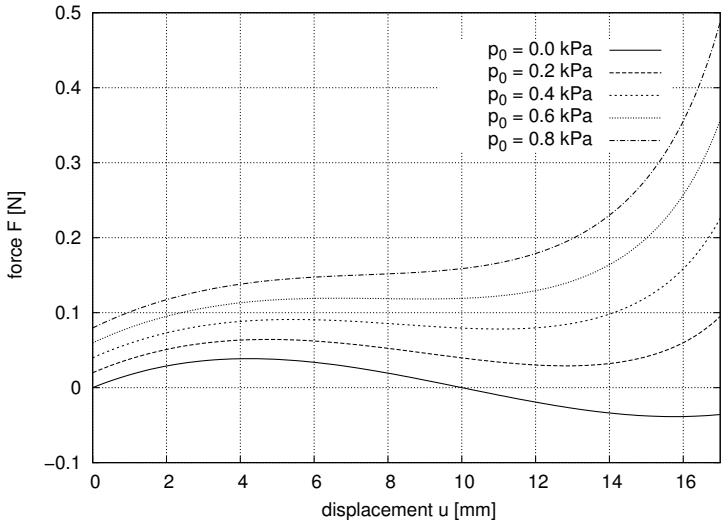

Figure 5.8: Load deflection curves of the snap-through problem with a volume dependent gas support $p = p(v)$, plotted for different initial pressures p_0.

Both sets of load deflection curves are depicted in figures 5.7 and 5.8 for different initial gas pressures p_0. It is clearly visible that in case a) of a gas pressure, which is independent of the structural displacements, all load deflection curves reach their singular point at $u \approx 4.5\,\text{mm}$, resulting in a snap-through of the structure. The only difference is in the corresponding buckling load, because in each curve a different internal pressure has to be overcome. However, considering the fact that in case b) the gas pressure is correlated with the enclosed volume via the isentropic state equation (2.81) or the isothermal state equation (2.82), the curves in figure 5.8 show that from a minimal in-

ternal pressure this volume dependence has a stabilizing effect on the load-deformation behaviour of the three hinged arch. The set of load deflection curves, depicted in figure 5.8, does not contain a singular point for internal pressures $p_0 \geq 0.8\,\text{kPa}$. For a further explanation figure 5.9 shows the tangential stiffnesses for different initial pressure p_0 and it is clear that for $p_0 \geq 0.8\,\text{kPa}$ they are permanently positive.

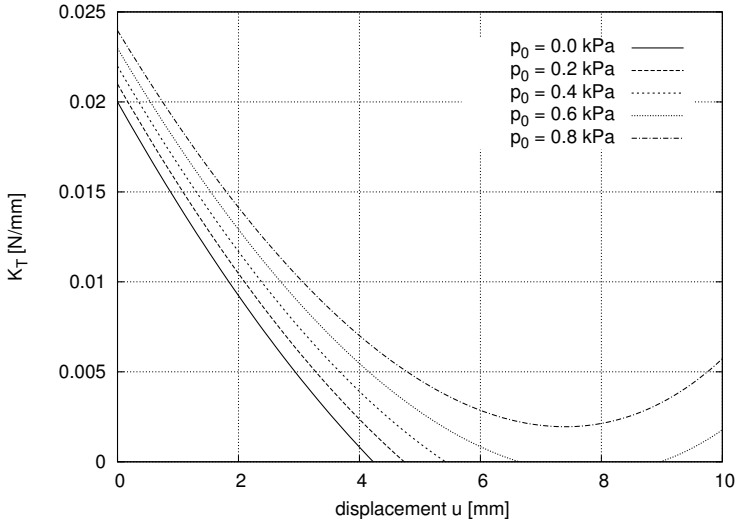

Figure 5.9: Developments of the tangential stiffnesses K_T of the snap-through problem with volume dependent gas support $p = p(v)$ plotted for different initial gas pressures p_0.

This example shows that for flexible structures with relatively small enclosed gas volumes the pressure support has a significant influence on the stability. However, for real structures in the field of civil engineering, featuring large gas volumes and high truss stiffnesses, this stabilizing effect is mostly negligible. This is due to the fact that usually in standard stability problems the structural displacements near the singular point are still rather small and the correlated volume changes are also quite small. Thus the incremental pressure changes caused by the structural displacements are much smaller than the geometric stiffnesses (see also HASSLER&SCHWEIZERHOF[39]). Nevertheless, if very flexible structures enclosing relatively small gas volumes have to be investigated, the algorithms derived in chapter 6.3 should be used for the eigenvalue computation.

Chapter 6

Numerical solution schemes

In the previous chapter the finite element method has been used to achieve a numerically solvable formulation of the weak form of equilibrium. In this process the equations have been presented both in a purely displacement dependent version and a hybrid version, using the internal state variables as additional unknowns. Since both formulations result in matrices with large bandwidth at a first view conflicting with an efficient solution, a vectorized solution scheme for the displacement dependent formulation is derived. This is compared with several iterative solutions of the hybrid equation system in a next step. Besides the computation of the state of equilibrium, the investigation of the stabilizing influence of a volume dependent fluid support is important as well. Therefore the third part of this chapter deals with the derivation of an efficient strategy for the computation of the eigenvalues and eigenmodes of the global stiffness matrix including all terms depending on fluid and gas loading.

6.1 Direct solution scheme

For each finite element in contact with fluid or gas, according to the previously presented algorithm, coupling vectors are generated, which form the coupling matrix $\underline{K}^{Cpl}$ by a dyadic combination. However, for each control volume these dyadic rank updates cause a fully occupied part of the global system matrix. In order to bypass the solution of an almost fully occupied system matrix, a general vectorized algorithm is discussed, which can be seen as a sequential application of the Sherman-Morrison formula, see also Faires&Burden[27], Rumpel[78] or Schweizerhof[87]. First a compact notation

$$\underline{A} = \underline{K} + \sum_{l=1}^{m} \underline{x}_l \underline{y}_l^T \ , \qquad \text{with} \qquad \underline{K} = \underline{K}^{el} + \sum_{i=1}^{n} \left(\underline{K}_i^g + \underline{K}_i^f \right) \tag{6.1}$$

is introduced. The load stiffness matrices $\underline{K}_i^g$ and $\underline{K}_i^f$ do not lead to a different band width, because they are matrices for the wetted surfaces of the elements with similar structure as the element stiffness matrix of the loaded element. Although the l^{th} rank update $\underline{x}_l$ and $\underline{y}_l^T$ may be unsymmetric in the most general case, compare equation

(4.69), however, the whole sum is symmetric. Since $\underline{x_l}$ and $\underline{y_l^T}$ represent the surfaces of the wetted elements, they are – depending on how many elements of the structure are in contact with fluid or gas – almost fully occupied, which leads to a large bandwidth of $\underline{A}$. With the right-hand side vector

$$\underline{f} = \underline{f}^{ex} - \underline{f}^{el} - \sum_{i=1}^{n} \left(\underline{f}_i^g + \underline{f}_i^f \right) \tag{6.2}$$

the solution can be written as:

$$\underline{d} = \underline{A}^{-1} \underline{f} \tag{6.3}$$

Reordering equation (6.1) accordingly

$$\underline{K} = \underline{A} - \sum_{l=1}^{m} \underline{x_l} \underline{y_l^T} \tag{6.4}$$

and subsequent left-hand side multiplication of equation (6.4) with $\underline{K}^{-1}$ gives after an additional right-hand side multiplication with $\underline{A}^{-1}\underline{f}$ the basis of a recursive rule for the solution vector.

$$\underline{d} \;=\; \underline{K}^{-1}\underline{f} - \underline{K}^{-1} \sum_{l=1}^{m} \underline{x_l} \underline{y_l^T} \underline{d} \tag{6.5}$$

6.1.1 Solution procedure for a rank-3-update of $\underline{K}$

In order to derive a general scheme for this recursive form, the solution scheme is shown for a stiffness matrix $\underline{K}$ with a rank-($m = 3$)-update. Afterwards the general algorithm for the computation in an arbitrary solution step i is set up. A special focus is here on a consequent vectorization of the equations to avoid storing fully populated stiffness matrices or fully populated sections of the stiffness matrix.

Starting point: recursive step $i = 0$

To reduce the expressions in the following steps the notations $\underline{d}_0 = \underline{K}^{-1}\underline{f}$ and $\underline{\Psi}_0 = -\underline{K}^{-1}$ are introduced. Thus from equation (6.5) a form is obtained, which gives more insight into the triple update of the conventional solution vector $\underline{d}_0$ with further unknown vectors resulting from the coupling vectors.

$$\underline{d} = \underline{d}_0 + \underline{\Psi}_0 \sum_{l=1}^{n=3} \underline{x_l} \underline{y_l^T} \underline{d} \qquad (\text{step } i = 0) \tag{6.6}$$

Starting from equation (6.6) we can proceed with the first real recursive step:

Recursive step $i = 1$

Separating the summand with index $l = i = 1$ from the sum in equation (6.6) gives us

$$\underline{d} = \underline{d}_0 + \underline{\Psi}_0 \ \underline{x}_1 \underline{y}_1^T \underline{d} + \underline{\Psi}_0 \sum_{l=2}^{m=3} \ \underline{x}_l \underline{y}_l^T \underline{d} \ . \tag{6.7}$$

By using the auxiliary vector

$$\underline{r}_{01} = \underline{\Psi}_0 \ \underline{x}_1 \tag{6.8}$$

we can abbreviate the solution to

$$\underline{d} = \underline{d}_0 + \underline{r}_{01} \underline{y}_1^T \underline{d} + \underline{\Psi}_0 \sum_{l=2}^{m=3} \ \underline{x}_l \underline{y}_l^T \underline{d} \ . \tag{6.9}$$

A further multiplication of (6.9) from the left side with the rank vector $\underline{y}_1^T$ then leads to

$$\underline{y}_1^T \underline{d} = \underline{y}_1^T \underline{d}_0 + \underline{y}_1^T \ \underline{r}_{01} \underline{y}_1^T \underline{d} + \underline{y}_1^T \ \underline{\Psi}_0 \sum_{l=2}^{m=3} \ \underline{x}_l \underline{y}_l^T \underline{d} \ . \tag{6.10}$$

Rewriting this equation results in:

$$\begin{aligned} & \underline{y}_1^T \underline{d} - \underline{y}_1^T \ \underline{r}_{01} \underline{y}_1^T \underline{d} \ = \ \underline{y}_1^T \underline{d}_0 + \underline{y}_1^T \ \underline{\Psi}_0 \sum_{l=2}^{m=3} \ \underline{x}_l \underline{y}_l^T \underline{d} \\ \Leftrightarrow \qquad & \left(1 - \underline{y}_1^T \underline{r}_{01}\right) \underline{y}_1^T \underline{d} \ = \ \underline{y}_1^T \underline{d}_0 + \underline{y}_1^T \ \underline{\Psi}_0 \sum_{l=2}^{m=3} \ \underline{x}_l \underline{y}_l^T \underline{d} \end{aligned} \tag{6.11}$$

Isolating the scalar term $\underline{y}_1^T \underline{d}$ on the left hand side yields along with the parameter

$$\beta_1 = \left(1 - \underline{y}_1^T \underline{r}_{01}\right)^{-1} \tag{6.12}$$

the following form:

$$\underline{y}_1^T \underline{d} = \beta_1 \underline{y}_1^T \ \underline{d}_0 + \beta_1 \underline{y}_1^T \underline{\Psi}_0 \sum_{l=2}^{m=3} \ \underline{x}_l \underline{y}_l^T \underline{d} \ . \tag{6.13}$$

Reinserting (6.13) in (6.9) gives

$$\underline{d} \ = \ \underline{d}_0 + \underline{r}_{01} \left(\beta_1 \underline{y}_1^T \ \underline{d}_0 + \beta_1 \underline{y}_1^T \underline{\Psi}_0 \sum_{l=2}^{m=3} \ \underline{x}_l \underline{y}_l^T \underline{d} \right) + \underline{\Psi}_0 \sum_{l=2}^{m=3} \ \underline{x}_l \underline{y}_l^T \underline{d} \ . \tag{6.14}$$

Rearranging the terms associated to the dyadic update ends the first recursive step:

$$\underline{d} \;=\; \underline{d}_0 + \beta_1 \underline{r}_{01} \underline{y}_1^T \; \underline{d}_0 + \Big(\beta_1 \underline{r}_{01} \underline{y}_1^T \underline{\Psi}_0 + \underline{\Psi}_0 \Big) \sum_{l=2}^{m=3} \; \underline{x}_l \underline{y}_l^T \underline{d} \; . \tag{6.15}$$

Computing the new interim solution

$$\underline{d}_1 = \underline{d}_0 + \beta_1 \underline{r}_{01} \underline{y}_1^T \underline{d}_0 = \underline{d}_0 + \beta_1 \underline{y}_1^T \underline{d}_0 \underline{r}_{01} \tag{6.16}$$

and introducing the updated auxiliary matrix

$$\underline{\Psi}_1 = \beta_1 \underline{r}_{01} \underline{y}_1^T \underline{\Psi}_0 + \underline{\Psi}_0 \tag{6.17}$$

(which actually does not need to be computed) then brings back the updated form of (6.6):

$$\underline{d} = \underline{d}_1 + \underline{\Psi}_1 \sum_{l=2}^{m=3} \underline{x}_l \underline{y}_l^T \underline{d} \qquad (\text{step } i = 1) \tag{6.18}$$

Now we have achieved a reduction from a rank-3-update to a rank-2-update. The next two sequential steps are performed analogously to the procedure outlined above, therefore only the necessary equations will be briefly presented.

Recursive step $i = 2$

Starting from the recursive equation (6.18) for the solution vector, we multiply it from the left with the rank vector $\underline{y}_2^T$. Isolating and reinserting the term $\underline{y}_2^T \underline{d}$ in equation (6.18) yields along with 2 auxiliary vectors

$$\underline{r}_{02} = \underline{\Psi}_0 \underline{x}_2 \qquad \text{and} \tag{6.19}$$

$$\underline{r}_{12} = \underline{\Psi}_1 \underline{x}_2 = \Big(\beta_1 \underline{r}_{01} \underline{y}_1^T \underline{\Psi}_0 + \underline{\Psi}_0 \Big) \underline{x}_2 = \beta_1 \underline{r}_{01} \underline{y}_1^T \underline{r}_{02} + \underline{r}_{02} \tag{6.20}$$

and the parameter

$$\beta_2 = \Big(1 - \underline{y}_2^T \underline{r}_{12} \Big)^{-1} \tag{6.21}$$

the next recursive rule for $\underline{d}$:

$$\underline{d} = \Big(\underline{d}_1 + \beta_2 \underline{r}_{12} \underline{y}_2^T \underline{d}_1 \Big) + \Big(\beta_2 \underline{r}_{12} \underline{y}_2^T \underline{\Psi}_1 + \underline{\Psi}_1 \Big) \sum_{l=3}^{m=3} \; \underline{x}_l \underline{y}_l^T \underline{d} \tag{6.22}$$

Since the dyadic update has now been reduced to the last remaining term, equation (6.22) can be written in more general form:

$$\underline{d} = \underline{d}_2 + \underline{\Psi}_2 \; \underline{x}_3 \underline{y}_3^T \underline{d} \; , \tag{6.23}$$

with

$$\underline{d}_2 = \underline{d}_1 + \beta_2 \underline{r}_{12} \underline{y}_2^T \underline{d}_1 = \underline{d}_1 + \beta_2 \underline{y}_2^T \underline{d}_1 \underline{r}_{12} \tag{6.24}$$

and

$$\underline{\Psi}_2 = \beta_2 \underline{r}_{12} \underline{y}_2^T \underline{\Psi}_1 + \underline{\Psi}_1 \; . \tag{6.25}$$

Recursive step $i = 3$

To compute the final solution the Sherman-Morrison formula is applied again. As done in the previous subsections, the recursive equation (6.23) is multiplied from the left with the remaining rank vector $\underline{y}_3^T$. Isolating and reinserting the term $\underline{y}_3^T \underline{d}$ in equation (6.23) yields after the 3rd step along with the 3 auxiliary vectors

$$\underline{r}_{03} = \underline{\Psi}_0 \underline{x}_3 \tag{6.26}$$

$$\underline{r}_{13} = \underline{\Psi}_1 \underline{x}_3 = \left(\beta_1 \underline{r}_{01} \underline{y}_1^T \underline{\Psi}_0 + \underline{\Psi}_0\right) \underline{x}_3 = \beta_1 \underline{r}_{01} \underline{y}_1^T \underline{r}_{03} + \underline{r}_{03} = \beta_1 \underline{y}_1^T \underline{r}_{03} \underline{r}_{01} + \underline{r}_{03} \tag{6.27}$$

$$\underline{r}_{23} = \underline{\Psi}_2 \underline{x}_3 = \left(\beta_2 \underline{r}_{12} \underline{y}_2^T \underline{\Psi}_1 + \underline{\Psi}_1\right) \underline{x}_3 = \beta_2 \underline{r}_{12} \underline{y}_2^T \underline{r}_{13} + \underline{r}_{13} = \beta_2 \underline{y}_2^T \underline{r}_{13} \underline{r}_{12} + \underline{r}_{13} \tag{6.28}$$

and the parameter

$$\beta_3 = \left(1 - \underline{y}_3^T \underline{r}_{23}\right)^{-1} \tag{6.29}$$

the final rule for the computation of the solution vector

$$\underline{d} = \underline{d}_3 = \underline{d}_2 + \beta_3 \underline{r}_{23} \underline{b}_3^T \underline{d}_2 = \underline{d}_2 + \beta_3 \underline{b}_3^T \underline{d}_2 \underline{r}_{23} \ . \tag{6.30}$$

Hence, the solution with the rank-($m = 3$)-update has been reduced to the triangularization of $\underline{K}$ and 4 forward-backward substitutions plus 10 scalar products and 7 vector summations.

General solution scheme

As shown at the example of a rank-3-update of the system matrix $m = 3$ sequential steps of the Sherman-Morrison algorithm were necessary to compute the solution vector. Further more, in each step i the auxiliary vectors $\underline{r}_{ji}$ with $i = 1..m$ and $j = 0..(i-1)$ and the parameter β_i had to be computed to get the current update of the last interim solution $\underline{d}_{i-1}$. Following this example a general solution algorithm for a stiffness matrix $\underline{K}$ featuring a rank-m-update can be developed, which is depicted in figure 6.1.

Memory requirements

For each new recursive step the number of auxiliary vectors, which have to be stored, increases by one. Thus for the most general case

$$\left(\underline{K} + \sum_{l=1}^{m} \underline{x}_l \underline{y}_l^T\right) \underline{d} = \underline{f} \tag{6.31}$$

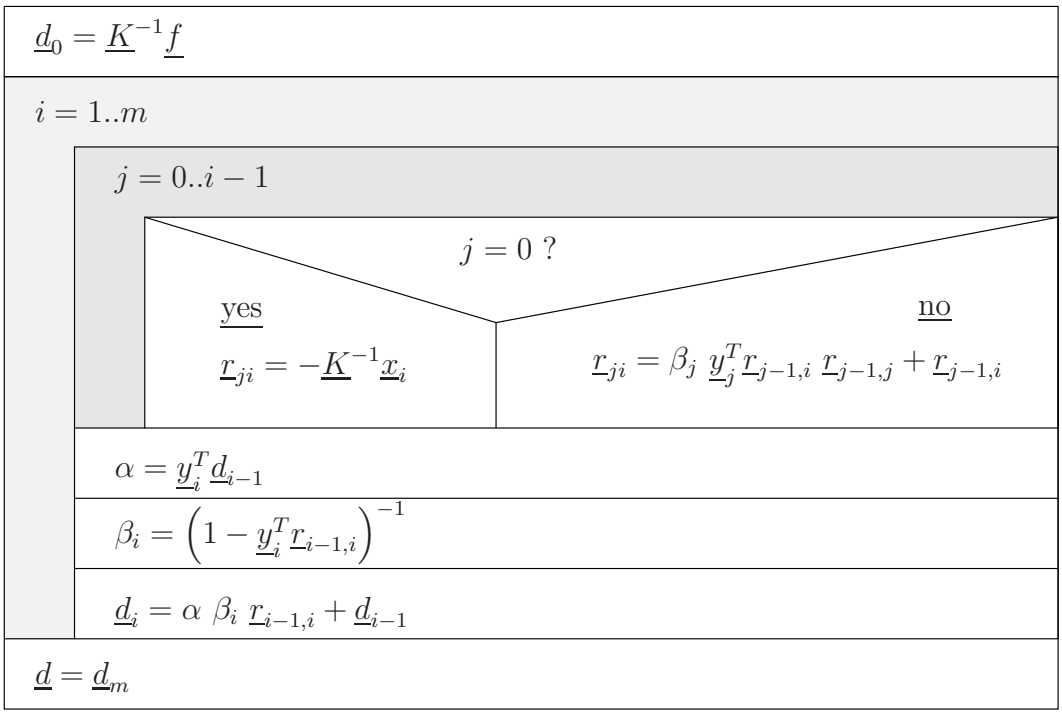

Figure 6.1: Recursive scheme for the computation of the auxiliary vectors $\underline{r}_{ji}$, the parameters β_i and the interim solutions $\underline{d}_i$ in the vectorized Sherman-Morrison algorithm for m updates

of a rank-m-updated system matrix $\underline{K}$, the memory requirements listed also in table 6.1 are as follows:

- $k = \sum_{i=0}^{m}(m-i)$ auxiliary vectors $\underline{r}_{ji}$,
- m parameters β_i ,
- 2 interim solutions $\underline{d}_i$ and $\underline{d}_{i-1}$.

As it can be seen the requirements given in table 6.1 demand sufficient memory to guarantee an efficient direct solution.

6.2 Iterative solution of the hybrid equation system

In the previous chapter with the Sherman-Morrison algorithm an efficient method for the solution of the merely displacement dependent equation system (4.74) has been presented. Although it is known that for badly conditioned equation systems with high condition numbers the direct solvers are more efficient than iterative Krylov-subspace

Step	auxiliary vectors	interim solutions	parameters
$i = 1$	$\underline{r}_{01}$	$\underline{d}_0,\ \underline{d}_1$	$\alpha,\ \beta_1$
$i = 2$	$\underline{r}_{01}$ $\underline{r}_{02}\quad \underline{r}_{12}$	$\underline{d}_1,\ \underline{d}_2$	$\alpha,\ \beta_1,\ \beta_2$
$i = 3$	$\underline{r}_{01}$ $\underline{r}_{02}\quad \underline{r}_{12}$ $\underline{r}_{03}\quad \underline{r}_{13}\quad \underline{r}_{23}$	$\underline{d}_2,\ \underline{d}_3$	$\alpha,\ \beta_1,\ \beta_2,\ \beta_3$
	$\vdots$		
$i = m$	$\underline{r}_{01}$ $\underline{r}_{02}\quad \underline{r}_{12}$ $\underline{r}_{03}\quad \underline{r}_{13}\quad \underline{r}_{23}$ $\vdots\qquad\quad \ddots$ $\underline{r}_{0m}\quad \underline{r}_{1m}\quad \underline{r}_{2m}\quad \cdots\quad \underline{r}_{m-1,m}$	$\underline{d}_{m-1},\ \underline{d}_m$	$\alpha,\ \beta_1,\ \beta_2,\ \ldots,\ \beta_m$

Table 6.1: Memory requirements for the vectorized Sherman-Morrison algorithm with m updates of the stiffness matrix

methods (see e.g. LENHARDT[54]), however, as shown in table 6.1, the memory requirements for the auxiliary vectors $\underline{r}_{ij}$ increase quadratically with increasing rank-updates. Therefore at this point an iterative solution of the hybrid equation system (4.52) will be discussed. In this case the memory requirements increase only linearly with increasing number of hybrid variables, because only one additional coupling column per unknown has to be stored in the system matrix. A more detailed investigation on the performance of several iterative solvers applied to such kind of equations can be found in MERKLE[59]. Therefore the results are only briefly presented here. For the one-dimensional gas filled system (elastic part k^{el}, cross-section A, gas pressure p^{kg}, external loading f^{ext}) depicted in figure 6.2, the linearized state of equilibrium can be

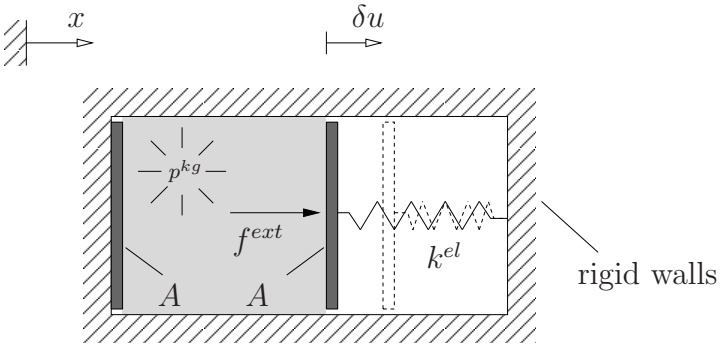

Figure 6.2: Virtual displacement δu acting on an equilibrated pneumatic one-degree of freedom system

given according to equation (4.52) and table 4.1 with $f = f^{ext} + p_t^{kg} A$ and $\alpha_t = \kappa \frac{p_t^{kg}}{\bar{v}_t^g}$

as follows:

$$\begin{pmatrix} k^{el} & A \\ A & -\frac{1}{\alpha_t} \end{pmatrix} \begin{pmatrix} \Delta d \\ \Delta p^{kg} \end{pmatrix} = \begin{pmatrix} f \\ 0 \end{pmatrix} \tag{6.32}$$

A left- and right-hand side multiplication of the coefficient matrix with the vector $[0,1]^T$ reveals the matrix being indefinite. Although scaling the second row with -1 would result in a positively definite coefficient matrix, its symmetry would be lost, leading to a higher numerical effort for the solution. Since in the above equation (6.32) a symmetric but indefinite coefficient matrix is at hand, several standard algorithms, such as the CG method or the Lanczos method, cannot be taken for the solution, because in this case the existence and the numerical stability of the triangulated Krylov-subspace projection of the system matrix are not guaranteed. Therefore in the thesis of MERKLE[59], as appropriate solution schemes for indefinite equation systems, the MINRES-method, the SQMR-method by FREUND&NACHTIGALL[30] as well as the SYMMLQ-method by PAIGE&SAUNDERS[68] have been compared to the direct solution presented in chapter 6.1. Further, the chosen iterative solvers were enhanced using a conventional and a generalized Jacobian preconditioner. However, the last one is only appropriate for the SQMR-method, because the preconditioning matrix is not positively definite.

6.2.1 Benchmark: Gas filled multi-chamber system

As a benchmark for the comparison of the different solution strategies, a structure with a variable number of control volumes $i = 1..n$ and internal gas pressures p^{kg} (see figure 6.3) was chosen. Each computation was made on a single node of the parallel computer system HP XC6000.

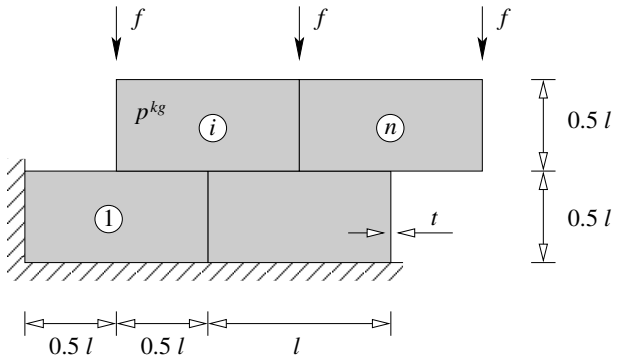

geometry and loading

$l = 10.0\,\text{mm}$

$t = 0.1\,\text{mm}$

$f = 18.75\,\text{N}$

initial pressure

$p_0^{kg} = 0.1\,\text{MPa}$

elastic material

$E = 7.5 \cdot 10^5\,\text{MPa}$

$\nu = 0.3$

Figure 6.3: Benchmark: multi-chamber system composed of $i = 1..n$ identical gas filled control volumes and subjected to an external loading

In a first step the different iterative solvers are compared with the direct solver in case of a conventional problem with increasing number of degrees of freedom. By setting

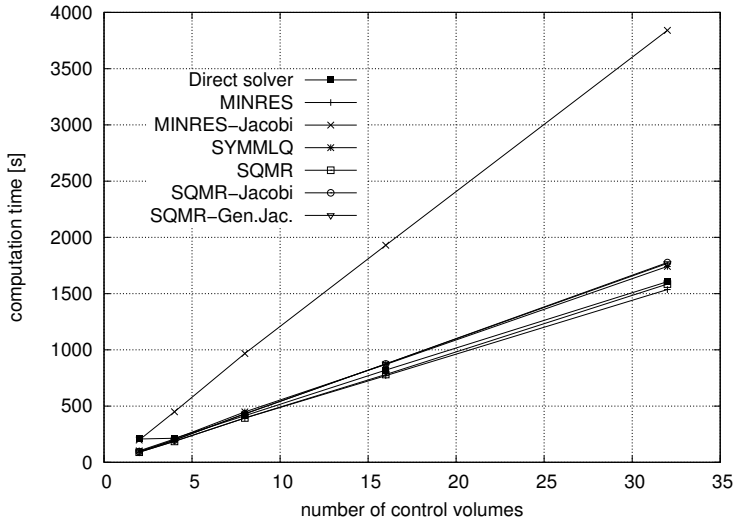

Figure 6.4: Computation times for the benchmark problem without volume coupling

$p^{kg} = 0$ the volume coupling is turned off. As depicted in figure 6.4 the MINRES-method with a Jacobian preconditioner is the slowest solver compared to the rest, requiring almost the same computation time. The MINRES and the SQMR schemes without a preconditioner are faster than the direct solver, whereas the SYMMLQ and the SQMR schemes with a preconditioner need more computation time than the direct solver. Obviously the chosen preconditioners are not able to enhance the convergence rate of the iterative solvers. Comparing the computation times of the iterative solvers

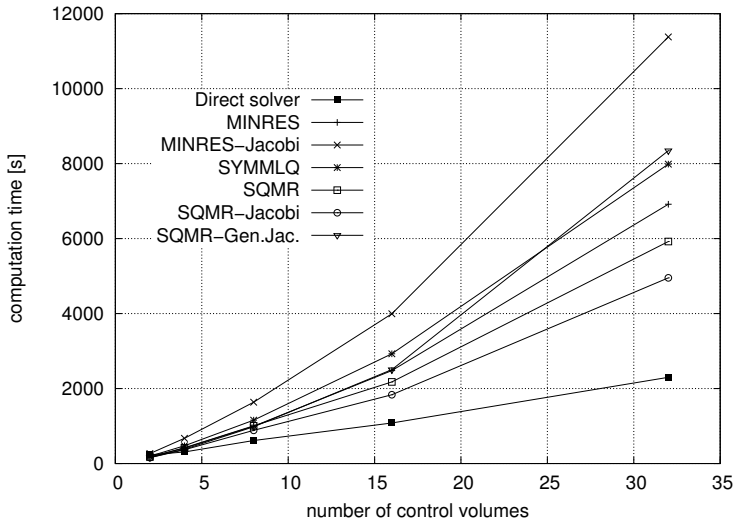

Figure 6.5: Computation times for the benchmark problem with volume coupling

and the direct solver, the benchmark with volume coupling, see figure 6.5, reveals

that the computation time for the direct solution algorithm only increases linearly with increasing number of control volumes. However, for the iterative solvers the computation time increases exponentially. Although it was shown that the number of iterations per Newton step remains constant from a certain number of control volumes on, the number of iterations and thus the number of operations, which is further increased by a preconditioner, is still very high with about 10000 iterations. Using state-of-the-art preconditioners, such as e.g. the ILU-preconditioner (incomplete LU decomposition) or its derivatives, see also MAYER[58], requiring only 100 iterations, would certainly be an appropriate remedy. However, they were not yet completely tested for this kind of problems, but currently under investigation.

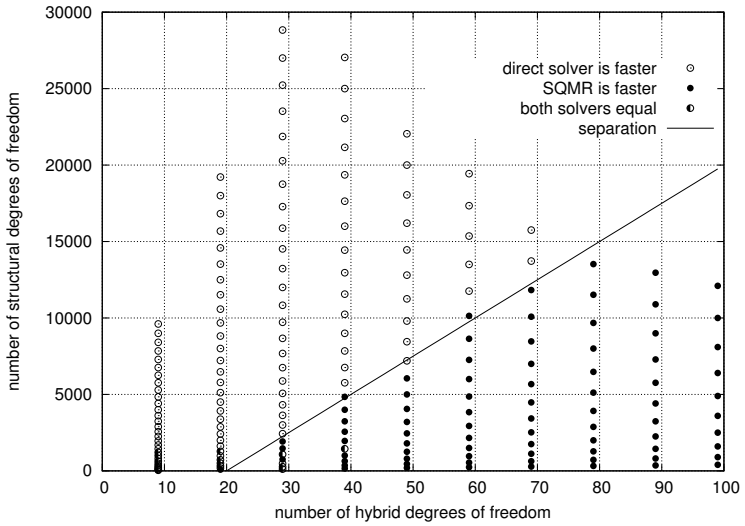

Figure 6.6: Comparison of computation times of direct solver and SQMR-method for an increase of both hybrid and structural degrees of freedom.

Finally a similar benchmark, now varying besides the hybrid unknowns also the number of structural degrees of freedom, is used to compare the SQMR-solver with the direct solver. As depicted in figure 6.6, a relatively small number of structural degrees of freedom with high number of control volumes (e.g. a honeycomb structure), leads to less computation time for the iterative solver compared to the direct one. At least concerning the previously mentioned solvers and preconditioners, the numerical examples performed give hints for the choice of an appropriate solution algorithm. As for increasing degrees of freedom the memory requirements of the direct solution scheme increase quadratically, see table 6.1, for very large systems an iterative solver will be the only choice.

6.3 Eigenvalue analysis

The focus of this section is on the eigenvalue analysis of a gas or fluid filled elastic structure with the goal to judge the stability of a problem. In Bažant[7] a mechanically exact example of a fluid filled pipe under axial loading is discussed, for which the buckling load P_{crit} is identical to the buckling load of an empty pipe and thus making an eigenvalue analysis apparently redundant. However, in this particular case a beam model (implying a uniaxial stress state, constant bending stiffness EI and a constant pressure p) was chosen for the pipe resulting in an eigenvalue problem $(EIw^{IV} + P_{crit}w'') = 0$ for the calculation of the critical buckling load P_{crit}, which is then independent of the internal pressure p. Considering the fact that actually in such an elastic thin-walled pipe, not a uniaxial stress state, but a plane stress state exists, means that the circumferential stresses caused by the pressure can have a major influence on the stiffness and thus may lead to significantly higher buckling loads as well, see also Stegmüller et al.[99]. A further reason for the investigation of the eigenvalues for such kind of problems is the coupling of the structural degrees of freedom and the internal state variables of the fluid presented in the previous chapters. Besides the geometric stiffness mentioned above, due to the volume coupling, an internal fluid loading has a further stabilizing influence on the tangent stiffness matrix $\underline{K}$, which is reflected in the rank-update

$$\underline{A} = \underline{K} + \alpha_t \underline{a}\underline{a}^T \ . \tag{6.33}$$

This rank-update essentially spoils the band structure of the stiffness matrix $\underline{K}$ and leaves an almost fully occupied matrix $\underline{A}$ and is thus producing additional numerical effort for the solution of the eigenvalues. To reduce the effort an algorithm based on the suggestions of Weissenburger[110] and Schweizerhof et al.[89] is presented here. To bypass the solution with such an almost fully populated system matrix in a first step the standard eigenvalue problem

$$\underline{K}\ \underline{\psi}_i = \lambda_i\ \underline{\psi}_i \tag{6.34}$$

has to be solved. With conventional algorithms, as for example a subspace iteration method, the eigenvalues λ_i and the eigenvectors $\underline{\psi}_i$ of the matrix $\underline{K}$, having the structure of a standard structural matrix, can be computed. In the next step the effect of the dyadic update of $\underline{K}$ with the rank-update $\alpha_t \underline{a}\underline{a}^T$ on the eigenvalues and -vectors will be investigated. Initially the special case of a single chamber only loaded with gas will serve as an example, however, in section 6.3.4 the general algorithm, applicable to a system with arbitrary combinations of fluid or gas loadings is provided.

6.3.1 Computation of shifted eigenvalues

Starting from the standard eigenvalue problem

$$\underline{A}\ \underline{\phi}_i = \chi_i\ \underline{\phi}_i \ , \tag{6.35}$$

where $\underline{\phi}_i$ is denoting the eigenvector, which is mapped to itself by the rule $\underline{A}$ and stretched with the eigenvalue χ_i. The modal vectors $\underline{\phi}_i$ can be assembled in the modal matrix $\underline{\Phi}$ and the associated eigenvalues χ_i in the spectral matrix $\underline{X}$. Rearranging equation (6.35) then leads to

$$\underline{A\Phi} = \underline{\Phi X} \; . \tag{6.36}$$

Subsequently the modal matrix $\underline{\Phi}$ can be separated into a modal factor matrix $\underline{\Xi}$ and the modal matrix $\underline{\Psi}$, which contains all eigenvectors $\underline{\psi}_i$ of the uncoupled stiffness matrix $\underline{K}$. Assuming they have already been computed by equation (6.34) using conventional eigenvalue solvers. Then $\underline{\Phi}$ can be written as:

$$\underline{\Phi} = \underline{\Psi\Xi} = \underline{\Psi} \begin{pmatrix} | & | & & | & & | \\ \underline{\xi}_1 & \underline{\xi}_2 & \dots & \underline{\xi}_i & \dots & \underline{\xi}_n \\ | & | & & | & & | \end{pmatrix} \; . \tag{6.37}$$

All modal vectors are normalized, thus

$$\underline{\Psi}^T \underline{\Psi} = \underline{I} \tag{6.38}$$

Inserting equation (6.37) in (6.36) and left-hand multiplication with $\underline{\Psi}^T$ yields

$$\begin{aligned} \underline{\Psi}^T \cdot | \quad \underline{A\Psi\Xi} &= \underline{\Psi\Xi X} \\ \underline{\Psi}^T \underline{A\Psi\Xi} &= \underline{\Psi}^T \underline{\Psi\Xi X} \\ \underline{\Psi}^T \underline{A\Psi\Xi} &= \underline{\Xi X} \; . \end{aligned} \tag{6.39}$$

With the notation

$$\underline{A}^\star = \underline{\Psi}^T \underline{A\Psi} = \underline{\Psi}^T \left(\underline{K} + \alpha_t \underline{aa}^T \right) \underline{\Psi} \tag{6.40}$$

a modified form of the eigenvalue problem (6.36) is obtained

$$\underline{A}^\star \underline{\Xi} = \underline{\Xi X} \; . \tag{6.41}$$

The modal factor matrix $\underline{\Xi}$ is mapped by the rule $\underline{A}^\star$ to itself again. Using the columns $\underline{\xi}_i$ of the modal factor matrix $\underline{\Xi}$ and the eigenvalues χ_i, equation (6.41) can be turned to the standard form of a special eigenvalue problem.

$$\underline{A}^\star \underline{\xi}_i = \chi_i \, \underline{\xi}_i \tag{6.42}$$

Substituting (6.40) into (6.42) results after some reordering in:

$$\begin{aligned} \left(\underline{\Psi}^T \left[\underline{K} + \alpha_t \underline{aa}^T \right] \underline{\Psi} - \chi_i \underline{I} \right) \underline{\xi}_i &= \underline{0} \\ \left(\underline{\Psi}^T \underline{K\Psi} + \alpha_t \underline{\Psi}^T \underline{aa}^T \underline{\Psi} - \chi_i \underline{I} \right) \underline{\xi}_i &= \underline{0} \end{aligned} \tag{6.43}$$

Using the spectral matrix $\underline{\Lambda}$ of $\underline{K}$

$$\underline{\Lambda} = \underline{\Psi}^T \underline{K\Psi} \tag{6.44}$$

along with the coupling vectors

$$\underline{\bar{a}} = \underline{\Psi}^T \underline{a} \tag{6.45}$$

transformed to the modal space, equation (6.43) simplifies to

$$\left(\underline{\Lambda} + \alpha_t \underline{\bar{a}\bar{a}}^T - \chi_i \underline{I}\right) \underline{\xi}_i = \underline{0} \; . \tag{6.46}$$

For this homogeneous set of equations non-trivial solutions $\underline{\xi}_i \neq \underline{0}$ only exist, if the determinant of the coefficient matrix $\left(\underline{\Lambda} + \underline{\bar{a}\bar{a}}^T - \chi_i \underline{I}\right)$ vanishes.

$$\det\left(\underline{\Lambda} + \alpha_t \underline{\bar{a}\bar{a}}^T - \chi_i \underline{I}\right) = 0 \tag{6.47}$$

Now two cases concerning the coordinates $\bar{a}_j$ must be considered:

Case 1: All coordinates unequal zero $\quad (\bar{a}_j \neq 0)$

In this case all new eigenvalues are different from the old ones: $\chi_i \neq \lambda_i$. This ensures the matrix $(\underline{\Lambda} - \chi_i \underline{I})$ not to be singular. Therefore it can be moved out of the operand in equation (6.47).

$$\det\left[\left(\underline{\Lambda} - \chi_i \underline{I}\right)\left(\underline{I} + \alpha_t \left[\underline{\Lambda} - \chi_i \underline{I}\right]^{-1} \underline{\bar{a}\bar{a}}^T\right)\right] = 0 \tag{6.48}$$

Using the multiplication rule of determinants on equation (6.48) results in

$$\det\left(\underline{\Lambda} - \chi_i \underline{I}\right) \; \det\left(\underline{I} + \alpha_t \left[\underline{\Lambda} - \chi_i \underline{I}\right]^{-1} \underline{\bar{a}\bar{a}}^T\right) = 0 \; . \tag{6.49}$$

An exact transformation given in PEARSON[72] or SCHWEIZERHOF[87] yields for the determinant of the rank-one-updated identity matrix $\underline{I}$:

$$\det\left(\underline{I} + \alpha_t \left[\underline{\Lambda} - \chi_i \underline{I}\right]^{-1} \underline{\bar{a}\bar{a}}^T\right) = 1 + \alpha_t \underline{\bar{a}}^T \left[\underline{\Lambda} - \chi_i \underline{I}\right]^{-1} \underline{\bar{a}} \tag{6.50}$$

Thus the following conditional equation for the eigenvalues χ_i is obtained:

$$\det\left(\underline{\Lambda} - \chi_i \underline{I}\right)\left(1 + \alpha_t \underline{\bar{a}}^T \left[\underline{\Lambda} - \chi_i \underline{I}\right]^{-1} \underline{\bar{a}}\right) = 0 \tag{6.51}$$

As the new eigenvalues are different from the old ones, $\chi_i \neq \lambda_i$, the determinant of the diagonal matrix $(\underline{\Lambda} - \chi_i \underline{I})$ is not equal zero. Consequently the second factor in equation (6.51) must be identical to zero to ensure the existence of non-trivial solutions. For the eigenvalues χ_i the characteristic polynomial $p(\chi)$ is obtained:

$$p(\chi) = 1 + \alpha_t \underline{\bar{a}}^T \left[\underline{\Lambda} - \chi \underline{I}\right]^{-1} \underline{\bar{a}} = 0 \tag{6.52}$$

Because $(\underline{\Lambda} - \chi \underline{I})$ is a diagonal matrix, the polynomial $p(\chi)$ can be simplified by summing up the product of the reciprocals of the j^{th} diagonal element with the square of the j^{th} coordinate $\bar{a}_j$.

$$p(\chi) = 1 + \alpha_t \sum_{j=1}^{n} \frac{\bar{a}_j \bar{a}_j}{\lambda_j - \chi} = 0 \tag{6.53}$$

Function (6.53) has poles at the eigenvalues λ_i of the stiffness matrix $\underline{K}$. Further on, function (6.53) has for a positive α_t the following limits between the poles (see also figure 6.7):

$$\lim_{\chi \to \lambda_j^+} = -\infty \ , \quad \lim_{\chi \to \lambda_{j+1}^-} = \infty \ , \quad \lim_{\chi \to -\infty} = 1 \quad \text{and} \quad \lim_{\chi \to \infty} = 1 \ . \tag{6.54}$$

These limits show that the polynomial will tend to $-\infty$, if the new eigenvalue χ_j is either slightly larger than the old eigenvalue λ_j or the polynomial will tend to ∞, if χ_j is slightly below the the old eigenvalue λ_{j+1}. As the characteristic polynomial $p(\chi)$ is strictly monotone between its poles, the new eigenvalues χ_i resp. the zero values of $p(\chi)$, must therefore lie somewhere in-between the poles. The pressure volume gradient α_t can be physically seen as a kind of spring constant of the gas. Negative values for α_t are therefore artificial and physically not possible. A closer look at the definition

$$\alpha_t = \kappa \frac{p_t^{kg}}{\bar{v}_t^g} \tag{6.55}$$

shows, that neither negative volumes $\bar{v}_t^g$ nor negative pressures p_t^{kg} exist and thus for a positive adiabatic exponent κ α_t is always greater zero. As depicted in Fig. 6.7 the

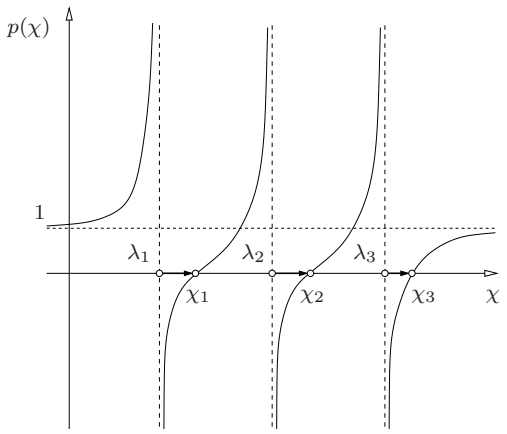

Figure 6.7: Eigenvalue shift at the example of a 3rd order polynomial $p(\chi)$ and $\alpha_t > 0$

new eigenvalues χ_i will increase for a positive pressure volume gradient α_t, resp. a gas/fluid support. Hence the coupling of an elastic structure with a gas or fluid filled control volume, storing additional strain energy, yields to an increase of the structural stiffness.

$$\lambda_1 < \chi_1 < \lambda_2 < \chi_2 < ... < \lambda_n < \chi_n \tag{6.56}$$

As already mentioned the polynomial $p(\chi)$ is strictly monotone between the poles λ_j, therefore an efficient method to localize the zeroes in $p(\chi)$ can be found by the bisection method. For a given tolerance *tol*

$$n > \log_2 \left(\frac{\lambda_{j+1} - \lambda_j}{tol} \right) \tag{6.57}$$

iterations are necessary to approximate the new eigenvalue χ_j, see also FAIRES&BURDEN[27]. Besides the fact, that the fluid loading has an effect on the structural stiffness it has to be considered that the right-hand side of the equation system is affected as well. Thus a small gain of stiffness cannot guarantee a large improvement of the overall stability of fluid loaded structures. However, for membranes the fluid/gas loadings are providing the only stiffness beyond the stresses in the structure created by the pressure.

Case 2: Coordinate $\bar{a}_j = 0$

Physically, the modified coupling vector $\underline{\bar{a}}$ represents the volume change of the structure. If a specific degree of freedom has no influence on the volume change, the associated coordinate $\bar{a}_j = 0$ of the coupling vector consequently will be zero. This means that the corresponding eigenvalue λ_j and eigenmode $\underline{\phi}_j$ are not affected by the gas support and therefore will remain untouched. The mathematical interpretation of this fact is that in this case the matrix

$$\underline{\Lambda} + \alpha_t \underline{\bar{a}}\underline{\bar{a}}^T - \chi_i \underline{I} \tag{6.58}$$

contains zero entries in the j^{th} row and the j^{th} column, except for the diagonal element. This has the effect that the j^{th} eigenvalue χ_j of (6.58) equals the old eigenvalue λ_j. Therefore in a first step of the algorithm, all zero entries must be filtered out of the coupling vector $\underline{\bar{a}}$ and the associated rows and columns in the spectral matrix $\underline{\Lambda}$ must be reduced likewise. Thus we obtain a reduced coupling vector $\underline{\hat{a}}$ without any zero entries and a reduced spectral matrix $\underline{\hat{\Lambda}}$. We can then proceed in analogy to case 1 (6.53) with the characteristic polynomial $\hat{p}(\chi_i)$ of a reduced order.

$$\hat{p}(\chi_i) = 1 + \sum_{j=1}^{m} \frac{\hat{a}_j \hat{a}_j}{\hat{\lambda}_j - \chi} = 0 \ , \qquad \text{with} \quad \chi \neq \lambda_j \ , \quad m < n \ . \tag{6.59}$$

As the particular new eigenvalues $\chi_i = \lambda_i$ have been filtered out of the set of all n eigenvalues, this polynomial can now be used to locate all remaining m new eigenvalues, which are affected by the volume coupling.

6.3.2 Computation of eigenvectors

For the computation of the corresponding eigenvectors equation (6.46) is considered again, focusing on the column $\underline{\xi}_i$ of the modal factor matrix $\underline{\Xi}$:

$$\left(\underline{\Lambda} + \alpha_t \underline{\bar{a}}\underline{\bar{a}}^T - \chi_i \underline{I}\right) \underline{\xi}_i = \underline{0} \ . \tag{6.60}$$

Rearranging this equation yields

$$\begin{aligned}(\underline{\Lambda} - \chi_i \underline{I})\,\underline{\xi}_i &= -\alpha_t \left(\underline{\bar{a}}\underline{\bar{a}}^T\right)\underline{\xi}_i \\ (\underline{\Lambda} - \chi_i \underline{I})\,\underline{\xi}_i &= -\alpha_t \underline{\bar{a}} \left(\underline{\bar{a}}^T \underline{\xi}_i\right) \\ \underline{\xi}_i &= -\alpha_t \left(\underline{\Lambda} - \chi_i \underline{I}\right)^{-1} \underline{\bar{a}} \left(\underline{\bar{a}}^T \underline{\xi}_i\right) \ . \end{aligned} \tag{6.61}$$

To eliminate the implicit form of $\underline{\xi}_i$ it can be normalized by its length, leading to

$$\underline{\xi}_i = -\frac{\alpha_t \left(\underline{\Lambda} - \chi_i \underline{I}\right)^{-1} \underline{\bar{a}} \ \left(\underline{\bar{a}}^T \underline{\xi}_i\right)}{||\alpha_t \left(\underline{\Lambda} - \chi_i \underline{I}\right)^{-1} \underline{\bar{a}} \ \left(\underline{\bar{a}}^T \underline{\xi}_i\right)||} = -\frac{\left(\underline{\Lambda} - \chi_i \underline{I}\right)^{-1} \underline{\bar{a}}}{||\left(\underline{\Lambda} - \chi_i \underline{I}\right)^{-1} \underline{\bar{a}}\ ||} \tag{6.62}$$

as the i^{th} column of $\underline{\Xi}$. With the multiplicative split (6.37) and the modal factor matrix $\underline{\Xi}$ composed accordant (6.62) the transformed modal matrix can then be computed:

$$\underline{\Phi} = \underline{\Psi}\underline{\Xi} = \underline{\Psi} \begin{pmatrix} | & | & & | & & | \\ \underline{\xi}_1 & \underline{\xi}_2 & \cdots & \underline{\xi}_i & \cdots & \underline{\xi}_n \\ | & | & & | & & | \end{pmatrix} \tag{6.63}$$

In the case of zero entries in the coupling vector the reduced modal matrix $\underline{\hat{\Phi}}$, which can also be computed according to this outlined scheme, must be amended by the old eigenvectors corresponding to the zero entries of $\underline{\bar{a}}$ to make it complete.

6.3.3 Efficiency considerations: How many eigenpairs needed?

In most engineering problems only a few lower eigenvalues are of interest. But an obvious disadvantage in the presented algorithm is the fact that – although only a few eigenvalues χ_i and the associated eigenmodes $\underline{\phi}_i$ of the system matrix $\underline{A}$ are to be computed – in a preceding computation both all eigenvalues λ_j of the global stiffness matrix $\underline{K}$ are necessary to set up the characteristic polynomial $p(\chi)$ and the complete modal matrix $\underline{\Psi}$ of $\underline{K}$ with all its decoupled eigenvectors is needed to obtain the new modal matrix $\underline{\Phi}$ via the product approach (6.63).

In this section a reduction of the general case with all n eigenvalues and n eigenmodes of $\underline{K}$ is discussed, showing that using only $m < n$ eigenpairs, usually lower ones, are sufficient. A central factor in the modal analysis within this scheme are the distances of the old eigenvalues λ_j among each other, because they determine the coupling. If all eigenvalues λ_{j+1} are considerably smaller than all following eigenvalues λ_{m+1}

$$\lambda_{j+1} \ll \lambda_{m+1} \ , \tag{6.64}$$

then we can assume for the new eigenvalues χ_j with

$$\lambda_j < \chi_j < \lambda_{j+1} \ll \lambda_{m+1} \ , \tag{6.65}$$

that they remain considerably smaller than λ_{m+1}:

$$\chi_j \ll \lambda_{m+1} \ . \tag{6.66}$$

Therefore – although for the computation of the first $j = 1..m$ shifted eigenvalues χ_j in the strict sense all old eigenvalues $\lambda_1 ... \lambda_j ... \lambda_n$ must be considered – all summands in the characteristic polynomial for $m+1 \leq j \leq n$ are negligible compared to the rest. Thus under the assumption $\bar{a}_j \ll \lambda_{m+1}$ (verification of the assumption at the end of section) we get

$$\begin{aligned} p(\chi) &= 1 + \alpha_t \sum_{j=1}^{m} \frac{\bar{a}_j \bar{a}_j}{\lambda_j - \chi} + \alpha_t \sum_{j=m+1}^{n} \frac{\bar{a}_j \bar{a}_j}{\lambda_j - \chi} = 0 \\ &\approx 1 + \alpha_t \sum_{j=1}^{m} \frac{\bar{a}_j \bar{a}_j}{\lambda_j - \chi} \ . \end{aligned} \tag{6.67}$$

Looking at this polynomial it is clear, that once the distance between the eigenvalues is large enough, then the updated lower eigenvalues χ_j remain almost unaffected by higher ones greater than λ_m. Thus both the search for the old eigenvalues λ_j with conventional methods and the search for the zeroes in $p(\chi)$ with the bisection method can be restricted to a minimum number m, which may reduce the computational effort considerably for large FE-problems. The same argument is valid to reduce the number of eigenvectors $\underline{\psi}_i$ of $\underline{K}$ necessary for the setup of the new modal matrix $\underline{\Phi}$. Looking at equation (6.62) again, the non-normalized vector can be written as

$$\underline{\xi}_i^\star = -\left(\underline{\Lambda} - \chi_i \underline{I}\right)^{-1} \underline{\bar{a}} = - \begin{bmatrix} \bar{a}_1 / \left(\lambda_1 - \chi_i\right) \\ \bar{a}_2 / \left(\lambda_2 - \chi_i\right) \\ \vdots \\ \bar{a}_n / \left(\lambda_n - \chi_i\right) \end{bmatrix} \tag{6.68}$$

and its norm is given by

$$|\underline{\xi}_i^\star| = \sqrt{\left(\frac{a_1}{\lambda_1 - \chi_i}\right)^2 + \left(\frac{a_2}{\lambda_2 - \chi_i}\right)^2 + \ \ldots \ + \left(\frac{a_n}{\lambda_n - \chi_i}\right)^2} \ . \tag{6.69}$$

As already demonstrated for large distances between the eigenvalues and with equation (6.66) the coordinates of $\underline{\xi}_i^\star$ can be approximated by

$$\xi_{ij}^\star = \frac{a_j}{\lambda_j - \chi_i} \quad \text{for} \quad j < m \tag{6.70}$$

and

$$\xi_{ij}^\star = 0 \quad \text{for} \quad j > m \ . \tag{6.71}$$

The norm of $\underline{\xi}_i^\star$ is less affected by eigenvalues λ_j with large distance to χ_i, because here the squares of the reciprocals of the distances are computed. Thus looking at equation (6.63)

$$\underline{\phi}_i = \begin{pmatrix} | & | & & | & & | \\ \underline{\psi}_1 & \underline{\psi}_2 & \dots & \underline{\psi}_j & \dots & \underline{\psi}_n \\ | & | & & | & & | \end{pmatrix} \underline{\xi}_i \ , \tag{6.72}$$

reveals, that the j^{th} coordinate in vector $\underline{\xi}_i$ obviously represents the influence of the old modal vector $\underline{\psi}_j$ of $\underline{K}$ on the computation of the shifted eigenvector $\underline{\phi}_i$ due to the rank-1-update, which gives an a posteriori control for $\underline{\Xi}$: To estimate the accuracy of the eigenmodes $\underline{\phi}_i$, computed with a reduced set of m eigenvalues λ_j and -vectors $\underline{\psi}_j$, the modal factor matrix $\underline{\Xi}$ must be considered. As the entries in the matrix $\underline{\Xi}$ are scaling factors for the coordinates of the old eigenmodes, their absolute magnitude gives a quantitative criterion on the mutual interference of the eigenmodes. In the case of a fully populated matrix either the mutual influence of the eigenvectors is obviously high or the previous assumption $\bar{a}_j \ll \lambda_{m+1}$ was not correct, which means that a new computation with a larger set of eigenvalues λ_j and -vectors $\underline{\psi}_j$ is probably necessary. This is the case if e.g. a symmetric structure has multiple equal or almost equal eigenvalues, but the chosen modal reduction basis does not consider all of them. In the case of a less populated modal factor matrix with a dominantly diagonal shape, a new computation with a larger modal set would not affect the solution remarkably. But in any case the criterion for choosing an appropriate modal basis depends on the user's decision how exact the answer should be, see also HASSLER&SCHWEIZERHOF[39].

6.3.4 Multiple rank-updates

Although it may seem that the derived algorithm is only valid for a rank-one-update of the stiffness matrix $\underline{K}$, multiple rank-updates can easily be taken into account by a sequential application of this method. I. e. in the case of a closed chamber, which is partially filled with a heavy incompressible fluid and an additional gas volume (see Fig. 3.1), according to equation (4.58) or HASSLER&SCHWEIZERHOF[40], the system matrix $\underline{A}$ in the equilibrium equations features a rank-2-update:

$$\underline{A} = \underline{K} + \alpha_t \left(\underline{a} + \underline{b}\right) \left(\underline{a} + \underline{b}\right)^T + \gamma_t \underline{b}\underline{b}^T \ , \tag{6.73}$$

where α_t again couples the total volume change $(\underline{a} + \underline{b})$ with the gas pressure change Δp^{kg} and the pressure volume gradient γ_t at time t couples the change of the fluid level $\Delta \underline{x}^o$ with the volume change $\underline{b}$ under the wetted shell surface. To compute the eigenvalues and -vectors the stiffness matrix with the first rank update is split according to equation (6.73), which leads to a matrix $\underline{A}^1$ only affected by the total volume change $(\underline{a} + \underline{b})$:

$$\underline{A}^1 = \underline{K} + \alpha_t \left(\underline{a} + \underline{b}\right) \left(\underline{a} + \underline{b}\right)^T \tag{6.74}$$

For this rank-one-update the eigenvalues and -vectors can be computed as described in the previous section. In the same manner the shift of eigenvalues and -vectors of $\underline{A}^1$ due to the second rank update can be computed.

$$\underline{A} = \underline{A}^1 + \gamma_t \underline{b}\underline{b}^T \tag{6.75}$$

A closer look at the characteristic equation for the determination of the eigenvalues χ of $\underline{A}$ reveals an interesting feature of the eigenvalues χ. In analogy to equation (6.49), the modified coupling vectors

$$\underline{\bar{a}} = \underline{\Psi}^T (\underline{a} + \underline{b}) \quad \text{and} \quad \underline{\bar{b}} = \underline{\Psi}^T \underline{b} \tag{6.76}$$

can be set up using the modal matrix $\underline{\Psi}$ of $\underline{K}$. These modified coupling vectors can then be used, along with the spectral matrix $\underline{\Lambda}$, to formulate the characteristic equation for the determination of the eigenvalues χ of the system matrix $\underline{A}$, now featuring a rank-two-update:

$$\det (\underline{A} - \chi \underline{I}) = \det \left(\underline{\Lambda} + \alpha_t \underline{\bar{a}}\underline{\bar{a}}^T + \gamma_t \underline{\bar{b}}\underline{\bar{b}}^T - \chi_i \underline{I} \right) = 0 \tag{6.77}$$

Similar to the procedure in section 6.3.1 the matrix $\underline{\Lambda} - \chi_i \underline{I}$ can be moved out of the operand in equation (6.77). A further application of the multiplication rule of determinants thus yields under the assumption $\det (\underline{\Lambda} - \chi_i \underline{I}) \neq 0$:

$$p(\chi) = \det \left(\underline{I} + [\underline{\Lambda} - \chi_i \underline{I}]^{-1} \left[\alpha_t \underline{\bar{a}}\underline{\bar{a}}^T + \gamma_t \underline{\bar{a}}\underline{\bar{a}}^T \right] \right) = 0 \ . \tag{6.78}$$

This characteristic equation still has poles at the eigenvalues λ_i of the stiffness matrix $\underline{K}$. The fact that $p(\chi)$ is also still strictly monotone between the poles and still features the limits (6.54) reveals, that although the rank updates lead to an increase of the eigenvalues χ_i, the relation

$$\lambda_i < \chi_i < \lambda_{i+1} \tag{6.79}$$

still holds, see also figure 6.8.

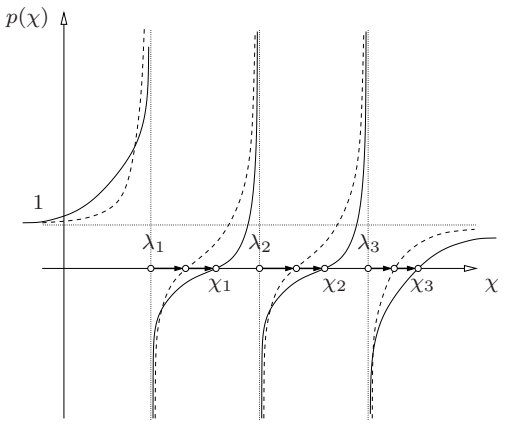

Figure 6.8: Double eigenvalue shift at the example of a 3rd order polynomial $p(\chi)$ as the characteristic equation for the determination of the eigenvalues of a rank-2-updated matrix $\underline{A} = \underline{K} + \alpha_t \left(\underline{a} + \underline{b}\right) \left(\underline{a} + \underline{b}\right)^T + \gamma_t \underline{b}\underline{b}^T$

Chapter 7

Numerical examples

The previously derived algorithms for the analytical description of fluid and gas filled structures are now used for the computation of several practical examples showing the specific effects of fluid and/or gas loading. At the example of the inflation and subsequent hydrostatic loading of a rubber dam the interaction of a fluid and a gas volume with the surrounding structure and external fluid loading is demonstrated. The deployment of the dam is performed using both gas and an incompressible fluid. The following example additionally considers the fluid compressibility, therefore as a practical application the high-pressure tube hydroforming of thin metal sheets is chosen. As the deformation dependent loading also effects the structural stability to a certain degree, a quantification of these effects is performed at an axially loaded steel cylinder under several fluid/gas loading conditions. In a further example the load-deflection and buckling behaviour of gas supported beams is investigated to judge the performance of conventional one-dimensional formulations for inflatable beams. The influence of multiple interacting fluid filled chambers on the computation of the inner state variables is investigated at the example of a buoyancy simulation of a cross-section of a double hull tanker, consisting of four separate chambers. As the last example, the transition from the analytical fluid description (wich is restricted to quasi-static processes) to the simulation of dynamical problems, such as wave propagation in fluids, is presented and thus tieing in with the field of acoustics by applying also a discretization of the fluid.

7.1 Rubber dam

The first application of the derived fluid-structure interaction algorithms is performed at the example of an inflatable dam. Inflatable dams, as depicted in figure 7.1, have several economical advantages compared to conventional barrages, as e.g. lever-, sector- or roller weirs. Due to their simple construction principle, neither complex control mechanisms nor a costly maintenance is necessary for regulating the retention water level elevation. Since most of these retaining structures were built during the last two decades, the technology is relatively young and partially afflicted with failures. A comprehensive study of rubber dams and their hydraulic design can be found in

GEBHARDT[31].

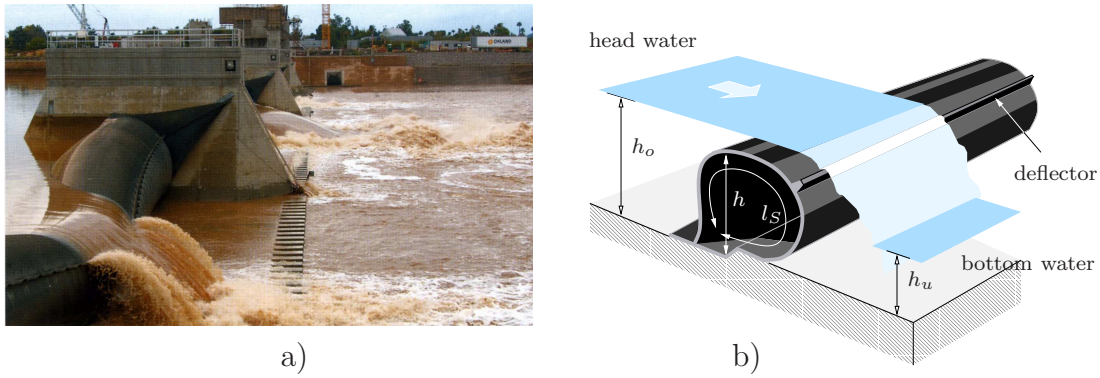

Figure 7.1: a) Photo and b) sketch of an inflated and overflowed rubber dam (source of photography: GEBHARDT ET AL.[32])

As in all subsequent computations the discretization of the rubber dam is performed using membrane elements, which are initially slack and thus kinematical, the computations are carried out with a Newmark time-integration scheme, also considering the inertia of the structure for the regularization of the equations. Since the negligence of the kinetic energy of the fluid is one of the basic assumptions of the derived formulations, both the filling process and the subsequent loading of the dam are performed quasi-statically, see also figure 7.2. Another possible solution procedure would be an

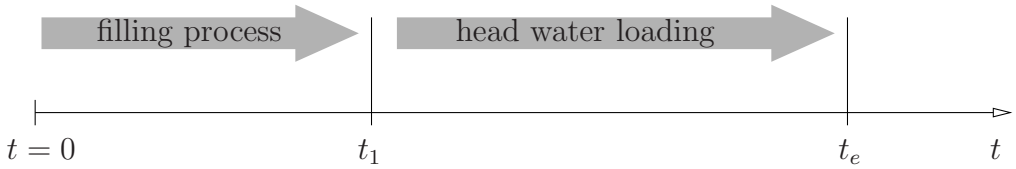

Figure 7.2: Time proportional load sequence for the dynamic computation of the gas or water inflated rubber dam subjected to head water loading

initial pressurizing of the dam using a dynamic solution scheme, in order to slightly prestress the structure. Since after this first step the structure features a sufficient stiffness, a static solution would then be possible after a restart of the computation. However, the condition number of the system matrix is considerably high and thus – even for small load step increments – leading to a diverging direct solution and to a large number of iterations per Newton step in case of an iterative solver. Hence, compared to an iterative static solution of the prestressed system for this example a completely dynamical solution is the more efficient way and thus preferred. To keep the number of Newton iterations per time step at a maximum of 2, the time steps for each computation are chosen to $\Delta t = 0.1\,\mathrm{s}$.

7.1.1 2D model of the rubber dam

Before computing the full three-dimensional model a two-dimensional cross-section model is taken to compare the numerical solution of the weir geometry with an analytical approach, validated in Gebhardt[31].

Air inflated rubber dam subjected to hydrostatic loading

An analytical solution of an air inflated and not overflowed rubber dam cross-section, depicted in figure 7.3, a completely static problem, is given in Anwar[3]. It is derived by a pure balance of forces at a cut free dam, assuming a dam curve tangential to the bottom at the unloaded side. Further, a pure membrane theory is assumed, which results in an exact half circle for the geometry at the bottom water as a solution of the differential equation describing the state of equilibrium.

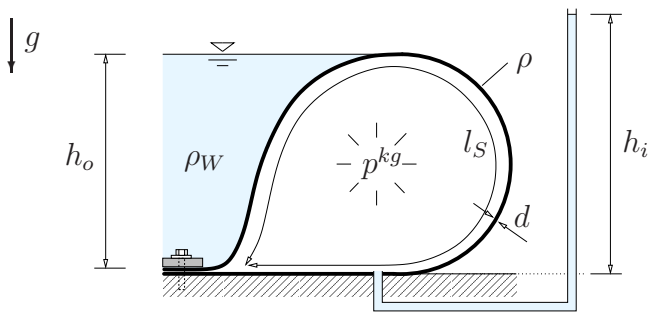

dam geometry
$l_S = 840\,\text{mm}$
$d = 0.7\,\text{mm}$
dam material (lin. elastic)
$E = 60\,\text{N/mm}^2$
$\nu = 0.4$
$\rho = 1.2 \cdot 10^3\,\text{kg/m}^3$
gravity and water density
$g = 9.81\,\text{m/s}^2$
$\rho_W = 1.0 \cdot 10^3\,\text{kg/m}^3$

Figure 7.3: Schematic diagram and material parameters of the air inflated rubber dam

The numerical model in this thesis is fixed by a vertical and horizontal displacement boundary condition; contact to the rigid bottom is modeled using a penalty formulation. For the cross-section with a length of $l_S = 840\,\text{mm}$ and a thickness of the membrane of $d = 0.7\,\text{mm}$ 100 geometrically nonlinear membrane elements are used. The appropriate parameters are given in figure 7.3. In this analysis the internal gas pressure p^{kg} is varied, resulting in different geometric curves for the dam, which is subjected to a hydrostatic loading at the head water, reaching to the weir crest. As visible in figure 7.4, for different coefficients of the internal pressure

$$\alpha = \frac{p^{kg}}{h_o \rho_W g} \,, \tag{7.1}$$

the analytical and numerical results for the weir geometry fit very well. An exception is the low pressurized dam with $\alpha = 0.52$, where the numerical and the analytical solutions slightly differ. Interestingly, this complies with experiments made by Gebhardt[31], where the measured weir curve was also situated slightly above the

analytical one for a low pressurized weir with $\alpha = 0.53$. The analytical solution is in this range numerically very sensitive and thus less accurate.

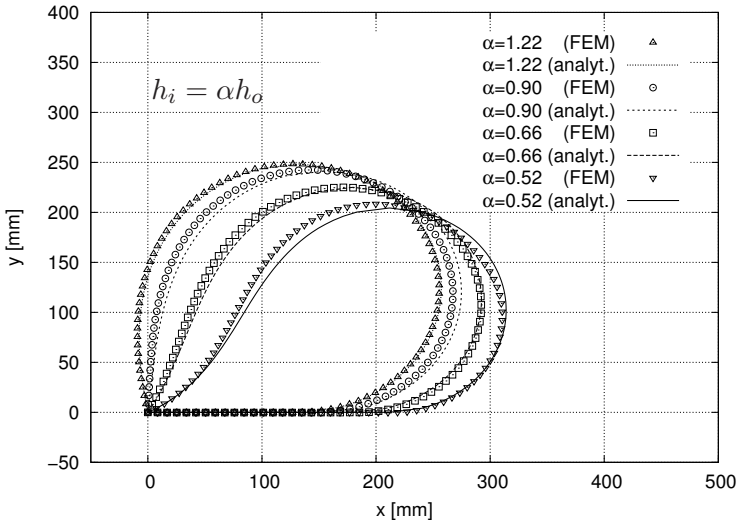

Figure 7.4: Air inflated rubber dam: weir geometries for different coefficients of the internal pressure α; comparison of analytical and numerical solution.

Water filled rubber dam subjected to hydrostatic loading

Since the slack membrane initially features almost no stiffness, numerical difficulties will be encountered, if the structure is subjected to an internal fluid overpressure, which causes large structural deformations and thus, depending on the bulk modulus K_0 of the fluid, eventually also large negative pressure increments for a completely filled structure. In order to bypass this difficulty the filling of the dam is achieved by an incompressible fluid with an additional small air bubble, which secures, that the structure is not completely fluid-filled and thus an incompressible filling medium can be chosen. The discretization of the water filled dam depicted in figure 7.5 was carried out using the same parameters as for the previous example. Although the derivations in ANWAR[3] also cover this case of a water filled dam, the solution contains several gaps and some unclear schemes, see GEBHARDT[31]. Therefore as an analytical solution the approach given in MLIT[60] is used for the analytical solution.

In analogy to the previous example the numerical and analytical weir geometries match very well for different coefficients α, see figure 7.6. An exception is again the low pressurized dam, with $\alpha = 1.18$, where the analytical dam curve is slightly below the numerical one. Again this complies with the experimental observations in GEBHARDT[31], where the measured geometry for the low pressurized weir with $\alpha = 1.04$ is situated slightly above the analytical one.

A possible reason for this effect could be that the solutions of the analytical dam curves can only be obtained by a numerical integration of their differential equations, using

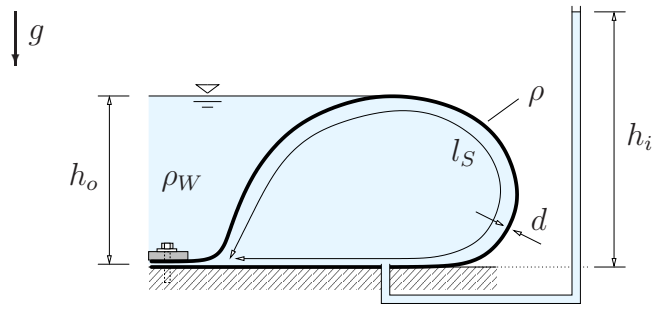

dam geometry

$l_S = 840\,\mathrm{mm}$

$d = 0.7\,\mathrm{mm}$

dam material (lin. elastic)

$E = 60\,\mathrm{N/mm^2}$

$\nu = 0.4$

$\rho = 1.2 \cdot 10^3\,\mathrm{kg/m^3}$

gravity and water density

$g = 9.81\,\mathrm{m/s^2}$

$\rho_W = 1.0 \cdot 10^3\,\mathrm{kg/m^3}$

Figure 7.5: Schematic diagram and material parameters of a rubber dam filled with water

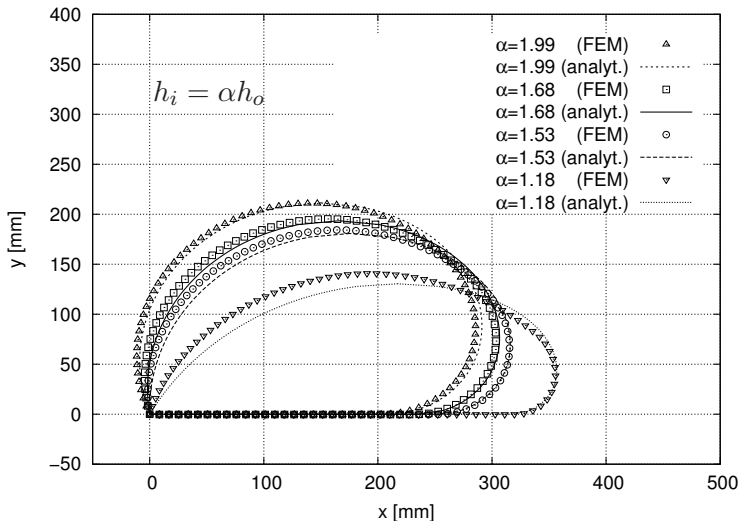

Figure 7.6: Water inflated rubber dam: weir geometries for different coefficients of the internal pressure α

elliptic integrals, as e.g. for the air inflated membrane

$$\xi = \sqrt{\frac{\alpha}{2}} \int\limits_{\arccos\left(\frac{\eta}{\alpha}-1\right)}^{\pi} \frac{1-\alpha\sin^2\psi}{\sqrt{1-\frac{\alpha}{2}\sin^2\psi}} d\psi \ , \tag{7.2}$$

where ξ is the unknown function for the membrane curve at the head water and which is depending on the dimensionless height $\eta = y/h_o \in [0,1]$. In case of an air filling the limit is $\alpha_{crit} = 0.50$ (from this value on the membrane at the head water touches the bottom) and in case of a water filling the limit is $\alpha_{crit} = 1.00$. Values below the critical ones would cause the numerical solution algorithm to fail, see also GEBHARDT[31], because these values mark the end of the domain of definition. Solutions for weir

curves with pressure coefficients close to the critical values $\alpha \approx \alpha_{krit}$ are therefore affected by numerical errors.

7.1.2 3D model of the rubber dam

In the following a three-dimensional model of a rubber dam, consisting of an uncoiled flexible tube, is investigated. The dam is clamped along its head water edge. For reasons of simplicity the dam is assumed to follow membrane kinematics, therefore no prestresses due to the uncoiling have to be considered. However, if the focus is rather on the design of the structure than on the pure geometry, a shell formulation would be the appropriate kinematical approximation, considering also the bending stresses in the vicinity of the clamped edge. Further, due to these large bending stresses resp. strains, a nonlinear elastic material law, such as a Neo-Hooke may be necessary. For reasons of symmetry only half of the weir, depicted in figure 7.7, is discretized using 60 element divisions for the length l, 40 for the width b and 20 for the cheek length a. All 6500 geometrically nonlinear 4-node membrane elements feature an isotropic St. Venant-Kirchhoff material. The application of a nonlinear material is not necessary in this case, as the membrane features indeed large deflections but only small strains. Geometry and material parameters are given in figure 7.7. For the contact between the cheeks of the weir and the bottom a penalty formulation is used.

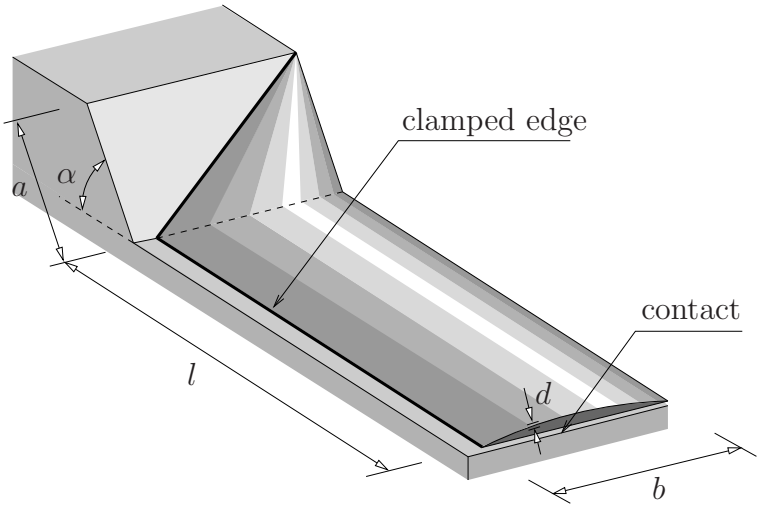

$$
\begin{aligned}
l &= 8000\,\text{mm} \\
b &= 3000\,\text{mm} \\
a &= 2000\,\text{mm} \\
d &= 20\,\text{mm} \\
\alpha &= 60^\circ \\
E &= 60\,\text{N/mm}^2 \\
\nu &= 0.4
\end{aligned}
$$

Figure 7.7: Geometry and material parameters of the uncoiled rubber dam

As the volume computing algorithm needs an initial volume not equal to zero, the geometry is generated in such a way, that the upper and lower membrane do not coincide. As depicted in figure 7.2 the filling and loading processes both for the air and for the water filled dam are performed, similar to the two-dimensional analyses, in sequential steps using a Newmark time-integration algorithm with small mass and

stiffness proportional Rayleigh damping parameters of $\alpha = 0.05$ for the mass matrix and $\beta = 0.05$ for the stiffness matrix.

Air inflated rubber dam subjected to hydrostatic loading

Inflation process:

The uncoiled flexible tube is first subjected to an increasing internal gas pressure p^{kg}, inflating the membrane in the time $t = 0\,\text{s}$ to $t = 10\,\text{s}$ without any hydrostatic loading. To keep the number of Newton iterations per time step at a maximum of 2, the time step is chosen to $\Delta t = 0.1\,\text{s}$. Figure 7.8 a) shows the completely deployed weir at time $t = 100\,\text{s}$.

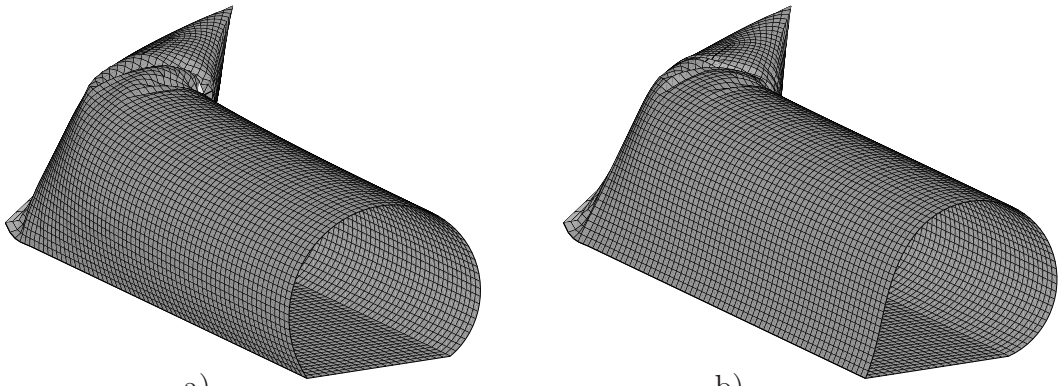

a) b)

Figure 7.8: a) Air filled rubber dam without hydrostatic loading. b) air filled rubber dam with head water level $h_o = 1600\,\text{mm}$ ($\alpha = 0.60$).

The inflation process can also be used to improve the rubber geometry against undesirable wrinkles in the vicinity of the cheeks of the weir, removing redundant material and thus unnecessary costs. Using a parameter study of the geometric variables, such as incline of the cheeks or the circumference of the weir, the final shape of the dam could be optimized with respect to a minimum of wrinkles. This is the subject of further investigations.

Hydrostatic loading:

In order to simulate a rubber dam with purely hydrostatic loading, but without an overflow, in the next loading phase, starting from $t = 100\,\text{s}$, the head water level is steadily increased, until it reaches the weir crest, see also figure 7.9. The influence of the hydrostatic head water loading on the dam height is marginal. As shown in figure 7.9 the dam height does not alter until $t = 170\,\text{s}$, which complies to a head water level of $h_o = 1400\,\text{mm}$, resp. 90% of the dam height. From this point on the dam height drops about 40 mm. First the hydrostatic load has almost no effect on the internal gas pressure of the dam. However, when approaching the weir crest the hydrostatic pressure causes a volume change of the structure, which complies with an

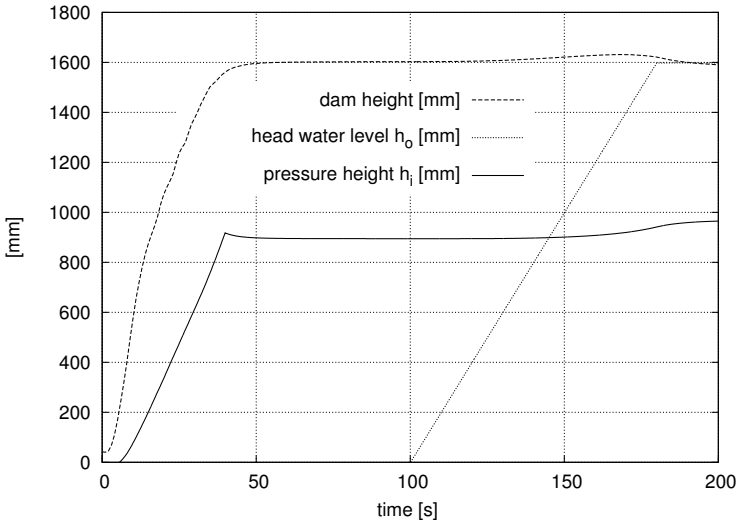

Figure 7.9: Air filled rubber dam: Developments of dam height, head water level h_o and pressure height $h_i = p^{kg}/\rho_W g$ over loading time t.

increase of the internal gas pressure of about 7%, see figure 7.9. In figure 7.8 b) the final shape of the rubber dam is depicted at time $t = 200\,\mathrm{s}$, having a coefficient of the internal pressure of $\alpha = 0.60$. Its shape at the center cross section is similar to the appropriate cross-section depicted in figure 7.6.

Water filled dam subjected to hydrostatic loading

Filling process:

The operators of water filled dams have learned to take care that the dam is completely filled with water, because air bubbles, permanently heading for the highest point, cause undesirable oscillations. As for the 2D case, in the simulation the numerical dilemma has to be faced again, that a very flexible structure is subjected to an internal fluid overpressure. According to equation (3.100) and depending on the chosen bulk modulus K_0, this would lead to large structural deflections and thus artificially large negative incremental changes $\Delta \boldsymbol{u}^o$ of the fluid level below the weir crest. Hence, the structure could be only partially filled or not filled at all. To bypass this numerical difficulty the whole retaining structure, including the controlling construction, has to be considered. This construction contains a water tank, which is located on a higher elevation than the weir. This difference of elevation to the weir complies with the hydrostatic overpressure. More details concerning the functionality of retaining structures can be found in GEBHARDT[31]. Further, this water reservoir features a free fluid surface, with the consequence that the fluid compressibility does not need to be considered and numerical difficulties can be avoided.

In order to save computation time a discretization of the water reservoir is not performed. Instead, the filling process can be managed in such a way that a small air

bubble is left in the structure, as is also done in section 7.1.1. With this air bubble essentially a free fluid level is present and thus the compressibility of the fluid can be neglected. The gas over-pressure inside the bubble then complies with the difference of the elevations of weir and the control construction.

However, in case of more complex three-dimensional geometries, as e.g. in the current example, this procedure fails due to numerical difficulties. Therefore in order to bypass the meshing of this controlling construction, which in fact is necessary from a geometric point of view, the computation is performed with a free fluid surface artificially set to infinity: $\partial\mathcal{B}^o = \infty$. Thus all incremental changes of the water level resulting from equation (3.100) are eliminated. Physically interpreted this means a controlling construction with a volumetric capacity much higher than that of the weir. The water level in this reservoir thus remains almost constant throughout the inflation of the weir. This artificial free fluid surface enables an entire filling of the flexible tube with an incompressible heavy fluid.

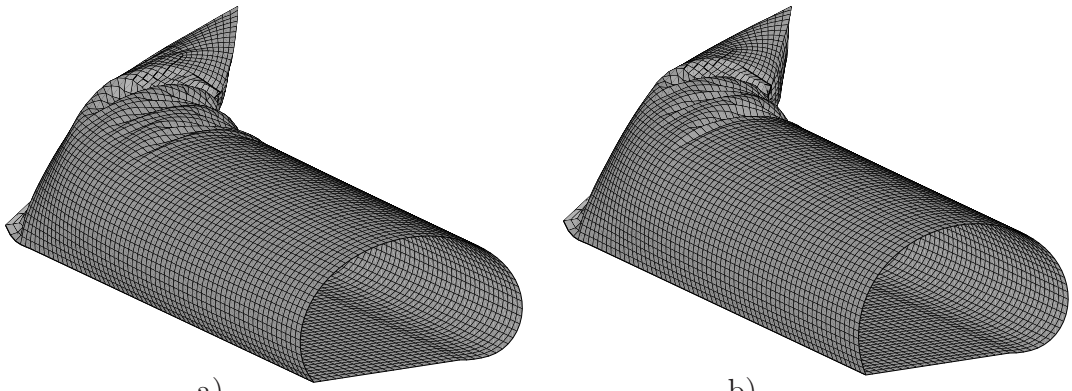

a) b)

Figure 7.10: a) Water filled rubber dam without external hydrostatic load and b) water filled rubber dam with head water level $h_o = 1370\,\text{mm}$ ($\alpha = 1.60$).

In figure 7.10 a) the completely filled dam is depicted at time $t = 220\,\text{s}$. The hydrostatic pressure at the bottom represents $h_i = 2000\,\text{mm}$.

Hydrostatic loading:

Figure 7.10 b) shows the final configuration at time $t = 300\,\mathrm{s}$ after the head water level has reached the dam crest. The diagram in figure 7.11 depicts the developments of

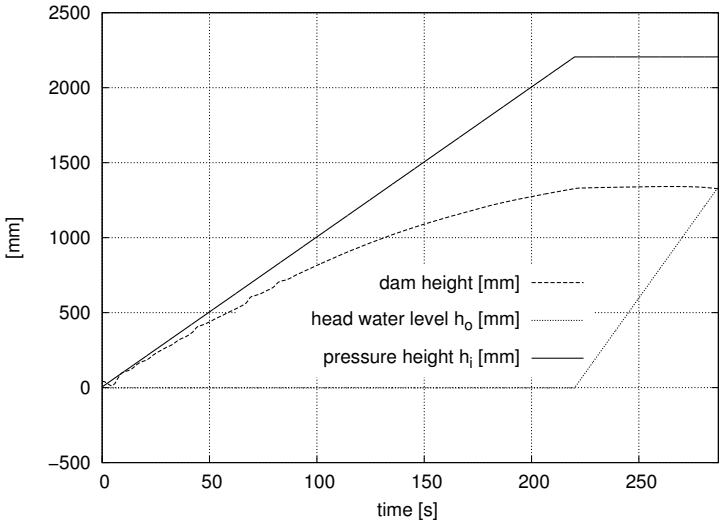

Figure 7.11: Water filled rubber dam: Developments of a) dam height, b) head water level h_o and c) pressure height $h_i = p^{kg}/\rho_W g$ over loading time t.

dam height, hydrostatic pressure at the bottom h_i and head water level h_o. The rise of the head water level has clearly less effect on the dam height than for the air filled dam.

7.2 High-pressure tube hydroforming

Metal sheet forming, using high-pressure tube hydroforming, is a relatively young technology, since first applications in Germany started in the middle sixties. Nowadays this technology is widely used, especially in the automotive industry, see e.g. SIEGERT[92]. Hydroforming is achieved using a piston to generate a pneumatic or hydraulic pressure to press the metal sheet against a matrix and thus obtaining the desirable shape. With this method e.g. in the sector of undercarriages varying cross-sections over the length of the component, varying thicknesses or multi chamber profiles can be achieved and thus an optimal functionality. Important is that the rather little local thinning of the final parts is leading to a fairly good quality. Since industry has permanently rising demands concerning the quality of hydroformed parts more exact computational

methods are required. The current example is typical and shows the influence of the volume dependence on the pressure of compression.

Geometry			Material (von Mises plasticity with isotropic hardening)		
l	$=$	$1000\,\mathrm{mm}$	E	$=$	$2.1 \cdot 10^5\,\mathrm{N/mm^2}$
$\varnothing$	$=$	$100\,\mathrm{mm}$	ν	$=$	0.3
t	$=$	$2\,\mathrm{mm}$	τ_0	$=$	$160\,\mathrm{N/mm^2}$
			H	$=$	$200\,\mathrm{N/mm^2}$

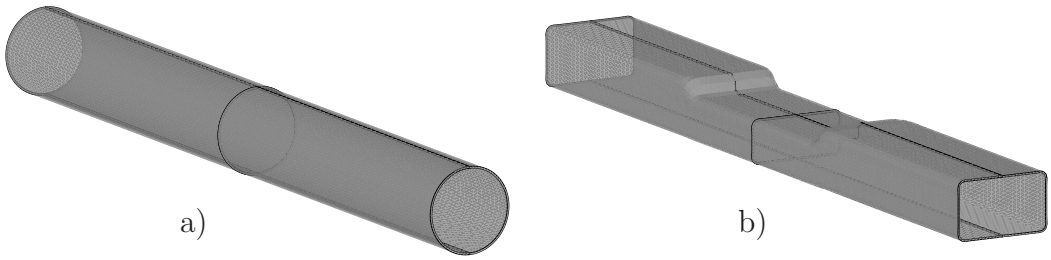

Figure 7.12: Geometry and material data; a) initial and b) desired geometry of the component

The initial geometry of the tube is given in figure 7.12 along with its measures. Taking advantage of the symmetry of the structure, only a quarter of the entire part is modeled and discretized with 4000 geometrically nonlinear solid shell elements (see also HAUPTMANN[41]), featuring an elastoplastic material law (initial yield stress τ_0 and isotropic hardening H).

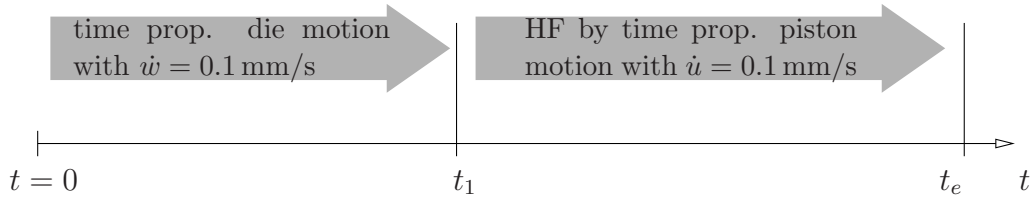

Figure 7.13: Time proportional load sequence for the static computation of a deep drawing process of a tube with a displacement controlled die with velocity $\dot{w} = 0.1\,\mathrm{mm/s}$ and a subsequent high-pressure tube hydroforming (HF) induced by a displacement controlled piston with a velocity $\dot{u} = 0.1\,\mathrm{mm/s}$.

In order to simulate a typical plastic shaping process, in a first step the tube is deformed by a displacement controlled die. Both the rigid die and the rigid matrix embedding the tube are modeled using a node-to-segment contact with a penalty formulation (see

Figure 7.14: a) Schematic diagram of the first deformation step of the component using a die with prescribed displacement w and b) FE-mesh after the deformation

e.g. KONYUKHOV&SCHWEIZERHOF[50]), with the segments – die and matrix – as rigid analytical surfaces. The penalty parameter ϵ is chosen to 5% of the Young's modulus, resp. $\epsilon = 1.0 \cdot 10^4\,\mathrm{N/mm^2}$. Figure 7.13 shows the load sequence for the static computation of the hydroforming of the tube. Since the convergence behaviour of simulations involving contact is rather sensitive with respect to the load step size, the displacement increments of both the die and the piston are chosen to $\Delta w = \Delta u = 0.1\,\mathrm{mm}$. This restricts the Newton iterations per load step to a maximum of 3.

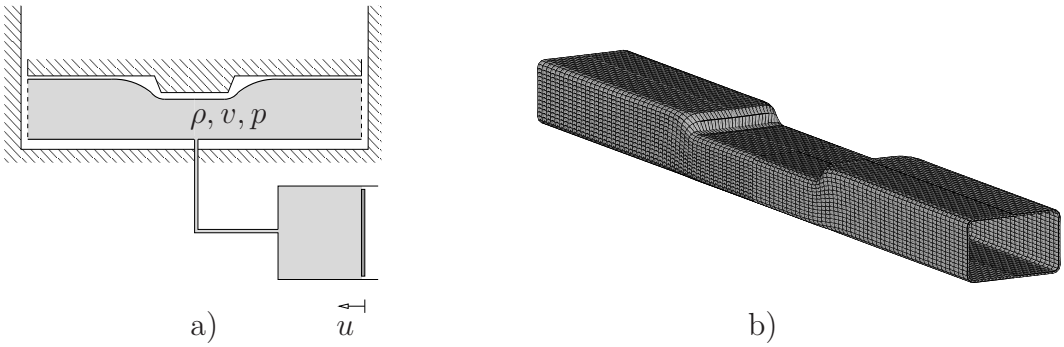

Figure 7.15: a) Schematic diagram of the high-pressure tube hydroforming with piston motion u and b) final geometry after plastic shaping with fluid pressure

As it can be seen in figure 7.14 b) the deformation with the die achieves the finally desired configuration only partially and the deformed tube still features an elliptical cross-section. Further, the die has has caused a snap-through of the tube surface. To achieve the final geometry in a next step the component is subjected to an internal fluid pressure, which is steadily increased by a piston motion u, depicted in figure 7.15 a). The bulk modulus of the fluid is chosen to that of water, with $K_0 = 2.2 \cdot 10^3\,\mathrm{MPa}$. In

reality, specific hydraulic oils have also stiffnesses of $K_0 = 1.5 \cdot 10^7$ MPa, much higher than that of water. However, considering the marginal volumetric deformations of the fluid in the hydroforming simulation this hardly makes any difference but a different piston motion. The finally achieved deformed configuration is given in figure 7.15 b). In a simulation of a high-pressure tube hydroforming process the thickness distribution over the component is of particular interest. As the fluid used for the compression practically causes uniform friction, locally constraint stresses, as arising e.g. in conventional deep drawing processes, are avoided. Thus the thickness distribution over the component is – as expected – more homogeneous.

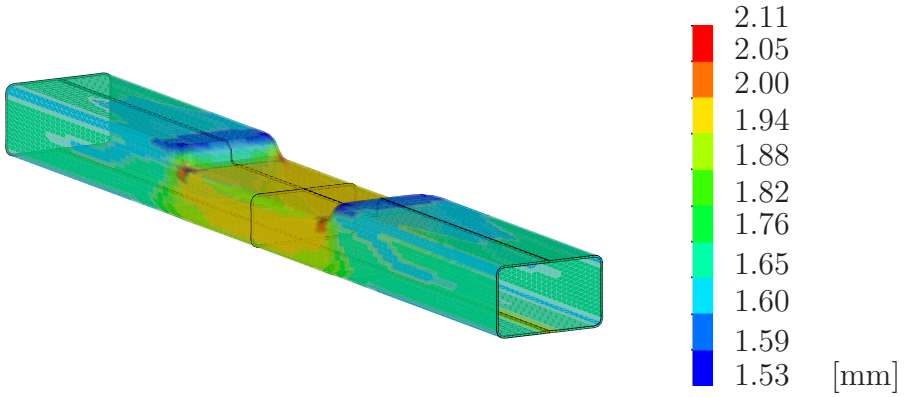

Figure 7.16: Contour plot of the thickness distribution in the hydroformed component

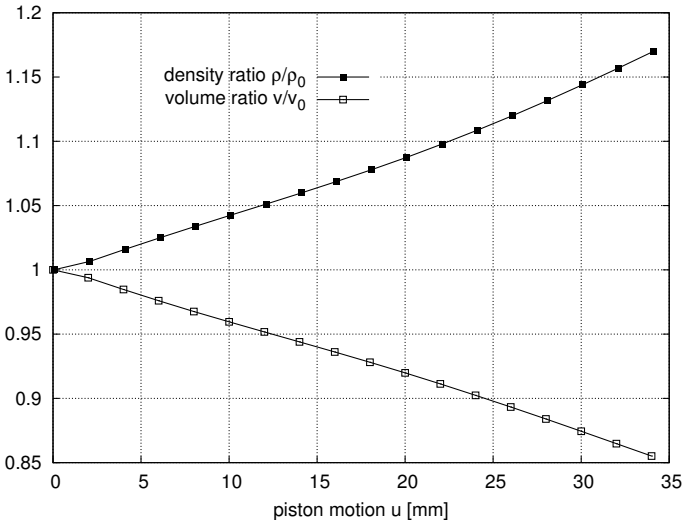

Figure 7.17: Developments of the inner state variables of the compressible fluid plotted over the piston motion u

Nevertheless, as visible in figure 7.16, the material is thinned out in regions with very high curvatures and in the outer parts, where the most plastic deformation in circumferential direction has taken place. Figure 7.17 depicts the developments of the

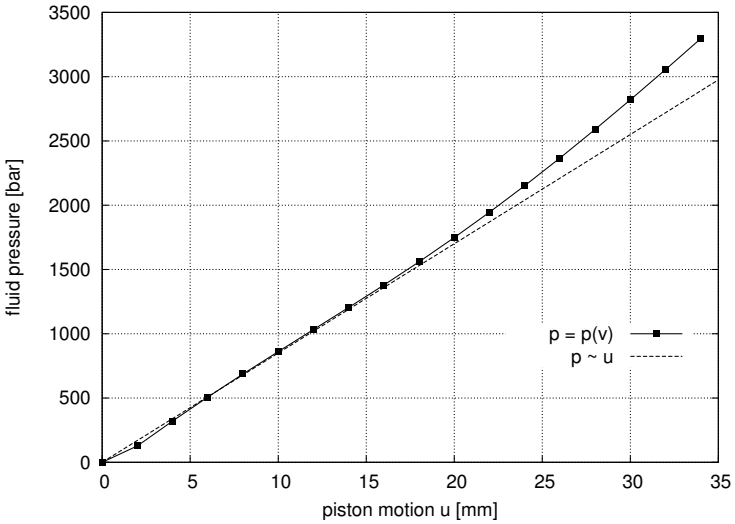

Figure 7.18: Development of a) the volume dependent fluid pressure $p = p(v)$ and b) a fluid pressure p proportional to the piston motion u versus the piston motion u

inner state variables of the compressible fluid, namely volume v and density ρ, related to their initial values and connected via mass conservation. Figure 7.18 shows an almost linear correlation between pressure and piston motion in the region of small pressures. This suggests that initially the volumetric expansion of the structure is proportional to the piston motion as well. However, with higher pressures the volumetric expansion is restricted by both the material hardening and the contact of the structure to the surrounding matrix. This yields a significant increase of the pressure, as the piston is steadily pressed into the fluid. After the final load step the pressure following the linear behaviour differs from the actual volume dependent pressure by about 16%.

7.3 Stability

7.3.1 Buckling analysis of fluid/gas filled cylinders

As the gas/fluid support and loading is included in the load vector and also leads to modifications in the stiffness matrix, in this section some numerical examples will be presented in order to discuss the influence of the fluid-structure interaction on the stability behaviour of thin-walled shell structures, especially the quantitative shifting of the eigenvalues and the coupling of the eigenmodes due to the volume dependence. In general the loading/support can be applied in any arbitrary sequence. The external loading will be incrementally increased and in chosen load steps both the standard eigenvalue problem (6.34) will be solved for a reduced modal basis and the appropriate eigenvalue shifting will be computed with the presented algorithm, see also figure 7.19.

The critical buckling load is obtained when the first zero eigenvalue appears.

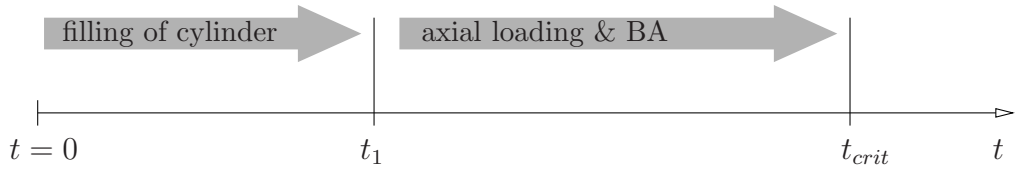

Figure 7.19: Time proportional load sequence for the static computation of the filling process and a subsequent axial loading with simultaneous buckling analysis (BA) of the gas/fluid filled cylinder

This section deals with closed steel cylinders under the following loading conditions:

a) empty cylinder

b) gas loaded cylinder

c) partially fluid filled cylinder

d) partially fluid and gas filled cylinder

e) completely fluid filled cylinder

The steel cylinder features a height of $h = 40\,\text{m}$, a radius of $r = 20\,\text{m}$ and a thickness ratio of $r/t = 1000$. The upper and lower caps are connected to the cylinder with a Navier support and modeled with fairly high stiffness, to prevent the cap from buckling before the global buckling state is reached. Further, the lower cap is in vertical direction completely fixed to the ground. In order to cover also unsymmetric buckling modes half of the cylinder ($\varphi = 180°$) is used for the computation considering symmetry. This affects only slightly the number of buckling waves in circumferential direction compared to a full model. For the discretization about 1400 linear solid shell elements (see HAUPTMANN&SCHWEIZERHOF[41]) with ANS/EAS enhancements are taken. First the internal fluid/gas support conditions are applied quasi-statically and afterwards the axial loading – directly imposed on the upper cap – is incrementally increased until the first eigenvalue equals zero and thus the critical buckling load is reached. Table 7.1 provides an overview over all simulations:

Empty cylinder

Starting with the empty cylinder under axial loading – load case a) – a critical buckling load of $F_{crit} = 420\,\text{MN}$ is achieved. Further on, the typical buckling mode with a high number of buckling waves along the lower boundary can be observed.

Load case	p_{max}	Δp	Buckling mode	Remarks
a) 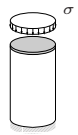	0 bar			• $F_{crit} = 420\,\text{MN}$ • buckling starts at lower boundary • high number of buckling waves
b) 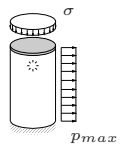	1.0 bar	0.2 bar	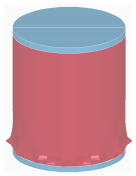	• $F_{crit}/F_{crit}^{empty} = 1.71$ • buckling mode with less waves • small differences in F_{crit} if $RHS \neq \underline{f}(\Delta v)$
c) 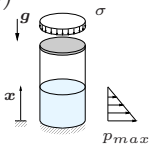	3.6 bar	0 bar		• $F_{crit}/F_{crit}^{empty} = 1.44$ • buckling starts at upper boundary • high number of buckling waves
d) 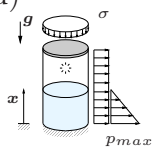	5.6 bar	0.3 bar	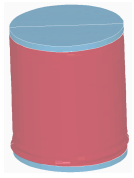	• $F_{crit}/F_{crit}^{empty} = 2.06$ • beam-like shear buckling and elephant foot buckling • -30% difference in F_{crit} if $RHS \neq \underline{f}(\Delta v)$ (if filling process is considered)
e) 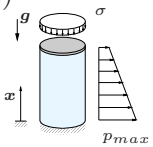	4.0 bar	2.3 bar		• $F_{crit}/F_{crit}^{empty} = 2.17$ • buckling along upper edge and elephant foot buckling along lower edge • -32% difference in F_{crit} if $RHS \neq \underline{f}(\Delta v)$

Table 7.1: Stability analyses of closed cylinder under axial loading with different internal pressure configurations – buckling modes are completed by reflection at symmetry plane

Gas filled cylinder

For a gas filled cylinder with an internal gas pressure of $p^{kg} = 1\,\text{bar}$ – load case b) – the buckling load is increased by a factor of 1.71 compared to the empty cylinder.

The buckling mode shows less buckling waves as in the first case, but they are still concentrated along the lower boundary, see Table 7.1. Neglecting the volume dependence of the right-hand-side vector (pressure increase due to structural deformation: $\Delta p^{kg} = 0.2\%$) only slightly affects the critical buckling load. In figure 7.20 this correlation between the volume change due to deformation and the internal gas pressure – performed via the adiabatic state equation – is depicted.

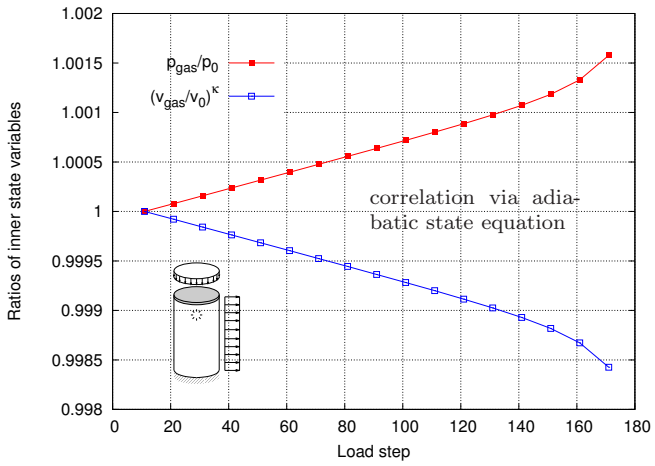

Figure 7.20: Distribution of inner state variables during complete loading process

Partially fluid filled cylinder

The partially fluid filled cylinder with a maximum pressure amplitude of $p_{max} = 3.6\,\text{bar}$ at the bottom – load case c) – has a critical buckling load of 600 MN, which is about a factor 1.44 higher as for the empty cylinder. However, although the pressure amplitude is much higher in this case as for the gas filled cylinder, the buckling load is still 16% lower. This is due to the fact that the hydrostatic distribution is linear in contrast to the constant gas pressure distribution and only affects elements below a water level of $x^o = 36\,\text{m}$. Further, for this cylinder a consideration of the volume dependence neither for the stiffness matrix nor for the right-hand-side vector leads to remarkable differences in the buckling load and the buckling mode. The buckling waves concentrate along the upper boundary, where the stiffening circumferential stresses show the lowest values.

Partially gas and fluid filled cylinder

Starting with an initial gas pressure of $p^{kg} = 20\,\text{mbar}$ and slowly increasing the interior water level (and thus decreasing the gas volume) to $x^o = 39\,\text{m}$ results for the partially gas and fluid filled cylinder – load case d) – in a critical load, which is about a factor of 2.06 higher as for the empty cylinder. The maximum pressure amplitude at the end

of the filling phase is $p_{max} = 5.6\,\text{bar}$. Neglecting the volume dependence of the right-hand-side during the filling phase would only result in a maximum pressure amplitude of $p_{max} = p^{kg} + \rho g x^o \approx 3.9\,\text{bar}$ and thus leads to a considerably lower estimate of the buckling load. The structural displacements caused by the axial loading lead to a further pressure increase of 0.3 bar. Hence, beginning the analysis directly (without simulating the filling process) with an already filled cylinder and with a comparable pressure amplitude of $p_{max} = 5.6\,\text{bar}$ would only slightly affect the critical buckling load. Due to the relatively high internal pressure the cylinder behaves almost as a rigid body and shows a kind of beam-like shear buckling in combination with an elephant foot buckling along the lower boundary.

Completely fluid filled cylinder

The last case is a completely fluid filled cylinder under axial loading – load case e). In comparison with the empty cylinder the buckling load F_{crit} of the fluid filled cylinder is about a factor 2.17 higher. The buckling mode clearly shows high frequency buckling waves along the upper edge and an elephant-foot type buckling wave along the lower boundary. A surprising fact is that although the almost same pressure amplitude and pressure distribution as in the case of the partially fluid and gas filled cylinder are acting, the buckling modes are different. But looking at the higher eigenvalues shows that in the critical buckling state the second and third eigenvalue (which corresponds to the beam-like shear buckling mode similar to the gas and fluid filled cylinder) are also very close to zero. Thus already a slight change in the pressure amplitude might have led to the same beam-like shear buckling mode as in the previous example. The axial loading, starting at load step 20 (current overpressure amplitude of $p_{max} = 4.0\,\text{bar}$), leads to a slight fluid volume compression of about 0.04%. In figure 7.21 the relation between volume change and density change is depicted. Despite the fact that this volume change is relatively small, it leads to a very high internal pressure with a chosen bulk modulus of the fluid of $K_0 = 0.5 \cdot 10^3\,\text{N/mm}^2$. Figure 7.22 depicts the development of the compressible pressure part p_t^{kf} during the loading process. This pressure increase from 3 bar to 5.3 bar (leading to $p_{max} = 6.3\,\text{bar}$) due to structural displacements is responsible for a buckling load, which is about 32% higher compared to a computation of F_{crit} neglecting the volume dependence of the right-hand-side.

Discussion

The previous examples showed that the internal gas/fluid pressures lead to high circumferential stresses. This hydrostatic pretensioning of the cylinders dominates the solution and therefore leads to considerably higher buckling loads in comparison to the empty cylinder (see also STEGMÜLLER ET AL.[99]). Depending on the pressure amplitude and the pressure distribution (constant or linear) the buckling modes also differ considerably.

But as already mentioned, in the cases of the steel cylinders considering the left-hand-

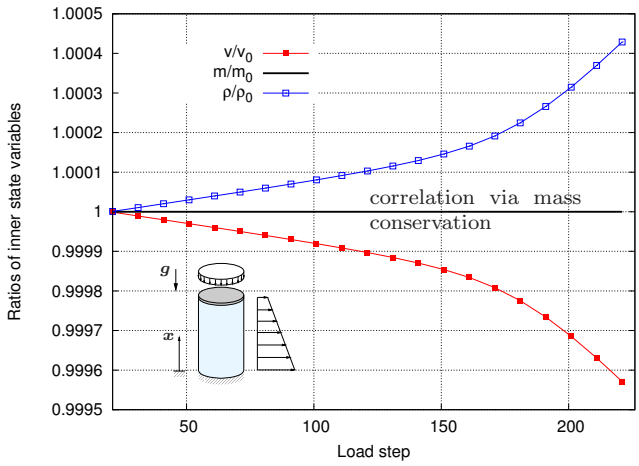

Figure 7.21: Distribution of inner state variables during loading process

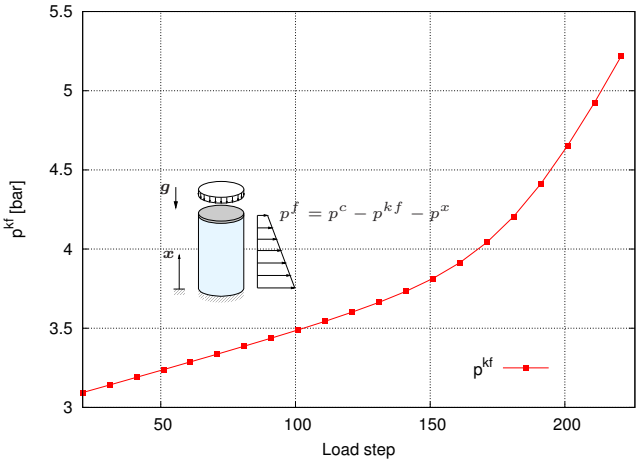

Figure 7.22: Development of pressure p^{kf} due to volume compression during loading process

side parts (stiffness matrix terms) of the volume coupling both in the equilibrium iterations and in the stability computation did not affect the solution to a high degree. Inspecting the modal factor matrix $\underline{\Xi}$, see equation (6.63), makes clear that there is almost no coupling between the old eigenvectors (computed without rank-update) and the new eigenvectors, because it is almost identical to the identity matrix $\underline{I}$. Thus for fairly stiff structures the rank-updates of the left-hand-side are negligible. On the other hand the examples showed that, although the volume changes were small, neglecting also the volume dependence of the right-hand-side vector resulted in different buckling loads for the same load case. Therefore at least the right-hand-side should be updated with the volume dependent information to achieve realistic results.

7.3.2 Buckling analysis of an inflatable beam

As there are several contributions in the literature dealing with inflatable beam elements, as e.g. FICHTER[28] or THOMAS&WIELGOSZ[101], in the following section the performance of such conventional inflatable beam formulations with respect to the prediction of the critical buckling load are investigated. For this purpose first the mechanics of the inflatable beam are briefly presented and then compared to the results obtained by a fully three-dimensional FE discretization of a beam using a volume dependent gas pressure support.

Mechanics of an inflatable beam

As it can be seen in figure 7.23, the resultant

$$P = p\pi R^2 \tag{7.3}$$

of the internal gas pressure p can be replaced by an equivalent force density $q(x)$ acting on the beam as an external loading.

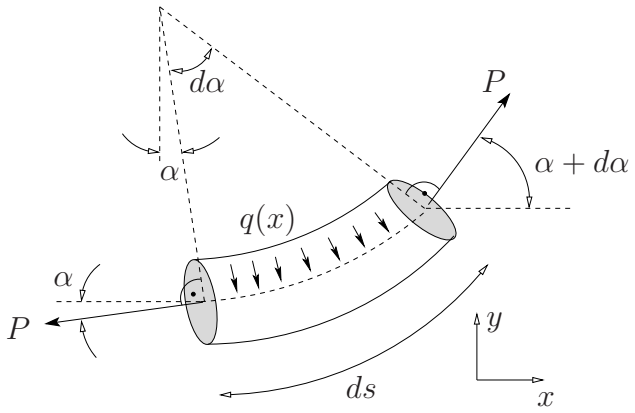

Figure 7.23: Replacement of internal pressure p by a redirecting force density $q(x)$

The equilibrium in vertical direction y then yields:

$$\sum F_y^i = 0: \quad -P\sin\alpha + P\sin(\alpha + d\alpha) - q(x)ds\cos\left(\alpha + \frac{1}{2}d\alpha\right) = 0 \tag{7.4}$$

Assuming small rotations $\alpha \ll 1$ of the cross section yields the linearizations

$$\sin\alpha \approx \alpha \quad \text{and} \quad \cos\alpha \approx 1 \tag{7.5}$$

and thus for the length ds of the differential beam element the approximation

$$ds = \sqrt{1 + \tan^2\alpha} \approx dx\ . \tag{7.6}$$

Inserting (7.3), (7.5) and (7.6) in equation (7.4) gives the pressure resultant P in terms of a force density $q(x)$.

$$q(x) = P\frac{d\alpha}{dx} = p\pi R^2 \frac{d\alpha}{dx} \tag{7.7}$$

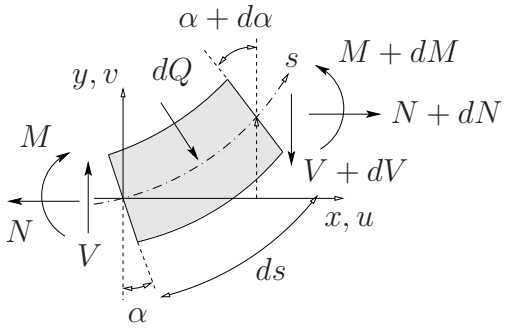

Figure 7.24: Equilibrium at a differential beam element under external load $dQ = q(x)ds$.

Applying the resultant

$$dQ = q(x)ds = p\pi R^2 \frac{d\alpha}{dx} ds \tag{7.8}$$

of the force density $q(x)$ as an external loading on the differential beam element ds leads according to figure 7.24 to the differential equations for the internal forces N, V and M of the beam.

$$\begin{aligned}
\frac{dN}{dx} + \boxed{p\pi R^2 \frac{d\alpha}{dx}\alpha} &= 0 \qquad \text{(a)} \\
\frac{dV}{dx} + \boxed{p\pi R^2 \frac{d\alpha}{dx}} &= 0 \qquad \text{(b)} \\
\frac{dM}{dx} - V - N\frac{dv}{dx} &= 0 \qquad \text{(c)}
\end{aligned} \tag{7.9}$$

Obviously in equations (7.9a) and (7.9b) the pretensioning effect of the gas pressure is included in the normal and transversal forces. Further, these equations show two major assumptions: both, the cross section with its radius R and the internal gas pressure p remain constant throughout the deformation. The effects of the circumferential stresses in the beam fabric are also not covered. According to this model the critical buckling load is reached, if the pretension due to the gas support is equalized by the compressive stresses of the bending moment caused by an external loading.

Buckling analysis of an inflatable beam using a membrane formulation

In the following the assumptions immanent to the inflatable beam model mentioned above are reviewed using a three-dimensional membrane formulation for the discretization of the inflatable beam along with a volume dependent gas pressure inside, see figure 7.25. The focus is especially on

- the deformation behaviour of the beam to check for the assumptions of small rotations $\alpha \ll 1$,
- the volume dependence of the internal gas support, to check for the assumption of a constant gas pressure and
- the development of the cross section, to check for its constant radius R.

Exploiting the symmetry a quarter of the beam is discretized with 638 bilinear membrane elements. Geometry and material data are also given in figure 7.25.

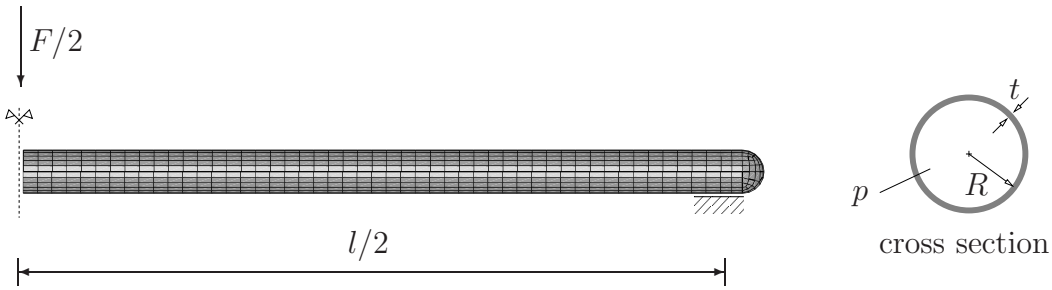

geometry:
$l = 2000\,\text{mm}$
$R = 30\,\text{mm}$
$t = 0.1\,\text{mm}$

material:
$E = 100\,\text{N/mm}^2$
$\nu = 0.4$
$\rho = 10^{-6}\,\text{kg/mm}^3$

mesh data:
discretization with 638 bilinear membrane elements

Figure 7.25: Geometry, material and mesh data of gas supported tubular beam

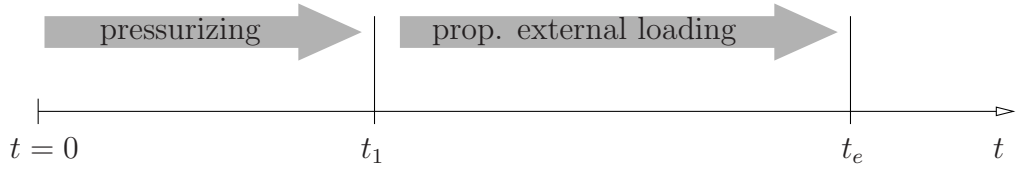

Figure 7.26: Load sequence for the buckling analysis of the gas supported beam

Figure 7.26 shows the load sequence for buckling analysis of the gas supported beam. As initially slack and thus kinematical membrane elements are chosen for the discretization

of the beam, a transient computation is performed using a Newmark-scheme for the time integration of the dynamic equilibrium equations. From a time $t = 0$ to t_1 the beam is pressurized at first. Afterwards a transversal load F acting at the midspan of the beam is steadily increased until the accompanying eigenvalue analysis, using the the scheme presented in chapter 6.3, detects the first zero eigenvalue of the global stiffness matrix $\underline{A}$ – see equation (6.33) – of the system and thus the critical buckling state.

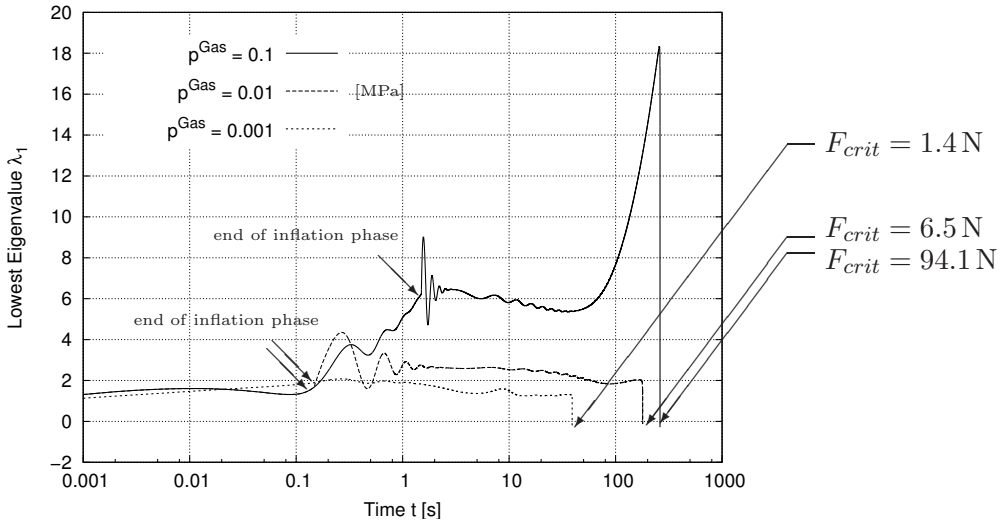

Figure 7.27: Pressurized tubular beam subjected to different internal gas pressures: Development of lowest eigenvalue of $\underline{K}$ under transverse loading F

Figure 7.27 shows the development of the lowest eigenvalues of $\underline{K}$ for a beam supported by three different gas pressures p. It is obvious that an increase of the internal pressure support leads to an increasing stiffness of the structure. The beam with a final pressure of $p = 0.001\,\mathrm{MPa}$ features a critical buckling load of merely $F_{crit} = 1.4\,\mathrm{N}$, a pressure of $p = 0.01\,\mathrm{MPa}$ increases the bearing capacity of the beam to $F_{crit} = 6.5\,\mathrm{N}$ and an internal pressure of $p = 0.1\,\mathrm{MPa}$ leads to a buckling load of $F_{crit} = 94.1\,\mathrm{N}$. The oscillations occurring in the eigenvalue curves are caused by the vertical and horizontal oscillations of the beam, due to the transient loading process simulation which become more evident for higher pressures, because of the relatively short inflation phase.

Figure 7.28 shows for a beam pressurized with an internal gas pressure of $p = 0.01\,\mathrm{MPa}$ and subjected to the critical buckling load F_{crit} the cross sections at the midspan and at the support. As it can be seen only some local deformations of the cross section occur in the vicinity of the support, for the rest of the beam the assumption of a constant circular cross section in the simple beam theory appears reasonable.

Besides the constant radius R of the cross section, a further assumption to be checked is the constant internal gas pressure throughout the deformation. Figure 7.29 shows the development of the volume change during the deformation process for the three differently pressurized beams, as the gas pressure is directly correlated with the volume

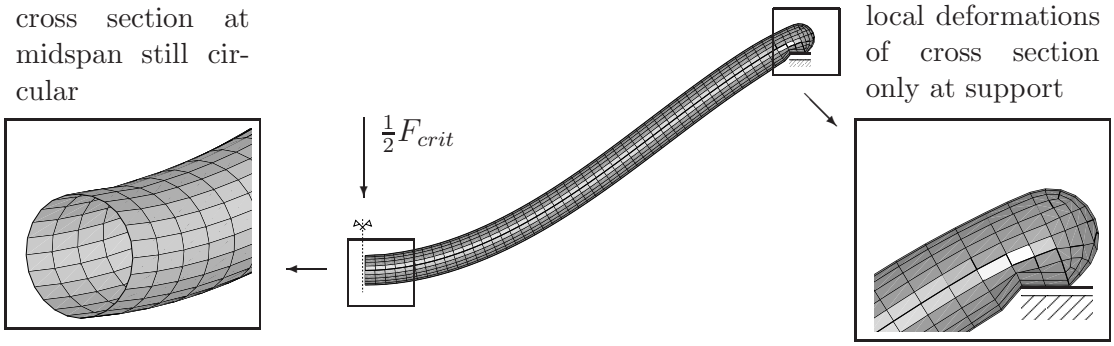

Figure 7.28: Beam with internal gas pressure of $p = 0.01\,\text{MPa}$ at critical buckling state: Cross sections at midspan of beam and at support

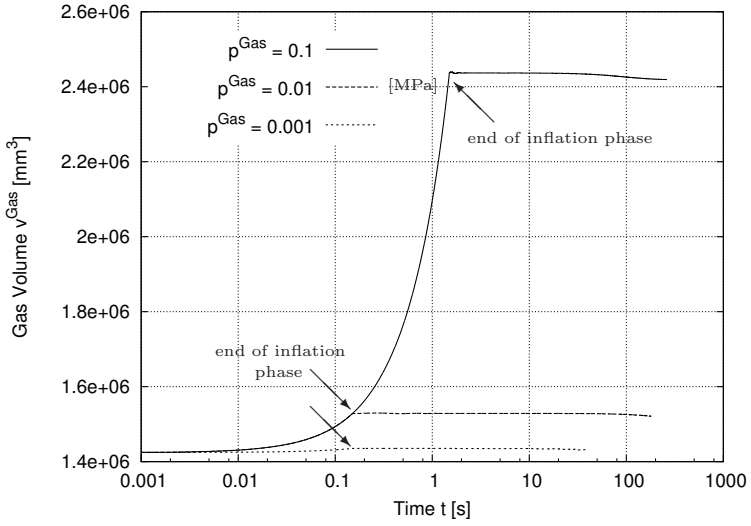

Figure 7.29: Pressurized tubular beam: Development of the volume change during the deformation process

change of the structure. Apart from the inflation process, no remarkable volume change during the loading process is apparent. Thus it can be stated that the stiffening effect of the volume change term $\alpha_t \underline{a}\underline{a}^T$ in the global stiffness matrix

$$\underline{A} = \underline{K} + \alpha_t \underline{a}\underline{a}^T \;, \quad \text{with} \quad \alpha_t = \kappa \frac{p_t}{v_t} \tag{7.10}$$

is negligible for large volumes v_t, as $\alpha_t \ll 1$. Figure 7.30 shows the development of the axial stresses in an upper side element of the three differently pressurized beams and makes clear that the effect of the geometrical stiffness is dominating over the stiffness term due to the volume dependence of the gas support, at least for higher gas pressures and large volumes v_t.

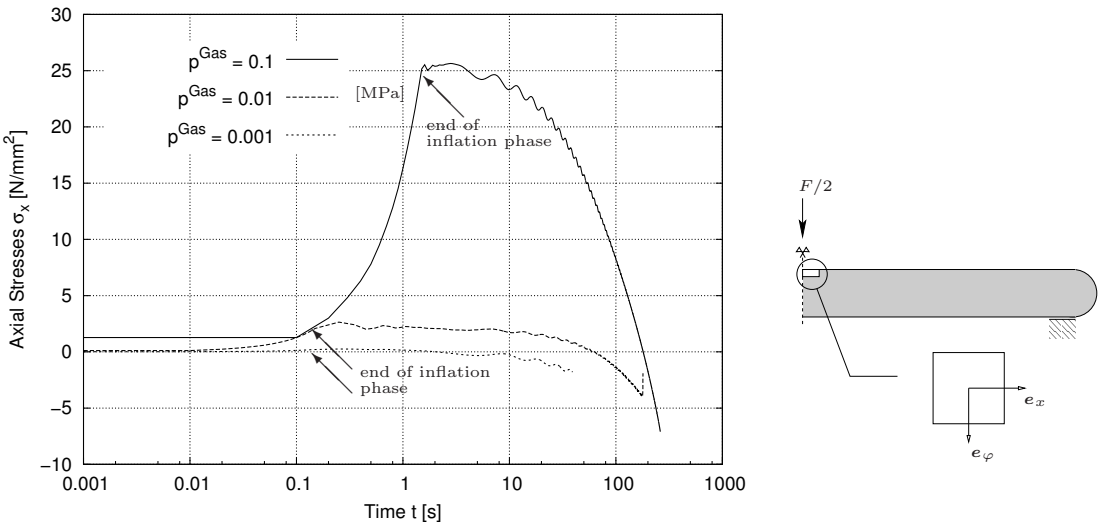

Figure 7.30: Pressurized tubular beam: Development of axial stress in upper side element during loading process

Figure 7.31 depicts the development of axial and circumferential stresses σ_{xx} and $\sigma_{\varphi\varphi}$, computed in an upper side element at the midspan of the beam (pressurized with $p = 0.01\,\text{MPa}$) and their correlation with the development of the lowest eigenvalue λ_1 of the system matrix $\underline{A}$. As already mentioned the inflation leads to a pretensioning of the structure both in axial direction $\boldsymbol{e}_x$ and in circumferential direction $\boldsymbol{e}_\varphi$ and thus to an increase of the eigenvalue from $\lambda_1 = 1.3$ at the beginning to a mean value of $\lambda_1 = 2.7$ at the end the inflation phase. The critical buckling state is reached at $t_{crit} = 200\,\text{s}$, when the lowest eigenvalue λ_1 is about zero. Remarkably in this diagram is the fact, that from $t = 60\,\text{s}$ on the beam still carries load although the axial stresses are "negative". Physically the membrane is not able to carry compression, as it starts wrinkling in this case. However, we have to remark that these negative normal stresses are only an artefact of the used insufficient element formulation, which is not able to capture the phenomenon of wrinkling. For more sophisticated membrane formulations capturing also the wrinkling phenomenon we refer to GIL&BONET[33]. Nevertheless, this example shows that for a buckling analysis of an inflatable beam both the normal and the circumferential stresses have to be taken into account. The simple beam theory assuming a unidirectional stress state is thus not applicable for the prediction of buckling loads.

Further, the beam theory assumes small rotations $\alpha \ll 1$. But in the critical buckling state, see figure 7.32, the rotation is with $\alpha = 40° = 0.7\,rad$ already relatively large. The diagram in figure 7.32 depicts the errors in the beam theory due to a linearization of the geometry. At the critical buckling state the error in the assumption $\sin\varphi \approx \varphi$ in equation (7.5) is with about 7% still low, but the error in the assumption $ds \approx dx$ in equation (7.6) is already 22%.

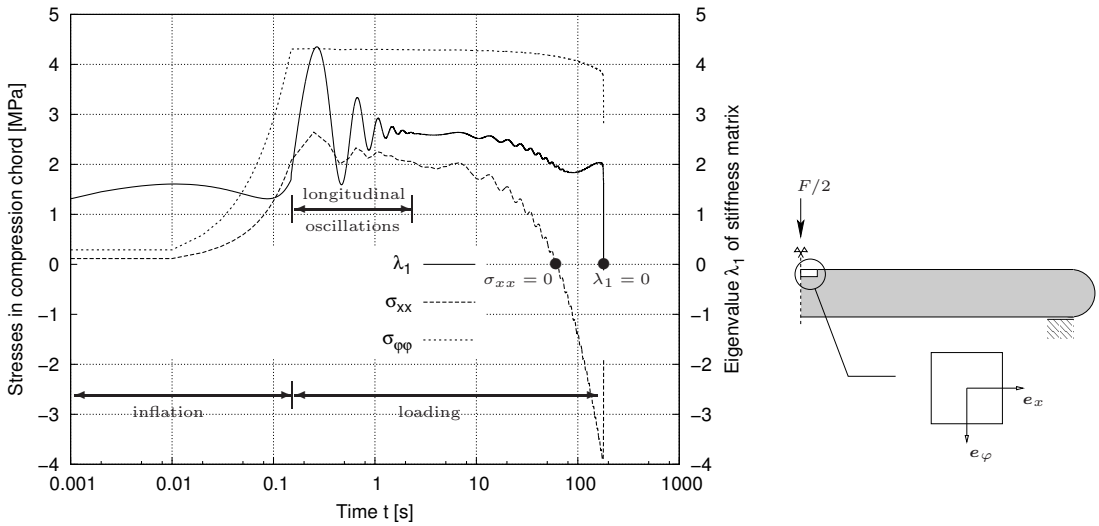

Figure 7.31: Development of axial and circumferential stresses σ_{xx} and $\sigma_{\varphi\varphi}$ in upper side element correlated with development of lowest eigenvalue λ_1 of stiffness matrix $\underline{A}$

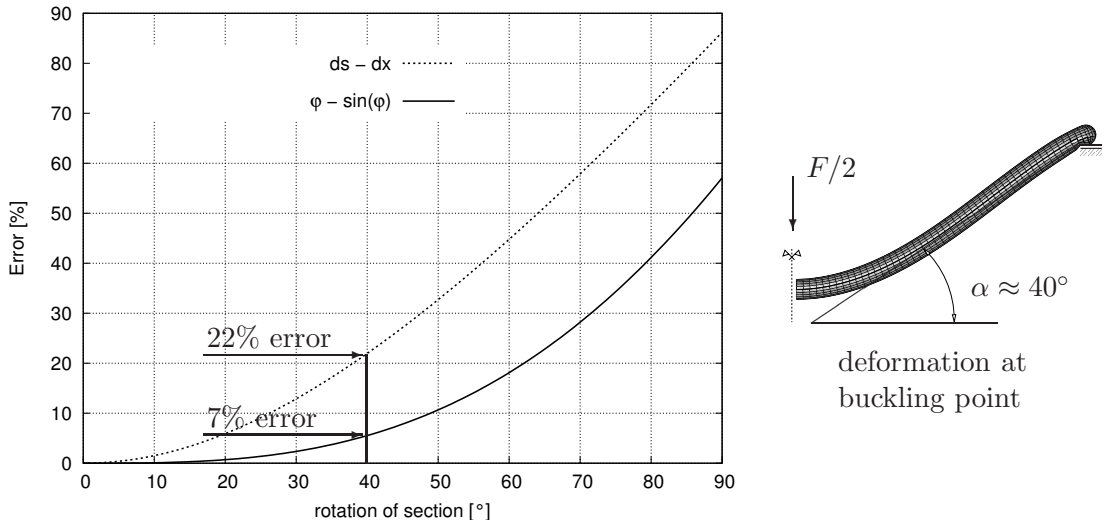

Figure 7.32: Pressurized tubular beam: Errors in theory due to a linearization of the geometry (critical buckling load reached at $\varphi = 40°$)

The assumption of small rotations thus leads to an underestimation of the differential element ds.

$$ds = \sqrt{1 + \tan^2 \alpha} > dx \tag{7.11}$$

According to equation (7.8), which represents the substitution of the internal gas pressure by a redirecting transversal force $dQ = q(x)ds = Pd\alpha$, for $\alpha \not\ll 1$ this leads to an underestimation of the stiffening effect of the internal gas pressure.

Although the simple beam formulation is applicable for load-deflection computations in the range of small rotations, as the assumptions of a constant radius and a constant pressure are valid, a buckling analysis should be performed using either a three-dimensional membrane formulation, as in this case, or more sophisticated beam models to account both for large rotations by a more precise kinematical assumption and the biaxial stress state in the beam, which has a major effect on the critical buckling load.

7.4 Buoyancy simulation

In the following the focus is on the investigation of the influence of multiple fluid filled control volumes on structural behaviour. As a practical example a buoyancy simulation of a cross-section of a double hull tanker, depicted in figure 7.33 a), is chosen.

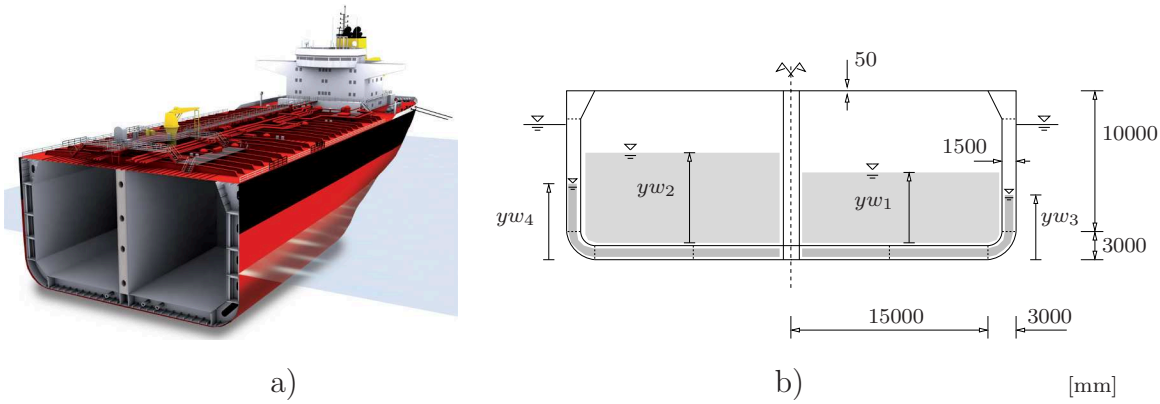

Figure 7.33: a) Cross-section of a double hull oil tanker (source: *www.schleswig-holstein.de*) and b) cross-section taken for the computation

This double hull, on one hand, is used to guarantee more safety in case of a disaster, on the other hand the filling of the additional volume between the inner and the outer hull can be used to control both the draught and the inclination of the ship during the loading and unloading process. The present cross-section consists then of four separate chambers with initially given fluid levels yw_i, $i = 1..4$ in addition to the outer fluid level. The geometry parameters used for the computation are given in figure 7.33 b). For an exaggerated influence of the structural displacements on the fluid levels the stiffeners between the plates in the cross-section, shown in 7.33 a), are not included in the model. The discretization is achieved using 450 solid shell elements with a linear elastic material model ($E = 2.1 \cdot 10^5\,\mathrm{N/mm^2}$, $\nu = 0.3$ and $\rho = 10^4\,\mathrm{kg/m^3}$). The parameters of the fluid are those of water. The complete sequence of the buoyancy computation of the ship cross-section is depicted in figure 7.34.

In a first load step the cross-section is released from an arbitrarily chosen position, thus without any Dirichlet boundary conditions into the water, see also figure 7.35

a). The computation is performed dynamically, considering the mass of the structure,

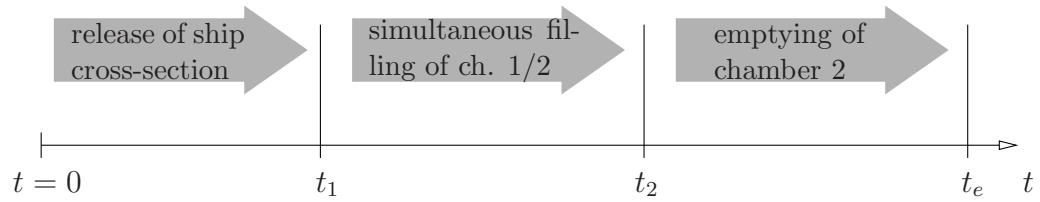

Figure 7.34: Time proportional load sequence for the dynamic buoyancy computation of a ship cross-section

using a Newmark time integration scheme. The time step is chosen to $\Delta t = 0.1\,\mathrm{s}$, which restricts the number of equilibrium iterations per time step to a maximum of 2. As it was shown at the one-dimensional example in section 5.3, the deformation dependent external fluid loading supports the structure in such a way, that a pure rigid body motion in vertical direction does not correspond to a zero eigenvalue in the global system matrix anymore. However, a pure static computation will be only possible, if the structure is horizontally fixed, as the eigenvalues corresponding to the rotational rigid body motion and the horizontal rigid body motion are not supported by the deformation dependent fluid loading (see section 5.1) and thus not necessarily positive.

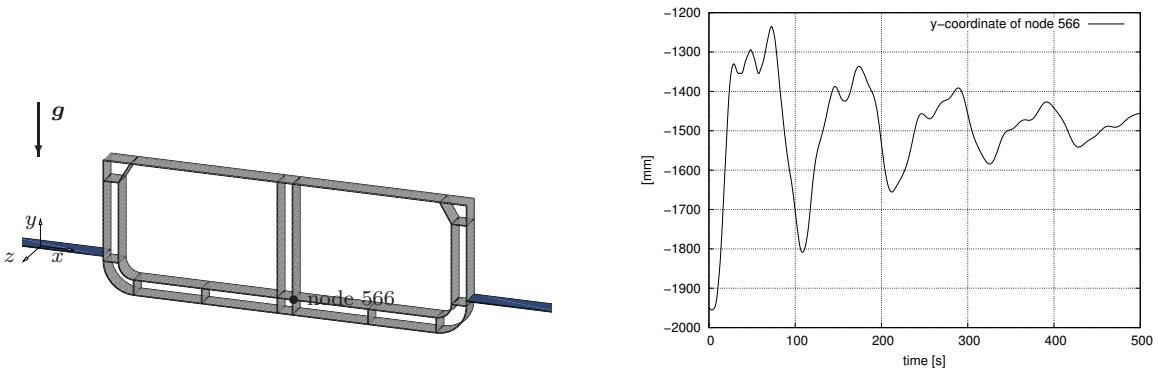

a) b)

Figure 7.35: a) Empty cross-section embedded in water and b) motion of node 566 relative to the water level

The oscillation about the vertical position of equilibrium, respectively the equilibrium of the dead load and the buoyancy of the displaced water, is depicted in figure 7.35 b). Although the lowest eigenmode, namely the rigid body motion of the cross-section, is dominating the oscillation of node 566, it is superpositioned by the vibration of the

structure, because, as already mentioned, the reinforcing planes in the cross-section are missing. To dissipate energy in the system and to enforce a final static position of rest, both numerical damping in the Newmark time integration algorithm and structural Rayleigh damping are used.

Starting at time $t_1 = 500\,\mathrm{s}$, after the structure has almost settled, both main chambers 1 and 2 are flooded with water. yw_1 and yw_2 denote the water level relative to node 566, see also figure 7.36 a). Figure 7.36 b) depicts the subsiding process of the ship into the water due to the additional fluid (dead) load.

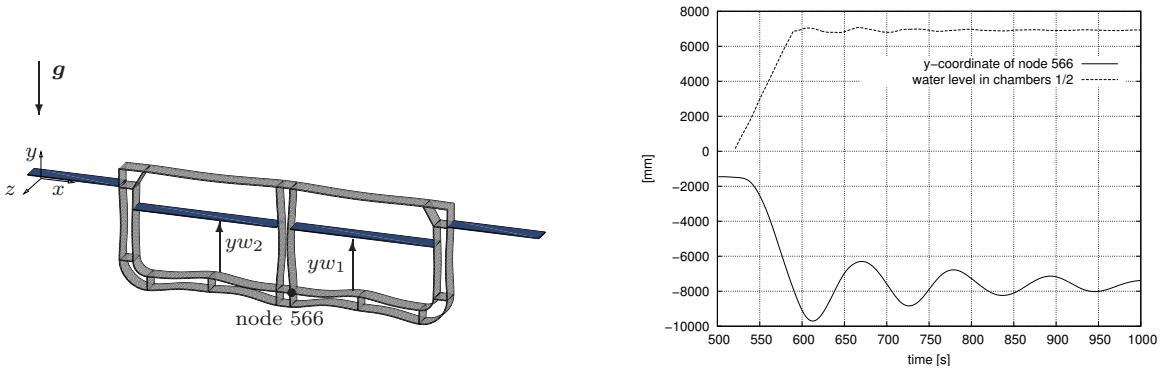

a) b)

Figure 7.36: a) Cross-section embedded into water and filled with water to an equal level in both tanks and b) motion of node 566 due to flooding of chambers 1 and 2; water level in chambers 1 and 2

The motion of node 566 is a result of the pseudodynamic simulation. The slight oscillations of the water level in the chambers result from the internal vibrations of the structure, causing small volume changes of the chamber and thus leading to oscillations of the water level, because the incompressible fluid conserves its volume. This effect will be amplified if one of the main chambers is emptied starting at time $t_2 = 1000\,\mathrm{s}$. This process is depicted in figure 7.37 b).

Thus, besides the present vertical motion, the unsymmetric distribution of mass causes a rotational motion as well. This can be seen comparing the motions of the two opposite corner nodes 157 and 1049. The oscillations of each water level are now slightly larger than in the previous loading case. However, in reality during the emptying process of chamber 2 the left auxiliary chamber 4 can be flooded as well in order to compensate and balance the rotational motion of the structure.

With this example we demonstrate that with the algorithms derived in this thesis we are also capable of simulating large quasi-static deformation problems of floating fluid filled vessels without using CFD-algorithms. Other possible examples for this kind of problems are e.g. pontoon bridges or airbags for lifting submarine structures.

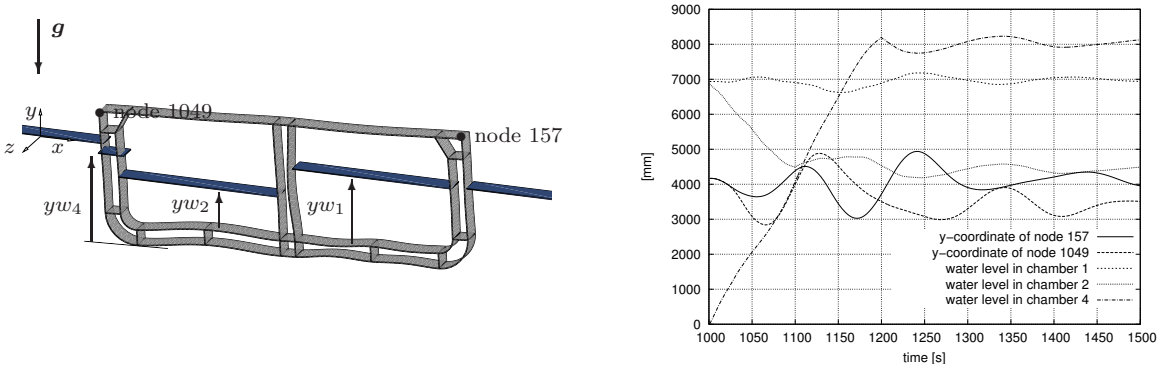

a) b)

Figure 7.37: a) Cross-section with different water levels in both chambers and b) motions of nodes 157 and 1049 during partial emptying of chamber 2 and filling of chamber 4

7.5 Acoustical simulation

The algorithms presented in this work can be used only for the computation of quasi-static problems, because they imply a homogeneous fluid phase where the inner state variables are position-invariant. However, if the focus is on the real vibration analysis of deployable thin-walled structures, as e.g. in the case of the rubber dams, see section 7.1, using conventional finite elements for the fluid, as e.g. proposed by SCHOTTÉ&OHAYON[83],[84] or BELYTSCHKO&KENNEDY[8], is not appropriate for the discretization during the filling process or during the inflation, because of the large deformations and thus the heavy fluid mesh distortions in this phase. This could possibly be overcome by applying the ALE-method, but at the expense of high computational effort due to the necessary mesh adaption in each time step. However, using the presented analytical surface integral description of a fluid for the simulation of the inflation and filling processes, the resulting informations, concerning the values of pressure, density and fluid level after filling/inflation, can be used e.g. in a subsequent modal analysis of the system.

The formerly analytically described fluid is now discretized with continuum fluid elements with the previously computed inner state variables as initial conditions. As a start the following derivations aim at the demonstration of the energetic equivalence of the final configuration after the inflation process, using first the analytical fluid description and then the initial configuration of the fully inflated system, now discretized with fluid elements.

If a system, consisting of a fluid domain $\mathcal{F}$ and a solid domain $\mathcal{B}$ and without any heat transfer $\delta\mathcal{Q}$ to the ambience, is in a state of equilibrium, the energy conservation in equation (3.3) will only contain the variations $\delta\mathcal{K}^{\mathcal{B}\cup\mathcal{F}}$ and $\delta\mathcal{U}^{\mathcal{B}\cup\mathcal{F}}$ of the kinetic and the

internal energy, as well as the virtual work $\delta \mathcal{A}^*_{ext}$ of the external forces.

$$\delta \mathcal{E} = \delta \mathcal{K}^{\mathcal{B} \cup \mathcal{F}} + \delta \mathcal{U}^{\mathcal{B} \cup \mathcal{F}} - \delta \mathcal{A}^*_{ext} = 0 \tag{7.12}$$

Introducing the virtual displacements $\delta \boldsymbol{u}$, the acceleration $\ddot{\boldsymbol{u}}$ and the density ρ, the variation of the kinetic energy of the fluid can be written as

$$\delta \mathcal{K}^{\mathcal{F}} = \int_{\mathcal{F}_0} \rho_0 \ddot{\boldsymbol{u}} \cdot \delta \boldsymbol{u} \, dV \ . \tag{7.13}$$

The stresses $\boldsymbol{S}$ and the virtual strains $\delta \boldsymbol{E}$ yield the variation of the internal energy:

$$\delta \mathcal{U}^{\mathcal{F}} = \int_{\mathcal{F}_0} \boldsymbol{S} : \delta \boldsymbol{E} dV \ . \tag{7.14}$$

Thus the weak form (7.12), as shown in chapter 4, can be used for a finite element formulation of the fluid-structure interaction. As, for the sake of efficiency, the inflation process shall be performed only quasi-statically, the variation of the kinetic energy of the fluid can be neglected in this first step.

$$\delta \mathcal{K}^{\mathcal{F}} = 0 \tag{7.15}$$

Further, the computation of the internal energy can be simplified by considering the fluid as a single-phase system. Thus the stress tensor can be given as:

$$\boldsymbol{S} = -p\boldsymbol{G} \ , \tag{7.16}$$

with p denoting the gas/fluid pressure and $\boldsymbol{G}$ denoting the second order metric tensor. Integrating over the initial fluid volume $\mathcal{F}_0$ and benefitting from the relation

$$\boldsymbol{G} : \delta \boldsymbol{E} = \mathrm{Tr}(\delta \boldsymbol{E}) = \delta v / v_0 \tag{7.17}$$

yields the variation of the internal energy of the fluid.

$$\delta \mathcal{U}^{\mathcal{F}} = -p \delta v \tag{7.18}$$

Thus for the variation of the fluid potential

$$\delta \mathcal{E}^{\mathcal{F}} = -p \delta v \tag{7.19}$$

remains. For a better understanding of the element matrices, we first refer again to the one-degree of freedom model, which has already been described in detail in chapter 5.2, see also figure 7.38. With the residual vector

$$f = f^{ext} - k^{el} u_t + p_t A \ , \tag{7.20}$$

containing the internal and external forces, the conditional equation for the unknown displacement increment Δu can be directly taken from equation (5.18)

$$\left(k^{el} + \kappa \frac{p_t}{v_t} A A \right) \Delta u = f \ . \tag{7.21}$$

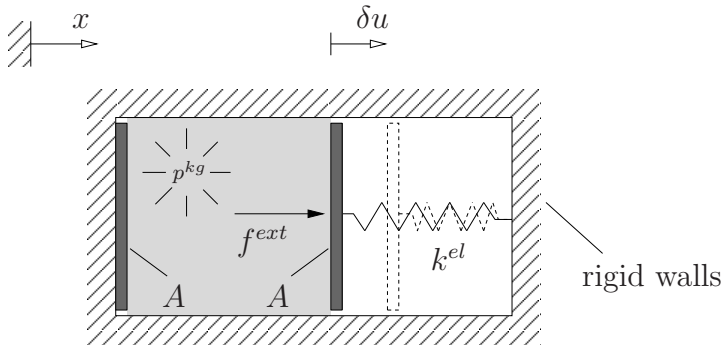

Figure 7.38: Virtual displacement δu acting on an equilibrated pneumatic one-degree of freedom system

Apart from the missing normal change part $\underline{K}^g$ this one-dimensional equation is identical to the n-dimensional equation (4.41) of a gas filled structure of arbitrary geometry, given in chapter 4.2.3. According to table 4.1 for the load case of a pure gas filled structure the following terms remain:

$$\left(\underline{K}^{el} + \underline{K}^g + \kappa \frac{p_t}{v_t} \underline{a}\underline{a}^T\right) \Delta \underline{u} = \underline{f} \ , \tag{7.22}$$

with

$$\underline{f} = \underline{f}^{ext} - \underline{f}^{el} - \underline{f}^g \ , \tag{7.23}$$

compare equation (4.43). As for the one-degree of freedom system, the virtual work due to volume compression is in this general case represented on the left-hand side by the product of the discrete areas $\underline{a}$. The current gas pressure p_t is acting as a load on the right-hand side of the equation. The inflation of the membrane shown in figure 7.39 is achieved using equation (7.22). For the computation of the pressure-volume gradient $\alpha_t = \kappa p_t / v_t$ an initial volume $v_0 > 0$ must be taken, provided e.g. by a slightly curved initial geometry, as depicted in figure 7.39. Figure 7.40 shows the inflation process of

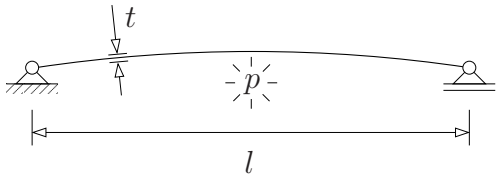

$$\begin{aligned} l &= 4\,\mathrm{m} \\ t &= 0.01\,\mathrm{m} \\ E &= 2.0 \cdot 10^7\,\mathrm{N/m^2} \\ \rho &= 1200\,\mathrm{kg/m^3} \\ p_{t=\infty} &= 6.75 \cdot 10^3\,\mathrm{Pa} \end{aligned}$$

Figure 7.39: Geometry and material parameters of the membrane; an initial volume $v_0 > 0$, necessary for the computation of α_t, is considered by a slightly curved initial geometry

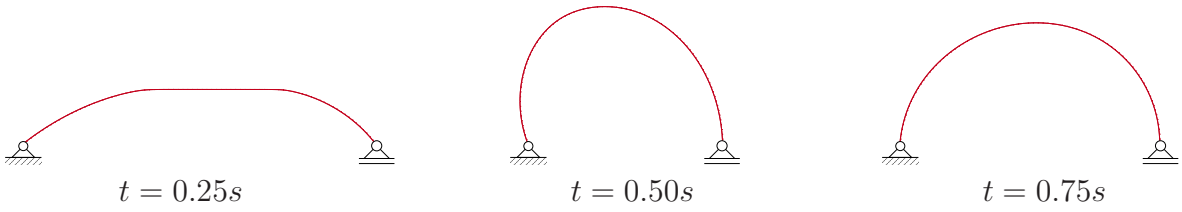

Figure 7.40: Inflation process of a membrane at different time steps using an analytical description of the gas

the membrane at different time steps t, using the previously discussed analytical gas loading.

After exploiting this meshfree but quasi-static description of the fluid, the solutions, namely the current displacement field $\underline{u}_t$ and the current gas pressure p_t, are used as initial conditions for the following dynamical simulation of the prestressed structure. Since in a modal analysis the fluid mesh does not undergo large deformations, conventional displacement based elements can be used for the discretization of the fluid in a first attempt, now considering also changes of the kinetic energy (7.13). For more details on better suited fluid elements see e.g. Wang&Bathe[109] or Belytschko&Kennedy[8]. Discretizing both the geometry $\underline{X}_e$ and the displacement field $\underline{u}_e$ of a fluid element with isoparametric shape functions $\underline{N}$

$$\underline{X}_e = \underline{N}\hat{\underline{X}}_e \quad \text{and} \quad \underline{u}_e = \underline{N}\underline{d}_e \tag{7.24}$$

(with $\hat{\underline{X}}_e$ denoting the discrete nodal coordinates and $\underline{d}_e$ the nodal displacements), the kinematics resp. the volume change of a fluid element with a volume Ω_e can be described. Introducing the matrix $\underline{B}$ in an updated Lagrangian formulation, where the current configuration with volume v_t serves as the new reference configuration, gives the virtual and the incremental volume changes on element level as follows:

$$\mathrm{Tr}(\delta \boldsymbol{E}) = \frac{\delta v}{v_t} = \underline{B}\delta\underline{d}_e \quad \text{and} \quad \mathrm{Tr}(\Delta \boldsymbol{E}) = \frac{\Delta v}{v_t} = \underline{B}\Delta\underline{d}_e \ . \tag{7.25}$$

With Δv and the material law (3.23) for an ideal gas under isentropic conditions the incremental pressure change

$$\Delta p = -\kappa p_t \frac{\Delta v}{v_t} = -\kappa p_t \underline{B}_t \Delta\underline{d}_e \ , \tag{7.26}$$

necessary for the linearized weak form, can be given as well. Finally the linearized weak form of equilibrium of the finite element, used in the following vibration analysis, yields at a time t

$$\delta \mathcal{E}^{\mathcal{f}}_{lin} = \delta \mathcal{E}^{\mathcal{f}}_t + \delta\underline{d}_e{}^T \int_{\Omega_e} \rho_t \underline{N}^T \underline{N} dv \ \Delta\ddot{\underline{d}}_e + \delta\underline{d}_e^T \int_{\Omega_e} \kappa p_t \underline{B}^T \underline{B} dv \ \Delta\underline{d}_e \ . \tag{7.27}$$

The last term in equation (7.27) is the analogon to the rank-update (7.22), with the difference, that the energy of the fluid in equation (7.22) is described using the surrounding structural surface $\partial\mathcal{B}$ instead of using a volume integral over the the fluid domain $\mathcal{F}$ as done in (7.27). Thus both formulations are identical, except for the inertia term, enabling an energetically equivalent and thus unproblematic data transfer from the meshfree fluid formulation to the discretized fluid. After the inflation process has come to a rest at time $t = \infty$, the fluid can be discretized with the previously derived continuum elements, as shown in figure 7.41.

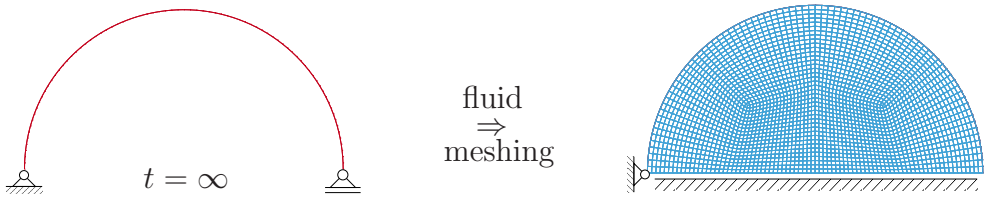

Figure 7.41: Meshing of the fluid with continuum elements considering the deformations and the internal pressure of the membrane after the inflation process has settled – all energy terms are correctly transfered.

For the fluid filled and completely deployed membrane structure an eigenvalue analysis can be performed (see e.g. figure 7.42), considering besides the fluid mass also the elastic strain energy stored in the membrane structure and in the gas due to its inflation.

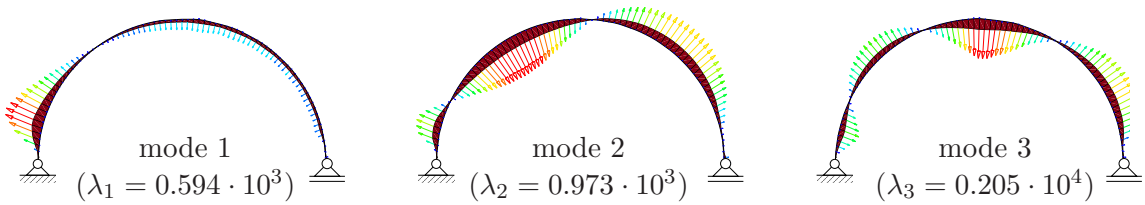

Figure 7.42: First three eigenmodes of the inflated membrane – gas domain discretized with fluid elements

Further on, the simulation of wave propagation can also be achieved, see figure 7.43. However, the mesh should be fine enough and regular if wave propagation is to be simulated using the finite element method without too much numerical dispersion.

The characteristical element length h is restricted to a maximum length, necessary for an element transition of the wave in the time Δt_L of the load application, see also SCHWEIZERHOF[88]. At a temperature of $T = 273\,\mathrm{K}$ and a pressure of $p = 6.75\,\mathrm{kPa}$ (matching $67.5\,\mathrm{mbar}$), according to equations (2.62) and (2.63), the density of the used gas (as it is the major component of air, nitrogen with a molar mass

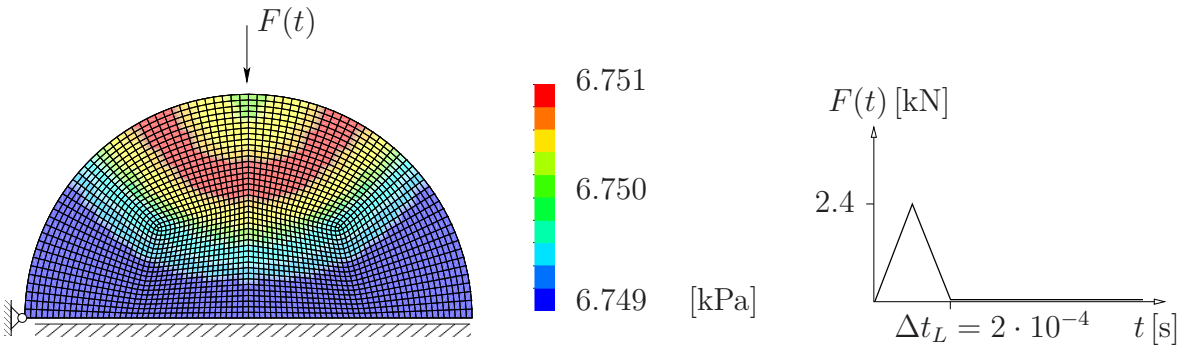

Figure 7.43: Wave propagation in a gas filled structure (at time $t = 0.0017\,\mathrm{s}$) due to an impulse excitation

of $M = 0.028\,\mathrm{kg/mol}$ is chosen) can be given as:

$$\rho = \frac{1}{\nu} = \frac{pM}{R_m T} = 0.0833\,\mathrm{kg/m^3} \tag{7.28}$$

With the density ρ and an adiabatic exponent of $\kappa = 1.0$ the velocity of the wave propagation yields $\omega = \sqrt{p/\rho} = 285\,\mathrm{m/s}$. If instead of Boyle's law the isentropic state equation (2.81) was used, with the adiabatic exponent $\kappa = 1.4$ for nitrogen, the velocity of the wave propagation would follow as $\omega = \sqrt{\kappa p/\rho} = 337\,\mathrm{m/s}$, which complies with the speed of sound in the air. Multiplication with the wave period $\Delta t_L = 2 \cdot 10^{-4}\,\mathrm{s}$ (see figure 7.43 right) for this example finally yields a critical element length of $h = \omega \Delta t_L = 0.055\,\mathrm{m}$. The chosen element length is $h \approx 0.033\,\mathrm{m}$, thus the mesh satisfies at least minimum requirements for a good approximation.

The description of the energy change of a fluid element is not necessarily bound to a volume integral formulation as done in (7.27) for a fully enclosed volume. A description using the boundaries $\partial\mathcal{F}^f$, $\partial\mathcal{F}^o$ or $\partial\mathcal{F}^g$ of the appropriate fluid or gas element can be taken as well. This allows a straightforward implementation of more complex gravitational effects, as e.g. a free fluid surface $\boldsymbol{x}^o$, because all derivations presented in chapter 3 can be further used, although now the integration has to be carried out over the boundary of the fluid element instead of integrating over the surrounding structural surface, as in the case of an analytical fluid description.

Conclusions/Outlook

Following previous works about displacement dependent pressure loads and static fluid-structure interaction (Schweizerhof&Ramm[90], Rumpel[78]), the focus of the present work is on a geometric description of all relevant physical properties of fluids or gases. Capturing the fluid and gas by its geometry or more precisely by its surrounding surface enables a meshfree and thus a very efficient description of the fluid resp. the gas. In order to achieve this formulation, as a start, the thermodynamical basics are presented, aiming on the derivation of constitutive material laws for an ideal gas, an incompressible fluid and a compressible fluid, which are – apart from the material parameters – only dependent on their geometry. In a next step, the principle of virtual work provides an energetic approach for the characterization of a state of equilibrium. After assembling all corresponding variations of the potential energies of the fluid and gas domains, they are transformed from a volume integral description to a surface integral description. Extending the works of Bonet et al.[15] and Rumpel[78], where the equilibrium equations for several load cases were derived separately, the current work provides an overall description of an elastic structure subjected to any combination of fluid and/or gas loading, contained either in a common control volume or in separated interacting chambers. The introduction of two dimensionless parameters enables a convenient selection of the desired load case.

In order to embed these equations in a numerical solution procedure, such as a Newton-scheme, they are subjected to a consistent linearization process. As already shown in Schweizerhof&Ramm[90] the consideration of appropriate boundary conditions is necessary for obtaining a self-adjoint (symmetric) and thus a path-independent formulation of the linearized weak form of equilibrium. Here the finite element method is used as the standard scheme for the numerical solution of the considered initial boundary value problems. Therefore a discretization of all energy terms yields the necessary element matrices, especially the so-called load stiffness matrices (representing the displacement dependence of the loading) and several vectors representing the coupling of the internal state variables of the fluid and gas with the structural displacements.

In order to briefly summarize the basic features of deformation dependent loadings, several analytical one-dimensional examples are used to derive the linearized equilibrium conditions and to compare them to the general formulation. Besides the physical meaning of the coupling matrices the focus is here also on detecting possible stabilizing influence factors the deformation dependent loading may have on the structure.

As the volume coupling of the fluid/gas loading/support leads to an almost fully populated stiffness matrix, a vectorized and thus an efficient solution strategy is presented, obtained by taking advantage of the special structure of the coupling matrices. Besides such a totally displacement dependent formulation a hybrid approach, with the internal state variables of the fluid as additional unknowns, is also given. A comparison of several standard iterative solution schemes (applied to the hybrid approach) with the previously mentioned vectorized algorithm for the displacement dependent formulation shows, that – for stiffness matrices and other additional vectors all fitting into the core memory of a computer – mostly this specific vectorized algorithm prevails. However, using more specific preconditioners and iterative solvers in combination with the hybrid approach is expected to be the best solution method for larger problems.

As the fluid or gas support has a certain stabilizing influence especially on soft structures, an additional focus of this work is on the derivation and discussion of an efficient procedure for the extraction of eigenvalues and eigenvectors, which is based on WEISSENBURGER[110] and SCHWEIZERHOF ET AL.[89], to obtain information on the stability of the overall problem.

Further, the numerical examples demonstrate the range of applications but also the restrictions of the fluid-structure interaction algorithms presented in this work. The deployment of a rubber dam using both gas and an incompressible fluid shows, that this formulation is capable of simulating large deformation problems. As the simulation of a high-pressure tube hydroforming process with a preceeding deep drawing step illustrates, these algorithms can be easily combined with other complex schemes, as e.g. contact analysis or nonlinear plasticity. Further, the quantification of the stiffening effect of deformation dependent loadings on the structure is performed both at the examples of several axially loaded steel cylinders filled with fluid and/or gas and at the example of a flexible gas supported beam. An additional example shows that even buoyancy simulations are possible without using CFD algorithms.

An obvious limitation of this formulation is the fact, that the applications are restricted to simulations of quasi-static processes, because each fluid has been initially idealized as a single phase system. However, the last example illustrates, that this meshless fluid description can be at least used to simulate inflation processes with large deformations as a preliminary for subsequent vibration analyses of the inflated and fluid filled structure, now incorporating a discretization of the fluid with appropriate elements.

Further, the surface integral description of all kinds of fluid or gas loadings would enable the derivation of specific fluid elements, capable of simulating also vibration processes of free fluid surfaces, as e.g. important in the field of aeronautical engineering, where e.g. the vibration mode analysis of liquid gas filled booster rockets appears to be still a challenge, see SCHOTTÉ&OHAYON[84].

Bibliography

[1] O. Andrianarison and R. Ohayon. Compressibility and gravity effects in internal fluid-structure vibrations: Basic equations and appropriate variational formulations. *Computer Methods in Applied Mechanics and Engineering*, 195:1958–1972, 2006.

[2] O. Andrianarison and R. Ohayon. Reduced models for modal analysis of fluid-structure systems taking into account compressibility and gravity effects. *Computer Methods in Applied Mechanics and Engineering*, 195:5656–5672, 2006.

[3] H.O. Anwar. Inflatable dams. *Journal of the Hydraulics Division, ASCE*, 93:99–119, 1967.

[4] H.D. Baehr. *Thermodynamik*. Springer-Verlag, Berlin, 2005.

[5] F. Barthold. *Theorie und Numerik zur Berechnung und Optimierung von Strukturen aus isotropen, hyperelastischen Materialien*. PhD thesis, Institut für Baumechanik und Numerische Mechanik der Universität Hannover, 1993.

[6] K.J. Bathe and E. Dvorkin. A four node plate bending element based on mindlin/reissner plate theory and a mixed interpolation. *International Journal for Numerical Methods in Engineering*, 21:367–383, 1985.

[7] Z.P. Bažant and L. Cedolin. *Stability of structures*. Oxford University Press, 1991.

[8] T.B. Belytschko and J.M. Kennedy. A fluid-structure finite element method for the analysis of reactor safety problems. *Nuclear Engineering and Design*, 38:71–81, 1976.

[9] A. Bermúdez, L. Hervella-Nieto, and R. Rodríguez. Finite element computation of three-dimensional elastoacoustic vibrations. *Journal of Sound and Vibration*, 219:279–306, 1999.

[10] D.T. Berry and H.T. Yang. Formulation and experimental verification of a pneumatic finite element. *International Journal for Numerical Methods in Engineering*, 39:1097–1114, 1996.

[11] M. Bischoff and E. Ramm. Shear deformable shell elements for large strains and rotations. *International Journal for Numerical Methods in Engineering*, 40:4427–4449, 1997.

[12] J. Bonet and S. Kulasegaram. Correction and stabilization of smooth particle hydrodynamics methods with applications in metalforming. *International Journal for Numerical Methods in Engineering*, 47:1189–1214, 2000.

[13] J. Bonet, S. Kulasegaram, M.X. Rodriguez-Paz, and M. Profit. Variational formulation for the smooth particle hydrodynamics (SPH) simulation of fluid and solid problems. *Computer Methods in Applied Mechanics and Engineering*, 193:1245–1256, 2004.

[14] J. Bonet and R.D. Wood. *Nonlinear Continuum Mechanics for Finite Element Analysis*. Cambridge University Press, 1997.

[15] J. Bonet, R.D. Wood, J. Mahaney, and P. Heywood. Finite element analysis of air supported membrane structures. *Computer Methods in Applied Mechanics and Engineering*, 190:579–595, 2000.

[16] R. Bouzidi, Y. Ravaut, and C. Wielgosz. Finite elements for 2D problems of pressurized membranes. *Computers and Structures*, 81:2479–2490, 2003.

[17] H. Bufler. Zur Potentialeigenschaft der von einer Flüssigkeit herrührenden Druckbelastung. *Zeitschrift für Angewandte Mathematik und Mechanik*, 65:130–132, 1985.

[18] H. Bufler. Konsistente und nichtkonsistente Druckbelastungen durch Flüssigkeiten. *Zeitschrift für Angewandte Mathematik und Mechanik*, 72:T 172–T 175, 1992.

[19] H. Bufler. Configuration dependent loading and nonlinear elastomechanics. *Zeitschrift für Angewandte Mathematik und Mechanik*, 73:T 20–T 33, 1993.

[20] L. Collatz. *Differentialgleichungen für Ingenieure*. Teubner, 1960.

[21] M.A. Crisfield. *Non-linear Finite Element Analysis of Solids and Structures. Volume 1: Essentials*. John Wiley, 1991.

[22] R. de Boer. *Vektor- und Tensorrechnung für Ingenieure*. Springer-Verlag, Berlin, 1982.

[23] A. Diaby, A. van Le, and C. Wielgosz. Buckling and wrinkling of prestressed membranes. *Finite Elements in Analysis and Design*, 42:992–1001, 2006.

[24] R. van Dijk, F. van Keulen, and J.C. Sterk. Simulation of closed thin-walled structures partially filled with fluid. *International Journal of Solids and Structures*, 37:6063–6083, 2000.

[25] S. Doll. *Zur numerischen Behandlung großer elasto-viskoplastischer Deformationen bei isochor-volumetrisch entkoppeltem Stoffverhalten*. PhD thesis, Institut für Mechanik der Universität Karlsruhe (TH), 1998.

[26] G.C. Everstine. A symmetric potential formulation for fluid-structure interaction. *Journal of Sound and Vibration*, 79:157–160, 1981.

[27] J.D. Faires and R.L. Burden. *Numerische Methoden*. Spektrum Akademischer Verlag, 1994.

[28] W.B. Fichter. A theory for inflated thin-wall cylindrical beams. *NASA Technical Note NASA TN D-3466*, 1966.

[29] R.E. Freeland, G.D. Bilyeu, G.R. Veal, and M.M. Mikulas. Inflatable deployable space structures Technology summary. *International Aeronautical Federation*, IAF-98-1.5.01, 1998.

[30] R.W. Freund and N.M. Nachtigal. QMR: A quasi-minimal residual method for non-hermitian linear systems. *Numerische Mathematik*, 60:315–339, 1991.

[31] M. Gebhardt. *Hydraulische und statische Bemessung von Schlauchwehren*. PhD thesis, Institut für Wasserwirtschaft und Kulturtechnik der Universität Karlsruhe (TH), 2006.

[32] M. Gebhardt, F. Nestmann, K. Schweizerhof, and B. Kemnitz. Grundlagen für die hydraulische und statische Bemessung von wasser- und luftgefüllten Schlauchwehren. *Wasserwirtschaft*, 03/2008:27–32, 2008.

[33] A.J. Gil and J. Bonet. Finite element analysis of partly wrinkled reinforced prestressed membranes. *Computational Mechanics*, 40:595–615, 2007.

[34] R.A. Gingold and J.J. Monaghan. Smoothed particle hydrodynamics, theory and application to non-spherical stars. *Monthly Notices of the Royal Astronomical Society*, 181:375–389, 1977.

[35] R.A. Gingold and J.J. Monaghan. Kernel estimates as a basis for general method for particle methods in hydrodynamics. *Journal of Computational Physics*, 46:429–453, 1982.

[36] F. Gruttmann and R.L. Taylor. Theory and finite element formulation of rubberlike membrane shells using principal stretches. *International Journal for Numerical Methods in Engineering*, 35:1111–1126, 1992.

[37] J. Hallquist. *LS-DYNA Theoretical Manual*. Livermore Software Technology Corporation, 1998.

[38] M.A. Hamdi and Y. Ousset. A displacement method for the analysis of vibrations of coupled fluid-structure systems. *International Journal for Numerical Methods in Engineering*, 13:139–150, 1978.

[39] M. Haßler and K. Schweizerhof. On the influence of fluid-structure-interaction on the static stability of thin walled shell structures. *International Journal of Structural Stability*, 7:313–335, 2007.

[40] M. Haßler and K. Schweizerhof. On the static interaction of fluid and gas loaded multi-chamber systems in a large deformation finite element analysis. *Computer Methods in Applied Mechanics and Engineering*, 197:1725–1749, 2008.

[41] R. Hauptmann and K. Schweizerhof. A systematic development of 'solid-shell' element formulations for linear and non-linear analysis employing only displacement degrees of freedom. *International Journal for Numerical Methods in Engineering*, 42:49–69, 1998.

[42] T.J.R. Hughes. *The Finite Element Method*. Dover Publications, 2000.

[43] T.J.R. Hughes, W.K. Liu, and T.K. Zimmerman. Lagrangian Eulerian finite elements formulation for viscous flows. *Computer Methods in Applied Mechanics and Engineering*, 21:329–349, 1981.

[44] K. Hutter. *Fluid- und Thermodynamik*. Springer-Verlag, Berlin, 2003.

[45] J.T. Katsikadelis and M.S. Nerantzaki. The ponding problem on elastic membranes: an analoug equation solution method. *Computational Mechanics*, 28:122–128, 2002.

[46] M.R. Kianoush and J.Z. Chen. Effect of vertical acceleration on response of concrete rectangular liquid storage tanks. *Engineering Structures*, 28:704–715, 2006.

[47] M. Kleiner, W. Homberg, and A. Brosius. Processes and control of sheet metal hydroforming. *Proceedings of the 6th ICTP on Advanced Technology of Plasticity*, 2:1243–1252, 1999.

[48] K. Knebel. *Stabilität von Stahlzylindern mit unilateralen Randbedingungen bei statischen und dynamischen Beanspruchungen*. PhD thesis, Institut für Mechanik der Universität Karlsruhe (TH), 1997.

[49] E. Kock and L. Olson. Fluid-structure interaction analysis by the finite element method – A variational approach. *International Journal for Numerical Methods in Engineering*, 31:463–491, 1991.

[50] A. Konyukhov and K. Schweizerhof. Covariant description for frictional contact problems. *Computational Mechanics*, 35:190–213, 2005.

[51] H. Landolt. *Zahlenwerte und Funktionen aus Physik, Chemie, Astronomie, Geophysik und Technik*. Springer-Verlag, Berlin, 1971.

[52] A. van Le and C. Wielgosz. Bending and buckling of inflatable beams: Some new theoretical results. *Thin-Walled Structures*, 43:1166–1187, 2005.

[53] A. van Le and C. Wielgosz. Finite element formulation for inflatable beams. *Thin-Walled Structures*, 45:221–236, 2007.

[54] I. Lenhardt. *Krylov-Unterraum-Verfahren für Gleichungssysteme aus der Strukturmechanik auf sequentiellen und parallelen Rechnern.* PhD thesis, Institut für Angewandte Mathematik der Universität Karlsruhe (TH), 1997.

[55] R.H. Luchsinger, A. Pedretti, A. Steingruber, and M. Pedretti. The new structural concept Tensairity: Basic principles. *Proceedings of the Second Conference of Structural Engineering, Mechanics and Computation*, A.A. Balkema/Swets Zeitlinger, Lisse. 2004.

[56] L.E. Malvern. *Introduction to the Mechanics of a Continuous Medium.* Prentice-Hall, 1969.

[57] J.E. Marsden and T.J.R. Hughes. *Mathematical Foundations of Elasticity.* Prentice-Hall, 1983.

[58] J. Mayer. A numerical evaluation of preprocessing and ILU-type preconditioners for the solution of unsymmetric sparse linear systems using iterative methods. *IWRMM Preprint*, 2007.

[59] A. Merkle. *Implementierung eines geometrisch nichtlinearen Interface-Elements zur Berechnung von statischen Fluid-Struktur-Kopplungen.* Diploma thesis, Institut für Mechanik der Universität Karlsruhe (TH), 2008.

[60] Ministry of Land, Infrastructure and Transport (MLIT), River Bureau. *Technische Richtlinie für Schlauchwehre, Translation from Japanese – Bundesanstalt für Wasserbau Karlsruhe.* Unpublished, 2000.

[61] H.J.P. Morand and R. Ohayon. *Fluid Structure Interaction.* John Wiley & Sons, 1995.

[62] T. Nakagawa, K. Nakamura, and H. Amino. Tiefziehen großer Blechformteile mit hydraulischem Gegendruck. *Neuere Entwicklungen in der Blechumformung*, 1998:51–69, 1998.

[63] R. Ogden. *Non-Linear Elastic Deformations.* Ellis Horwood and Jon Wiley, 1984.

[64] R. Ohayon. Intelligent adaptive fluid structure interaction systems. *Computational Mechanics*, WCCM VI in conjuction with APCOM'04, Sept. 5-10, 2004, Beijing, China.

[65] L.G. Olson and K.J. Bathe. A study of displacement-based fluid finite elements for calculating frequencies of fluid and fluid-structure systems. *Nuclear Engineering and Design*, 76:137–151, 1983.

[66] M. Pagitz and S. Pellegrino. Buckling pressure of "pumpkin" balloons. *International Journal of Solids and Structures*, 44:6963–6986, 2007.

[67] M. Pagitz, Y. Xu, and S. Pellegrino. Stability of lobed balloons. *Advances in Space Research*, 37:2059–2069, 2006.

[68] C.C. Paige and M.A. Saunders. Solution of sparse indefinite systems of linear equations. *SIAM Journal on Numerical Analysis*, 12:617–629, 1975.

[69] A. Palisoc, G. Veal, C. Cassapakis, G. Greschik, and M. Mikulas. Geometry attained by pressurized membranes. *Proc. SPIE, Space Telescopes and Instruments*, 3356:747–757, 1998.

[70] H. Parisch. *Festkörper-Kontinuumsmechanik*. Teubner, 2003.

[71] C.E. Pearson. General theory of elastic stability. *Quarterly of Applied Mathematics*, 14:133–144, 1956.

[72] J.D. Pearson. Variable metric methods of minimization. *Computer Journal*, 12:171–178, 1969.

[73] A. Pedretti, A. Steingruber, M. Pedretti, and R.H. Luchsinger. The new structural concept Tensairity: FE-modeling and applications. *Proceedings of the Second Conference of Structural Engineering, Mechanics and Computation*, A.A. Balkema/Swets Zeitlinger, Lisse, 2004.

[74] A. Pflüger. *Stabilitätsprobleme der Elastostatik*. Springer-Verlag, Berlin, 1964.

[75] T. Raible. *Concepts for Nonlinear Orthotropic Material Modeling with Applications to Membrane Structures*. PhD thesis, Institut für Baumechanik und Numerische Mechanik der Universität Hannover, 2003.

[76] S. Reese. *Theorie und Numerik des Stabilitätsverhaltens hyperleastischer Festkörper*. PhD thesis, Institut für Baumechanik und Numerische Mechanik der Universität Hannover, 1994.

[77] M. Riemer, J. Wauer, and W. Wedig. *Mathematische Methoden der Technischen Mechanik*. Springer-Verlag, Berlin, 1993.

[78] T. Rumpel. *Effiziente Diskretisierung von statischen Fluid-Struktur-Problemen bei großen Deformationen*. PhD thesis, Institut für Mechanik der Universität Karlsruhe (TH), 2003.

[79] T. Rumpel and K. Schweizerhof. Volume-dependent pressure loading and its influence on the stability of structures. *International Journal for Numerical Methods in Engineering*, 56:211–238, 2003.

[80] T. Rumpel and K. Schweizerhof. Hydrostatic fluid loading in non-linear finite element analysis. *International Journal for Numerical Methods in Engineering*, 59:849–870, 2004.

[81] T. Rumpel, K. Schweizerhof, and M. Haßler. Efficient finite element modelling and simulation of gas and fluid supported membrane and shell structures. *Textile Composites and Inflatable Structures, E. Onate, B. Kröplin (eds.)*, pages 153–172, 2005.

[82] H. Schneider. *Flüssigkeitsbelastete Membranen unter großen Deformationen.* PhD thesis, Institut für Mechanik (Bauwesen) der Universität Stuttgart, 1990.

[83] J.S. Schotté and R. Ohayon. Effect of gravity on a free-free elastic tank partially filled with incompressible liquid. *Journal of Fluids and Structures*, 18:215–226, 2003.

[84] J.S. Schotté and R. Ohayon. Incompressible hydroelastic vibrations: finite element modelling of the elastogravity operator. *Computers and Structures*, 83:209–219, 2005.

[85] J. Schröder. *Theoretische und algorithmische Konzepte zur phänomenologischen Beschreibung anisotropen Materialverhaltens.* PhD thesis, Institut für Baumechanik und Numerische Mechanik der Universität Hannover, 1996.

[86] K. Schweizerhof. *Nichtlineare Berechnung von Tragwerken unter verformungsabhängiger Belastung.* PhD thesis, Institut für Baustatik der Universität Stuttgart, 1982.

[87] K. Schweizerhof. *Quasi-Newton Verfahren und Kurvenverfolgungsalgorithmen für die Lösung nichtlinearer Gleichungssysteme in der Strukturmechanik.* Institut für Baustatik der Universität Karlsruhe (TH), 1989.

[88] K. Schweizerhof. *Finite Elemente für Feld- und zeitvariante Probleme, Vorlesungsmitschrieb.* Institut für Mechanik der Universität Karlsruhe (TH), 2003.

[89] K. Schweizerhof and U. Andelfinger. Effiziente Erdbebenberechnung einfacher Sekundärstrukturen in großen Bauwerken. *Ingenieur Archiv*, 57:267–276, 1987.

[90] K. Schweizerhof and E. Ramm. Displacement dependent pressure loads in nonlinear finite element analyses. *Computers and Structures*, 18:1099–1114, 1984.

[91] M.J. Sewell. On configuration-dependent loading. *Archive for Rational Mechanics and Analysis*, 23:327–351, 1967.

[92] K. Siegert. *Vortragstexte zur Veranstaltung „Internationale Konferenz Hydroumformung in Fellbach bei Stuttgart, am 28. u. 29. Oktober 2003“.* MAT-INFO Werkstoff-Informationsgesellschaft mbH, 2003.

[93] K. Siegert and B. Lösch. Hydroblechumformung. *Hydroumformen von Rohren, Strangpreßprofilen und Blechen*, 1:263–289, 1999.

[94] J.C. Simo and F. Armero. Geometrically non-linear enhanced strain mixed methods and the method of incompatible modes. *International Journal for Numerical Methods in Engineering*, 33:1413–1449, 1992.

[95] J.C. Simo, F. Armero, and R.L. Taylor. Improved versions of assumed enhanced strain tri-linear elements for 3d finite deformation problems. *Computer Methods in Applied Mechanics and Engineering*, 110:359–386, 1993.

[96] J.C. Simo and M.S. Rifai. A class of mixed assumed strain methods and the method of incompatible modes. *International Journal for Numerical Methods in Engineering*, 29:1595–1638, 1990.

[97] M. Souli, A. Ouahsine, and L. Lewin. ALE formulation for fluid-structure interaction problems. *Computer Methods in Applied Mechanics and Engineering*, 190:659–675, 2000.

[98] A.J.M. Spencer and R.S. Rivlin. Isotropic integrity bases for vectors and second-order tensors, Part I. *Archive for Rational Mechanics and Analysis*, 9:45–63, 1962.

[99] H. Stegmüller, F.W. Bornscheuer, and E. Ramm. Stability and ultimate load analysis of liquid filled conical shells. *Institut für Baustatik der Universität Stuttgart*, Mitteilung Nr. 4, 1984.

[100] H. Tan and H. Baier. Inflation and deployment simulation for folded tubes made of rigidizable fabric prepreg. *Computational Mechanics*, WCCM VI in conjuction with APCOM'04, Sept. 5-10, 2004, Beijing, China.

[101] J.C. Thomas and C. Wielgosz. Deflections of highly inflated fabric tubes. *Thin-Walled Structures*, 42:1049–1066, 2004.

[102] C. Truesdell. *Rational Thermodynamics*. Springer-Verlag, New York, 1984.

[103] C. Truesdell and W. Noll. *The Non-Linear Field Theories of Mechanics*. Handbuch der Physik, Band III/3, (Editor: S. Flügge), Springer-Verlag, 1965.

[104] C.Y. Tuan. Ponding on circular membranes. *International Journal of Solids and Structures*, 35:269–283, 1998.

[105] J.C. Virella, L.A. Godoy, and L.E. Suarez. Fundamental modes of cylindrical tank-liquid systems under horizontal motions. *Engineering Structures*, 28:1450–1461, 2006.

[106] F. Vollertsen, R. Breede, and M. Beckmann. Process layout and forming results from deep drawing using pressurized membranes. *Proceedings of the Institution of Mechanical Engineers, Part B: Journal of Engineering Manufacture*, 215:977–990, 2001.

[107] R. Wagner and T. Raible. Wann trägt Luft wirklich? *Bauen mit Textilien*, 3:7–15, 2000.

[108] W.A. Wall. *Fluid-Struktur Interaktion mit stabilisierten Finiten Elementen*. PhD thesis, Institut für Baustatik der Universität Stuttgart, 1999.

[109] X. Wang and K.J. Bathe. Displacement/pressure based mixed finite element formulations for acoustic fluid-structure interaction problems. *International Journal for Numerical Methods in Engineering*, 40:2001–2017, 1997.

[110] J.T. Weissenburger. Effect of local modifications on the vibration characteristics of linear systems. *ASME Journal of Applied Mechanics*, 35:327–332, 1968.

[111] C. Wielgosz, J.C. Thomas, and P. Casari. Strength of inflatable fabric beams at high pressure. *AIAA/ASME/ASCE/AHS Structures, Structural Dynamics and Material Conference, Denver*, 43:1292, 2002.

[112] P. Wriggers. *Nichtlineare Finite-Element-Methoden*. Springer-Verlag, Berlin, 2001.

[113] H. Ziegler. *An introduction to thermomechanics*. North-Holland Publishing Company, 1977.

[114] O.C. Zienkiewicz and R.L. Taylor. *The Finite Element Method, Vol. 1*. Butterworth-Heinemann, 2000.

[115] O.C. Zienkiewicz and R.L. Taylor. *The Finite Element Method, Vol. 2*. Butterworth-Heinemann, 2000.

Appendix A

Mathematical basics

A.1 Linearizations

Linearizations are necessary for the solution of complex nonlinear initial boundary value problems, if they are to be embedded in numerical solution schemes, such as the Newton-Raphson method.

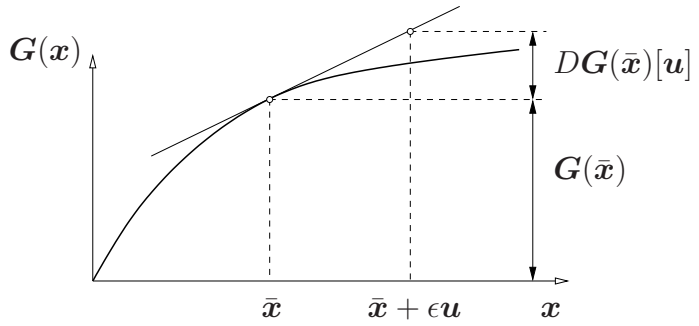

Figure A.1: Linearization of a function $\boldsymbol{G}(\boldsymbol{x})$

A Taylor series expansion of a function $\boldsymbol{G}(\boldsymbol{x})$ at a position $\bar{\boldsymbol{x}}$, defined in the n-dimensional space $\mathcal{R}^n$, performed about an artificially introduced parameter ϵ yields (after neglecting higher order terms) the linearization

$$\boldsymbol{G}(\bar{\boldsymbol{x}} + \epsilon\boldsymbol{u}) \approx \boldsymbol{G}(\bar{\boldsymbol{x}}) + D\boldsymbol{G}(\bar{\boldsymbol{x}})[\boldsymbol{u}] \ . \tag{A.1}$$

The directional derivative $D\boldsymbol{G}(\bar{\boldsymbol{x}})[\boldsymbol{u}]$ of $\boldsymbol{G}(\boldsymbol{x})$ at the position $\bar{\boldsymbol{x}}$ in direction of $\boldsymbol{u}$ can be obtained using the chain rule:

$$\begin{aligned} D\boldsymbol{G}(\bar{\boldsymbol{x}})[\boldsymbol{u}] &= \epsilon \frac{d}{d\epsilon} \left[\boldsymbol{G}(\bar{\boldsymbol{x}} + \epsilon\boldsymbol{u})\right]\Big|_{\epsilon=0} = \epsilon \frac{\partial}{\partial \boldsymbol{x}} \boldsymbol{G}(\bar{\boldsymbol{x}} + \epsilon\boldsymbol{u})\Big|_{\boldsymbol{x}=\bar{\boldsymbol{x}}} \frac{d}{d\epsilon}(\bar{\boldsymbol{x}} + \epsilon\boldsymbol{u})\Big|_{\epsilon=0} \\ &= \frac{\partial \boldsymbol{G}(\boldsymbol{x})}{\partial \boldsymbol{x}}\Big|_{\boldsymbol{x}=\bar{\boldsymbol{x}}} \epsilon\boldsymbol{u} \end{aligned} \tag{A.2}$$

If the infinitesimal size $\epsilon\boldsymbol{u}$ is denoting a real increment, it is given the notation $\epsilon\boldsymbol{u} = \Delta\boldsymbol{u}$, whereas in the case of a virtual increment it is given the designation $\epsilon\boldsymbol{u} = \delta\boldsymbol{u}$.

A.2 Some fundamentals of variational calculus

As the variational calculus is used in this thesis as a basic method for the derivation of a stationary potential energy value, describing a state of equilibrium, it shall be briefly illustrated here. More detailed information on the variational calculus can be found e.g. in RIEMER ET AL.[77]. The goal of variational calculus is the determination of a function $q(t)$ maximizing or minimizing the integral $\jmath[q]$ of the functional

$$\jmath[q] = \int_{t_1}^{t_2} F(q, \dot{q}, t)\ dt\ , \quad \dot{q} = \frac{dq}{dt} \tag{A.3}$$

for a given basic function $F(q, \dot{q}, t)$. Assuming a solution $q(t)$ a thereof slightly varying function

$$\bar{q}(\epsilon, t) = q(t) + \epsilon\eta(t)\ , \epsilon \ll 1 \tag{A.4}$$

can be introduced, which differs from q by $\epsilon\eta(t)$. The variation of the function q thus yields

$$\delta q = \bar{q} - q = \epsilon\eta(t)\ , \epsilon \ll 1\ . \tag{A.5}$$

A Taylor series expansion of $\bar{q}(\epsilon, t) = q(t) + \epsilon\eta(t)$ about the variational parameter

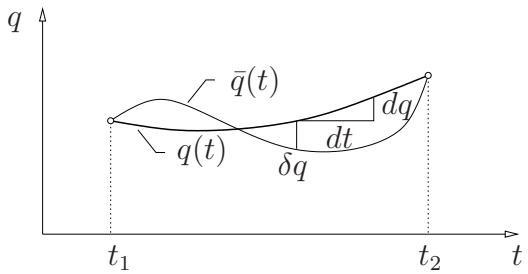

Figure A.2: Variation $\delta q = \bar{q} - q$

gives

$$\begin{aligned} \bar{q}(\epsilon, t) &= \bar{q}|_{\epsilon=0} + \left.\frac{\partial\bar{q}}{\partial\epsilon}\right|_{\epsilon=0} \epsilon + \left.\frac{1}{2!}\frac{\partial^2\bar{q}}{\partial\epsilon^2}\right|_{\epsilon=0} \epsilon^2 + \cdots \\ &= q(t) + \left.\frac{\partial\bar{q}}{\partial\epsilon}\right|_{\epsilon=0} \epsilon + O(\epsilon^2) \end{aligned} \tag{A.6}$$

Comparing equations (A.4) and (A.6) shows, that neglecting higher order terms

$$\delta q := \left.\frac{\partial \bar{q}}{\partial \epsilon}\right|_{\epsilon=0} \epsilon \tag{A.7}$$

defines the first variation of a function q. It complies with a derivation of q to ϵ and it has to be performed orthogonal to the time axis. Thus it yields

$$\delta t \equiv 0 \ . \tag{A.8}$$

Further the terms

$$\frac{d}{dt}\delta q = \frac{d}{dt}\epsilon\eta = \epsilon\dot{\eta} \quad \text{and} \quad \delta\frac{dq}{dt} = \dot{\bar{q}} - \dot{q} = \epsilon\dot{\eta} \tag{A.9}$$

can be used to verify the permutation relation

$$(\delta q)^{\cdot} = \delta\dot{q} \ . \tag{A.10}$$

In analogy the integral permutation relation

$$\delta\jmath = \delta\int_{t_1}^{t_2} F \ dt = \int_{t_1}^{t_2} \delta F \ dt. \tag{A.11}$$

is valid. The fact that the variation δq is perpendicular to the time axis t can be interpreted as the variation being only a virtual process. According to equation (A.11) the variation of the functional becomes the variation of the basic function F.

$$\begin{aligned} \delta F &= \bar{F} - F \\ &= F(q+\epsilon\eta, \dot{q}+\epsilon\dot{\eta}, t) - F(q,\dot{q},t) \end{aligned} \tag{A.12}$$

A Taylor series expansion of $\bar{F}$ about ϵ gives

$$\begin{aligned} \bar{F} &= F(q+\epsilon\eta, \dot{q}+\epsilon\dot{\eta}, t) \\ &= \bar{F}\big|_{\epsilon=0} + \left.\frac{\partial \bar{F}}{\partial \epsilon}\right|_{\epsilon=0} \epsilon + O(\epsilon^2) \\ &= F + \left.\left(\frac{\partial F}{\partial \bar{q}}\frac{\partial \bar{q}}{\partial \epsilon} + \frac{\partial F}{\partial \dot{\bar{q}}}\frac{\partial \dot{\bar{q}}}{\partial \epsilon}\right)\right|_{\epsilon=0} \epsilon + O(\epsilon^2) \\ &= F + \left(\frac{\partial F}{\partial q}\eta + \frac{\partial F}{\partial \dot{q}}\dot{\eta}\right) + O(\epsilon^2) \end{aligned} \tag{A.13}$$

Inserting equation (A.13) in (A.11) and neglecting higher order terms yields the first variation of the functional

$$\delta\jmath = \int_{t_1}^{t_2} \left(\frac{\partial F}{\partial q}\eta + \frac{\partial F}{\partial \dot{q}}\dot{\eta}\right)\epsilon \ dt \ . \tag{A.14}$$

Using partial integration the second term can be transformed to

$$\int_{t_1}^{t_2} \frac{\partial F}{\partial \dot{q}} \dot{\eta}\, dt = \left(\frac{\partial F}{\partial \dot{q}} \eta \right) \Bigg|_{t_1}^{t_2} - \int_{t_1}^{t_2} \frac{d}{dt} \left(\frac{\partial F}{\partial \dot{q}} \right) \eta\, dt \ . \tag{A.15}$$

Since the test function satisfies the boundary conditions $\eta(t_1) = \eta(t_2) = 0$, the boundary term in equation (A.15) vanishes and for the first variation of the functional

$$\delta \jmath = \int_{t_1}^{t_2} \left(\frac{\partial F}{\partial q} - \frac{d}{dt} \frac{\partial F}{\partial \dot{q}} \right) \epsilon \eta\, dt \tag{A.16}$$

a form remains, which has been reduced to the variation $\delta q = \epsilon \eta$ of the unknown function $q(t)$. With

$$\delta \jmath = 0 \tag{A.17}$$

it can be stated that the integral value of a stationary functional does not change in a first approximation, if an adjacent function $\bar{q}$ is used instead of the unknown function q. However, equation (A.17) is only a necessary condition for finding an extreme value of the functional (besides the stable states of equilibrium also instable states may exist).

A.2.1 Eulerian equation of the variational problem

The fundamental lemma of the variational calculus posts, that the only possibility satisfying equation (A.16) for all times t and for arbitrary variations δq is eliminating the integrand. This yields the Eulerian equation of the variational problem for the determination of $q(t)$.

$$\frac{\partial F}{\partial q} - \frac{d}{dt} \frac{\partial F}{\partial \dot{q}} = 0 \tag{A.18}$$

A.3 Legendre transformation

The Legendre transformation aims on an exchange of the independent variable x in a function $f(x, y)$ with another independent variable u, which is the derivative of f to x:

$$u = \left. \frac{\partial f}{\partial x} \right|_y \tag{A.19}$$

The transformed function $g(u, y)$ can be derived as follows: The value of $f(x, y)$ can be alternatively written as

$$f(x, y) = f(x_0, y) + \left. \frac{\partial f}{\partial x} \right|_y \Delta x \ , \quad \text{with} \quad \Delta x = x - x_0 \ . \tag{A.20}$$

Inserting equation (A.19) in (A.20) gives with $x_0 = 0$ the transformed function $g(u, y)$ as the intersection of the contribution in x-direction of the tangential plane in $f(x, y)$ with the plane $x = 0$, see also figure A.3. Thus the transformed function

$$g(u, y) = f(x, y) - xu \tag{A.21}$$

is obtained by the difference of the original function $f(x, y)$ and the product of the variables xu which are to be swapped. Hence, a function $f(x, y)$ is then not exclusively

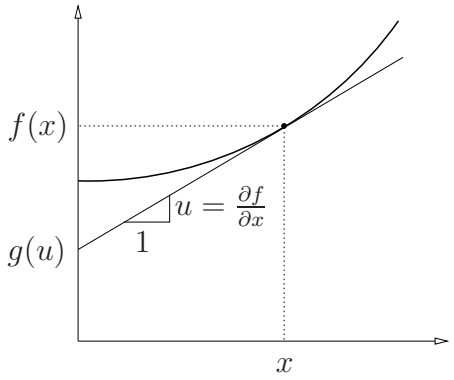

Figure A.3: Geometric interpretation of the Legendre transformation

given by its point set, but also by the tangential planes coating the function. Building the total differential of $g(u, y)$ proves along with equation (A.19) that the function $g(u, y)$

$$dg = \left.\frac{\partial f}{\partial x}\right|_y dx + \left.\frac{\partial f}{\partial y}\right|_x dy - x du - u dx = \left.\frac{\partial f}{\partial y}\right|_x dy - x du \tag{A.22}$$

features only u and y as independent variables.

A.4 Some fundamentals of tensor calculus

A.4.1 Triple product

The volume of a parallelepiped is given by

$$v = \boldsymbol{a} \cdot (\boldsymbol{b} \times \boldsymbol{c}) = \epsilon_{ijk} a^i b^j c^k = \epsilon_{ijk} a^j b^k c^i = (\boldsymbol{a} \times \boldsymbol{b}) \cdot \boldsymbol{c} \; . \tag{A.23}$$

If the columns of the deformation gradient $\boldsymbol{F} = \partial \boldsymbol{x} / \partial \boldsymbol{X}$ are regarded as three tangent vectors spanning a parallelepiped, its volume dv/dV complies with the determinant of the deformation gradient.

$$\det \boldsymbol{F} = J = dv/dV \tag{A.24}$$

A.4.2 Product of two tensors

$$(\boldsymbol{a} \otimes \boldsymbol{b})(\boldsymbol{c} \otimes \boldsymbol{d}) = a^i b^j c^j d^k (\boldsymbol{e}_i \otimes \boldsymbol{e}_k) = (\boldsymbol{b} \cdot \boldsymbol{c})(\boldsymbol{a} \otimes \boldsymbol{d}) \tag{A.25}$$

A.4.3 Expanding double cross products

$$(\boldsymbol{b} \times \boldsymbol{a}) \times \boldsymbol{c} = (\boldsymbol{a} \otimes \boldsymbol{b} - \boldsymbol{b} \otimes \boldsymbol{a})\boldsymbol{c} \tag{A.26}$$

A.4.4 Separation of a matrix

By the following rule an arbitrary $m \times m$-matrix can be separated in a symmetric and an antisymmetric part:

$$\boldsymbol{M} = \frac{1}{2}(\boldsymbol{M} + \boldsymbol{M}^T) + \frac{1}{2}(\boldsymbol{M} - \boldsymbol{M}^T) \tag{A.27}$$

A.4.5 Trace of a tensor

The trace of a tensor is given by a contraction of its dual base vectors.

$$\mathrm{Tr}(\boldsymbol{A}) = \left(G^{ij}\boldsymbol{G}_i \otimes \boldsymbol{G}_j\right) : \left(A_{kl}\boldsymbol{G}^k \otimes \boldsymbol{G}^l\right) = G^{ij} A_{kl} \delta_i{}^k \delta_j{}^l = A_{il} G^{il} \tag{A.28}$$

A.4.6 Convective coordinates on a surface

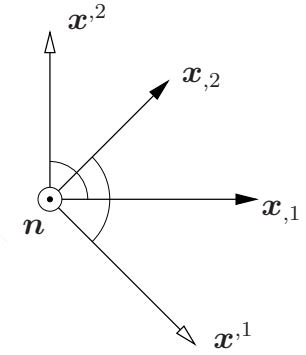

Transformation of the convective base vectors using the normal $\boldsymbol{n}$

$$\boldsymbol{x}_{,1} = -\boldsymbol{n} \times \boldsymbol{x}^{,2} \tag{A.29}$$

$$\boldsymbol{x}_{,2} = \boldsymbol{n} \times \boldsymbol{x}^{,1} \tag{A.30}$$

Figure A.4: Orientation of convective coordinates

A.4.7 Gauß' theorem

For the transformation of volume integrals in surface integrals Gauß' theorem can be used. It states that the change of a tensor field $\boldsymbol{t}$ in a control volume $\mathcal{B}$ equals the

quantity of this field emitted over the boundary $\partial\mathcal{B}$.

$$\int_{\mathcal{B}} \operatorname{div} \boldsymbol{t}\, dv = \int_{\partial\mathcal{B}} \boldsymbol{t}\boldsymbol{n}\, da \tag{A.31}$$

$\boldsymbol{n}$ denotes the normal vector on the surface.

A.5 Computation of the volume

The computation of the volume v of a body in terms of boundary integrals can be performed using Gauß' theorem and the relation $\operatorname{div}\boldsymbol{x} = 3$.

$$v(\boldsymbol{x}) = \int_{\mathcal{B}} dv = \frac{1}{3}\int_{\mathcal{B}} \operatorname{div}\boldsymbol{x}\, dv = \frac{1}{3}\int_{\partial\mathcal{B}} \boldsymbol{x}\cdot\bar{\boldsymbol{n}}\, da\ , \quad \text{with} \quad \bar{\boldsymbol{n}} = \frac{\boldsymbol{n}}{|\boldsymbol{n}|} \tag{A.32}$$

Using equations (3.34) and (3.35) the previous integration can also be achieved in convective coordinates ξ^i:

$$v(\boldsymbol{x}) = \int_{\mathcal{B}} dv = \frac{1}{3}\int_{\partial\mathcal{B}} \boldsymbol{x}\cdot\boldsymbol{n}\, d\xi^1 d\xi^2\ , \tag{A.33}$$

with the non-normalized normal vector $\boldsymbol{n}$.

A.5.1 Variation of the volume

The virtual change of the volume δv can be derived by an application of the directional derivative in direction $\delta\boldsymbol{u}$ along with the chain rule. This yields a separation of the volume change in a displacement part $\delta v^{\delta u}$ and a normal change part $\delta v^{\delta n}$:

$$\delta v = Dv(\boldsymbol{x})[\delta\boldsymbol{u}] = \frac{1}{3}\int_{\partial\mathcal{B}} (\delta\boldsymbol{u}\cdot\boldsymbol{n} + \boldsymbol{x}\cdot\delta\boldsymbol{n})\, d\xi^1 d\xi^2 = \delta v^{\delta u} + \delta v^{\delta n} \tag{A.34}$$

For the complete description of δv the variation of the normal

$$\boldsymbol{n} = \boldsymbol{x}_{,1}\times\boldsymbol{x}_{,2} \tag{A.35}$$

on the structural surface is necessary. Its virtual change follows from

$$\delta\boldsymbol{n} = D\boldsymbol{n}(\boldsymbol{x})[\delta\boldsymbol{u}] = \delta\boldsymbol{u}_{,1}\times\boldsymbol{x}_{,2} + \boldsymbol{x}_{,1}\times\delta\boldsymbol{u}_{,2}\ . \tag{A.36}$$

Regarding the second summand in equation (A.34), inserting equation (A.36) gives

$$\delta v^{\delta n} \;=\; \frac{1}{3}\int_{\partial\mathcal{B}} (\delta\boldsymbol{u}_{,1}\times\boldsymbol{x}_{,2})\cdot\boldsymbol{x} + \boldsymbol{x}\cdot(\boldsymbol{x}_{,1}\times\delta\boldsymbol{u}_{,2})\, d\xi^1 d\xi^2\ . \tag{A.37}$$

Reordering with the triple product (A.23) yields

$$\delta v^{\delta n} = \frac{1}{3}\int_{\partial\mathcal{B}} \delta\boldsymbol{u}_{,1}\cdot(\boldsymbol{x}_{,2}\times\boldsymbol{x}) + (\boldsymbol{x}\times\boldsymbol{x}_{,1})\cdot\delta\boldsymbol{u}_{,2}\; d\xi^1 d\xi^2 \; . \tag{A.38}$$

Using partial integration the surface integral can be separated in a domain part and a boundary part with normal $\boldsymbol{n}^s$.

$$\begin{aligned}\delta v^{\delta n} &= \frac{1}{3}\int_s [n_1^s(\boldsymbol{x}_{,2}\times\boldsymbol{x}) + n_2^s(\boldsymbol{x}\times\boldsymbol{x}_{,1})]\cdot\delta\boldsymbol{u}\; ds \\ &\quad -\frac{1}{3}\int_{\partial\mathcal{B}} (\underbrace{\boldsymbol{x}_{,21}\times\boldsymbol{x}+\boldsymbol{x}\times\boldsymbol{x}_{,12}}_{=\boldsymbol{0}} + \underbrace{\boldsymbol{x}_{,2}\times\boldsymbol{x}_{,1}+\boldsymbol{x}_{,2}\times\boldsymbol{x}_{,1}}_{=-2\boldsymbol{n}})\cdot\delta\boldsymbol{u}\; d\xi^1 d\xi^2\end{aligned} \tag{A.39}$$

The normal vector $\boldsymbol{n}^s$ still lies in the $\boldsymbol{x}_{,1}\times\boldsymbol{x}_{,2}$-plane, but it is orthogonal to the boundary s, see also figure A.5. This results in:

$$\delta v^{\delta n} = \underbrace{\frac{1}{3}\int_s [n_1^s(\boldsymbol{x}_{,2}\times\boldsymbol{x}) + n_2^s(\boldsymbol{x}\times\boldsymbol{x}_{,1})]\cdot\delta\boldsymbol{u}\; ds}_{\delta v_s^{\delta n}} + \frac{2}{3}\int_{\partial\mathcal{B}} \boldsymbol{n}\cdot\delta\boldsymbol{u}\; d\xi^1 d\xi^2 \; . \tag{A.40}$$

A transformation of the covariant base vectors $\boldsymbol{x}_{,1}, \boldsymbol{x}_{,2}$ on the structural surface to an in-plane boundary normal $\boldsymbol{n}^s$ and an in-plane boundary tangent $\boldsymbol{t}^s$ accordingly

$$\begin{pmatrix} \boldsymbol{n}^s \\ \boldsymbol{t}^s \end{pmatrix} = \begin{pmatrix} n_1^s & n_2^s \\ n_2^s & -n_1^s \end{pmatrix} \begin{pmatrix} \boldsymbol{x}_{,1} \\ \boldsymbol{x}_{,2} \end{pmatrix} \tag{A.41}$$

results in a uniform description of the first summand of equation (A.40).

$$\begin{aligned}\delta v_s^{\delta n} &= \frac{1}{3}\int_s [n_1^s(\boldsymbol{x}_{,2}\times\boldsymbol{x}) + n_2^s(\boldsymbol{x}\times\boldsymbol{x}_{,1})]\cdot\delta\boldsymbol{u}\; ds \\ &= \frac{1}{3}\int_s [n_1^s(\boldsymbol{x}_{,2}\times\boldsymbol{x}) - n_2^s(\boldsymbol{x}_{,1}\times\boldsymbol{x})]\cdot\delta\boldsymbol{u}\; ds \\ &= -\frac{1}{3}\int_s (\boldsymbol{t}^s\times\boldsymbol{x})\cdot\delta\boldsymbol{u}\; ds\end{aligned} \tag{A.42}$$

This boundary integral

$$\delta v_s^{\delta n} = -\frac{1}{3}\int_s (\boldsymbol{t}^s\times\boldsymbol{x})\cdot\delta\boldsymbol{u}\; ds \tag{A.43}$$

vanishes, because in case of a closed fluid surface no boundary is apparent and in case of several fluid layers the boundary terms cancel each other, because their tangents

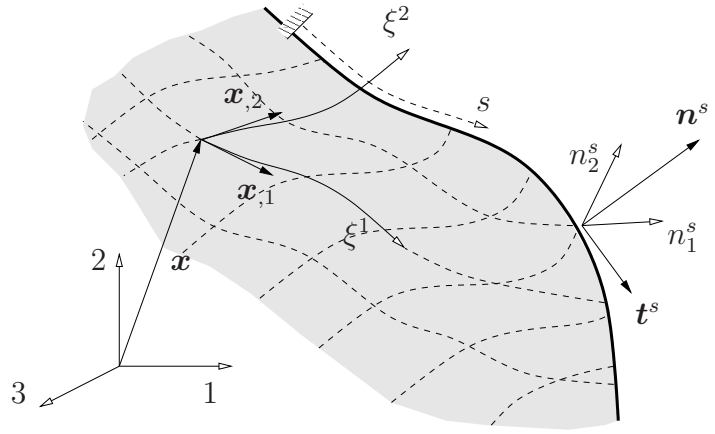

Figure A.5: Boundary normal $\boldsymbol{n}^s = [n_1^s, n_2^s]^T$ and boundary tangent $\boldsymbol{t}^s = [n_2^s, -n_1^s]^T$

point in opposite directions. If the fluid is not completely enclosed, term (A.43) can be eliminated by applying appropriate boundary conditions, which means $\delta\boldsymbol{u}|_s = \boldsymbol{0}$, on s. After eliminating the boundary integral, the variation of the volume according to equation (A.34) can be given as:

$$\delta v = \frac{1}{3}\int\limits_{\partial\mathcal{B}} \boldsymbol{n}\cdot\delta\boldsymbol{u}\; d\xi^1 d\xi^2 + \frac{2}{3}\int\limits_{\partial\mathcal{B}} \boldsymbol{n}\cdot\delta\boldsymbol{u}\; d\xi^1 d\xi^2 = \int\limits_{\partial\mathcal{B}} \boldsymbol{n}\cdot\delta\boldsymbol{u}\; d\xi^1 d\xi^2 \tag{A.44}$$

A more detailed physical interpretation is given in Rumpel&Schweizerhof[79].

A.6 First order volume moment

In order to transform the first order volume moment in a surface integral description, in a first step the projections of the particular volumes dv_i under each side of the differential volume element dv have to be calculated. They are obtained by the scalar product of the normalized area normal $\bar{\boldsymbol{n}}_i$ and the position vector $\boldsymbol{x}_i$ to the side.[1]

$$dv_{(i)} = \boldsymbol{x}_{(i)}\cdot\bar{\boldsymbol{n}}_{(i)}\; da_{(i)} \tag{A.45}$$

The appropriate first order volume moment then follows as

$$d\bar{\boldsymbol{s}}_{(i)} = dv_{(i)}\; \boldsymbol{x}_{C(i)}\;. \tag{A.46}$$

Capturing the volume moment by the coordinates of the center of gravity $\boldsymbol{x}_{Ci}$ is not a proper method, because it is in contrast to a formulation in terms of its surface. However, as depicted in figure (A.6), it can be written

$$\boldsymbol{x}_2 = \begin{pmatrix} x_{21} \\ x_{22} \\ x_{23} \end{pmatrix} = \begin{pmatrix} x_{C21} \\ 2\; x_{C22} \\ x_{C23} \end{pmatrix}\;, \tag{A.47}$$

[1]No summation over bracketed indices (i).

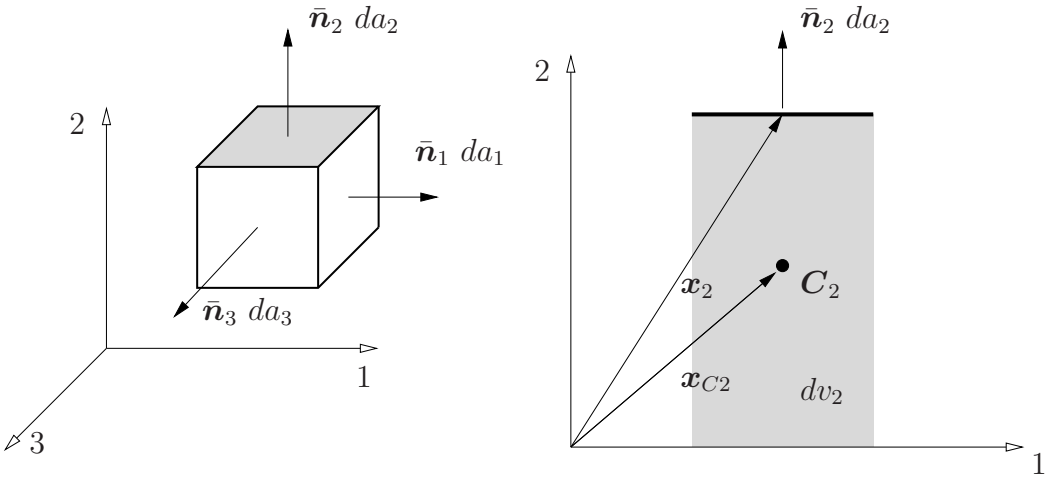

Figure A.6: Projection of the volume under da_2 in 2-direction

which means that the description of each volume moment can be achieved using the position vector $\boldsymbol{x}_i$ to the surface instead of using the center of gravity $\boldsymbol{x}_{Ci}$. In this case within the computation the fact must be considered, that one of the three coordinates of the center of gravity is doubly weighted. Thus the averaging factor is now 1/4 instead of 1/3. The resulting first order volume moment $d\bar{\boldsymbol{s}}$ is finally obtained by the average of all particular volume moments.

$$\begin{aligned} d\bar{\boldsymbol{s}} &= \frac{1}{4}\left[\begin{pmatrix} 2\ x_{C11} \\ x_{C12} \\ x_{C13} \end{pmatrix} dv_1 + \begin{pmatrix} x_{C21} \\ 2\ x_{C22} \\ x_{C23} \end{pmatrix} dv_2 + \begin{pmatrix} x_{C31} \\ x_{C32} \\ 2\ x_{C33} \end{pmatrix} dv_3\right] \\ &\quad + \frac{1}{4}\left[\begin{pmatrix} 2\ x_{C41} \\ x_{C42} \\ x_{C43} \end{pmatrix} dv_4 + \begin{pmatrix} x_{C51} \\ 2\ x_{C52} \\ x_{C53} \end{pmatrix} dv_5 + \begin{pmatrix} x_{C61} \\ x_{C62} \\ 2\ x_{C63} \end{pmatrix} dv_6\right] \\ &= \frac{1}{4}\sum_{i=1}^{6} \boldsymbol{x}_i(\boldsymbol{x}_i \cdot \bar{\boldsymbol{n}}_i)\ da_i \end{aligned} \tag{A.48}$$

Since the normals of the sides 4..6 point in negative direction the moments of their projected volumes $dv_4..dv_6$ are negative as well. Generally the first order volume moment can be described in terms of surface integrals as follows:

$$\bar{\boldsymbol{s}} = \int_{\mathcal{B}} \boldsymbol{x}\ dv = \frac{1}{4}\int_{\partial\mathcal{B}} \boldsymbol{x}(\boldsymbol{x} \cdot \bar{\boldsymbol{n}})\ da\ . \tag{A.49}$$

It has to be mentioned that this formula is only valid if the volume features a closed surface. Using again the relations (3.34) and (3.35) this integration can be transformed to convective coordinates ξ^i.

$$\bar{\boldsymbol{s}} = \int_{\mathcal{B}} \boldsymbol{x}\ dv = \frac{1}{4}\int_{\partial\mathcal{B}} \boldsymbol{x}(\boldsymbol{x} \cdot \boldsymbol{n})\ d\xi^1 d\xi^2\ . \tag{A.50}$$

A.6.1 Variation of the first order volume moment

For the complete description of the variation of the gravitational potential of a fluid its first order volume moment has to varied. For that purpose, according to equation (A.50), the volume integral is transformed into a surface integral. Thus for the projection of the variation of the first order volume moment yields:

$$\begin{aligned} \boldsymbol{g}\cdot\delta\bar{\boldsymbol{s}} &= \boldsymbol{g}\cdot D\bar{\boldsymbol{s}}(\boldsymbol{x})[\delta\boldsymbol{u}] \\ &= \frac{1}{4}\,\boldsymbol{g}\cdot\int_{\partial\mathcal{B}}\delta\boldsymbol{u}(\boldsymbol{x}\cdot\boldsymbol{n})+\boldsymbol{x}(\delta\boldsymbol{u}\cdot\boldsymbol{n})+\boldsymbol{x}(\boldsymbol{x}\cdot\delta\boldsymbol{n})\;d\xi^1d\xi^2 \\ &= \frac{1}{4}\int_{\partial\mathcal{B}}(\boldsymbol{g}\cdot\delta\boldsymbol{u})(\boldsymbol{x}\cdot\boldsymbol{n})+(\boldsymbol{g}\cdot\boldsymbol{x})(\delta\boldsymbol{u}\cdot\boldsymbol{n})+(\boldsymbol{g}\cdot\boldsymbol{x})(\boldsymbol{x}\cdot\delta\boldsymbol{n})\;d\xi^1d\xi^2 \end{aligned} \tag{A.51}$$

In analogy to equation (A.38) the last summand from equation (A.51) can be transformed using (A.36).

$$\begin{aligned} \boldsymbol{g}\cdot\delta\bar{\boldsymbol{s}}^{\delta n} &= \frac{1}{4}\int_{\partial\mathcal{B}}(\boldsymbol{g}\cdot\boldsymbol{x})(\boldsymbol{x}\cdot\delta\boldsymbol{n})\;d\xi^1d\xi^2 \\ &= \frac{1}{4}\int_{\partial\mathcal{B}}(\boldsymbol{g}\cdot\boldsymbol{x})\left[\delta\boldsymbol{u}_{,1}\cdot(\boldsymbol{x}_{,2}\times\boldsymbol{x})+(\boldsymbol{x}\times\boldsymbol{x}_{,1})\cdot\delta\boldsymbol{u}_{,2}\right]\;d\xi^1d\xi^2 \end{aligned} \tag{A.52}$$

As before by partial integration the differential operator is shifted from the test function $\delta\boldsymbol{u}$ and thus a separation in a field term and a boundary term with boundary normal $\boldsymbol{n}^s$ is achieved. Hence equation (A.52) can be given as:

$$\begin{aligned} \boldsymbol{g}\cdot\delta\bar{\boldsymbol{s}}^{\delta n} &= \frac{1}{4}\int_{s}(\boldsymbol{g}\cdot\boldsymbol{x})\left[n_1^s(\boldsymbol{x}_{,2}\times\boldsymbol{x})+n_2^s(\boldsymbol{x}\times\boldsymbol{x}_{,1})\right]\cdot\delta\boldsymbol{u}\;ds \\ &\quad-\frac{1}{4}\int_{\partial\mathcal{B}}\left[(\boldsymbol{g}\cdot\boldsymbol{x}_{,1})(\boldsymbol{x}_{,2}\times\boldsymbol{x})+(\boldsymbol{g}\cdot\boldsymbol{x}_{,2})(\boldsymbol{x}\times\boldsymbol{x}_{,1})\right]\cdot\delta\boldsymbol{u}\;d\xi^1d\xi^2 \\ &\quad-\frac{1}{4}\int_{\partial\mathcal{B}}(\boldsymbol{g}\cdot\boldsymbol{x})\underbrace{\left[(\boldsymbol{x}_{,2}\times\boldsymbol{x})_{,1}+(\boldsymbol{x}\times\boldsymbol{x}_{,1})_{,2}\right]}_{=-2\boldsymbol{n}}\cdot\delta\boldsymbol{u}\;d\xi^1d\xi^2 \end{aligned} \tag{A.53}$$

Using an appropriate coordinate transformation (A.41) the boundary term can be transformed similar to (A.42). Equation (A.53) can thus be written as:

$$\begin{aligned} \boldsymbol{g}\cdot\delta\bar{\boldsymbol{s}}^{\delta n} &= -\frac{1}{4}\int_{s}(\boldsymbol{g}\cdot\boldsymbol{x})(\boldsymbol{t}^s\times\boldsymbol{x})\cdot\delta\boldsymbol{u}\;ds \\ &\quad-\frac{1}{4}\int_{\partial\mathcal{B}}\left[(\boldsymbol{g}\cdot\boldsymbol{x}_{,1})(\boldsymbol{x}_{,2}\times\boldsymbol{x})+(\boldsymbol{g}\cdot\boldsymbol{x}_{,2})(\boldsymbol{x}\times\boldsymbol{x}_{,1})\right]\cdot\delta\boldsymbol{u}\;d\xi^1d\xi^2 \\ &\quad+\frac{1}{4}\int_{\partial\mathcal{B}}2(\boldsymbol{g}\cdot\boldsymbol{x})(\boldsymbol{n}\cdot\delta\boldsymbol{u})\;d\xi^1d\xi^2\;. \end{aligned} \tag{A.54}$$

Using the relations (A.29) and (A.30) for a transformation from a co- to a contravariant basis the second integral in the previous equation can be rewritten.

$$
\begin{aligned}
&-\frac{1}{4}\int_{\partial\mathcal{B}} [(\boldsymbol{g}\cdot\boldsymbol{x}_{,1})(\boldsymbol{x}_{,2}\times\boldsymbol{x}) + (\boldsymbol{g}\cdot\boldsymbol{x}_{,2})(\boldsymbol{x}\times\boldsymbol{x}_{,1})]\cdot\delta\boldsymbol{u}\; d\xi^1 d\xi^2 \\
&\quad = \; -\frac{1}{4}\int_{\partial\mathcal{B}} \left[(\boldsymbol{g}\cdot\boldsymbol{x}_{,1})(\boldsymbol{n}\times\boldsymbol{x}^{,1}\times\boldsymbol{x}) + (\boldsymbol{g}\cdot\boldsymbol{x}_{,2})(\boldsymbol{x}\times\boldsymbol{x}^{,2}\times\boldsymbol{n})\right]\cdot\delta\boldsymbol{u}\; d\xi^1 d\xi^2
\end{aligned}
\tag{A.55}
$$

This expression can be further transformed by expanding the double cross product according to (A.26).

$$
\begin{aligned}
&-\frac{1}{4}\int_{\partial\mathcal{B}} \left[(\boldsymbol{g}\cdot\boldsymbol{x}_{,1})(\boldsymbol{n}\times\boldsymbol{x}^{,1}\times\boldsymbol{x}) + (\boldsymbol{g}\cdot\boldsymbol{x}_{,2})(\boldsymbol{x}\times\boldsymbol{x}^{,2}\times\boldsymbol{n})\right]\cdot\delta\boldsymbol{u}\; d\xi^1 d\xi^2 \\
&\qquad = \; -\frac{1}{4}\int_{\partial\mathcal{B}} \left[(\boldsymbol{g}\cdot\boldsymbol{x}_{,1})(\boldsymbol{x}^{,1}\otimes\boldsymbol{n} - \boldsymbol{n}\otimes\boldsymbol{x}^{,1})\boldsymbol{x}\right. \\
&\qquad\qquad \left. + \; (\boldsymbol{g}\cdot\boldsymbol{x}_{,2})\left(\boldsymbol{x}^{,2}\otimes\boldsymbol{n} - \boldsymbol{n}\otimes\boldsymbol{x}^{,2}\right)\boldsymbol{x}\right]\cdot\delta\boldsymbol{u}\; d\xi^1 d\xi^2
\end{aligned}
\tag{A.56}
$$

Expanding this term with

$$
(\boldsymbol{g}\cdot\boldsymbol{x}_{,3})(\boldsymbol{x}^{,3}\otimes\boldsymbol{n} - \boldsymbol{n}\otimes\boldsymbol{x}^{,3})\boldsymbol{x} = \boldsymbol{0}\;, \tag{A.57}
$$

which vanishes because of

$$
\boldsymbol{x}_{,3} = \boldsymbol{x}^{,3} = \boldsymbol{n}\;, \tag{A.58}
$$

leads to the following formulation:

$$
\begin{aligned}
&-\frac{1}{4}\int_{\partial\mathcal{B}} [(\boldsymbol{g}\cdot\boldsymbol{x}_{,1})(\boldsymbol{x}_{,2}\times\boldsymbol{x}) + (\boldsymbol{g}\cdot\boldsymbol{x}_{,2})(\boldsymbol{x}\times\boldsymbol{x}_{,1})]\cdot\delta\boldsymbol{u}\; d\xi^1 d\xi^2 \\
&\qquad = \; -\frac{1}{4}\int_{\partial\mathcal{B}} [(\boldsymbol{g}\cdot\boldsymbol{x}_{,1})(\boldsymbol{x}^{,1}\otimes\boldsymbol{n} - \boldsymbol{n}\otimes\boldsymbol{x}^{,1})\boldsymbol{x} \\
&\qquad\qquad + (\boldsymbol{g}\cdot\boldsymbol{x}_{,2})(\boldsymbol{x}^{,2}\otimes\boldsymbol{n} - \boldsymbol{n}\otimes\boldsymbol{x}^{,2})\boldsymbol{x} \\
&\qquad\qquad + (\boldsymbol{g}\cdot\boldsymbol{x}_{,3})(\boldsymbol{x}^{,3}\otimes\boldsymbol{n} - \boldsymbol{n}\otimes\boldsymbol{x}^{,3})\boldsymbol{x}]\cdot\delta\boldsymbol{u})\; d\xi^1 d\xi^2
\end{aligned}
\tag{A.59}
$$

Rewriting the tensor products in this relations according to (A.25) yields:

$$
\begin{aligned}
&-\frac{1}{4}\int_{\partial\mathcal{B}} [(\boldsymbol{g}\cdot\boldsymbol{x}_{,1})(\boldsymbol{x}_{,2}\times\boldsymbol{x}) + (\boldsymbol{g}\cdot\boldsymbol{x}_{,2})(\boldsymbol{x}\times\boldsymbol{x}_{,1})]\cdot\delta\boldsymbol{u}\; d\xi^1 d\xi^2 \\
&\qquad = \; -\frac{1}{4}\int_{\partial\mathcal{B}} \delta\boldsymbol{u}\cdot\left[(\boldsymbol{x}^{,1}\otimes\boldsymbol{x}_{,1})(\boldsymbol{g}\otimes\boldsymbol{n}) - (\boldsymbol{n}\otimes\boldsymbol{g})(\boldsymbol{x}_{,1}\otimes\boldsymbol{x}^{,1})\right. \\
&\qquad\qquad + (\boldsymbol{x}^{,2}\otimes\boldsymbol{x}_{,2})(\boldsymbol{g}\otimes\boldsymbol{n}) - (\boldsymbol{n}\otimes\boldsymbol{g})(\boldsymbol{x}_{,2}\otimes\boldsymbol{x}^{,2}) \\
&\qquad\qquad \left. + (\boldsymbol{x}^{,3}\otimes\boldsymbol{x}_{,3})(\boldsymbol{g}\otimes\boldsymbol{n}) - (\boldsymbol{n}\otimes\boldsymbol{g})(\boldsymbol{x}_{,3}\otimes\boldsymbol{x}^{,3})\right]\boldsymbol{x}\; d\xi^1 d\xi^2\;.
\end{aligned}
\tag{A.60}
$$

Introducing the identity tensor

$$\boldsymbol{I} = \boldsymbol{x}_{,1} \otimes \boldsymbol{x}^{,1} + \boldsymbol{x}_{,2} \otimes \boldsymbol{x}^{,2} + \boldsymbol{x}_{,3} \otimes \boldsymbol{x}^{,3} = \boldsymbol{I}^T \tag{A.61}$$

simplifies this expression to

$$\begin{aligned} -\frac{1}{4}\int_{\partial\mathcal{B}} &[(\boldsymbol{g}\cdot\boldsymbol{x}_{,1})(\boldsymbol{x}_{,2}\times\boldsymbol{x}) + (\boldsymbol{g}\cdot\boldsymbol{x}_{,2})(\boldsymbol{x}\times\boldsymbol{x}_{,1})]\cdot\delta\boldsymbol{u}\; d\xi^1 d\xi^2 \\ &= -\frac{1}{4}\int_{\partial\mathcal{B}} \delta\boldsymbol{u}\cdot[(\boldsymbol{g}\otimes\boldsymbol{n}) - (\boldsymbol{n}\otimes\boldsymbol{g})]\,\boldsymbol{x}\;\; d\xi^1 d\xi^2 \\ &= -\frac{1}{4}\int_{\partial\mathcal{B}} [(\boldsymbol{g}\cdot\delta\boldsymbol{u})(\boldsymbol{x}\cdot\boldsymbol{n}) - (\boldsymbol{g}\cdot\boldsymbol{x})(\boldsymbol{n}\cdot\delta\boldsymbol{u})]\;\; d\xi^1 d\xi^2\;. \end{aligned} \tag{A.62}$$

Inserting (A.62) in equation (A.54) and combining all terms finally yields the projection of the variation of the first order volume moment in gravitational direction.

$$\boldsymbol{g}\cdot\delta\bar{\boldsymbol{s}} = \int_{\partial\mathcal{B}} (\boldsymbol{g}\cdot\boldsymbol{x})(\boldsymbol{n}\cdot\delta\boldsymbol{u})\; d\xi^1 d\xi^2 - \frac{1}{4}\int_s (\boldsymbol{g}\cdot\boldsymbol{x})(\boldsymbol{t}^s\times\boldsymbol{x})\cdot\delta\boldsymbol{u}\; ds \tag{A.63}$$

Although in equation (3.28) by using $\bar{\boldsymbol{s}} = \boldsymbol{s}^f + \boldsymbol{s}^o$ a formal separation of the fluid domain was achieved and thus a boundary s was generated, due the relations

$$\boldsymbol{x}^o|_s = \boldsymbol{x}|_s\;, \quad \boldsymbol{t}^{os} = -\boldsymbol{t}^s \quad \text{and} \quad \delta\boldsymbol{u}^o|_s = \delta\boldsymbol{u}|_s \tag{A.64}$$

and after combining the previously separated terms both boundary parts cancel each other. Thus only the domain parts remain in equation (A.63).

$$\boldsymbol{g}\cdot\left(\delta\boldsymbol{s}^f + \delta\boldsymbol{s}^o\right) = \int_{\partial\mathcal{B}^f} (\boldsymbol{g}\cdot\boldsymbol{x}^f)(\boldsymbol{n}^f\cdot\delta\boldsymbol{u}^f)\; d\xi^1 d\xi^2 + \int_{\partial\mathcal{B}^o} (\boldsymbol{g}\cdot\boldsymbol{x}^o)(\boldsymbol{n}^o\cdot\delta\boldsymbol{u}^o)\; d\xi^1 d\xi^2 \tag{A.65}$$

If no closed surface is present, the virtual work boundary term in (A.63) can only be eliminated by applying either an appropriate boundary condition on s, using $\delta\boldsymbol{u}|_s = \boldsymbol{0}$ or by defining $p = \rho\boldsymbol{g}\cdot\boldsymbol{x} = 0$ on s as the appropriate von Neumann boundary condition.

A.7 Derivatives of the invariants in direction of the strains

$$\frac{\partial I_{\boldsymbol{C}}}{\partial\boldsymbol{C}} = \frac{\partial}{\partial\boldsymbol{C}}\mathrm{Tr}(\boldsymbol{C}) = \frac{\partial}{\partial\boldsymbol{C}}(\boldsymbol{C}:\boldsymbol{G}) = \boldsymbol{G} \tag{A.66}$$

$$\frac{\partial II_{\boldsymbol{C}}}{\partial\boldsymbol{C}} = \frac{\partial}{\partial\boldsymbol{C}}\mathrm{Tr}(\boldsymbol{C}^2) = \frac{\partial}{\partial\boldsymbol{C}}(\boldsymbol{C}\boldsymbol{C}):\boldsymbol{G} = 2\boldsymbol{G}\boldsymbol{C}\boldsymbol{G} \tag{A.67}$$

$$\frac{\partial III_{\boldsymbol{C}}}{\partial\boldsymbol{C}} = \frac{\partial}{\partial\boldsymbol{C}}J^2 = III_{\boldsymbol{C}}\boldsymbol{C}^{-1} = J^2\boldsymbol{C}^{-1} \tag{A.68}$$

$$\frac{\partial J}{\partial \boldsymbol{C}} = \frac{\partial J}{\partial III_{\boldsymbol{C}}} \frac{\partial III_{\boldsymbol{C}}}{\partial \boldsymbol{C}} = \frac{1}{2} J \boldsymbol{C}^{-1} \tag{A.69}$$

$$\frac{\partial \ln J}{\partial \boldsymbol{C}} = \frac{1}{J} \frac{\partial J}{\partial \boldsymbol{C}} = \frac{1}{2} \boldsymbol{C}^{-1} \tag{A.70}$$

Curriculum vitae

Name	Marc Haßler
Date of birth	December 16, 1976
Place of birth	Wadern, Germany
Primary and secondary	1983 – 1987 Elementary school Lockweiler
	1987 – 1996 Hochwald Gymnasium Wadern General qualification for university entrance
Military service	1996 – 1997
Study	1997 – 2003 Course of study of civil engineering at the Universität Karlsruhe (TH), Germany Specialization: structural steelwork Graduated as Diplom-Ingenieur
Occupation	2003 – 2009 Research assistant at the Institut für Mechanik, Universität Karlsruhe (TH), Germany
	since 2009 Computational engineer at MTU Aero Engines GmbH, Munich, Germany